INTERNATIONAL ACADEMIC RESEARCH AND REVIEWS IN

SCIENCE AND MATHEMATICS

March 2023

EDITOR
PROF. DR. HASAN AKGÜL

SERÜVEN YAYINEVİ

Genel Yayın Yönetmeni / Editor in Chief • C. Cansın Selin Temana

Kapak & İç Tasarım / Cover & Interior Design • Serüven Yayınevi

Birinci Basım / First Edition • © Mart 2023

ISBN • 978-625-6399-77-8

Serüven Yayınevi / Serüven Publishing
Türkiye Adres / Turkey Address: Kızılay Mah. Fevzi Çakmak 1. Sokak Ümit Apt No: 22/A Çankaya/ANKARA
Telefon / Phone: 05437675765
web: www.seruvenyayinevi.com
e-mail: seruvenyayinevi@gmail.com

Baskı & Cilt / Printing & Volume
Sertifika / Certificate No: 47083

International Academic Research and Reviews in Science and Mathematics

March 2023

Editor

Prof. Dr. Hasan AKGÜL

CONTENTS

CHAPTER 1

THE NEWEST SYNTHESIZED COUMARIN-BASED CHEMOSENSORS IN 2023

Hülya ÇELİK ONAR[1], Hasniye YAŞA[2]

1 Assoc.Prof., İstanbul University-Cerrahpaşa, Engineering Faculty, Chemistry Department, Organic Chemistry Devision Avcılar, İstanbul, Turkey ORCID: 0000-0003-2573-5751

2 Assoc.Prof., İstanbul University-Cerrahpaşa, Engineering Faculty, Chemistry Department, Organic Chemistry Devision Avcılar, İstanbul, Turkey ORCID: 0000-0003-3171-9096

Chemosensors are molecular devices that respond to their target and produce a visual signal, indicating the sensitivity of the device. Chemosensors are composed of two parts: the binding portion and the signaling portion. By non-covalent interactions, the binding component interacts with the analyte. On the other hand, the signaling component displays visibly discernible changes in color or chemical composition. Several factors, including binding power, solvent molecules and size, have an impact on chemosensors. The success of a chemosensor is closely related to both its selectivity and sensitivity for a very small amount of analyte. The number of chemosensor binding sites can be increased to enhance these features [1]. Chemosensors are referred to as molecules that alter their emission or absorption characteristics when they come into contact with other molecules. Chemosensors have been received a lot of attention due to their affordability, great sensitivity, and environmental friendliness [2].

Fluorescent sensors, a type of optical sensing units, are molecules that can change their fluorescent properties in the presence of an analyte. A fluorescent sensor consists of light source, supramolecular part, optical source, photomultiplier or photodiode parts. Fluorescent sensors are widely used in industries such as clinical biochemistry, analytical chemistry, medicine and the environment, due to their advantages over other types of technology such as high selectivity, high sensitivity, simple operation and fast reaction [3].

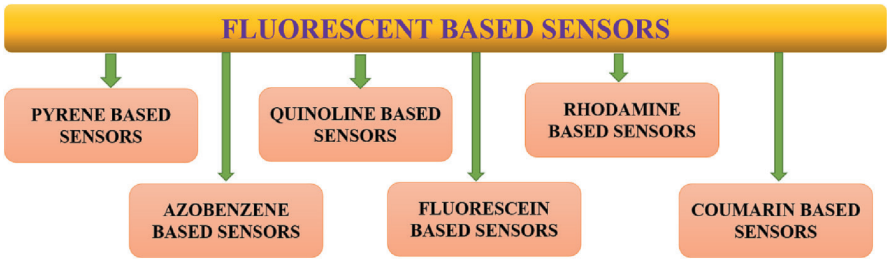

Proton transfer plays an important role in many chemical reactions and in various biological systems. A large number of coumarin derivatives that allow proton transfer, has been successfully used as fluorescent probe, a chemosensor for various anions, cell imaging, photo stabilizer and drug delivery applications [4].

Along with numerous applications in medicine, chemistry, life sciences and biotechnology, research in recent years has focused on highly sensitive and selective fluorescent probes to detect metal ions. An important metal in all living organisms, aluminum also plays a significant role in human life activities and is a fundamental component of enzyme-catalyzed

reactions and biotechnological transformations. Al^{3+} ions can be found in a variety of environments, including natural waterways, plants, and animals. The health risks associated with excessive aluminum exploration include breast cancer, osteomalacia, Alzheimer's disease, Parkinson's disease, and osteoporosis.

In addition to their effective biological applications, coumarin-based Schiff bases have been widely used as effective fluorescent probes for detecting metal ions in recent years due to their simplicity of modification, visible emission wavelength, excellent resolution, strong fluorescent quantum yield and good cell penetration. The first fluorescent substance to be discovered in humans is coumarin. The creation of superior fluorescent probes is also based on the excimer mechanism, fluorescence resonance energy transfer (FRET), photoinduced electron transfer (PET), and intramolecular charge transfer (ICT) [5]. A new coumarin-based Schiffbase (7MIZ) was created by Ravichandran et al.and its true nature determined by X-ray single crystal studies and other spectral techniques. The probe (7MIZ) acted as a highly selective fluorescence sensor for the detection of Al^{3+} ion among other metal ions (chloride saltsA sharp increase in emission intensity is observed at 482 nm when the probe captures the Al^{3+} ion, which is explained as the CHEF (chelation enhanced fluorescence) effect [5].

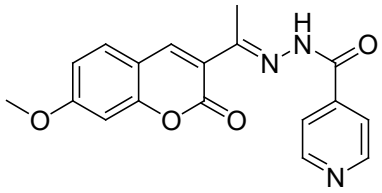

7MIZ

Yang et al. in this paper also created a fluorescence probe **1** based on coumarin hydrazides Schiff base. Since Al^{3+} can bind to the probe at all three places: carbonyl oxygen, C=N bond and hydroxyl oxygen, fluorescence increases and an increase is observed in the molecular plane. It has been stated that the Probe1, which shows a strong selectivity for Al^{3+} and a detection limit as small as 0.12 μM, can be used successfully in real water samples and biological systems [6].

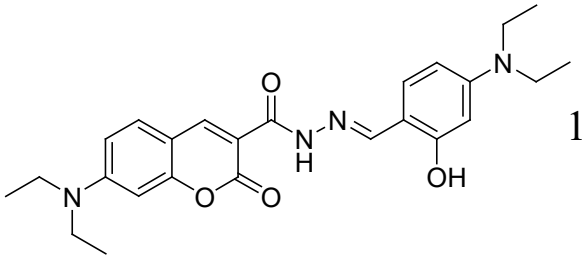

1

One of the most crucial metal ions for biological activities is magnesium. Due to its role in both phosphate metabolism and chlorophyll, magnesium is essential for plants. The formation of the human body's skeleton depends heavily on magnesium and It plays a role in several physiological processes that occur in people, including as enzyme activation, cell growth, DNA and RNA synthesis, and the creation of enzyme cofactors. However, Mg^{2+} ion overload can cause a number of diseases such as muscle dysfunction and lung and cardiovascular tumors. As a result, Mg^{2+} ion detection is crucial for both chemistry and biology research [7].

Zinc is a crucial component of many metalloenzymes and is involved in a wide range of biological processes, including gene transcription, reproduction, the transmission of brain signals, and the contraction of muscles. Epilepsy, Alzheimer's disease, and cerebral ischemia are just a few of the illnesses that can develop in humans when Zn^{2+} levels are too high or too low. Due to the critical role that Zn^{2+} ion plays in human physiology, it is important to recognize and detect it [7].

By combining 7-hydroxy-4-methyl-2-oxo-2H-chromene-8-carbaldehyde with benzo[d] thiazol-2-amine, the coumarin-based probe HL was created. FTIR, NMR, and mass spectra were used to describe HL in addition to X-ray crystallography. It was stated that HL was selective, sensitive and reversible for the detection of Mg^{2+} and Zn^{2+} ions [7].

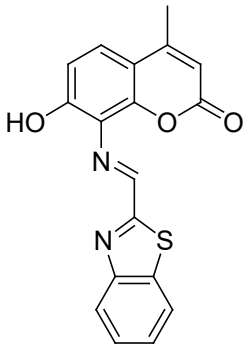

HL

Copper is a vital micronutrient for numerous physiological processes, including metabolism, enzyme functioning, and immunological function. It is the third most prevalent transition metal after zinc and iron. Anemia, vitiligo, irregular bone growth, gastrointestinal issues, and mental impairment can all result from a copper shortage in the body. This work includes the synthesis and characterization of methyl (E)-2-((7-(diethylamino)-2-oxo-2H-chromen-3-yl)methylene)hydrazine-1-carboxylate (SJL), a very sensitive fluorescent probe. As a result of the study, it was stated that the probe showed a magnificent fluorescence quenching reaction against Cu^{2+} with a quenching efficiency of 82.3% in aqueous solution and produced a permanent complex. SJL works best in the pH range of 5 to 9 and can be transformed into test strips to ascertain Cu^{+2}. The probe has been specially utilized to observe copper ions in Hela cells and glassfish larvae [8].

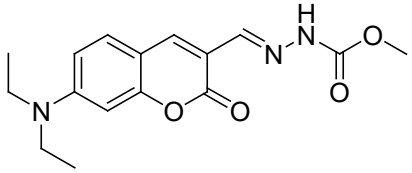

SJL

In this study, the CNH probe, 3-((Z)-1-((E)-((2-hydroxynaphthalen-1-yl)methylene)hydrazono)ethyl)-2H-chromen-2-one, was perfectly synthesized and the its structure was elucidated using IR, ^{1}HNMR, ^{13}C NMR, HRMS. Cu^{2+} and F^{-} ions were detected colorimetrically by a synthetic probe with a detection limit of 1.4 10-6 M in THF and DMF solutions. The color shift in the probe following the binding of Cu^{2+} ions is due to ligand-to-metal charge transfer, as demonstrated by UV-Vis spectra [9].

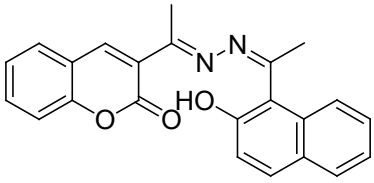

CNH

A different study developed the XS-1 probe containing coumarin, 1,3,4-thiadiazole, and Schiff base nuclei to detect the Cu^{+2} ion. According to the study, bonding caused the probe's fluorescent color to shift from colorless to brilliant green and the solution's hue to change from light pink to bright yellow [10].

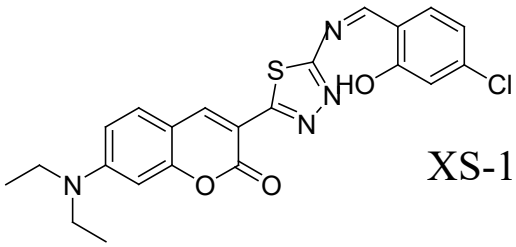

XS-1

Hg pollution continues to be a major issue because of the increased amount of Hg released into our ecosystem through volcanic emissions, oil refining, and rubbish incineration. Again, research indicates that Hg is one of the most prevalent, highly hazardous, and non-biodegradable substances, and that Hg^{2+} is the form of mercury that is found in nature in the greatest abundance. In the food chain, Hg^{2+} can build up in human bodies and result in a number of conditions affecting the brain, kidneys, and nervous system. Thus, it is essential to monitor the amount of Hg^{2+} in the environment [11].

A recent half-century saw an increase in developing and industrial activities, which hastened the prevalence of Hg^{2+} in the environment. The Hg^{2+} ions pollution became a major threat to environmental preservation, animal and plant survival, and human health on a global scale. The human body can easily absorb the very deadly Hg^{2+} ion through respiration, the food chain, and even the skin. Mercury's bioaccumulation and biomagnification in the human body harms the immune system, liver, kidney, central nervous system, and immune system. Hence, Hg^{2+} ion detection is quite important. A novel probe (S1), thionocarbonate-coumarin-thiourea triad-based, was synthesized by Li et al. The probe changed from colorless to blackish brown when the Hg^{2+} ion was added, resulting in a 70-fold increase in fluorescence of the probe. As a result, the probe successfully performed Hg^{2+} bioimaging in real cells and plants while maintaining good biocompatibility [12].

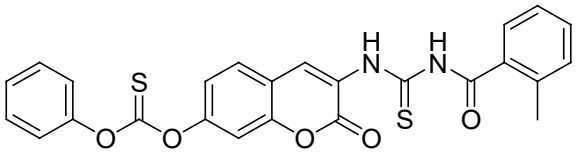

S1

In this work, HCCA-modified filter paper was prepared for the fluorescent detection of Hg^{2+}. This coumarin-based fluorescent probe consists of N-(7-hydroxy-coumarin-3-yl)carbamothioyl) acetamide (HCCA),

hexamethylene diisocyanate and Pristine paper. Elemental analysis, FTIR, XPS, and SEM were used to confirm that the coumarin derivative was successfully grafted chemically on paper. The modified paper's fluorescent hue changed from colorless to bright blue, and it was shown to be very selective and sensitive to Hg^{2+} [11].

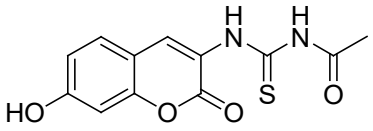

HCCA

One of the most essential trace elements, iron ion (Fe^{3+}), is particularly crucial for biological functions such muscular contraction, nerve conduction, and enzyme catalysis. Human health-wise, low levels of Fe^{3+} can cause anemia and liver cirrhosis, while high levels of Fe^{3+} can cause anorexia and a number of age-related illnesses. In addition, since Fe^{3+} is one of the most abundant heavy metal ions in the world and is widely used in industrial production, it is found at a high rate in domestic garbage and industrial wastes [13].

Dialdehyde cellulose and a coumarin derivative were used in a condensation procedure to create the new fluorescent probe DAC-NCH, which has a particular response to Fe^{3+}. It was determined that 91.7 nM was the lowest value for detection limit for Fe^{3+} with the DAC-NCH [13].

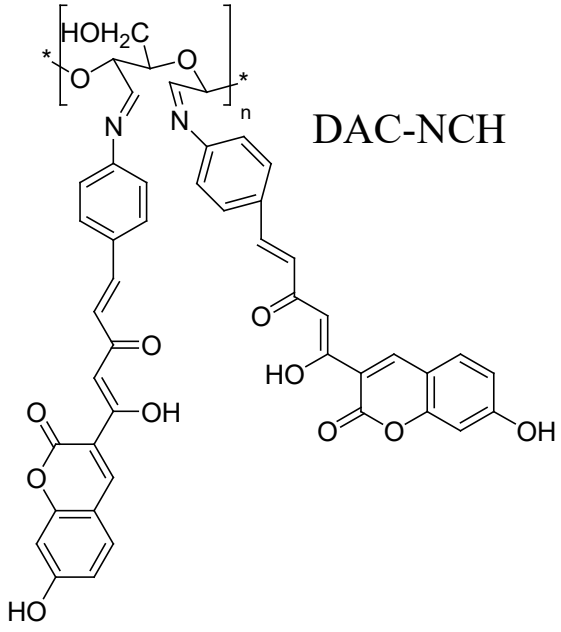

DAC-NCH

As anions make up around 70% of the enzyme sites, they are considered to be the most crucial component of biochemical processes. The fluoride ion (F^-), one of these anion, is the most significant trace element in the human body. Practically, F^- ions have a positive effect on human health and are crucial for treating osteoporosis and avoiding dental caries. The WHO has established a suitable F content in drinking water of 1.5 mg/L. Having too many F^- ions might have detrimental effects on your health. Fluorine is transformed to HF in the stomach (due to acidic condition). Lipid bilayers have HF permeability that is identical to water's, allowing it to move throughout the body. Fluorosis in bones and teeth is brought on by an excess of F^- ions. In addition to causing fluorosis, too much fluoride can negatively impact children's ability to gauge their neurodevelopmentFluoride is an essential trace element found in the human body and is a strong Lewis base. Deficiency or excess can cause significant adverse effects on human health and the environment. In this situation, it is imperative to design sensors that can detect fluoride ions with greater sensitivity and selectivity than other biologically competitive anions. Due to coumarins' favorable derivatization characteristics, low toxicity, high fluorescence quantum yield, significant Stokes shift, and superior photo stability, coumarin-based fluoride ion sensors have been developed. Researchers were drawn to develop receptors for the recognition and sensing of various biologically significant cations and anions because of coumarin derivatives' excellent photo stability, higher fluorescence quantum yield, enormous Stokes shift, good solubility in aqueous as well as organic medium, and less toxicity. Several receptors have been found for the specific detection of various hazardous anions based on the coumarin moiety [14]. Hence, the development of chemosensors with exceptional selectivity and high sensitivity for the detection of F ions is crucial. Here, a brand-new Schiff base based on coumarin has been created to detect F^- ions. When F^- ions were added, the chemosensor immediately displayed a strong color shift (light yellow to purple). The competing anions' impact on the chemosensor are lessened. The binding constant was found to be $1.61\ 10^{-4}$, and the limit of detection was projected to be as low as $1.1\ 10^{-6}$. As a result, F^- ions in the toothpaste sample could be detected with WJ-F. The color of the probe changed from light yellow to purple when bound with F^- ions, and a red shift was observed in the absorbance band. The reaction between WJ-F and F^- ions was monitored using the 1H NMR method to determine the deprotonation of the N-H protons causing the extreme color change [1].

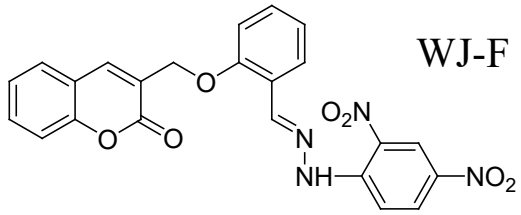

Cyanide (CN) is a chemical that some bacteria, fungus, and algae in the environment create. It is present in over 2,000 different plant species, some of which are edible, such as flaxseed and bamboo shoots. The World Health Organization recommends limiting the amount of CN in drinking water to 1.9 μM. Moreover, CN can block cells from utilising oxygen during mitochondrial oxidation, resulting in internal hypoxia that harms the cardiovascular and neurological systems and respiratory system. The preservation of human health depends on the identification of CN in the environment and food [15].

In order to detect the cyanide ion, Manivannan et al. created the JE5 probe. After detecting the cyanide ion, the probe's color changes from dark blue to pale yellow. The probe JE5's limits of detection were established to be 1.99 M and 0.97 nM, respectively, using UV-Visible and fluorescence methods [16].

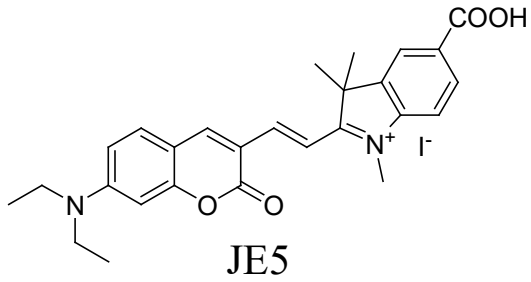

A coumarin-based near-infrared fluorescent probe (CCB) was created by Pan et al. to simultaneously measure mitochondrial viscosity and CN-flating. The capability of this colorimetric method to detect CN with a detection limit as low as 0.22 M was stressed [15].

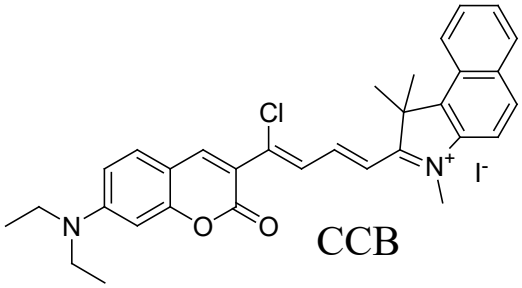

CCB

Although hydrazine (N_2H_4) is a very important chemical in the industry, it can cause serious harm to people and the environment. This study developed a novel fluorescent probe CHY based on coumarin for the detection of hydrazine. The CHY probe showed clear fluorescence with hydrazine, while initially no fluorescence. Moreover, it possesses a broad pH range of 5 to 9, great selectivity, potent anti-interference, and high sensitivity to hydrazine detection. The Environmental Protection Agency recommends a standard of 3.12 10^{-7} M, where the limit of detection (LOD) of CHY for hydrazine is calculated as 2.4 10^{-8} M [17].

CHY

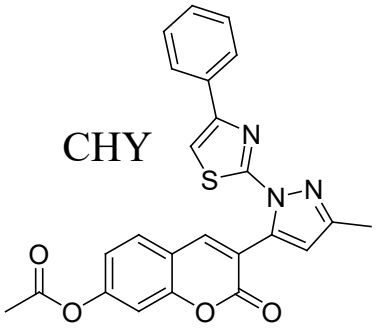

A common chemical reagent that is detrimental to both the environment and human health is hydrazine. Thus, it is essential to create a quick and accurate method for hydrazine identification. In this study, a novel fluorescent cellulose-based probe (ACBC-CA) for the selective and sensitive detection of hydrazine was rationally created. ACBC-CA was created by employing coumarin-based derivative as the fluorophore and cellulose acetate as the structural foundation. In reaction to hydrazine, ACBC-CA showed a sizable "turn-on" fluorescence response as well as a noticeable fluorescence color change from colorless to bright yellow. According to calculations, hydrazine's ACBC-CA detection threshold is 1.2 10^{-7} M. Furthermore, genuine environmental water and soil samples were effectively used to use ACBC-CA to find hydrazine [18].

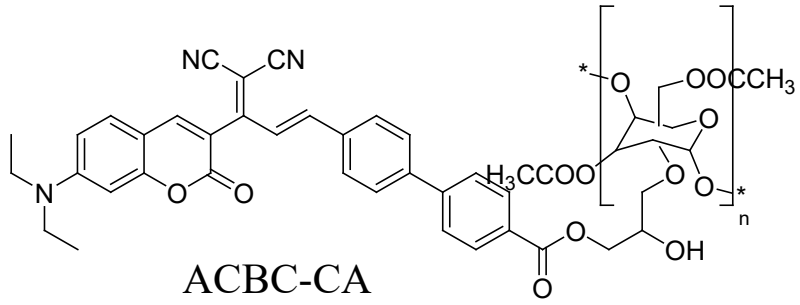

ACBC-CA

There has been a lot of recent study on azo dyes incorporating coumarin thiophene as chemosensors, laser dyes, NLO materials, and organic light-emitting diodes. Three azo dyes (6a-c) containing coumarin thiophene were created in this study, and in different solvents, UV-vis spectroscopy was used to analyze their photophysical properties. In DMSO/H_2O, acidochromic characteristics were also studied, and all products displayed them. To find out whether the produced chemicals might be reused, reversibility studies were conducted. Products 6a-6c were also looked into for possible hydroxide sensor applications. The goal of this study is to design and create a visual chemosensor that can detect hydroxide and pH [19].

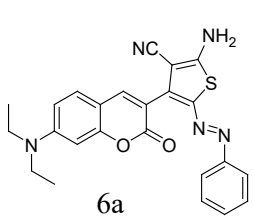

6a

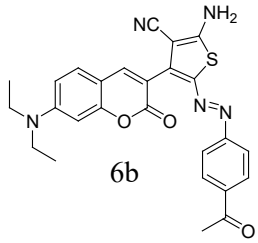

6b

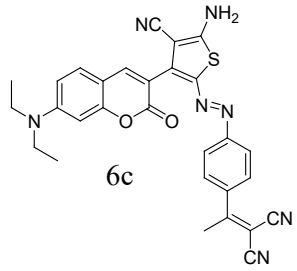

6c

To create visual chemosensors that can sense hydroxide and pH, two new thiazolylazo dyes (4 and 5) containing coumarin-thiophene moiety were created in this work. FT-IR, $^{1}H/^{13}C$ NMR, and HRMS methods were used to describe the obtained compounds. It was investigated how several solvents with varying polarities affected the dyes' absorption spectra. UV-Vis spectroscopy was used to examine how sensitive dyes are to acidic and basic media in organic and aqueous solutions. Furthermore, colorimetric modifications were discovered [2].

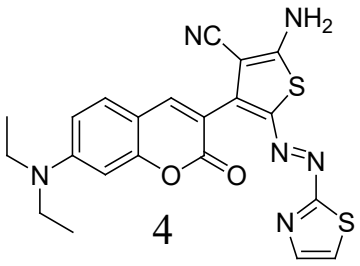

4

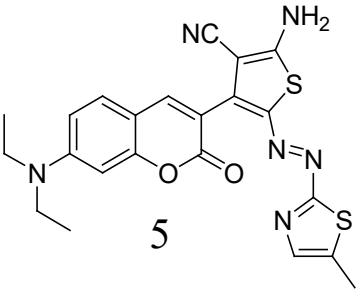

5

Chemical nerve agents are extremely poisonous substances because they can permanently inhibit the enzyme acetylcholinesterase (AChE) and increase the neurotransmitter acetylcholine (ACh) above normal levels in living things. This leads to the paralysis of the respiratory system, the immobilization of the muscles, and the eventual death of living things. Chemical nerve agents which have frequently been used in deadly terrorist attacks, are therefore used as Chemical Warfare Agents (CWAs). Due of their comparable mobility and reduced toxicity, diethylchlorophosphate (DCP) is frequently used as a substitute for sarin nerve agents. The development and design of DATC for the selective detection of sarin surrogate diethylchlorophosphate (DCP) in solution and gas phases, respectively, has been completed. In the presence of DCP, a ratiometric shift and a yellow to colorless conversion are observed in the UV-visible absorption spectrum. The excited state due to intramolecular proton transfer process (ESIPT) in DATC causes the observation of switch-on fluorescence at 480 nm [20].

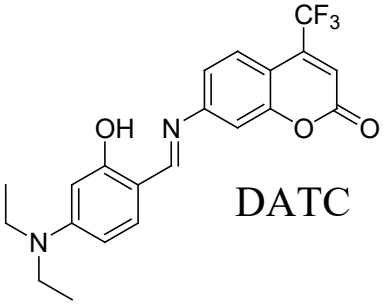

DATC

In this study, It was reported the identification of a new fluorescent imaging probe (XCYC-3) generated from coumarin that may be used to detect Aβ plaques both in vitro and in vivo. In contrast to Aβ monomers, this probe exhibits stronger fluorescence amplification to Aβ aggregates, and transgenic mice's brain slices can clearly stain Aβ plaques with a high

signal-to-noise ratio. The in vivo tests, in particular, show that XCYC-3 is a promising fluorescent probe for identifying cerebral Aβ plaques in animal models. Namely, one of the main clinical features of Alzheimer's disease (AD) is senile plaques, which are primarily composed of the protein Amyloid-β (Aβ). XCYC-3 can be used for Aβ recognition [21].

XCYC-3

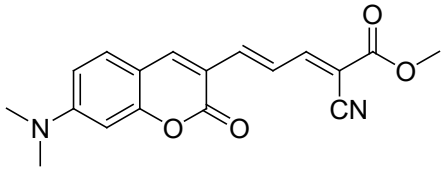

Hypochlorous acid (HClO), an important reactive oxygen species (ROS), is very important for the human immune system and its task is to maintain the normal functions of organisms. Intracellular redox balance is regulated by HClO produced from mitochondria. However, abnormal HCIO levels are linked to cancer, neurological damage and immune system problems. In conclusion, rapid and accurate monitoring of HCIO in mitochondria is crucial for early diagnosis of various diseases. Therefore, a mitochondrial-targeted HDCl probe, a hybrid of coumarin, quaternized pyridine and N,N-dimethylthiocarbamate, was developed to detect HClO in living cells. Very low detection limit of 2.8 nM for HClO in phosphate buffer solution (PBS). and with its ultra-fast (5 s) response characteristics, the HDCl probe exhibits great sensitivity, good selectivity and triggers a significantly increased fluorescence signal at 641 nm [22].

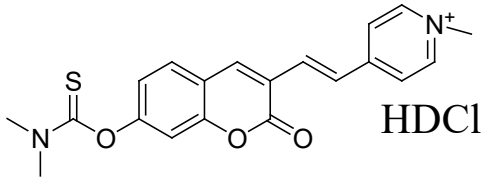

A phenylmethane dye with mild alkalinity known as neutral red (NR) is frequently used in manufacturing and daily life as a redox indicator, biological stain and acid-base indicator. Although the use of dyes has greatly increased economic prosperity and improved human life, it has also had a substantial negative impact on the environment, especially with relation to dye wastewater. The health of people and the environment are seriously threatened by dye wastewater. A fluorescent probe was synthesized for the detection of neutral red by using monoaldehyde-3-acetylcoumarin based on the Fluorescence resonance energy transfer (FRET) principle by Yi et

al. The probe has a linear range of 0-30 μM and a detection limit of 8.68 μM and is noted to be highly selective for neutral red [23].

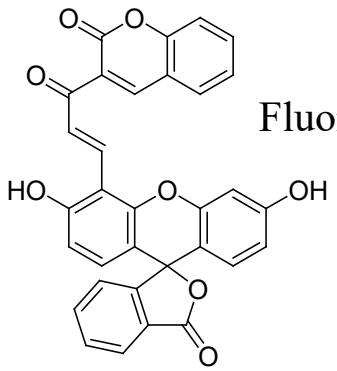

Fluorescent probe

The role of mitochondrial Ca^{2+} in various pathological circumstances can be studied with the aid of inhibitors of the mitochondrial calcium uniporter (MCU). This study introduces RuOCou, a novel fluorogenic MCU inhibitor. This substance is a fluorescent axial coumarin carboxylate ligand-containing version of the well-known MCU inhibitor Ru265. A possible theranostic MCU inhibitor, this fluorogenic prodrug could be used to treat human diseases linked to MCU activity [24].

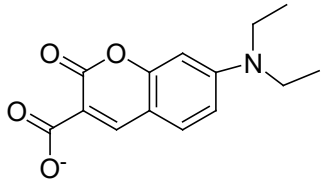

Coumarin carboxylate ligand use in MCU inhibitor

REFERENCES

1. N. Ahmed, W. Zareen, Z. Shafiq, S. F. de Alcˆantara Morais, M. Khalid, A. A. Carmo Braga, K. S. Munawar, Y. Yong. 2023. A coumarin based Schiff Base: An effective colorimetric sensor for selective detection of F^- ion in real samples and DFT studies. Spectrochim. Acta A Mol. Biomol. Spectrosc. 286, 121964-121977. https://doi.org/10.1016/j.saa.2022.121964

2. M. Yahya, R. Metin, B. Aydıner, N. Seferoğlu, Z. Seferoğlu. 2023. The syntheses, photophysical properties and pH−sensitive studies of heterocyclic azo dyes bearing coumarin–thiophene–thiazole. Anal Sci . 1-14. https://doi.org/10.1007/s44211-023-00281-0.

3. M. Rajasekar, V. Ranjitha, K. Rajasekar. 2023. Recent advances in Fluorescent-based cation sensors for biomedical applications. Results Chem. 5, 100850-100880. https://doi.org/10.1016/j.rechem.2023.100850.

4. H. Roohi, T. Pouryahya. 2023. TD-DFT study of the excited state intramolecular proton transfer (ESIPT) mechanism and photophysical properties in coumarin–benzothiazole derivatives: substitution and solvent effects. Mol. Syst. Des. Eng. 1-19. https://doi.org/10.1039/d2me00263a.

5. D. Ravichandran, M. Ranjani, G. Prabu Sankar, R. Shankar, M. Karthi, S. Selvakumar, R. Prabhakaran. 2023. Coumarin-Picolinohydrazone derived Schiffbase as fluorescent sensor(OFF-ON) for detection of Al^{3+} ion: Synthesis, Spectral and theoretical studies. J. Mol. Struct. 1273, 134329-134338. https://doi.org/10.1016/j.molstruc.2022.134329.

6. G. Yang, P. Li, Y. Han, L. Tang, Y. Liu, H. Xin, K.N. Wang, S. Zhao, Z. Liu, D. Cao. 2023. A coumarin hydrazide Schiff base fluorescent probe for sensitively sensing Al^{3+} in living cells. Mater. Chem. Phys. 295, 127145-127150. https://doi.org/10.1016/j.matchemphys.2022.127145.

7. D. Singh, S. Tomar, S. Sing, G. Chaudhary, A. P. Singh, R. Gupta. 2023. A fluorescent pH switch probe for the 'turn-on' dual-channel discriminative detection of magnesium and zinc ions. J. Photochem. Photobiol. A: Chem.435, 114334-114347. https://doi.org/10.1016/j.jphotochem.2022.114334.

8. J. Shi, M. Wang, X. Pang, Y. Liu, W. Liu, Y. Huo, F. Shen, S. Li, L. Zhao, D. Cao. 2023. highly sensitive coumarin-based fluorescent probe for visual detection of Cu2C in aqueous solution and its bioimaging in living cells. J. Mol. Struct.in press. https://doi.org/10.1016/j.molstruc.2023.135062.

9. S. Gond, P. Yadav, A.K. Singh, V.P. Singh. 2023. A novel 3-acetyl coumarin based AIE luminophore for colorimetric recognition of Cu^{2+} and F^-ions. J. Mol. Struct. 1273, 134317-134329. https://doi.org/10.1016/j.molstruc.2022.134317.

10. J. Zhao, H. Xu, L. Qin, Y. Hu, C. Lü, Y. An. 2023. A 1,3,4-thiadiazole functionalized Schiff base based fluorescence enhancement and colorimetric probe for detection of Cu (II) ion and its potential applications. Chem. Phys.

565, 111740-111749. https://doi.org/10.1016/j.chemphys.2022.111740.

11. X. Liu, R. Gao, L. Han, C. Kan, J. Xu. 2023. A smartphone readout device for portable and sensitive estimation of Hg^{2+} via coumarin-modified paper. Talanta. 252, 123849-123858. https://doi.org/10.1016/j.talanta.2022.123849.

12. H. Li, J. Li, Z. Pan, T. Zheng, Y. Song, J. Zhang, Z. Xiao. 2023. Highly selective and sensitive detection of Hg^{2+} by a novel fluorescent probe with dual recognition sites. Spectrochim. Acta A Mol. Biomol. Spectrosc. 291, 122379-122393. https://doi.org/10.1016/j.saa.2023.122379.

13. X. Wang, Z. Meng, X. Tian, J. Kou, K. Xu, Z. Wang, Y. Yang. 2023. A novel coumarin derivative-grafted dialdehyde cellulose-based fluorescent sensor for selective and sensitive detection of Fe^{3+}. Spectrochim. Acta A Mol. Biomol. Spectrosc. 292, 122378-122394. https://doi.org/10.1016/j.saa.2023.122378.

14. B. R. Swain, R. Satapathy. 2023. Development of coumarin derivatives as fluoride ion sensor. Tetrahedron. In press. https://doi.org/10.1016/j.tet.2023.133310.

15. W. Pan, L. Han, X. Cao, S. Shen, X. Pang, Y. Zhu. 2023. Dual-response near-infrared fluorescent probe for detecting cyanide and mitochondrial viscosity and its application in bioimaging. Food Chem. 407, 135163-135171. https://doi.org/10.1016/j.foodchem.2022.135163.

16. R. Manivannan, Y. A. Son. 2023. Blue light emitting fluorophore for the effective detection of cyanide ion and electronic test kit development for real time measurement. Dyes Pigm. 210, 110941-110950. https://doi.org/10.1016/j.dyepig.2022.110941.

17. X. Tian, M. Li, Y. Zhang, S. Gong, X. Wang, Z. Wang, S. Wang. 2023. A coumarin-based fluorescent probe for hydrazine detection and its applications in real water samples and living cells. J. Photochem. Photobiol. A: Chem.437, 114467-114474. https://doi.org/10.1016/j.jphotochem.2022.114467.

18. J. Kou, Z. Meng, X. Wang, Z. Wang, Y. Yang. 2023. Coumarin functionalized cellulose-based fluorescent probe for detection of hydrazine and its applications in environmental analysis. React. Funct. Polym. 182, 105453-105462. https://doi.org/10.1016/j.reactfunctpolym.2022.105453.

19. M. Yahya, N. Seferoglu, G. Kaplan, Y. Nural, A. Barsella, Z. Seferoglu. 2023. Synthesis, nonlinear optical properties, photophysical, and theoretical studies of azo dye bearing coumarin-thiophene. J. Mol. Struct. 1273, 134257-134268. https://doi.org/10.1016/j.molstruc.2022.134257.

20. M. Mahato, S. Ahamed, N. Tohora, T. Sultana, S. Ghanta, S.K. Das. 2023. A Coumarin151 derived ratiomteric and turn on chemosensor for rapid detection of sarin surrogate. Microchem. J. 185, 108240-108247. https://doi.org/10.1016/j.microc.2022.108240.

21. Y. Cao, X, Liu, J. Zhang, Z. Liu, Y. Fu, D. Zhang, M. Zheng, H. Zhang, M.H. Xu. 2023. Design of a Coumarin-Based Fluorescent Probe for Efficient In

Vivo Imaging of Amyloid−β Plaques. ACS Chem. Neurosci.1-10. https://doi.org/10.1021/acschemneuro.2c00468.

22. Y. Huo, Y. Ji, D. Chen, S. Pu. 2023. Fast responding of mitochondrial HClO using a coumarin-based fluorescent probe in living cells and zebrafish. Dyes Pigm. 209, 110940-110947. https://doi.org/10.1016/j.dyepig.2022.110940.

23. C. Yi, F. Yan, X. Wei, Y. Wu, X. Wang, J. Xu. 2023. Design and characterization of high performance fluorescent probe for neutral red based on fluorescein monoaldol-3-acetyl coumarin. J. Photochem. Photobiol. A: Chem. 439, 114592-114599. https://doi.org/10.1016/j.jphotochem.2023.114592.

24. Z. Huang, S. N. MacMillan, J. J. Wilson. 2023. A Fluorogenic Inhibitor of the Mitochondrial Calcium Uniporter. Angew. Chem. 62, e202214920-e202214924. https://doi.org/10.1002/anie.202214920.

CHAPTER 2

CORROSION AS A METAL DISEASE (EXAMPLE STUDY: USE OF INHIBITORS TO PROTECT BRASS FROM CORROSION IN ACIDIC ENVIRONMENT)

Gülden ASAN[1]

1 Hitit University, Vocational School of Technical Sciences, guldenasan@hitit.edu.tr, Çorum,Türkiye ORCID: 0000-0002-6075-159X

1. INTRODUCTION

Corrosion can be defined as the chemical and electrochemical change of substances, especially metals and alloys, due to the effect of the environment, or the breakdown or physical dissolution of the substance without being dependent on mechanical factors. All metals and alloys are unstable in the earth's atmosphere and they want to corrode and return to their more stable forms (Hansson, 2011). Therefore, corrosion is a natural and spontaneous reaction. Studies are carried out to prevent this reaction in the industry. Because corrosion creates a great burden on the economies of countries (Javaherdashti, 2000). The loss of the corroded metal both disrupts the production process and harms the environment and worker health with chemicals spilled into the environment. Scientists and engineers make great efforts to solve this problem (Hou et al., 2017). In order to compare the corrosion resistance of metals and alloys with each other, the corrosion rate of each should be given quantitatively. The reduction in mass can be tracked to indicate a material's resistance to corrosion. It is known that corrosion occurs electrochemically. The amount of metal dissolved in a corrosion event is directly proportional to the amount of current flowing. Electrochemical methods for measuring the corrosion rate were generally introduced after the 1950s (Üneri, 1969). The measurement of the corrosion rate was based on the determination of mass reduction until recently. The biggest disadvantage of this method was that it took a long time to determine the corrosion rate and it gave an average rate as a result. Electrochemical methods, on the other hand, give much faster and more reliable results in determining the corrosion rate. The galvanostatic method is one of the first methods to measure the corrosion rate. In order to obtain an anodic or cathodic polarization curve with this method, a certain current is applied to these electrodes by changing the resistance R by connecting the metal as an anode, and the resulting potential is measured with a voltmeter. In the potentiostatic method, polarization data is obtained by measuring the direction and amount of the current after the potential of the metal is adjusted. In the mixed potential theory, three basic methods are used to determine the corrosion rate (Üneri, 2011). These:

1- Tafel extrapolation method: In this method, the anodic and cathodic Tafel curves for the corroded metal are determined experimentally and the linear parts of them are extended and the corrosion rate ($I_{cor.}$) and corrosion potential ($E_{cor.}$) for that system are determined from the cut-off points.

2- The method of extrapolation of the cathodic polarization curve to the corrosion potential: in this method, the polarization curve is obtained only for the cathodic branch. The method of determining the corrosion rate with the help of cathodic polarization curves was proposed by Stern in 1955.

3- Linear polarization method or polarization resistance method: it has been widely used recently to determine the corrosion rate. This method was first proposed by Simmons in 1955 and by Skold and Larson in 1957. The theoretical foundations of the method were given by Stern and Geary in 1957. The method is applied according to both alternating current and direct current techniques. This method has many different application areas. Some; in determining the corrosion rate of pipes buried underground, in determining the corrosion rate of metals used in surgeries to living things, and in determining the rate of corrosion under severe nuclear radiations, etc. available (Üneri, 2011).

2. CORROSION TYPES

The main types of corrosion can be given as follows:

1- General corrosion

2- Galvanic or metal couple corrosion

3- Crevice corrosion

4- Pitting corrosion

5- Intergranular corrosion

6- Selective corrosion (parting)

7- Erosion corrosion

8- Stress Corrosion Cracking

These types of corrosion occur more or less together (Üneri, 2011).

2.1. General Corrosion

With the same chemical or electrochemical reaction across a large or entire surface, the metal surface wears out uniformly on all sides. General corrosion can also be called homogeneous dispersion corrosion. General corrosion protection methods include painting, use of inhibitors and cathodic protection (Üneri, 2011). Picture 1 shows an example of general corrosion.

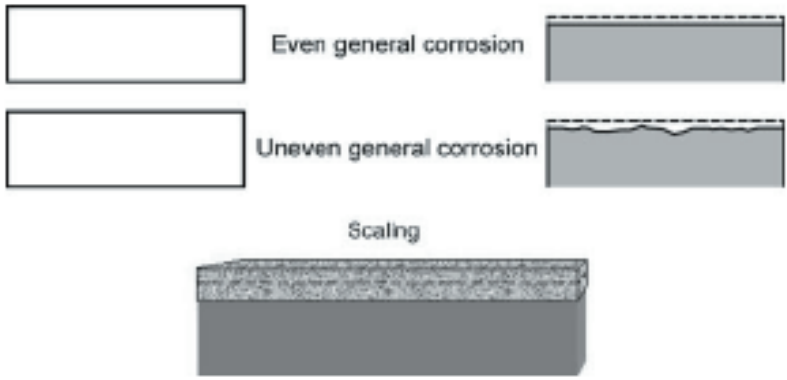

Picture 1: *Example of general corrosion (Zehra, Mobin, & Aslam, 2022)*

2.2. Galvanic or Metal Couple Corrosion

If two dissimilar metals are immersed in a corrosive or conductive medium, a potential difference usually arises between them. When two such metals are connected to each other by a conductor, electrons flow from one to the other under this potential difference. The corrosion of the metal, which has low resistance to corrosion, increases compared to the unbonded state. The more durable metal, on the other hand, reduces corrosion compared to the unbound state. The metal that is less resistant to corrosion becomes the anode, and the more resistant metal becomes the cathode. In this type of corrosion, the cathode either does not corrode at all or corrodes very little (Üneri, 2011). Picture 2 shows an example of galvanic corrosion.

Picture 2: *Example of Galvanic Corrosion (Zehra, Mobin, & Aslam, 2022)*

2.3. Crevice Corrosion

In most cases, severe local corrosion occurs in cracks, crevices, or covered areas on the metal surface in a corrosive environment. This type

of corrosion generally occurs in narrow areas with stagnant solutions and gasket surfaces, surface deposits in the gaps under the bolt and rivet heads (Üneri, 2011). Picture 3 shows an example of crevice corrosion.

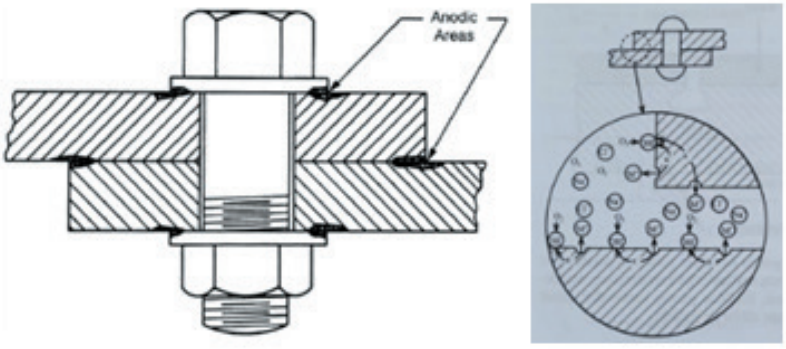

Picture 3: *Example of Galvanic Corrosion (Zehra, Mobin, & Aslam, 2022; Üneri, 2011)*

2.4. Pitting Corrosion

If holes and pits occur on a metal surface as a result of corrosion, this type of corrosion is called pitting corrosion. These pits can sometimes be far from each other and sometimes very close. If they are too close to each other, they give the appearance of a rough surface. In general, the diameters of the pits are equal to or less than the depth of the pits. Pitting corrosion is the most destructive and hidden type of corrosion (Üneri, 2011). Picture 4 shows an example of pitting corrosion.

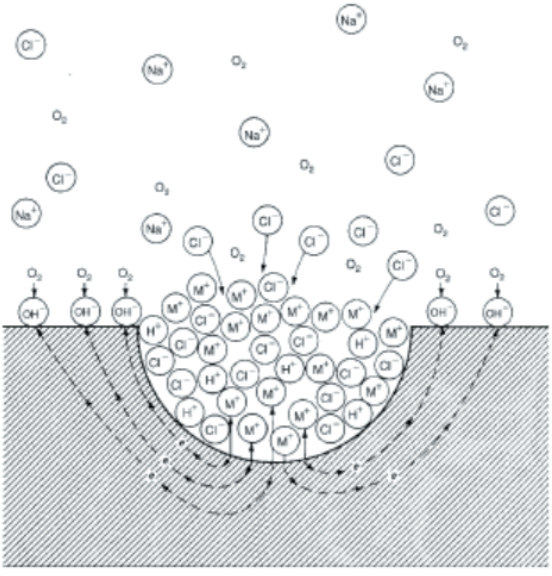

Picture 4: *Example of Pitting Corrosion (Zehra, Mobin, & Aslam, 2022)*

2.5. Intergranular Corrosion

If a metal or alloy is corroded, the wear is usually the same all over the surface. But under certain conditions the interfaces of the grains are very prone to reactions. As a result, intergranular corrosion occurs. The alloy breaks down or loses its strength. The most distinctive feature of intergranular corrosion is that although the mass reduction is very small, the corrosion rate is very high in the regions of the crystal lattice boundaries (Üneri, 2011). Picture 5 shows an example of intergranular corrosion.

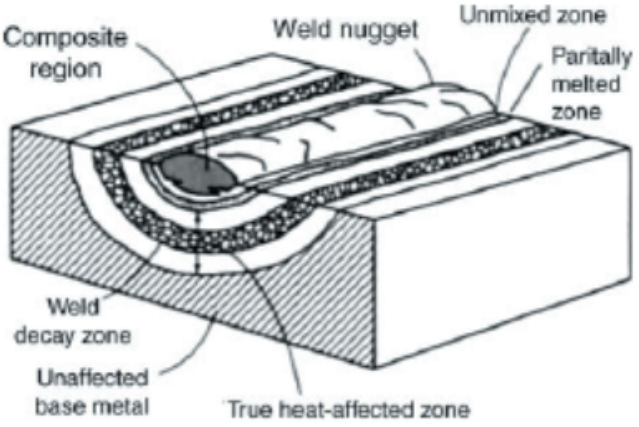

Picture 5: *Example of Intergranular Corrosion (Zehra, Mobin, & Aslam, 2022)*

2.6. Selective corrosion (parting)

The wear of a component of an alloy by corrosion is called selective corrosion or selective corrosion. The best-known example of this type of corrosion is the removal of zinc from brass by corrosion. This phenomenon is called disinfection. The same phenomenon is seen in other alloys. Aluminium, iron, cobalt, chromium or other elements are selectively removed from the alloy. It is also called partial wear by metallurgists (Üneri, 2011). Picture 6 shows an example of selective corrosion.

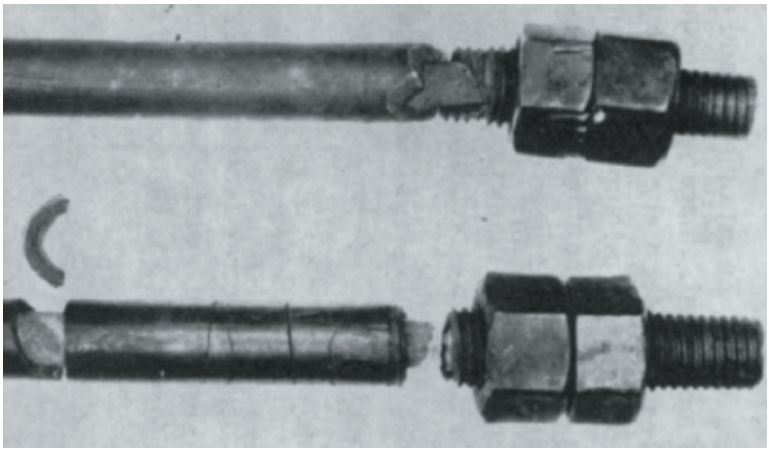

Picture 6: *Example of Selective Corrosion (Zehra, Mobin, & Aslam, 2022)*

2.7. Erosion Corrosion

The increase in the rate of wear or fragmentation of the metal due to the relative movement between a metal and the corrosive medium is called erosion corrosion. Usually this movement is quite rapid and there is a mechanical wear or abrasion effect. It dissolves away from the metal surface as metal ions or forms solid corrosion products. These corrosion products are mechanically removed from the metal surface. The appearance of erosion corrosion is peculiar. Most metals or alloys are susceptible to erosion corrosion. The susceptibility of many to corrosion is due to a kind of film (passivity) formed on their surface. Examples of this are aluminum, lead and stainless steels. When these protective films are worn or damaged, metals and alloys rapidly erosion corrosion. Soft and easily damaged or mechanically weathered metals such as copper and lead are highly susceptible to erosion corrosion (Üneri, 2011). Picture 7 shows an example of erosion corrosion.

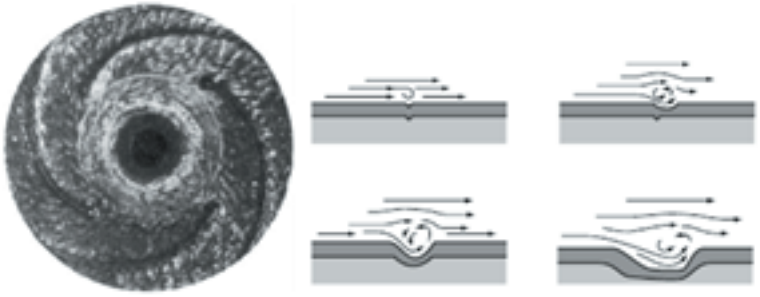

Picture 7: *Example of Erosion Corrosion (Zehra, Mobin, & Aslam, 2022)*

2.8. Stress Corrosion Cracking

Most of the machine parts and metal structures in a corrosive environment are under mechanical stress. For example, high pressure vessels, steam boilers, cylinder liners of internal combustion engines. Suppose a metal is corroded by the release of hydrogen and at the same time some parts are under tension. We think that the hydrogen entering the metal causes a crack in the regions where the stress is excessive and the corrosive solution affects the metal in these cracks. When a crack occurs on the metal surface, the inside of the crack may behave completely differently from the surface of the metal. For example, while the metal surface is covered with oxide, there is no oxide layer on the metal surface in the crack. Metal dissolution occurs mostly in the crack, and hydrogen release occurs on the metal surface. Stress corrosion cracking; It is the result of the joint effect of external or internal tensile forces and local corrosion. Stress corrosion cracking is very rare in pure metals, and in some cases it does not occur at all. However, stress corrosion cracking is very common in alloys (Üneri, 2011). Picture 8 shows an example of stress corrosion cracking.

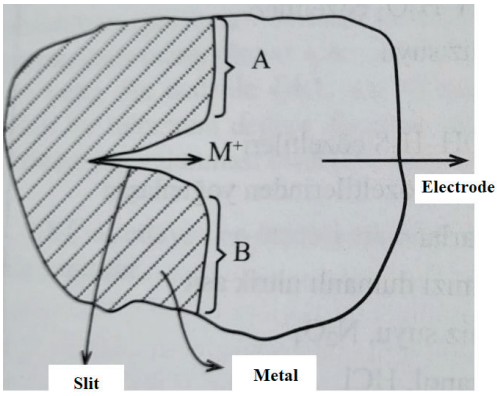

Picture 8: *Example of Stress Corrosion Cracking (Üneri, 2011)*

3. THE CONCEPT OF PASSIVITY IN CORROSION

When the potential of a metal is increased above a critical size by applying an external anodic potential or adding an oxidizer to the environment, if the corrosion rate decreases significantly, the metal is said to be passivation. Passivity can also be defined simply as the loss of a metal's ability to react chemically under certain environmental conditions. Although passivity seems to be an opportunity to reduce corrosion from an engineering point of view, attention should be paid to the possibility of transitioning from a passive state to an active state. Passivity has been widely studied since it was first observed in the 1840s because of its unique

properties and importance for engineering applications. Passivity is based on a thin film formed on the metal surface. The film is estimated to be 30 Ångström or less thick. It is estimated that the film contains a significant amount of water of hydration, is very thin and sensitive, and changes when it separates from the metal surface or when the metal is separated from the corrosive environment. Thus, the nature of passive film and thus the nature of passivity has not yet been fully elucidated. Recent electrochemical investigations have significantly increased the knowledge in the field of corrosion and passivity. It has been understood that this film consists of metal oxides and hydroxides. Not all metals show passivity, but there are many alloys that show passivity in their solutions. Iron, chromium, nickel, titanium and their alloys, such as stainless steels, are the most important of the passivating metals (Üneri, 2011).

4. CORROSION PROTECTION METHODS

Corrosion protection methods; material selection, changing the medium (reducing the temperature, reducing the velocity, removing oxygen or oxidants, changing the concentration), inhibitors, design, pretreatment of metal surfaces, coatings, anodic protection, cathodic protection.

Let's take a look at these methods in order:

4.1. Material Selection

The most common way to prevent corrosion is to choose metals and alloys suitable for the area of use. There are some general rules that can be applied and generally true about the corrosion resistance of metals and their alloys. Nickel, copper and their alloys are often used for reducing or non-oxidizing media such as acids and aqueous solutions. For oxidizing conditions, alloys containing chromium are used. Titanium and its alloys have the best corrosion resistance for very strong oxidizing conditions. In general, the corrosion resistance of a pure metal is better than that of a metal with additives or small amounts of other elements. But pure metals are often expensive, too soft and weak. For this reason, pure metals are generally used only in some special places. A good example of a pure metal is aluminum, and aluminum more than 99.5% pure isn't expensive either. Commercial pure aluminum is used in the hydrogen peroxide industry. Because hydrogen peroxide breaks down if other elements are found. If it is not pure enough, there will be local corrosion of aluminum utensils due to decomposition of the iron contained in the aluminum. Another pure metal example is arc fused zirconium. Zirconium obtained in this way is more resistant to corrosion than zirconium melted by induction. When choosing a material, it is desirable that the metal or alloy be cheaply manufactured and resistant to corrosion (Üneri, 2011).

4.2. Changing The Medium

Changing the medium affects corrosion. Lowering the temperature generally causes a significant reduction in the corrosion rate. Reducing the rate is often a useful method to control corrosion. Generally, speed increases corrosion, but there are some exceptions. Passivating metals and alloys, such as stainless steel, generally show greater corrosion resistance in active environments than in stationary environments. Movements that are too fast should always be avoided because they can create erosion corrosion. Removal of oxygen or oxidants is an ancient corrosion control technique. The water sent to the boiling pots was passed through a large amount of steel, removing the air. Today, in modern practice, air can be deoxygenated using vacuum treatment, inert gas spraying or oxygen-consuming substances. The effect of the corrosive substance concentration on the corrosion resistance will naturally decrease if the corrosive substance concentration can be lowered in the environment (Üneri, 2011).

4.3. Inhibitors

The effect of inhibitors on corrosion resistance: An inhibitor is a chemical substance that, when added in a small amount to a medium, effectively controls, reduces or prevents the reaction of a metal with its environment. Inhibitors can also be thought of as retarding catalysts. A wide variety of types and compositions of inhibitors have been found. Inhibitors slow the rate of corrosion by reducing the rates of either anode reactions or cathode reactions, or both.

An anodic inhibitor increases the anodic polarization, thus shifting the corrosion potential in the positive direction. Cathodic inhibitors change the corrosion potential to negative. Mixed inhibitors have less effect on the potency and the direction of the potential change is determined by the relative magnitudes of the anodic and cathodic effects. Inhibitors are added to many systems. Such as metal cleaning baths, cooling systems, various refinery units, oil pipelines, chemical processes, steam generators, balancing tanks, oil and gas production and storage areas. In general, anodic inhibitors are anions. Anions migrate towards the anode sites. Often, they passivate the metal under the influence of oxygen. Anodic inhibitors are generally inorganic substances; Many inorganic inhibitors such as orthophosphate, silicate, nitrite and chromate and organic benzoate. Non-oxidizing inhibitors are only effective with the contribution of dissolved oxygen. Although anodic inhibitors are very effective and widely used, they have some undesirable properties. When the amount of inhibitor is not sufficient or gradually decreases, it is encountered that the entire anode surface cannot be covered. As a result, small anode and large cathode pairs occur. This situation is very dangerous and pitting corrosion is observed. For this

reason, anodic inhibitors are often referred to as “dangerous inhibitors”.

Inhibitors that slow down the corrosion rate by acting on the cathodic reaction, such as hydrogen reduction in acidic environments and oxygen reduction in neutral or nearly neutral environments, are called cathodic inhibitors. Generally, these inhibitors are cations. They migrate to the cathode regions. They precipitate chemically or electrochemically and insulate the surface. Cathodic inhibitors are safe inhibitors as they do not cause localized corrosion such as pitting corrosion and thus do not increase corrosion. Even if they are found in insufficient amount in the environment, they do not pose a danger. Although these inhibitors are known to be less effective than anodic inhibitors in protecting metal against corrosion, they are widely used in practice because they do not show the danger of increasing corrosion.

Adsorption inhibitors make up the largest class of inhibitors. In general, these inhibitors are organic compounds. By adsorbing on the metal surface, they reduce the metal dissolution and reduction reactions on the metal surface. These types of inhibitors generally have a dual effect, as they are adsorbed on the entire surface of the metal. That is, they inhibit both anodic and cathodic events. But the effects are often not the same (Üneri, 2011).

4.4. Design

The design of a material is important for its corrosion resistance. It should be noted how much the thickness can be reduced in the design of pipes, tanks and other components, as the corroded material decreases in thickness over time. In general, 2 times the thickness required for the desired life of a material is taken. If the life of a structure is supposed to be ten years and the corrosion rate of this structure is estimated to be 32 mm in 10 years, the structure should be made with a thickness of 64 mm. In addition, the thickness of the material must comply with the mechanical requirements such as pressure, mass and stress. There are many rules for the most corrosion-resistant design of the structure. Some of them are as listed below.

Welding rather than rivets should be used in tanks and other containers. Riveted connections can cause crevice corrosion. Ease of emptying and cleaning should be considered in the design of tanks and other equipment. After the tank is emptied, the bottom of the tank should be inclined towards the drain hole so that the liquid does not collect at the bottom. In Picture 9, wrong designs and the right design to be preferred are given.

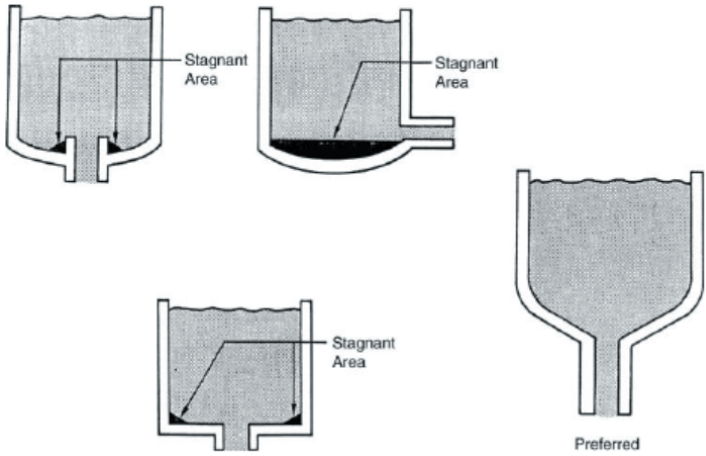

Picture 9. *Three different designs with stagnant areas and the correct design without stagnant areas are given as example (Zehra, Mobin, & Aslam, 2022).*

Parts of a system that are expected to corrode quickly should be made in such a way that they can be easily replaced. Excessive concentration and mechanical stresses should be avoided in a corrosive environment. Mechanical and residual stress cause crevice corrosion. This rule should be followed especially when using materials that are prone to stress corrosion cracking, such as stainless steel and brass. Electrical contact between dissimilar metals should be avoided to prevent galvanic corrosion. If possible, the same material should be used in all parts of the building or various metals should be insulated from each other. Sharp bends in piping systems should be avoided. Rapid erosion occurs in places of sharp bends and other fluid flow rates. This is especially important where materials prone to erosion corrosion such as lead, copper and their alloys are used. Round bends are also better and easier to paint and cover. Hot spots should be avoided during heat transfer processes. Heat exchangers and other heat carrier arrangements should be made in such a way that the temperature change is the same everywhere. The uneven distribution of temperature causes local heating and the corrosion rate increases. In addition, hot spots introduce stresses that will cause stress corrosion cracking. A design should be used to prevent the ingress of oxygen. The reduction of oxygen during corrosion is one of the most common cathodic reactions. Corrosion can often be reduced or prevented if oxygen is removed. The most general rule for design is to avoid heterogeneity. Dissimilar metals, vapor fields, uneven heat, inhomogeneous voltage distributions and other differences in a system cause corrosion damage. As a result, an effort should be made to provide the same conditions as possible in the whole system while designing (Üneri, 2011).

4.5. Pretreatment of Metal Surfaces

Before applying various types of coatings on metal surfaces, metal surfaces must be carefully cleaned from dirt such as oil and salt, oxide layers and oxides such as rust. In addition, the surface may require a polishing to be suitable for the process in question. This pre-treatment is very important especially in electroplating and enamel processes. Pretreatment is usually done for two purposes. The primary purpose is to remove organic materials such as oil and grease. The other purpose is to remove inorganic materials such as oxide layer, crust, rust and other corrosion products and to give the surface a suitable shine. Both processes are done in a variety of ways, depending on the situation, and can be repeated several times. All coating methods generally require washing and degreasing before pickling and sometimes sand cleaning. Mineral oils and greases (hydrocarbons such as petrolatum, etc.) are removed with organic solvents. For fatty acids oils such as lanolin and some waxes (waxes), saponification of fatty acid esters in the base solution is preferred. In order to understand that the metal surface is freed from oil, it is understood that the surface is completely wet with water and that it does not leave any stains after the water is removed (Üneri, 2011).

4.6. Coatings

It provides a sufficient barrier between the metal and its environment by coating the metallic and inorganic materials on the metal surface in a very thin way. The primary task of the metallic coating is to provide an effective barrier. Metal plating is done electrolytically, by flame spraying, cladding, hot dipping and steam precipitation. The inorganic coating is formed by spraying, diffusion or chemical conversion. Sputtering is usually applied by high temperature firing and firing. A complete barrier must be provided either way. Porosity or other defects cause rapid local corrosion due to the metal-pair effect. Coatings; It can be classified as metallic coatings, inorganic coatings, organic coatings and chromating (coatings made by chemical conversion). Metallic coatings can be electroplated. The metal to be protected for coating is hung as the cathode and connected to the direct current source with the help of a suitable electrode. The nature of the coating; It depends on various factors including temperature, current density, time and composition of the electrolysis bath. These variables can be adjusted so that the coating is thick (eg 0.5 mm) or thin (eg 10-4 - 10-5 mm), shiny or opaque, soft (lead) or hard (chrome), brittle or stretchable. Hard coating is used to fight against erosion corrosion. Covering; it may be a single metal, several layers of metal, or in the form of an alloy (eg brass). If coating is to be done with a more noble metal than the metal to be coated, the coating must be very tight. If pores or scratches occur, dangerous small

anode-large cathode pairs are formed and pitting corrosion occurs. Coating with a more noble metal than the metal to be coated is also called “cathodic coating”. The most important example of this type of coating is electrolytic nickel coating on steel. In some cases, steel is first plated with copper. But with the improved nickel plating baths, it has been possible to make a tight nickel plating directly on the steel without the need for copper plating. This type of coating is more resistant to corrosion than copper-nickel layers, especially in the industrial atmosphere (Üneri, 2011).

4.7. Anodic Protection

This technique has been developed using the principles of electrode kinetics and is explained by theories of electrochemical kinetics and current potential curves. If an anodic current is applied to a metal, the rate of dissolution of the metal increases. In general, this is the case of metals that cannot show active-passive transition. If a carefully controlled anodic current is applied to metals that show active-passive transition, such as iron, nickel, chromium, titanium and their alloys, the metals become passivated after a certain potential and the rate of dissolution of the metal decreases. It is only possible to protect a metal anodicly using a potentiostat. The potentiostats consist of an electrical source that gives current to the electrolysis circuit on the one hand, and a component that regulates the current source to regulate the current intensity required to keep the potential of a metal in the electrolysis cell at a predetermined value. The potentiostat has three ends. Of these, the positive end is connected to the structure, the negative end is connected to the cathode (platinum or platinum coated), and the reference lead is connected to the comparison electrode (reference electrode, for example, calomel electrode). The potentiostat keeps the potential between the structure and the comparator electrode constant while operating. The potential suitable for shielding is determined by electrochemical measurements (Üneri, 2011).

4.8. Cathodic Protection

This technique is based on the theory of electrochemical corrosion. If each open area on the metal surface collects the given current, the metal will not corrode. This is exactly what cathodic protection does. Direct current is applied from an external source to flow over the entire surface of the structure. If the amount of current is adjusted appropriately, the corrosion current discharged from all anodic areas on the structure will overcome and a net current will flow from these points to the structure surface. Then the whole surface will be cathodic and the cathodic protection will be complete. Cathodic protection; pipelines, ships, ports, etc. It is applied to structures that are buried or immersed in electrolyte environments such

as soil and water.

Cathodic protection is applied by two methods. The first of these is by applying external current and the second is the galvanic anode (sacrificial anode). In cathodic protection by applying an external current, the structure is electrically negative, and as a result, the structure behaves like a cathode. The second electrode is electrically positive and completes the circuit as the auxiliary anode. Current is carried by electrons in the external circuit. Electrolyte solutions do not contain free electrons. Therefore, the current must be carried by positively and negatively charged ions. The current flowing through the electrolyte solution (soil and sea water also act as an electrolyte) equal to but in the opposite direction to that passing through the external circuit occurs as a positive current, that is, as the current carried by the positively charged ions. Cathodic protection can only be applied when the structure to be protected and the auxiliary electrode are both in electronic and electrolytic contact state.

In cathodic protection with galvanic anode (sacrificial anode): If two dissimilar metals are electrically connected in an electrolyte solution, it can be observed with a voltmeter that current flows between the two metals due to the difference in the electrochemical potentials of these metals. The metal (noble) with a larger electropositive potential becomes the cathode and is protected from corrosion. The more electronegative (active) metal becomes the anode. The electric current passing between the two metals accelerates the dissolution (corrosion) of the anode. Thus it is sacrificed. Therefore, it must be renewed periodically. The flow of electric current flows towards the cathode with electrons in the external circuit, while in the corrosive electrolyte the current is carried by ions. The voltage of the galvanic anode / protected structure system (potential difference between anode and cathode) must be large enough to overcome the corrosion of the structure by the corrosion cells formed on the corroded structure surface. For this, active metals such as zinc, magnesium and aluminum are selected as anodic metals. The currents obtained even from these active anodes are limited to relatively small amounts. Therefore, cathodic protection with galvanic anodes (sacrificial anodes) can normally be applied where the amount of current required for protection is small (Üneri, 2011).

5. EXAMPLE STUDY: USE OF INHIBITORS TO PROTECT BRASS FROM CORROSION IN ACIDIC ENVIRONMENT

Brass; It is the general name of the yellow colored alloys obtained by adding zinc to copper. Brass alloy is preferred in the industry because of its corrosion resistance, very good thermal and electrical conductivity, easy

processing and relatively inexpensive (Gadow & Elabbasy, 2017). Due to its decorative appearance due to its yellow color, it finds use in decorative elements, architectural coatings, electrical fixtures, musical instruments, radiators, firearm cartridge casings, bullet capsules in the weapon industry, pipes, screws, and in different geometries such as rods, sheets, pipes. . In addition to finding a wide application area in the industry, brass is also frequently used in architecture and cultural objects. However, when exposed to a humid atmosphere, brass rusts by forming oxide layers. Corrosion protection plays an important role in reducing losses in economies, protecting cultural heritage and public safety (Ramdé, Rossi, & Bonou, 2016). In the most general sense, we can define corrosion as a destructive electrochemical attack on the metal by its environment (Cevallos-Morillo et al., 2021). When the corroded material becomes unable to function, it may cause the production to stop. When the chemicals contained in the broken part are dispersed to the environment, they not only cause environmental pollution, but more importantly, they may come to the employees and cause death or even serious injury. Occupational accidents can occur in many different sectors as a result of metal parts breaking off due to corrosion. For all these reasons, corrosion causes billions of dollars in economic loss, significant safety hazards and environmental pollution every year (Gülden Asan, 2021; Chaubey, Savita, Qurashi, Chauhan, & Quraishi, 2021; Kesavan, Gopiraman, & Sulochana, 2012). Different methods are used to protect metals from corrosion. These can be counted as changing the environment, use of alloy, appropriate design, surface coatings and use of anti-corrosion inhibitor. Inhibitors used in corrosion protection; can be divided into organic inhibitors and inorganic inhibitors. Inorganic inhibitors usually have either cathodic or anodic action. Since organic inhibitors have both cathodic and anodic effects, they are superior to inorganic inhibitors. We can also classify inhibitors according to the reactions they inhibit. These; They are anodic, cathodic or mixed inhibitors with both anodic and cathodic properties. Anodic inhibitors of anodic reactions, cathodic inhibitors; They are inhibitors that prevent or slow down the occurrence of cathodic reactions. Mixed inhibitors, as the name suggests, try to inhibit both cathodic and anodic reactions. Mixed inhibitors are also called adsorption inhibitors because they generally act by adhering to the surface. There are 3 different interactions between the adsorption inhibitors and the metal surface. Depending on the type of this interaction, chemical adsorption or physical adsorption takes place. Thirdly, inhibitor molecules can form a thin film layer on the metal surface by inhibiting the anodic and cathodic areas on the metal surface (Taghavikish, Dutta, & Choudhury, 2017). Since inorganic inhibitors are generally toxic, organic inhibitors are preferred as corrosion inhibitors. Inhibitors used in corrosion protection; can be divided into organic inhibitors and inorganic inhibitors. Corrosion protection forms of

inhibitors are generally adsorbed on the metal surface, forming a protective film layer, and interrupting the interaction of the medium and the metal surface. Heteroatoms such as nitrogen, sulfur and phosphorus that can donate electrons in organic inhibitors increase the corrosion inhibitory effectiveness (Abdallah, Al-Agez, & Fouda, 2009; ASAN, 2020; Chakravarthy, Mohana, & Pradeep Kumar, 2014). Because non-environmentally friendly inhibitors threaten the environment and human health with their toxic effects, they are not suitable for corrosion protection purposes. Therefore, the use of environmentally friendly inhibitors called green inhibitors has become widespread (Chevalier et al., 2014; El-Etre & Ali, 2017; Tan et al., 2021). These eco-friendly inhibitors, which are also used in corrosion protection, have found application since the mid-1900s. Generally, plant extracts were used in these studies. All kinds of parts of the plant, including stem, root bark, leaves, fruits, fruit peel, flowers, seeds and nuts, were used to obtain plant sap. Studies have shown that since the raw material is abundant, these inhibitors can be easily isolated and thus cost less. These obtained green inhibitors are used to protect various metals and metal alloys from corrosion (Al, Cu, Zn, brass etc.) (Ndukwe, 2022; Tan et al., 2021). In this study, the effect of environmentally friendly nicotinamide on the corrosion of brass in 0.1 M hydrochloric acid solution was investigated. The Tafel Polarization method, which is widely used, was used in corrosion measurements because it provides fast measurement and reliable results (G. Asan & Asan, 2020). It is not possible to escape from acidic environments in industry and the corrosive effect of acid is quite dangerous (Raja, Qureshi, Abdul Rahim, Osman, & Awang, 2013). For this reason, acidic medium was chosen in the study. Nicotinamide, on the other hand, has a high inhibitory activity because it has a cyclic structure containing heteroatoms such as nitrogen and oxygen. Nicotinamide, which is also a vitamin B3, was preferred in this study because it is an environmentally friendly corrosion inhibitor.

5.1. Materials and Methods

Electrochemical behavior of brass was investigated by taking alternating voltammogram of brass in 0.1 M hydrochloric acid medium. The corrosion rate was then measured by the Tafel Polarization method. Then, in order to determine the optimum concentration, 3 different nicotinamide concentrations were prepared and added to this solution. In order to determine which retention time is optimal for the added inhibitor concentration, this measurement was called the zero-minute measurement at the first moment the inhibitor was added. Corrosion rates were then measured at 15, 30, 45 and 60 minutes holding times. Corrosion rates were measured with Ivium Technologies De Regent 178 5611 HW Eindhoven model device.

A three-pronged balloon was used as a corrosion cell. Brass electrode as working electrode, platinum plate counter electrode and saturated calomel electrode as reference electrode were used. Before the measurements, the brass electrode with a surface area of 1 cm^2 and embedded in the resin was cleaned with sandpaper and washed with distilled water. The saturated calomel electrode was used by placing it in the lugin. Hydrochloric Acid solution was prepared from Merck brand 37 % Hydrochloric Acid solution. Nicotinamide solutions were also prepared from Sigma Aldrichin Nicotinamide. The molecular formula of Nicotinamide is given in Picture 10.

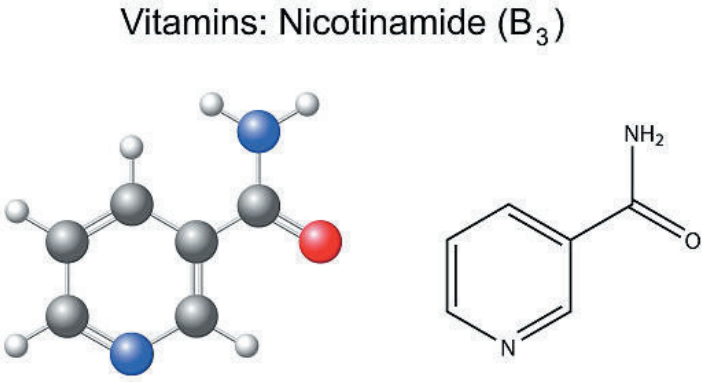

Picture 10. *Molecular formula of nicotinamide*

5.2. Results and Discussion

In order to determine the electrochemical behavior of brass in 0.1 M hydrochloric acid solution, a voltammogram alternating between -1.0 V and +0.2 V is taken and given in Figure 1. When Figure 1 is examined, two small anodic peaks originating from copper were observed between –0.5 V and -0.23 V in the forward potential scanning. When scanning was continued, after remaining passive until around 0.1 V, the current started to increase with the oxidation of copper and zinc by giving electrons. At +2.0 V the current reached about 25 mA. In the reverse potential scanning of brass, reduction peaks of Cu^{2+}, Cu^{+} and Zn^{2+} were observed.

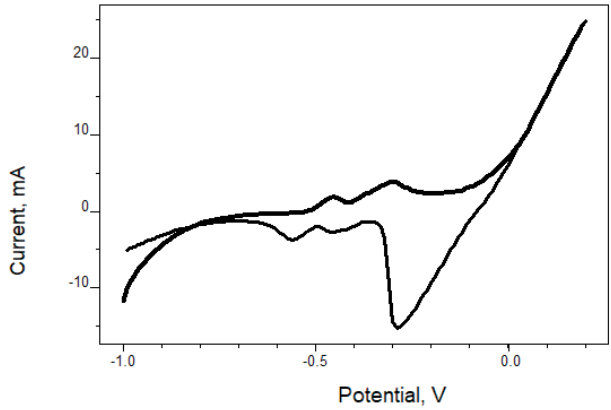

Figure 1. *Cyclic voltammogram (CV) of Brassin in 0.1 M Hydrochloric acid solution*

After observing the electrochemical behavior of brass in hydrochloric acid medium, the corrosion rate was measured by Tafel polarization method without adding nicotinamide. Then, the minute measurement was taken at the first moment when 500 ppm nicotinamide was prepared and added to the solution. Then, by adding 500 ppm nicotinamide, corrosion rates were measured in 4 different times (15, 30, 45 and 60 minutes), respectively. The % inhibitory activity was calculated from the measured corrosion rates. With the increase of the inhibitor retention time, it gained time to adhere to the nicotinamide brass surface and contributed to the formation of a protective layer (Ravichandran & Rajendran, 2005). It has also been seen in previous studies that increasing the holding time shifts the corrosion potential to positive and decreases the corrosion rate (Gülden Asan & Asan, 2020). The corrosion rates and calculated % inhibitor efficiencies at all these times are given in Table 1.

Table 1. *Corrosion rates and calculated % Inhibitor Efficiency values from the Tafel polarization curves given by Brass Electrode by adding 500 ppm nicotinamide to 0.1 M HCl solution at different holding times*

Concentration, ppm	Residence time, minute	E_{cor}, V	I_{cor}, (μA)	Corrosion Rate, mm/y	% Inhibitor Efficiency
0	0	-0.506	17.990	0.0589	---
500	0	-0.518	2.698	0.00883	85.0
	15	-0.503	2.009	0.00658	88.8
	30	-0.475	1.670	0.00546	90.7
	45	-0.465	0.949	0.00311	94.7
	60	-0.457	0.804	**0.00263**	**95.5**

Tafel polarization curves taken at different holding times were superimposed and given in Figure 2. As can be seen from the figure and the table, the corrosion potential shifted to some positive values when the holding time of the brass electrode increased in the nicotinamide environment. Looking at Table 1, the lowest corrosion rate was 0.00263 mm/year and the inhibitory efficiency was 95.5% in the 60 minuteholdingtime.

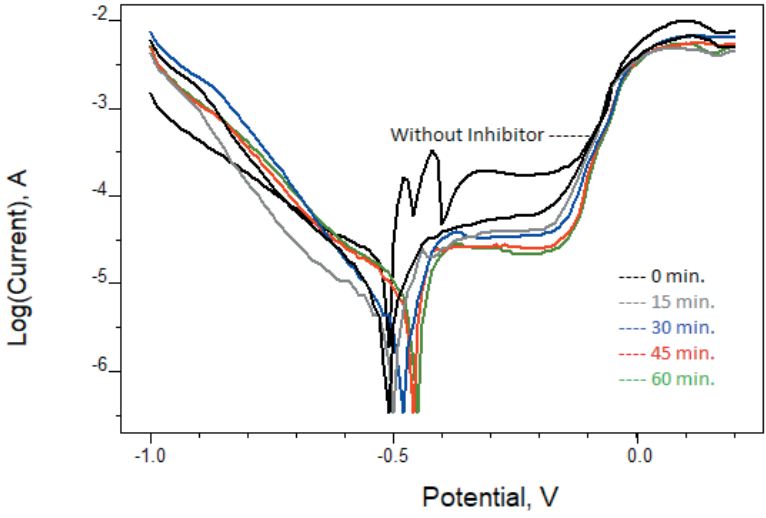

Figure 2. *Overlapping of Tafel polarization curves given by Brass Electrode by adding 500 ppm nicotinamide to 0.1 M HCl solution at different holding times*

In order to examine the effect of nicotinamide concentration on brass corrosion, 750 ppm and 1000 ppm nicotinamide were added to 0.1 M HCl solution after 500 ppm, and optimum retention time was determined at all

concentrations. Looking at Table 2 and Figure 3, the best corrosion rate was 0.00116 mm/y and the inhibitory efficiency was 98.0% in 60 minutes of holding. Compared to 500 ppm nicotinamide, an increase in inhibitor efficiency was observed with increasing inhibitor concentration.

Table 2. *Corrosion rates and calculated % Inhibitor Efficiency values from the Tafel polarization curves given by Brass Electrode by adding 750 ppm nicotinamide to 0.1 M HCl solution at different holding times*

Concentration, ppm	Residence time, minute	E_{cor}, V	I_{cor}, (µA)	Corrosion Rate, mm/y	% Inhibitor Efficiency
0	0	-0.506	17.990	0.0589	---
750	0	-0.469	2.573	0.00842	85.7
	15	-0.447	1.682	0.00550	90.7
	30	-0.424	1.004	0.00328	94.4
	45	-0.411	0.418	0.00137	97.7
	60	-0.440	0.356	**0.00116**	**98.0**

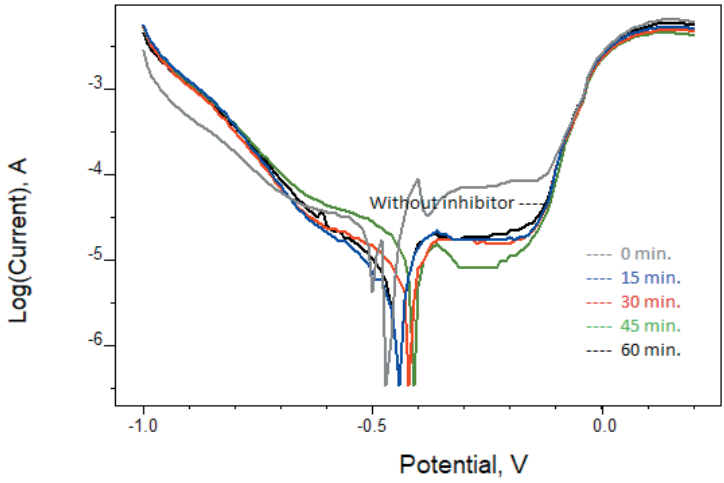

Figure 3. *Overlapping of Tafel polarization curves given by Brass Electrode by adding 750 ppm nicotinamide to 0.1 M HCl solution at different holding times*

Nicotinamide concentration was increased to 1000 ppm. By adding nicotinamide to 0.1 M HCl solution, the optimum time was determined as in the other two concentrations. When Table 3 and Figure 4 were examined, the lowest corrosion rate was 0.00111 mm/y and the inhibitory efficiency was 98.1% in 60 minutes of waiting. A concentration higher

than 1000 ppm was not tried, since approximately the same values were obtained with the addition of 750 ppm Nicotinamide and 60 minutes of soaking, and 1000 ppm nicotinamide 60 minutes of soaking. The highest inhibitory efficiency was determined as 98.1%. Although there was some positive shift in corrosion potentials, this shift was limited.

Table 3. *Corrosion rates and calculated % Inhibitor Efficiency values from the Tafel polarization curves given by Brass Electrode by adding 1000 ppm nicotinamide to 0.1 M HCl solution at different holding times*

Concentration, ppm	Residence time, minute	E_{cor}, V	I_{cor}, (μA)	Corrosion Rate, mm/y	Inhibition Efficiency %
0	0	-0.506	17.990	0.0589	---
1000	0	-0.518	2.67	0.00874	85.2
	15	-0.457	0.940	0.00308	94.8
	30	-0.465	0.774	0.00253	95.7
	45	-0.452	0.602	0.00197	96.7
	60	-0.420	0.338	0.00111	98.1

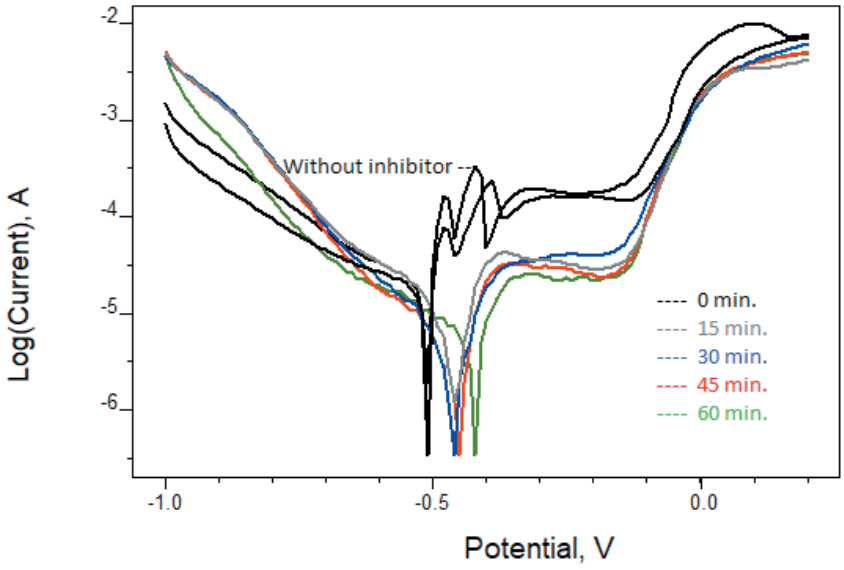

Figure 4. *Overlapping of Tafel polarization curves given by Brass Electrode by adding 1000 ppm nicotinamide to 0.1 M HCl solution at different holding times*

The % inhibitory efficiency values obtained at 5 different holding times (0, 15, 30, 45 and 60 minutes) of the addition of Nicotinamide at three different concentrations (500 ppm, 750 ppm and 1000 ppm) are given in Figure 5 for comparison.

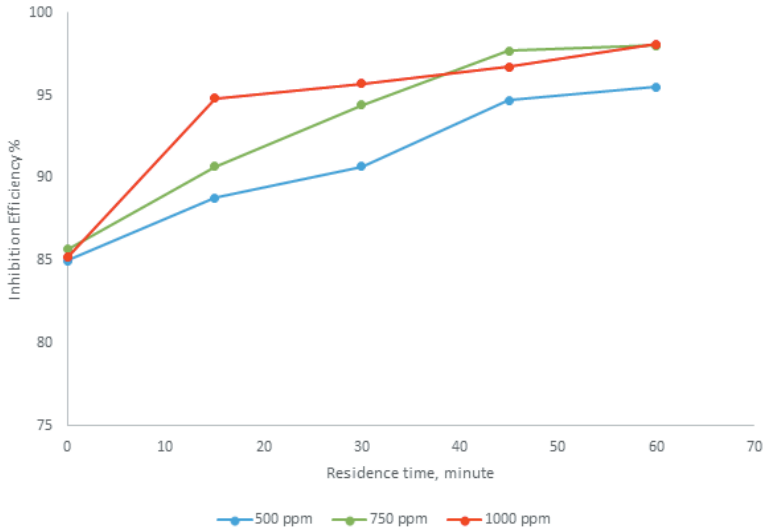

Figure 5. *Collective display of % inhibitory activity values obtained for Brass at different holding times in 0.1 M HCl solution containing 500 ppm, 750 ppm and 1000 ppm nicotinamide*

5.3. Conclusion

As a result, nicotinamide proved to be an effective corrosion inhibitor for brass. When Figure 5 is examined, it is seen that the inhibitory efficiency increases with the increase of the holding time. While the rate of increase in inhibitory activity was slower in 500 ppm Nicotinamide and 750 ppm nicotinamide, the inhibitory activity reached 94.8% rapidly in 1000 ppm nicotinamide in 15 minutes. Although the retention time was increased in 500 ppm Nicotinamide, the maximum inhibitory efficiency remained at 95.5%. This showed us that a concentration of 500 ppm is not enough for very good protection. Inhibitory activity of 750 ppm and 1000 ppm Nicotinamide reached 98% in 60 minutes of soaking. The inhibitory efficiency obtained with the addition of 750 ppm nicotinamide in 15 minutes and 30 minutes at intermediate times between the two, until only 98% inhibitory efficiency was reached, was lower than the inhibitory effectiveness values obtained with the addition of 1000 ppm nicotinamide. A nicotinamide concentration of 1000 ppm should be preferred when a faster increase in inhibitory activity is desired, or 750 ppm if a slow but controlled increase in inhibitory activity is desired. The most crucial importance of the study is nicotinamide vitamin B3, which has a very good solubility in aqueous media, that is, being an environmentally friendly inhibitor should be the biggest reason for preference.

REFERENCES

Abdallah, M., Al-Agez, M., & Fouda, A. S. (2009). Phenylhydrazone derivatives as corrosion inhibitors for -α-brass in hydrochloric acid solutions. *International Journal of Electrochemical Science*, 4(3), 336–352.

ASAN, A. (2020). KlorürlüOrtamlaNikotinamidiPirincin Korozyonuna KarİnhibitEtkisinin. *Euroasia Journal of Mathematics, Engineering, Natural and Medical Sciences*, 7(11), 1–2. Retrieved from https://doi.org/10.38065/euroasiaorg.233

Asan, G., & Asan, A. (2020). Corrosion protection of AISI 1010 using doped MoS<inf>2</inf> conductive polymers. *Journal of the Turkish Chemical Society, Section A: Chemistry*, 7(1). Retrieved from https://doi.org/10.18596/jotcsa.497889

Asan, Gülden. (2021). Protection of Copper From Corrosion With Nicotinamide Inhibitor. *Hittite Journal of Science & Engineering*, 8(3), 273–277. Retrieved from https://doi.org/10.17350/hjse19030000239

Asan, Gülden, & Asan, A. (2020). Inhibitor effect of nicotinamide on corrosion of aluminum. *Journal of Molecular Structure*, 1201, 127184. Retrieved from https://doi.org/10.1016/j.molstruc.2019.127184

Cevallos-Morillo, C., Cisneros-Pérez, P., Llive, R., Ricaurte, M., Reinoso, C., Meneses, M. A., … Palma-Cando, A. (2021). Croton lechleri extracts as green corrosion inhibitors of admiralty brass in hydrochloric acid. *Molecules*, 26(24), 1–12. Retrieved from https://doi.org/10.3390/molecules26247417

Chakravarthy, M. P., Mohana, K. N., & Pradeep Kumar, C. B. (2014). Corrosion inhibition effect and adsorption behaviour of nicotinamide derivatives on mild steel in hydrochloric acid solution. *International Journal of Industrial Chemistry*, 5(2), 1–21. Retrieved from https://doi.org/10.1007/s40090-014-0019-3

Chaubey, N., Savita, Qurashi, A., Chauhan, D. S., & Quraishi, M. A. (2021). Frontiers and advances in green and sustainable inhibitors for corrosion applications: A critical review. *Journal of Molecular Liquids*, 321, 114385. Retrieved from https://doi.org/10.1016/j.molliq.2020.114385

Chevalier, M., Robert, F., Amusant, N., Traisnel, M., Roos, C., & Lebrini, M. (2014). Enhanced corrosion resistance of mild steel in 1 M hydrochloric acid solution by alkaloids extract from Aniba rosaeodora plant: Electrochemical, phytochemical and XPS studies. *Electrochimica Acta*, 131, 96–105. Retrieved from https://doi.org/10.1016/j.electacta.2013.12.023

El-Etre, A. Y., & Ali, A. I. (2017). A novel green inhibitor for C-steel corrosion in 2.0 mol·L− 1 hydrochloric acid solution. *Chinese Journal of Chemical Engineering*, 25(3), 373–380. Retrieved from https://doi.org/10.1016/j.cjche.2016.08.017

Gadow, H. E., & Elabbasy, H. M. (2017). Electrochemical study on the efficiency

of Curcuma extract as a green inhibitor for corrosion of α-brass in 1MHCl. *International Journal of Electrochemical Science*, 12(7), 5867–5887. Retrieved from https://doi.org/10.20964/2017.07.13

Hansson, C. M. (2011). The impact of corrosion on society. *Metallurgical and Materials Transactions A: Physical Metallurgy and Materials Science*, 42(10), 2952–2962. Retrieved from https://doi.org/10.1007/s11661-011-0703-2

Hou, B., Li, X., Ma, X., Du, C., Zhang, D., Zheng, M., … Ma, F. (2017). The cost of corrosion in China. *Npj Materials Degradation*, 1(1). Retrieved from https://doi.org/10.1038/s41529-017-0005-2

Javaherdashti, R. (2000). How corrosion affects industry and life. *Anti-Corrosion Methods and Materials*, 47(1), 30–34. Retrieved from https://doi.org/10.1108/00035590010310003

Kesavan, D., Gopiraman, M., & Sulochana, N. (2012). Green Inhibitors for Corrosion of Metals : A Review Correspondence : *Chemical Science Review and Letters*, 1(1), 1–8.

Ndukwe, A. I. (2022). Green Inhibitors for Corrosion of Metals in Acidic Media: a Review. *Academic Journal of Manufacturing Engineering*, 20(2), 36–50.

Raja, P. B., Qureshi, A. K., Abdul Rahim, A., Osman, H., & Awang, K. (2013). Neolamarckia cadamba alkaloids as eco-friendly corrosion inhibitors for mild steel in 1M HCl media. *Corrosion Science*, 69, 292–301. Retrieved from https://doi.org/10.1016/j.corsci.2012.11.042

Ramdé, T., Rossi, S., & Bonou, L. (2016). Corrosion inhibition action of sulfamethoxazole for brass in acidic media. *International Journal of Electrochemical Science*, 11(8), 6819–6829. Retrieved from https://doi.org/10.20964/2016.08.39

Ravichandran, R., & Rajendran, N. (2005). Electrochemical behaviour of brass in artificial seawater: Effect of organic inhibitors. *Applied Surface Science*, 241(3–4), 449–458. Retrieved from https://doi.org/10.1016/j.apsusc.2004.07.046

Taghavikish, M., Dutta, N. K., & Choudhury, N. R. (2017). Emerging corrosion inhibitors for interfacial coating. *Coatings*, 7(12). Retrieved from https://doi.org/10.3390/coatings7120217

Tan, B., Xiang, B., Zhang, S., Qiang, Y., Xu, L., Chen, S., & He, J. (2021). Papaya leaves extract as a novel eco-friendly corrosion inhibitor for Cu in H2SO4 medium. *Journal of Colloid and Interface Science*, 582, 918–931. Retrieved from https://doi.org/10.1016/j.jcis.2020.08.093

Üneri, S. (1969). The Utility of Linear Polarization Method For The Determination of The Corrosion Rate. *Fen Fakültesi Tebliğler Dergisi*, 36–62.

Üneri, S. (2011). *Korozyon ve Önlenmesi*. Ankara: Korozyon Derneği.

Zehra, S., Mobin, M., & Aslam, R. (2022). *Corrosion prevention and protection methods*. *Eco-Friendly Corrosion Inhibitors: Principles, Designing and Applications*. Retrieved from https://doi.org/10.1016/B978-0-323-91176-4.00023-4

CHAPTER 3

CAUSES OF WORKPLACE ACCIDENTS IN THE FORESTRY INDUSTRY AND PREVENTATIVE STEPS

Ali Bahadır KÜÇÜKARSLAN[1]

1 PhD Candidate, İstanbul Commerce University, bahadirkucukarslan@gmail.com, https://orcid.org/0009-0000-2580-146X

1. Introduction

Today, the availability of scarce production raw materials and the personnel with the technical know-how to process these products have become crucial factors. Because of this, companies have begun to give their staff extra attention in order to continuously benefit from their technical expertise. In this context, over the past 50 years, occupational health and safety (OHS) measures have been implemented for workers in many nations, particularly in European nations. The Occupational Health and Safety Law No. 6331 was adopted in Turkey on June 20, 2012. Because of this, it can be said that over the past seven years, interest in OHS studies has grown in Turkey. Due to these advancements, scientific research on occupational health and safety, which addresses issues like safe work practices in all industries, the prevention of workplace accidents, and the eradication of occupational diseases, has accelerated.

Mass production and consumption of goods and services have been brought about by factors like population growth, industrialization, the expansion and diversification of human needs, and the adoption of economic development. But as a result of the industrial revolution, the working class began to bear the cost of this social welfare. because those who are involved in mass production during this time are exposed to occupational diseases and work-related accidents. However, it has been recognized that these unfavorable working conditions are inconsistent with social justice, and legal regulations pertaining to workplace accidents and occupational diseases have begun to be made. Initially originating in quickly industrializing nations like England and the USA, these improvement movements aimed to improve working conditions for workers later spread to other nations that started the industrialization process (Ozgür, 2017).

Due to overuse and misuse of natural resources as well as the employment of workers in unfavorable conditions, the industrial revolution, which resulted from the classical understanding of development, pollutes the environment. Globally, however, action has been taken since the 1970s to halt this unfavorable development; in place of the traditional conception of development, the idea of sustainable development, also known as the green economy, has started to be applied. The adoption of a sustainable development strategy, however, was insufficient to completely eliminate and/or significantly reduce the negative effects experienced by the employees. For this reason, measures have been started to be taken on OHS at international and national levels. The United Nations Environment Program's 2011 report features one of the initiatives that have been undertaken at the global level over the past 20 years in this area. One of the three widely acknowledged objectives of the green economy is described in this report as "reviving the global economy, preventing job losses and creating new job

opportunities while also helping to protect the most vulnerable segments of society" (Yalcin, 2016). Another one of these initiatives is the "resource efficiency" indicator with the "sustainable consumption and production" theme that is one of the European Union's (EU) Sustainable Development Indicators (EUROSTAT, 2011; Aksu, 2011). It is clear from these two initiatives that resource efficiency, protecting society's most vulnerable groups, and other OHS-related concerns are prioritized.

Studies that seek to eliminate both long-term and short-term health issues that may arise as a result of the work done are commonly referred to as occupational safety studies. With the help of these studies, it is hoped to reduce the likelihood of occupational accidents occurring during or as a result of work, to prevent health issues that may be brought on by the workplace, and to take preventative measures against occupational diseases. With this in mind, OHS practices cover all types of paid or unpaid work, not just very dangerous or heavy work (CASGEM, 2014). OHS laws and regulations have been passed as a result of our nation's efforts to harmonize with the EU. This concept, which was initially accepted as "Occupational Health and Safety," was changed to "Occupational Health and Safety" in 2012 with the Law No. 6331, as can be seen by looking at these laws.

It is well known that the nation's development is correlated with its level of economic growth. It is widely acknowledged that employment and capital growth are the main drivers of economic growth. Scientific research has shown that other factors, besides employment growth and capital accumulation, have a significant impact on total factor productivity (TFP), which in turn affects the rate of economic expansion. Because of this, nations have begun to concentrate their development efforts on total factor productivity. Parallel to these developments, TFP was highlighted in Turkey's 10th Development Plan, where it was stated that the 0.2 percentage point increase in TFP was what caused the average growth (4.3%) during the relevant period. For this reason, it was aimed to improve the perception of productivity, improve production processes, increase added value and contribute to the target during the relevant plan period (Bayrakçeken, 2018; TPFV.ORG, 2019). With reference to GDF (2012) in Turkey's 10th Development Plan Sustainable Forest Management Special Expertise Commission Report, forestry, which is one of the 59 sectors contributing to the Turkish economy, is a labor-intensive sector (employment multiplier 0.291) has been reported to provide employment opportunities. In this report, it is also stated that forestry works can provide employment opportunities for the largely unskilled labor force without requiring further training (T.R. Ministry of Development, 2014). Special attention should be given to Turkey's OHS practices, both to increase TFP and as a re-

quirement of national-international OHS legislation. However, as in other sectors in Turkey, the concept of OHS in the forestry sector has not been fully adopted and OHS practices have not been developed sufficiently. For this reason, scientific studies are needed for the adoption of the concept of OHS in all sectors of the Turkish economy and for the implementation of its applications adequately. Although the number of scientific studies on this subject has increased, it is not sufficient.

The purpose of this study is to investigate the causes of occupational accidents in the forestry industry and the possible countermeasures within the context of the relevant literature. It is anticipated that the results of this study will contribute to the body of literature on occupational health and safety (OHS) in the forestry industry.

2. Occupational Health and Safety Concept and Basic Principles

Initially, the concept of OHS was included in certain articles of the Labor Law No. 4857, which was put into effect on May 22, 2003. However, on June 30, 2012, the OHS Law No. 6331 was enacted, and its own legal basis was established for this concept. According to the hierarchy of norms, adherence to laws and constitutions, which are the infrastructure of OHS, came to the fore. Despite the abolition of the OHS regulation in this process, thanks to the regulations enacted, the work accelerated in order for the operation to operate more efficiently and the process progressed in this direction (Güler, 2017).

Due to the low level of consciousness, it has been seen that there is a bottleneck in the studies carried out to create an OHS culture. However, creating a positive OHS culture emerges as the best process management that can be accepted in order to provide efficiency, as opposed to creating an obstacle to operation and production (Aktay, 2014).

For the OHS process to progress efficiently, it is of great importance that the mechanisms of the state controlling the legal process, employers and their representatives, and workers fulfill and accept the inspections and measures. Being indifferent to the issue of OHS and only considering it legally poses a great danger (Erol, 2015).

When OHS studies are mentioned, training, risk assessment analyzes and emergency plans come to mind first. However, the essence of OHS studies is to protect the safety of work and workers. For this reason, by adopting a proactive approach, it is revealed how to take precautions against work accidents, how to minimize emergencies before they occur, or how to overcome the situation with the least damage. In particular, training activities are of great importance to ensure that employees are aware of

their dangers and risks, and to explain how to behave towards them (Balkır, 2012).

2.1. The Importance of Occupational Health and Safety

The World Health Organization defines health as a state of complete physical, mental and social well-being and not merely the absence of disease or infirmity. Ensuring the life, freedom and security of employees is both a human and a constitutional right. OHS has 3 main objectives: protecting employees, creating a safe working environment, minimizing environmental risks for employees and the working environment. It is important to determine the factors that threaten people's most basic right to life, to prevent them, to create a safe working environment for people and to ensure their continuity (Yılmaz et al., 2016).

In developed countries, OHS has moved from a reactive approach to a proactive approach, thus ensuring that employees live a healthy life not only in their workplace situation, but also when they arrive at their homes. In our country, 5% of the gross national product is lost due to not taking OHS measures. The most important point to remember is that the work done for OHS is not an expense, but one of the most important requirements to ensure production and efficiency (Akıllı & Aydoğdu, 2013).

2.2. Importance for Employer and Employee

Employers are responsible for ensuring the safety of their employees. The fact that the insured has technical knowledge does not remove the employer's oversight obligation. Employers are obliged to avoid risks that may occur to their employees, to analyze risks and to struggle with these risks at their source. They have responsibilities such as providing their employees with appropriate personal protective equipment and regularly checking them, creating instructions suitable for the job, eliminating hazards at their source, and using collective protection methods (Ulusoy, 2013). In addition, employers are obliged to keep records of work accidents and occupational diseases and report these data to the Social Security Institution. Employees are expected to receive health checks, organize training, receive their requests, opinions and suggestions and respond to them.

Employees, on the other hand, have obligations such as using the machinery and devices in the workplace in accordance with the instructions, not using them for different and different purposes, using the personal protective equipment provided to them in appropriate and necessary times, and informing the employer or employer's representatives and employee representatives about the negative situations that may occur. Apart from

this, having the right to avoid working in the presence of an imminent danger plays an important role in the protection of employees (Erol, 2015).

2.3. Social and Economic Importance

Turkey ranks 3rd in the world and 1st in Europe in occupational accidents. According to official data, it is seen that an average of 172 workers have a work accident per day, and as a result, four workers have lost their lives, and six workers have been permanently disabled. In countries where the unemployment level is high, workers worry about getting wages before the safety of the work environment. Because employees are worried about not being able to find a job to earn their living due to labor market conditions, fear of being excluded from the labor market and being excluded from social security, they prefer to work in unhealthy conditions and do not care about occupational safety measures. As of 2013, the number of fatal occupational accidents in Turkey has reached 1,235 (Çetin & Karatay Gögül, 2015).

Factors such as compensation paid for reasons such as loss of limb or life of employees, occupational diseases, increased periods of incapacity for work, and retirement due to disability increase the cost of labor and disrupt the continuity of the workforce. In addition, in workplaces where occupational accidents occur, other employees experience deficiencies in morale and motivation, and the quantity and quality of production decrease. For this reason, states attach importance to social development in their development strategies. In Turkey, the current situation of occupational health and safety is revealed in the Development Plans and short and long term targets are specified (DPT, 2014).

One of the basic inputs is the work of adding value on the basis of labor. As in the past, the fear of unemployment and work accident death compensation constitute the soft underbelly of the employment policy. Therefore, workers should pursue their legal rights and support the development of OHS coverage in Turkey (Şahin, 1987).

3. Perception of Occupational Health and Safety

3.1. Occupational Health and Safety Culture

Health and safety are considered to be the two essential elements of personal and social development, and today many businesses are working to increase the level of security. When we look at these studies, it is seen that most of them are aimed at establishing an enterprise safety management system and creating an OHS culture. After the importance of OHS culture in preventing accidents has been accepted, many definitions have

been made about this concept. Özkan & Lajunen (2003) and Cox & Flin (1998) stated that the term OHS culture was first used in a report prepared by the OECD Nuclear Agency in 1987 after the 1986 Chernobyl nuclear accident, and this concept "depends on the adequacy, style and quality of the health and safety programs of the institution. It is a product of the values, attitudes, competencies and behavior patterns of individuals and groups who decide to insist on the practice". However, although the importance of the concept of OHS culture has been emphasized in various ways, it has been seen that studies on its detailed definition and measurability are not sufficient (Kol, 2016).

3.2. Occupational Health and Safety Climate

The concept of OHS climate is a concept that has been used before compared to the concept of OHS culture. The concepts of OHS culture and OHS climate are used interchangeably by some. Unwritten organizational rules for OHS culture can be called; OHS climate, on the other hand, is the dominating influences on a certain functional area, such as health and safety, and determines the perception of employees about that subject, in other words, what is rewarded, what is supported and what is expected. In fact, culture is deeper, affected by many different functional areas and takes longer to change; the climate changes quickly and is affected more quickly by the leadership (ÇASGEM, 2017; Şerifoğlu & Sungur, 2007).

3.3. Effective Factors on Perception of Occupational Health and Safety

In order to determine the perceptions on OHS, it is first necessary to determine the factors affecting them. Developments made or to be made on OHS can have positive effects on the perceptions of employees, management and administrators. For this reason, it is important not to ignore the following factors in determining perceptions. The most important thing to remember is that these vital issues must be handled together. OHS is a very important issue, and the development of this issue seems possible with industrialization, the state, academics, professional formations and labor force. The 5 factors that affect the improvements to be made in OHS are summarized below:

- Legislation, sanctions and penalties,
- Effective and innovative OHS programs (company level or project specific),
- Academic and vocational education (general and private),
- To conduct research to better understand the causes of accidents, to

develop methods, tools and technologies to prevent work accidents and occupational diseases,

• To ensure cooperation between industry, government and academics, with the contributions of professional chambers and unions, in order to continuously improve OHS.

Although great progress has been made in the field of OHS in the USA in the last 20 years, it is stated that there are still steps to be taken for the future. These steps are;

• Accessing small contractors for training and compliance,

• Knowledge/technology transfer to the international OHS community,

• It can be counted as increasing cooperation between stakeholders to improve OHS.

• However, in order to take these steps, the following must also be done;

• Developing better OHS program implementation strategies and methods,

• Doing more research and identifying hazards/providing precautions,

• Making improvements (better and useful databases) in data collection and analysis in the field of OHS (Usmen & Baradan, 2011).

4. What Leads to Accidents at Work and What Preventative Steps Can Be Taken

Even though there are likely to be a great number of interconnected factors that contribute to the occurrence of occupational accidents, there is always the possibility that the accident was brought on by issues that were not anticipated and were not planned for in advance. It is generally accepted that unsafe situations and unsafe behaviors are among the causes of accidents that occur on the job. According to the findings of the studies, only ten percent of occupational accidents are the result of unsafe working conditions, whereas the remaining eighty-eight percent are the result of unsafe behaviors. It is not sufficient for an organization, region, or even the country to be engaged in a struggle on their own if the goal is to reduce the occurrence of accidents and diseases. The use of chemicals that are harmful to everyone, the failure to protect the environment, and the accumulation of hazardous waste all contribute to an increase in the severity of the adverse effects experienced by workers as well as by the environment. According to research conducted by the EU OHS Agency, it has been determined that the primary focus should be placed on the prevention of this

scenario in smaller businesses (Ozdemir, 2016).

Employees' carelessness, absentmindedness, and other factors are cited as the causes of their potentially hazardous behaviors;

- Work that is both careless and disorganized.
- They did not make use of any of their own individual protectors.
- Unsafe handling of apparatus or instruments
- Despite warnings, unsafe operation; this compromises the integrity of the security equipment.
- Insecure loading, transportation, stowing, placement, etc.
- Joking, surprising, removing,
- It is possible to count as operations that are carried out in a manner that is not in accordance with the instructions, etc.

Dangerous situations can be brought on by a number of factors, including machine-borne hazards, environmental hazards, administrative hazards, and management hazards. It provides a list of potential dangers, issues, and so on that may arise if engineering measures are not taken (Yılmaz, 2013).

5. The Reasons for Workplace Accidents in the Forestry Industry and the Preventative Steps That Should Be Taken

Forestry businesses, like any other type of business, each have their own unique culture, as well as distinct attitudes and behaviors that stem from the employees and administrative staff members working within the organization. There are some aspects of the businesses that are viewed as moving in a positive direction, but there are other aspects of the businesses that show the exact opposite of this scenario. The forestry industry is vulnerable to the effects of external conditions; as a result, there will be work-related accidents and other incidents, which will require corrective actions such as administrative measures, engineering measures, and adjustments to machinery and equipment. Even though it is designed to stop problems from occurring, it is not enough on its own. Because the composition of the soil is that of a living organism, and because the soil is an essential component of our lives even as it is subject to transformation at any given time. In particular, wildfires and other such events. In these kinds of situations, the dissimilarities between the previous state of the environment and the current state of the environment can make the intervention more difficult and increase the vital risks for the workers. The lack of protective clothing and equipment for workers, as well as a lack of food and drink, makes this situation even more difficult (Menemenciolu, 2006).

As a result, forestry works are subject to challenging weather conditions and terrain conditions as a result of their natural environment.

When compared to other industries, the object of work in the forestry sector is nature itself, and the conditions under which the work is performed are influenced by the outdoors. Because of the nature of the forestry work group, it is in the work group that requires the worker to go to the work and falls into the heavy and dangerous work group such as mining. In addition, the forestry work group is in the work group that requires the worker to wear protective gear. In addition, the fact that a sizeable portion of forestry work cannot be completed with the assistance of machinery compels workers in the forestry industry to perform a variety of tasks at a variety of times. According to Acar & Şentürk (1997), the ever-increasing complication of technology combined with an increase in production numbers has made it difficult to ensure human health and occupational safety, as well as contributed to an increase in the consumption of natural resources and an increase in certain environmental risks.

Training for people who work in forests is the most important preventative measure that can be taken for occupational health and safety. Every year, there are approximately a half a million people who find employment in forest areas. Training for these workers, obtaining information that will help them protect themselves, and ensuring that personal protective equipment (PPE) is used, among other things, are all necessary. Efficiency makes it possible to forestall the occurrence of losses. Therefore, even if only a 1% improvement is achieved in order to reduce the number of accidents that occur at work, the annual value will increase by thousands of dollars (Engür, 2014).

On the land, "unevenness" is understood to mean "a bumpy place with a lot of slope, soil," when the word is used in reference to the terrain. Working on sloped terrain in this way always requires more attention and careful planning than working on flat terrain does. Cutting and felling trees, moving trees around, and other tree-related tasks. It is a well-known fact that the business of trading is one of the most hazardous occupations. According to Menemencioglu (2012), it has been observed that the increased use of machinery in forestry activities has resulted in a decrease of nearly 70 percent in the number of occupational accidents and injuries.

The elevation differences on the land are responsible for the development of a variety of forest types. The treatment administered to each distinct species, as well as the machinery and apparatus that must be utilized in accordance, are each different. A machine cannot do its work because of the slope, which is another disadvantage. Because with the technology that is available today, it is not possible to work with machines on a particular

slope. This situation increases the risk of accidents as it requires working with human power. When it comes to texture in forestry, the soil structure is understood. There are differences between the cultivation of fine-textured soils, the cultivation of coarse-textured soils or sandy soils (Başkan, 2004). For this reason, field studies to be carried out without considering these differences during the work require workers to work with different precautions and technical knowledge.

6. Literatür Özeti

Yılmaz et al. in 2016, the direct effect of organizational safety climate perception on safety behavior and employee performance in shipyards was evaluated, and it was revealed that the perception of safety climate most affected safety behavior and employee performance.

Tüzüner & Özaslan, in 2011, determined that the safety climate perceptions of health care workers were below the determined average. With this research, it has been determined that the perception of safety climate differs statistically in terms of the departments in which the health care workers work, but it does not show a statistically significant difference depending on the gender, age group, education level, total professional experience, and work experience in the place where they work. The fact that nurses see the work on OHS themselves, are more exposed to the risk of infection than the majority, and their knowledge of OHS management systems have caused them to realize the deficiencies in this regard more clearly.

In Uslu, 2014, the demographic characteristics of the participants and the similarities in other sectors related to OHS were explained, and it was stated that the relationship between safe behavior and safety culture was statistically significant in the positive direction. As a result, it was pointed out that the perception of safety culture increased with the increase of safe behaviors in businesses.

According to Tümer, in 2011, health is accepted as a human capital element as important as education, which determines the productivity and quality of people in the production process. OHS, on the other hand, is summarized as the activities carried out in order to be protected from all kinds of negative conditions that may occur during work. It has been emphasized that the magnitude of the damage caused by work accidents and occupational diseases will depend entirely on luck if the managers do not identify the hazards and identify the risks that can be controlled in advance.

According to Şerifoğlu and Sungur, 2007, the management's encouragement and rewarding of employees, making near-miss records widespread, and effective use of internal communication can prevent negative

consequences. In this case, it is stated that the top management, considering the cost, believes that the contribution to OHS will have a positive effect and puts it into practice by making a commitment, as the most important factor in ensuring continuity and effectiveness.

ÇASGEM examined the current situation in order to determine the perception of OHS in Turkey in 2017, and the demographic-socioeconomic characteristics, OHS perceptions and ELO of the participants were questioned. In addition, a SWOT (identification of strengths and weaknesses, opportunities and threats) meeting was held with expert participants. At this meeting, the strongest aspect of the OHS perception in Turkey was the implementation of the OHS Law, the most important weakness was the lack of OHS culture at the desired level, the most important opportunity was the updating of the legislation studies, and the most important threat was the deficiencies in the OHS data.

Eroglu et al. In 2002, it is stated that protective clothing and equipment are not given importance in forestry activities in Turkey, but this is not valid for forest workers fighting fires where the risk is very high, and the risk of injury and even death increases in forestry activities because protective clothing and equipment are used at very low levels. . As a result, it was stated that workers working in forestry activities should have protective clothing and equipment that are durable enough to protect themselves from injuries and deaths in accordance with national and international standards.

Yılmaz, In 2009, the effectiveness of the OHS boards in Turkey was evaluated by taking into account the observations and evaluations of the experts working in the workplaces. It has been stated that occupational safety experts, together with other OHS measures, make a positive contribution to reducing the number of occupational accidents, and that the communication-cooperation function of these boards is as important as the accident reduction function.

In the 10th Development Plan 2014-2018; It has been reported that the current situation with OHS in Turkey, the improvement of working conditions, trade union freedoms and the legislation on collective bargaining agreements have been put into effect, and related legal arrangements have been made. In addition, it was stated that the issues of increasing employment, primarily youth and women, preventing work accidents and unregistered employment, and increasing the quality of the workforce maintain their importance. Regarding these issues; It is aimed to improve working conditions, develop OHS culture, increase compliance with OHS standards, and train sufficient number and quality of personnel who are experts in OHS issues.

In 2016, the MoLSS stated that OHS in forestry is a prerequisite for

environmentalism and effective use of natural resources, emphasizing that forestry is one of the riskiest industries in many countries, that forestry workers are highly likely to retire early, have occupational diseases and occupational accidents. as "General principles, legal framework and general duties, health and safety structure at enterprise level; Labor; Safety rules for vehicles, machinery and harmful chemicals; Work Clothes and Personal Protective Equipment; Testing and Certification of Equipment; First Aid, Emergency Rescue and Occupational Health Services; Shelters, Storage and Nutrition Reporting, Recording, Notification and Investigation of Occupational Accidents and Occupational Diseases Technical guides for occupational health and safety in the forestry work site, .." topics are explained.

Gümüş & Türk (2017) emphasized that all forest fire workers are experienced and healthy men. It was stated that 82% of forest fire workers were satisfied with their wages and all agreed that their jobs were very dangerous and difficult, but they did not use clothing and equipment to protect themselves against burning.

In 2009, Gifford emphasized the necessity of solving occupational safety and health problems in forestry as a priority, and the necessity of developing a safety culture in all forestry activities, due to the increase in health problems among forestry workers in many European countries and the high level of accident rates in forestry work. Cutting and felling trees, transporting, falling from height as safety risks in forestry; Handling, using chemicals (for example, pesticides), noise and vibration were stated as health risks. has been disclosed. In addition, the necessity of working in open fields and the harsh weather conditions in these areas, poisonous plants and insects, snakes and other dangerous animals, ergonomics in forestry work should be improved, because an average of 73 forest workers per year died due to occupational accidents in 15 EU member countries during the 1999-2004 period. It has been emphasized that the number of those who receive the report of being unable to work for more than 3 days approaches 26,000 on average per year, and that these figures will increase with the increase in the number of member countries.

In its 1998 study on health and safety in forestry activities, the ILO mentioned that forestry is usually carried out by small groups, in remote areas, and that this poses a greater challenge than other industry jobs. He referred to the necessity of using personal protective equipment in the forestry sector for situations such as overheating of the body in ambient conditions, infection from the contact of plants and animals, poisoning. It has revealed the course of action that employees should comply with in matters such as high risk (tree felling, scuffing..). It was emphasized that employers, employees and subcontractors should comply with the deter-

mined procedures and instructions. Otherwise, it shows a high probability of accidents.

Conclusion

Forestry activities are one of the most challenging and demanding jobs, and one of the jobs with the highest probability of causing an accident due to lack of precautions and/or attention. It is very important to use personal protective clothing and equipment to prevent accidents, especially due to adverse outdoor conditions and fatigue. For this reason, personal protective equipment in forestry works should be subject to the control of the relevant supervisors continuously, without being left to the initiative of the employees. Due to the strong communication between forestry workers, near miss and accident records should definitely be recorded. It should be sensitive about the improvement of the machinery and equipment used, but it should be ensured that the machine-equipment improvements are made in accordance with the standards. It should be investigated why the rate of those who are satisfied with IOBM employees cannot reach 90% and why they accept work accidents that may happen to them as fate. Measures that will bring the IOBM's IOP level to 5 points, which is 3 points, should be determined immediately.

FAO, (2016) It is seen as the difficulty of working life that employees are exposed to situations such as falling trees and branches, chainsaw kickbacks and tree tripping, exposure to whole body and hand vibration, and working open to chemical and biological risk factors. In addition, it is emphasized that employees work with piece rates and that there is no organization that will take into account their own health and safety measures.

OGM Personnel Department Legal Counseling has requested work accidents in the fields under the responsibility of OGM and the compensation and expenses paid/to be paid for these work accidents. It is stated in Annex-2 that compensation payments were made to a total of 22 civil servants and workers who lost their lives or were injured during the efforts to extinguish forest fires from 2009 to 15.03.2019 (OGM, 2019). It is expected that the average number of people who lost their lives due to occupational accidents in the last 10 years is very high (ILO, 1998). This situation makes us think that OHS records are not kept in accordance with the legislation. However, if the OHS data is recorded and reported in detail, it will increase the awareness of the occupational accidents to be experienced and will enable the efforts to prevent them to be faster. Another negative point to be emphasized here is that employees who have had a fatal occupational accident are registered only if they are OGM personnel. Because especially the tree cutting works are given to the neighboring villagers by tender method and the forest villagers here are seen as a kind of

employer, it causes the occupational accidents during these activities not to be included in the OGM records.

As a result of the research conducted by Tunay & Bozkurt in 2018, a survey study was conducted for forest villagers who perform forestry works with vahidi price. According to the results of the survey, it is seen that 56% of the employees have had a work accident. It has been determined that the main causes of occupational accidents are factors such as the difficulty of the working environment, fatigue-sleeplessness, not taking work seriously-carelessness.

It is not possible to obtain positive results from OHS practices without knowing the working environment and the past experiences of the employees. In this study, it was determined that the subject groups participated in the OHS studies at a moderate level and somewhat. Undoubtedly, safe behaviors and ensuring a safe situation are among the biggest factors that can eliminate work accidents. For this reason, the activities to be organized to keep the OHS safety perception of the employees high will both bring awareness to the employees and appear as a preventive factor for accidents. Indeed, it has been observed that those who have to work with risks and dangers in the business environment bring different solutions for themselves, develop themselves more in order to get rid of the situation with the least damage and are more conscious than their colleagues.

REFERENCES

Acar, H.H., & Şentürk, N. (1997). Orman işçiliği ve Doğu Karadeniz Bölgesindeki durumu üzerine bir araştırma. *İ.Ü. Orman Fakültesi Dergisi*, *47*(1-4), 46- 47.

Akıllı, H., & Aydoğdu, Ö. (2013). İş sağliği ve güvenliğinin önemi. *Maden Tetkik ve Arama Genel Müdürlüğü, MTA Doğal Kaynaklar ve Ekonomi Bülteni*, *16*.

Aksu, C. (2011). Sürdürülebilir kalkınma ve çevre, http://cevre.mf.duzce.edu.tr/Dokumanlar/cevre_mf/Dosyalar/S%C3%9CRD%C3%9CR%C3%9CLEB%C4%B0L%C4%B0R%20Kalk%C4%B1nma%20ve%20%C3%87evre.pdf

Aktay, N. (2014). İş sağlığı ve güvenliği eğitiminin iş güvenliği kültürüne etkisi (Yayımlanmamış Yüksek Lisans Tezi). İstanbul Üniversitesi Sosyal Bilimler Enstitüsü, İstanbul.

4857 Sayılı İş Kanunu.

6331 Sayılı İş Sağlığı ve Güvenliği Kanunu.

Balkır, Z.G. (2012). İş sağlığı ve güvenliği hakkının korunması: İşverenin İş sağlığı ve güvenliği organizasyonu. *Sosyal Güvenlik Dergisi*, *1*, 56-91.

Başkan, O. (2004). Gölbaşı yöresi topraklarının mühendislik-fiziksel özellik ilişkilerinde jeoistatistik uygulaması (Yayımlanmamış Doktora Tezi). Ankara Üniversitesi Fen Bilimleri Enstitüsü, Ankara.

Bayrakçeken, G. (2018). Sürdürülebilir kalkınma ve toplam faktör verimliliği için elverişli ortam, http://tfvp.org

Camkurt, M.Z. (2013). Çalışanların kişisel özelliklerinin iş kazalarının meydana gelmesi üzerindeki etkisi. *TÜHİS İş Hukuku ve İktisat Dergisi*, *24*(1), 74-76.

Cox, S., & Flin, R. (1998). Safety Culture: Philosopher's stone or man of straw?. *Work & Stress*, *12*(3), 189-201.

ÇASGEM (2014). *Avrupa Birliği'nde iş sağlığı ve güvenliği*. Ankara: Çalışma ve Sosyal Güvenlik Eğitim ve Araştırma Merkezi.

ÇASGEM (2017). Türkiye'de iş sağlığı ve güvenliği algısı. Ankara: Uzerler Matbaacılık Tanıtım Sanayi Tic. Ltd.

Çetin, M., & Karatay Gögül, P. (2015). Türkiye'deki iş kazaları ve işçi ölümlerinin ekonomik boyutu ve politika önerisi. Sosyoloji Konferansları, No: 51.

ÇSGB (2016). *Orman işlerinde iş sağlığı ve güvenliği*. Ankara: Çalışma ve Sosyal Güvenlik Bakanlığı Genel Yayın No: 49.

DPT (2014). *10. kalkınma planı*. Ankara: Devlet Planlama Teşkilatı.

Engür, M.O. (2014). *Odun üretiminde çalışanların eğitimi ağaç kesme ve boylama operatörü*. Ankara: CTA Ltd.

Erol, S. (2015). İş sağlığı ve güvenliği konusunda işveren, çalışan ve devletin rolü. *ASSAM Uluslararası Hakemli Dergi*, *4*, 116-138.

EUROSTAT (2011). Sürdürülebilir kalkınma göstergeleri. http://epp.eurostat.ec.europa.eu/portal/page/portal/sdi/indicators

FAO (2016). Occupational Health and Safety in Forestry – Issues of Relevance in Tropical Concessions, http://www.fao.org/forestry/45322- 0d44ab967c-53c998c7d84672da59993b0.pdf

Gifford, M. (2009). *Safety and health in the European forestry sector – The impact of more open markets and of increased regulation*. Working Paper No 264.

Güler, U. (2017). Peyzaj uygulama alanlarında iş sağlığı ve güvenliği: Ankara örneğinde şantiye hizmetlerinin değerlendirilmesi (Yayımlanmamış Yüksek Lisans Tezi). Ankara Üniversitesi Fen Bilimleri Enstitüsü, Ankara.

Gümüş, S., & Türk, T. (2007). *Orman yangın işçilerinde işçi sağlığı ve güvenlik verilerinin tespitine yönelik araştırma*. Ankara: Seçkin Yayıncılık.

ILO (1998). Safety and health in forestry work, https://www.ilo.org/wcmsp5/groups/public/---ed_protect/---protrav/---safework/documents/normativeinstrument/wcms_107793.pdf

Kol, İ. (2016). İş sağlığı ve güvenliğinde operasyonel disiplin (Yayımlanmamış Yüksek Lisans Tezi). Gedik Üniversitesi Sosyal Bilimler Enstitüsü, İstanbul.

Menemencioğlu, K. (2012). Tarım ve orman işçiliğinde çalışma yeri koşulları ve karşılaşılan sorunlar. *Türk Bilimsel Derlemeler Dergisi*, *5* (2), 72-76

Menemencioğlu, K. (2006). Ormancılıkta üretim işlerinde çalışma koşulları ve iş kazaları üzerine bir araştırma. *Süleyman Demirel Üniversitesi Orman Fakültesi Dergisi*, *2*(1), 1- 4.

OGM (2019). OGM Personel Dairesi Başkanlığı Hukuk Müşavirliği, Nakdi ve Yangın Tazminatı Ödemeleri.

Özkan, T., & Lajunen, T. (2003). Güvenlik kültürü ve iklimi. *Pivolka*, *2*(10), 3-4.

Şahin, H. (1987). Türkiye'de istihdam sorununun nedenleri ve çözüm yolları. *İstanbul Üniversitesi İktisat Fakültesi Mecmuası*, *43*, 335-345.

Şerifoğlu, U. K., & Sungur, E. (2007). İşletmelerde sağlık ve güvenlik kültürünün oluşturulması; tepe yönetimin rolü ve kurum içi iletişim olanaklarının kullanımı. *İstanbul Üniversitesi İşletme İktisadı Enstitüsü Yönetim Dergisi*, *58*, 1-17.

T.C. Kalkınma Bakanlığı (2014). Türkiye 10. Kalkınma Planı (2014-2018) Sürdürülebilir Orman Yönetimi Özel İhtisas Komisyonu Raporu, Ankara, Türkiye.

TPFV.ORG (2019). Toplam Faktör Verimliliği Nedir? http://tfvp.org/tfv-nedir/

Tunay, M., & Bozkurt, A. (2018). Ormancılık çalışmalarında iş güvenliği analizinin uygulanması. *Mühendislik Bilimleri ve Tasarım Dergisi*, *16*(2), 195-

202.

Tüzüner, V. L., & Özaslan, B. Ö. (2011). Hastanelerde iş sağlığı ve güvenliği uygulamalarının değerlendirilmesine yönelik bir araştırma. *İstanbul Üniversitesi İşletme Fakültesi Dergisi*, *2*, 138-154.

Ulusoy, M.E. (2013). İşverenin iş sağlığı ve güvenliği açısından işyerinde örgütlenme yükümlülüğü (Yayımlanmamış Yüksek Lisans Tezi). Selçuk Üniversitesi Sosyal Bilimler Enstitüsü, Konya.

Uslu, V. (2014). İşletmelerde iş güvenliği performansı ve iş güvenliği kültürü algılamaları arasındaki ilişki: Eskişehir ili metal sektöründe bir araştırma (Yayımlanmamış Yüksek Lisans Tezi). Eskişehir Osmangazi Üniversitesi Sosyal Bilimler Enstitüsü, Eskişehir.

Usmen, M., & Baradan, S. (2011). İnşaat sektöründe işçi sağlığı ve iş güvenliği alanındaki iyileştirmeleri etkileyen faktörler: ABD örneği. *Türkiye Mühendislik Haberleri*, *5*, 41- 48.

Yalçın, A. Z. (2016). Sürdürülebilir kalkınma için yeşil ekonomi düşüncesi ve mali politikalar, çankırı karatekin üniversitesi. *İktisadi ve İdari Bilimler Fakültesi Dergisi*, *6* (1), 749-775.

Yılmaz, A.İ. (2013). İş sağlığı ve güvenliğinde kaza zinciri teorisinin önemi ile açık işletmelerdeki tehlikeli hareket ve tehlikeli durumlar. *Yer Altı Kaynakları Dergisi*, *3*, 32.

Yilmaz, E. A., Öziç, H., & Akbulut, A. (2016). Güvenlik özgürlük dengesi bağlamında Türkiye'deki "iç güvenlik paketi" tartışmaları. *Dumlupınar Üniversitesi Sosyal Bilimler Dergisi*, 132-146.

Yiğit, A. (2011). *İş güvenliği ve işçi sağlığı*. Bursa: Alfa Aktüel Yayınları.

Yorulmaz, M. (2016). Tersane işletmelerinde örgütsel güvenlik ikliminin incelenmesi. *International Journal of Social Science*, *46*, 304-318.

CHAPTER 4

SIMULATION IN PARTICLE PHYSICS

Çağın KAMIŞCIOĞLU[1]

1 Assoc. Prof. Dr. Ankara University, Faculty of Engineering, Physics Engineering Department, Ankara, Türkiye ORCID:0000-0003-2610-6447

1.Introduction

The aim of physics is to understand the events, functioning and order in the universe, to make inferences for the future, to develop new concepts, theories and models, and to put them into practice. For this purpose, it regularly examines, observes, interprets and explains the events in the universe and nature. It examines all relations related to matter, motion and energy in the universe with systematic and scientific approaches. With these studies, it makes significant contributions to the understanding of the events in nature and the universe, and gradually to the development of humanity. For this reason, it is difficult to explain the events in nature without physical science. In other words, many events in the environment we live in are explained by the laws, theories and rules of physical science. In this process, various branches of physical science are used. Among these, particle physics has a special importance (Kamışcıoğlu, 2017; 2020).

Particle physics is the science of the smallest particle or particle, which includes studies aimed at finding the basic building blocks of the universe. These are also called subatomic particles. Subatomic particles combine among themselves to form the earth, stars, other planets, that is, the entire universe. However, different branches of science examine each dimension in the universe. Particle physics, on the other hand, focuses on the internal structure of the atomic nucleus and studies at the subatomic level. Many particles reaching our Earth from space are of high energy. But detecting these particles or discovering their nature is not easy. For this, experimental environments are required. In experimental physics, the physical state realized in the experimental environment is examined. This situation is not easy for high-energy or subatomic particles. Special mechanisms and advanced technology are required to obtain these particles or to increase them to high energies. For this purpose, CERN, known today by the abbreviation of the European Center for Nuclear Research or its French name Conseil Européen pour la Recherche Nucléaire, is the world's largest particle physics laboratory. With its establishment in 1954, it is a laboratory that shapes particle physics today. In this laboratory, subatomic particles are studied with various projects and collaborations. In the projects, the characteristic features of subatomic particles are tried to be revealed. The particle beams obtained for this purpose are collided with each other with different particles or nuclei. These interactions are resolved by detecting the resulting particles. However, a lot of data is collected in experiments (CERN, 2023).

To convert the vast amounts of data collected in particle collider experiments into precise measurements of nature, particle physicists need to build models in high-dimensional data. To this end, experimental particle physicists use complex computer simulations for the occurrence of ele-

mentary particle collisions, particle decays, interactions with the detector, particles resulting from the interaction, and their detection and kinematic investigations.

Simulation modeling is essentially imitating the real world. However, this imitation is created safely and efficiently. Thus, it provides an important analysis method that is easily verified and understood. With this aspect, it examines complex systems and asks "what if?" They offer clear solutions for scenarios. Therefore, Particle Physics Simulations are definitely useful and complementary to subatomic physics. Especially in the process of researching and examining high-energy particles, simulations are very supportive.

2.What is Simulation?

Simulation is a concept that is widely used in fields such as education, health, economy, agriculture, industry, aviation and shipping. Various explanations have been made in dictionaries, encyclopedias and scientific books to explain this concept. Some of the important ones are listed below.

Simulation is explained as "simulation" in Turkish Language Society Current Turkish Dictionary (TDK,2023). This concept comes from the English word "simulation", which means "to do the same or the same, to imitate, to imitate". In general, it is the reenactment of an event or situation in accordance with its originality. For this, a real event or process is visualized based on time. So an artificial model is created.

In scientific books, simulation is described as "a mathematical model that describes the operation of a real-world system over time". For seismication, artificial records of a real system are first created, and inferences are made by observing and examining them. Thus, both real and conceptual systems are modeled and studied. The simulation model is used to describe and analyze the operation of a real system, whether done manually or by computer (Banks & Carson, 1984).

In some sources, simulation is given as "time-based imitation of a system, operation and process in the real world". The evolving behavior of a system over time is studied by developing a simulation model. This developed model creates a conceptual framework and defines the system. The model usually contains a set of assumptions about the functioning of the system. These assumptions are expressed in mathematical, logical and symbolic relationships between entities or objects. Simulation is also an indispensable problem-solving tool. It becomes an important tool for solving real world problems (Banks, Carson, Nelson & Nicol, 2005).

In Encyclopedia Britannica, simulation is given as "a research or teaching technique that reproduces real events and processes in education, science and industry under certain test conditions" (Encyclopedia Britan-

nica, 2023). In this explanation, simulation is considered as both a research and a teaching technique.

As can be seen, simulation is the process of creating an artificial model in order to better understand a theoretical or real-world system, operation or process and to evaluate different strategies. This developed artificial model is used to conduct various experiments, to investigate and reveal the system in detail. In this respect, simulation is both a modeling and a research and teaching technique.

3. Benefits

As a modeling technique, simulation has three basic stages. These are information, scenario and analysis. Preparing each step is a mathematical process that requires very complex operations. First, the rules, relations and operating process of the real system are determined together with various variables. Then, the interaction of events, new situations that develop as the simulation progresses, and even new rules are created. Thus, it includes many design options such as text, test, animation, visuals, vocalization, practice, application. The simulation tools used in this process range from paper-pencil, board game production to complex computer-aided interactive systems (Encyclopedia Britannica, 2023). As a modeling technique, it provides a number of benefits for conducting various experiments, investigating the represented system in detail, solving existing problems and teaching students well.

Simulation as a research technique provides various benefits to practitioners in applied sciences. Experiment simulations, for example, allow researchers to perform experiments or demonstrations in a "virtual lab environment" without using rare materials or expensive machinery. In the automotive industry, sample automobiles are subjected to wind tunnel tests. In particular, computer simulations save hundreds of hours devoted to pre-example generation and testing. Time compression is another cost-saving feature in simulation. Events that have lasted for centuries are brought to life in a few minutes in the simulation. For example, astronomers can report events that take millions of years, such as the collision of two galaxies, in a few minutes with computer simulations to demonstrate theoretical explanations of galactic movements (Banks & Carson, 1984).

Simulation as a teaching technique prevents false learning by providing students with appropriate solutions on vital issues. In this respect, it provides important contributions to students. Simulation is an active teaching technique that supports learning. It facilitates gaining knowledge and skills, reinforcing learning, developing self-confidence, group discussion and teamwork. For example, in the field of medicine, it helps young doctors to make rapid diagnosis and treatment to keep the patient alive. Air-

craft pilot trainees learn what to do in realistic and emergency situations with advanced simulation devices such as flight simulators. Simulations enable students to better understand the complex effects of physical and social environmental factors. For example, agricultural students observe how to grow good rice under the constant threat of pests, fire, and floods (Encyclopedia Britannica, 2023).

4. Types of Simulation

Simulation is used in different fields such as education, health, economy, industry, aviation, shipping and agriculture. Therefore, there are several types and cover a wide range. Researchers are doing some studies to classify them. However, these studies are far from covering all simulations in the field. Based on the studies in the field by Myers (2012) and especially Axelrod's (2007) classification of simulation in social sciences, four types of simulations were determined. These are listed under the titles of entertainment, evaluation, experimentation and educational simulations according to purpose (Axelrod, 2007; Myers, 2012).

Entertainment Simulations: The primary purpose of these is to entertain, excite, satisfy or engage the user on an emotional level. Entertainment simulations often include video games. These simulations are designed for entertainment rather than learning (Myers, 2012).

Evaluation Simulations: These are used for testing and evaluating various system or device designs. For example, the impact of a traffic management system on traffic in city planning or simulations used in chemistry to evaluate the biodegradability of compounds (Punch vd., 1996).

Experiment Simulations: These are designed to experiment or gain experience. It is used to model a scientific experiment or a situation involving various analysis and decision making (Myers, 2012). For example, supporting a theory or discovery, creating new relationships or principles, solving existing problems. According to some researchers, these simulations with deductive or inductive content are more effective and are accepted as "a third way of doing science" (Axelrod, 2007).

Educational Simulations: These are used for education and training purposes. The general aim is to transfer the knowledge in the field and the skills gained in practice. Proponents of educational simulations suggest simplifying some aspects of simulations so that students can analyze them better. In educational simulations, students are given the opportunity to control the system in order to understand the basis of a real system, learn all its principles and gain skills (Garson, 2009; Maier & Grossler, 2000).

Educational simulations are divided into two subspecies by some researchers. For example, Clark (2005) discusses e*ducational* simulations in

two sub-titles as informative and operational. Informative ones are models based on theoretical principles and concepts that give information about facts about a system. They are designed for knowledge teaching. Transactional ones are models based on the sequence of stages and processes implemented in a system. These include field-specific principles or processes, as well as skills such as research, discovery, problem solving, and learning by experiment. In other words, it is designed for the purpose of gaining skills (Clark, 2005).

A similar understanding is seen in research and studies by Alessi & Trollip (2001). As a result of a series of investigations, these researchers group the training simulations into two groups as instructive and skill-building. Each of these has a different purpose and content. A qualified training simulation unites these categories.

1) Instructive Simulations: The main purpose of didactic simulations is "What is this?" is to answer the question. There are two types in this group, physical and repeated simulations (Myers, 2012)

a.Physical simulations: In these simulation programs, a physical object or event is shown on the computer screen. It is aimed for the student to examine and learn this in detail. For example, simulations such as photosynthesis event in basic sciences, chemical reactions, electrical circuits, electric motor in engineering, computer circuits are examples of this.

b. Repeated simulations: These are very similar to physical simulations. It is intended to teach an object or event like them. However, here, the event is examined in more detail by changing the simulation parameters and the process is repeated with different parameters until the desired result is reached. These are also called scientific discovery simulations. The student runs them over and over, changing the parameters and observing the results. For example, time is slowed down and accelerated, very slow or very fast events are easily examined. The student sees the stages of development more easily. Genetic biology experiments can be given as an example (Alessi & Trollip, 2001).

2) Skill Simulations: The purpose of these is "How to do it?" is to answer the question. Process and conditional simulations aimed at gaining skills are covered in this group.

a. Process simulations: The purpose of using process simulations is to teach the necessary steps and stages to reach a goal. Flight simulation programs, programs showing the operation of a device or troubleshooting programs can be given as examples of these simulations (Myers, 2012).

b. Conditional simulations: These simulations are about the behavior of individuals or institutions under different situations and conditions.

Here, alternative solutions are presented to the student in different situations and it is aimed to see the results. These simulations are mostly used in medicine, law and business world (Alessi & Trollip, 2001).

5. Simulation in Particle Physics

Simulation becomes even more important in particle physics. Because particle physics aims to find the most basic building blocks of the universe. In other words, it is the science of the smallest particle or particle. It is studied to observe the internal structure of the atomic nucleus and the subatomic level. In particle physics, it is investigated what the matter consists of and for this purpose, it is examined down to the smallest particle. Their relations with each other, their interactions and their basic features are emphasized. Observing subatomic particles in practice is quite difficult. It is not possible to observe directly under normal conditions, since they are invisible and their lifetime is very short. For this reason, it is tried to be observed through special sensors or experiments (Kamışcıoğlu, 2022). To carry out these researches, planned and regular experiments are carried out. In this process, the main components that make up the universe are determined, defined, reconstructed and decomposed in a controlled way (Kamışcıoğlu, 2017). Simulation provides important contributions to these experiments.

In many scientific fields that rely on statistical inference, such as experimental particle physics, simulations are used to bridge or map theoretical models to experimental data. Thus, model predictions can be tested against experimental results.

A simulation applies mathematical methods and methods to complex analysis or big data and predicts what might happen, generates actions or scenarios. So in what situations is this simulation used?

When it is not possible to do the real experiment,

When the real experiment is too expensive or too long,

When the planned experiment has not been implemented yet,

When the real experiment is dangerous.

Today, it is possible to generate data using various simulation tools such as MadGraph (Alwall, J vd. 2014), Sherpa (Gleisberg, T., vd. 2009), Pythia (Sjöstrand, T., vd. 2015), Herwig (Corcella, G. vd.2001) and GEANT4 (Collaboration, T.G, 2003; Geant, 2023). The term used for data from these instruments is Monte Carlo.

5.1. Monte Carlo

Monte Carlo Method was invented by John von Neumann and Stanislaw Ulam during World War II to improve decision making under uncertain conditions. It is named after a well-known casino town called Monaco. The reason for this is that chance and random results, which form the basis of the modeling approach, also form the basis of games such as dice and roulette (Metropolis, 1987).

Monte Carlo assumes that the system can be described by modelable probability density functions (PDF) without the need to write equations. In this method, random distributions are sampled using appropriate computer codes and the behavior of a physical system or state is reconstructed. With Monte Carlo Simulations it is possible to design, optimize and analyze a physical state. So it is also very useful in High Energy Physics. For example,

- in experiments where particles with high data are collided,

- to reproduce collision events,

- to obtain various kinematic distributions,

- to reconstruct and understand the response of the detector,

- to detect system variables,

- to reveal the interaction of particles with matter is very important for background modeling

- developing new idea and efficiency calculations.

For a high-energy particle, certain steps are followed in the simulation. However, if it is desired to be basically glazed, it starts with the random generation of one or more particles with a certain momentum with the help of a generator. The particle then moves freely to interact. It performs an interaction depending on the possible geometric or physical process defined. Boundary conditions, environment, etc. parameters are taken into account. As a result of the interaction, new particles can be produced, destroyed or scattered. This produced particle is tracked depending on the parameters tested. The result is this interaction will be the output.

The Monte Carlo method focuses on repeated random samples. As seen in Figure 1, a Monte Carlo simulation first assigns a random value to the variable with uncertainty. The created model is run and a result is obtained. Then the process is repeated so that many different values are assigned to the relevant variable. After the simulation is complete, the results are averaged to arrive at an interpretation.

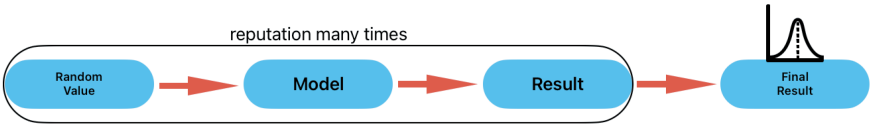

Figure 1. The Monte Carlo method

Monte Carlo simulation is crucial in all phases of experimental particle physics in terms of the design and development of the detector concept, exploration of the physics scope, modelling, optimization of the reconstruction software, and analysis results. The two most important core parts for this simulation software package are modeling and detector simulation. While modeling creates a physics background, detector modeling involves particle and detector interaction.

CompHep, CalcHEP, CMSJet, ORCA, which are used in High Energy Physics at the modeling stage, can be given as examples. As event generators, Pythia, Geant4, Herwig, Sherpa can be used for full simulation or for special purposes aMC@NLO, POWHEG, Vincia, Dire are examples. When we look at the statistics in High Energy Physics, the Geant4 simulation toolkit holds the lead in terms of the number of citations of recent publications (Ayyıldız, 2016; Soyez, 2020).

Today, high-performance and high-tech collider experiments are carried out in High Energy Physics. In these experiments where new concepts are tested, each collision of particles with a detector or another particle is called an "event". These events are quite complex. Each one of them should be analyzed one by one and their physical processes should be revealed. For this reason, a series of signals or traces occurring in the detector are the most important elements.

In the last stage, as given in Figure 2, the data obtained from the simulation and the data obtained from the nature are compared. The validity of the detector is determined while the used physics model or data acceptance becomes clear. Differences, if any, are reviewed and interpreted.

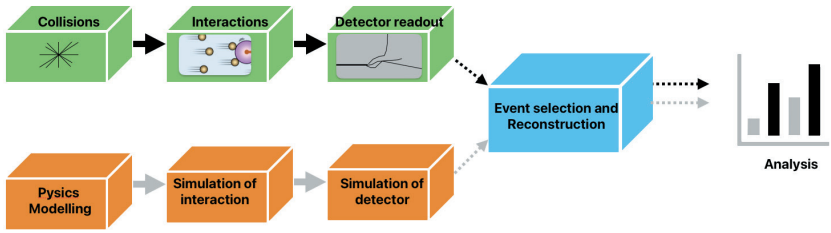

Figure 2. The Monte Carlo method step vs nature data steps.

6. Conclusion

As can be seen, simulation is widely used in many disciplines to serve different purposes. In Particle Physics, as in other disciplines, simulation has proven itself and has shown tangible successes. The widespread use of GEANT4 demonstrates its impact on experimental fields. There is a need for advanced simulation methods that can model future experiments and facilities. For this purpose, more advanced simulations should be planned and necessary resources should be created for existing and future experiments by cooperating with various fields.

References

Alessi S. M.& Trollip S. R. (2001). Multimedia for Learning: Methods and Developments. Needham Heights, Massachusetts: Allyn and Bacon.

Alwall, J., Frederix, R., Frixione, S., Hirschi, V., Maltoni, F., Mattelaer, O., Shao, H. S., Stelzer, T., Torrielli, P., and Zaro, M.(2014). The automated computation of tree-level and next-to- leading order differential cross sections, and their matching to parton shower simulations, Journal of High Energy Physics 2014 (2014) 7, 79.

Axelrod, R. (2007). Advancing the art of simulation in the social sciences. In J. P. Rennard (Ed.), *Handbook of research on nature inspired computing for economics and management* (s. 90-100). Hershey, PA: Idea Group Reference.

Ayyıldız, M.(2016).Yüksek Enerji Fiziğinde Kullanılan Simülasyon Teknikleri. (Yüksek Lisans Tezi).İnönü Üniversitesi, Fen Bilimleri Enstitüsü, Fizik Anabilim Dalı.

Banks, J. & Carson, J. S. (1984). Discrete-Event System Simulation. Prentice-Hall, NewJersey.

Banks,J., Carson,J.S. Nelson,B.L, & Nicol,D.M. (2005). *Discrete-Event System Simulation,* Fourt Edition, Pearson New International Edition.

CERN (2023) https://home.cern/about adresinden 14 mart 2023 tarihinde erişilmiştir.

Clark, R. C. (2005). Multimedia learning in e-courses. In R. Mayer (Ed.), *The Cambridge handbook of multimedia learning* (s. 589-616). New York: Cambridg University Press.

Collaboration, T. G.(2003). Geant4 – a simulation toolkit, Nuclear Instruments and Methods in Physics Research Section A: Accelerators, Spectrometers, Detectors and Associated Equipment 506 (2003) 3, 250.

Corcella, G., Knowles, I. G., Marchesini, G., Moretti, S., Odagiri, K., Richardson, P., Seymour, M. H., and Webber, B. R.(2001). HERWIG 6: An Event generator for hadron emission reactions with interfering gluons (including supersymmetric processes), JHEP 01 (2001) 10.

Encyclopedia Britannica (2023). Simulation | scientific method - Encyclopedia Britannica https://www.britannica.com. adresinden 11 şubat 2023 tarihinde erişilmiştir.

Garson, G. D. (2009). Computerized simulation in the social sciences. *Simulation & Gaming, 40*(2), s. 267-279.

Geant (2023) https://geant4.web.cern.ch/ adresinden 14 mart 2023 tarihinde erişilmiştir.

Gleisberg, T., Hoeche, S., Krauss, F., Schonherr, M., Schumann, S., Siegert, F.,

and Winter, J. (2009). Event generation with SHERPA 1.1, JHEP 02 (2009) 7.

Kamışcıoğlu, Ç. (2017). OPERA Dedektöründeki Nötrino-Kurşun Yüklü Akım Etkileşmelerinde Hadron Çokluk Dağılımlarının İncelenmesi, (Yayımlanmamış doktora tezi). Ankara Üniversitesi, Fen Bilimleri Enstitüsü, Ankara.

Kamışcıoğlu, Ç. (2020). *Parçacık Fiziğindeki Gelişmeler ve Yönelimler,* Güncel Fen Bilimleri Çalışmaları, Ankara: Akademisyen Kitabevi A.Ş.,E-ISBN 978-605-258-877-2, 1.Baskı

Kamışcıoğlu, Ç. (2022). Investigation of High School Textbooks in terms of Particle Physics. Parçacık Fiziği Açısından Lise Ders Kitaplarının İncelenmesi. *The Journal of Limitless Education and Research, Sınırsız Eğitim ve Araştırma Dergisi, 7*(1), 131 - 167.

Maier, F. H., & Grossler, A. (2000). What are we talking about--A taxonomy of computer simulations to support learning. *System Dynamics Review, 6*(2), 135- 148.

Metropolis, N. (1987). The Beginning of the Monte Carlo Method. Los Alamos Science Special Issue 1987.Vol. 15, 1987, pp. 125-130.

Myers,R.D.(2012). Analyzing Interaction Patterns To Verify A Sımulation/Game Model, Doctor of Philosophy in the Department of Instructional Systems Technology of the School of Education, Indiana University

Punch, B., Patton, A., Wight, K., Larson, B., Masscheleyn, P., & Forney, L. (1996). A biodegradability evaluation and simulation system (BESS) based on knowledge of biodegradation pathways. In W. J. G. M. Peijnenburg & J. Damborsky (Eds.), *Biodegradability Prediction* (pp. 65-73). The Netherlands: Kluwer Academic Publishers.

Sjöstrand, T., Ask, S., Christiansen, J. R., Corke, R., Desai, N., Ilten, P., Mrenna, S., Prestel, S., Rasmussen, C. O., and Skands, P. Z.(2015). An Introduction to PYTHIA 8.2, Comput. Phys. Commun. 191 (2015) 159.

Soyez, G.(2020).Event Generators for High-Energy Physics,(e)LHCP 2020, May 25-29 2020,IPhT, CNRS, CEA Saclay.

CHAPTER 5

IMPORTANCE OF ANALYSIS PHENOLIC COMPOUNDS BY HPLC

Elif APAYDIN[1]

1 Giresun University, Central Research Laboratory Application and Research Center

1. Reactive oxygen species (ROS)

While oxidation is a very important process for living organisms, oxygen is known as the molecule of both life and death. Oxygen is essential for aerobes but lethal or growth arresting for anaerobes. Incomplete reduction of oxygen also leads to the formation of reactive oxygen species (ROS). These cell-damaging reactive oxygen species cause cell death when antioxidant defense systems are insufficient. Reactive oxygen species need to be at low levels to function in most biochemical processes with intramolecular transduction in cell differentiation and cell growth arrest, immune protection and defense against microorganisms (Ghosh & Myers, 1998; Yin, Yin & He, 1995; Bae, Kang & Seo, 1997; Lee, Galoforo & Berns, 1998). The occurrence of high levels of reactive oxygen species, or the inability to remove them, can lead to oxidative stress, which can cause very serious metabolic breakdowns and damage biological molecules (Chopra & Wallace, 1998; Wojtaszek, 1997). Antioxidants are generally defined as substances that prevent the formation of free radicals. Antioxidants, which are naturally present in metabolism or ingested with food, significantly delay or inhibit the oxidation process when present in low concentrations. In other words, an antioxidant is a substance that significantly delays/prevents the oxidation of an oxidizable substrate such as lipids, proteins, carbohydrates and nucleic acids when present in lower concentrations(Yin, Yin & He, 1995). Some free radicals and their damages are given in the Table 1.

Table 1 *Free Radicals and Properties of Some Free Radical Producing Species (Halliwell, 1994)*

Name	Symbol	Property
Hydrogen radical	$H^{\bullet}$	The simplest known radical
Hydroxyl radical	$OH^{\bullet}$	The most reactive oxygen metabolite radical. Attacks all molecules in the human body
Superoxide radical	$O_2^{\bullet-}$	First intermediate product of oxygen metabolism
Hydrogen peroxide	H_2O_2	Low reactivity, poor molecular damage properties
Singlet oxygen	O_2	Short half-life, strongly oxidative form
Perhydroxy radical	$HO_2^{\bullet-}$	Rapidly dissolves in lipids and increases lipid peroxidation
Peroxyl radical	$ROO^{\bullet-}$	Less effective than perhydroxyl, lecolyzes lipids
Trichloromethyl radical	$CCl_3^{\bullet}$	CCl4 metabolism, a radical produced in the liver
Thiyl radical	$RS^{\bullet}$	General name for species with sulfur and unpaired electrons

Alkoxyl radical	$RO^{\bullet}$	Organic peroxides are broken down and oxygen metabolites are formed.
Nitrogen monoxide	NO	It is produced in vivo from L-arginine
Nitrogen dioxide	NO_2	It is produced by the reaction of NO with oxygen. Found in polluted air, cigarette smoke, etc.

2. Phenolic Compounds

Phenolic compounds are formed by the direct bonding of one or more phenolic groups to the aromatic ring. The term phenolic covers a very wide and various range of compounds, and the grouping is also very diverse. Harborne and Simmonds (1964) made a classification according to the number of carbons in the molecule (Harborne & Simmonds, 1964).

Table 2 *Classification Phenols According to The Number of Carbons*

Structure	Symbol
C_6	simple phenolics
C_6-C_1	phenolic acids
C_6-C_2	phenylacetic acids and acetophenones
C_6-C_3	cinnamyl aldehydes, cinnamic acids
C_6-C_3	coumarins
C_{15}	flavan, flavanone, flavanonol, anthocyanidins
C_{18}	betacyanines

Antioxidants are molecules responsible for restricting radical formation, inhibiting radical reactions, neutralizing the radicals formed and eliminating damaged molecules with the mechanisms of action of phenolic and flavonoids in their structures (Aruoma, Spencer, Warren, Jenner, Butler & Halliwell, 1997). Flavonoids are the most abundant phenolic compounds found in plants in the human diet. Food origin flavonoids, flavonols and phenolic compounds such as kaempferol, gallic acid, quercetin and myricetin have a rich biological spectrum including antibacterial, antiviral, antiallergic and antioxidant (Huang, Ou & Prior, 2005). There are studies suggesting that flavonoid consumption reduces coronary heart disease (Hertog, Feskens, Hollman, Katan & Kromhout, 2005). In a study conducted in Japan, it was reported that plasma total cholesterol and LDL-cholesterol concentrations decreased with increased intake of flavonoids (quercetin, myricetin, kaempferol and luteolin), while another study in Finland showed that consumption of apples and onions rich in quercetin decreased chronary mortality (Knekt,Jarvinen,Reunanen & Maatela, 1996).

3. HPLC (High Performance Liquid Chromatography)

Phenolic and flavonoid substances are known to function as free radical scavengers or reaction complements and exhibit antioxidant behavior that prevents oxidation. It is possible to detect these behaviors by some spectroscopic and chromatographic methods. Since these compounds are UV active and absorb in the visible region, they can be analyzed by some spectroscopic and chromatographic methods. High performance liquid chromatography (HPLC) is a powerful enstrumental technique for the rapid analysis and identification of secondary metabolites and bioactive compounds in plant samples. It provides very efficient and fast analytical separation (Rice Evans, Miller, Bolwell Bramley & Pridham, 1995; Kalaycıoğlu & Öner, 1994).Chromatography was first used in 1906 by a Russian botanist Tswett. He was able to separate pigments in leaves using a $CaCO_3$ column and petroleum ether.

Figure 1 *Russian botanist Mikhail Tswett*

Figure 2 *The First Seperation of Pigments*

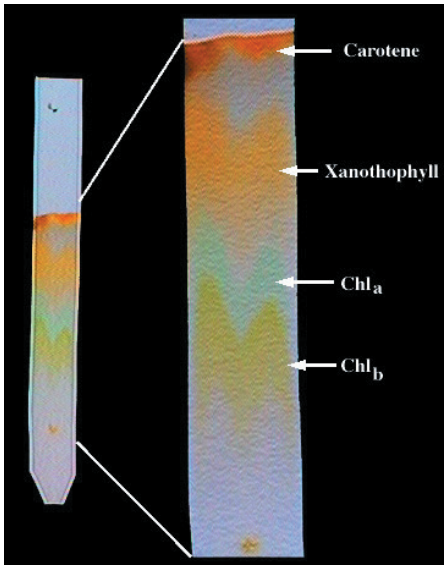

Figure 3 *Classical Column Chromatography*

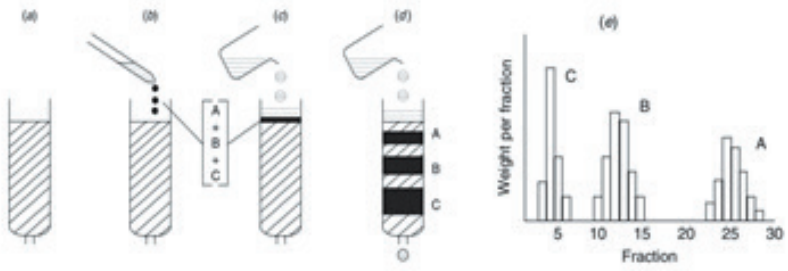

In chromatographic separation, substances are separated in two immiscible phases. In HPLC, the mobile phase runs the analytes through the column as the stationary phase and transfers them to the detector system. The retention time (tR) of each substance in the mixture is determined by its chemical affinity for the mobile phase. Substances that are more affinities to the mobile phase move faster. The concentration profile of each substance leaving the column is called a peak. The table of peaks is called a chromatogram (Bidlingmeyer, 1993).

Figure 4 *Simple Schematic Representation of HPLC Units (https://www.knauer.net/en/Systems)*

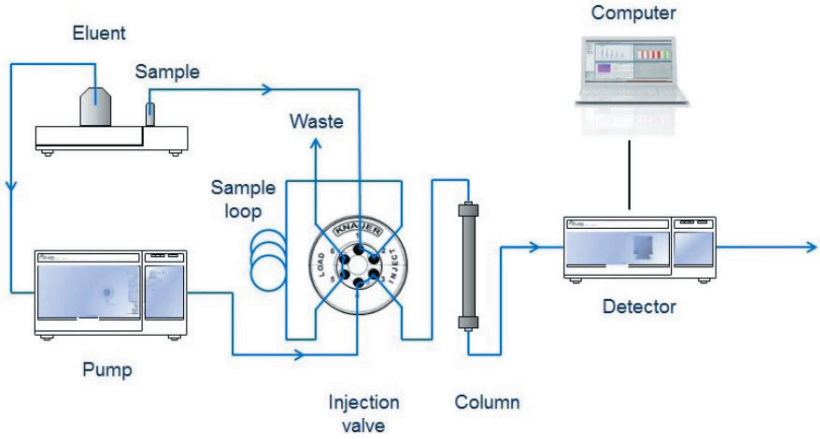

Fig. 1 Schematic layout of a HPLC system

3.1. Pump

The liquid chromatography pumps transport the mobile phase through theHPLC system to other units in a controlled and accurate manner at a flow rate selected according to the column type. It provides 200-600 atm (2000-5000 psi or 20-60 MPa) pressure. The processes in which various mobile phases are used for different periods of time with two or more pump systems are known as gradient elution systems, while systems in which a single mobile phase is used are defined as isocratic elution systems (Dorsey, Cooper, Siles, Foley & Barth, 1996).

The most important factor in HPLC separations is the polarity of the stationary phase and the liquid mobile phase. So it is difined as normal phase and reverse phase chromatography. If the stationary phase is polar and the mobile phase is apolar, it is defined as normal phase chromatography, while if the stationary phase is apolar and the mobile phase is polar, it is defined as reverse phase chromatography.

3.2. Autosampler/ Injection:

Wiht recent technology manuel injection has been end, automatic enjection with software control.

Figure 5 *Six-Port Sample Injection Valve*

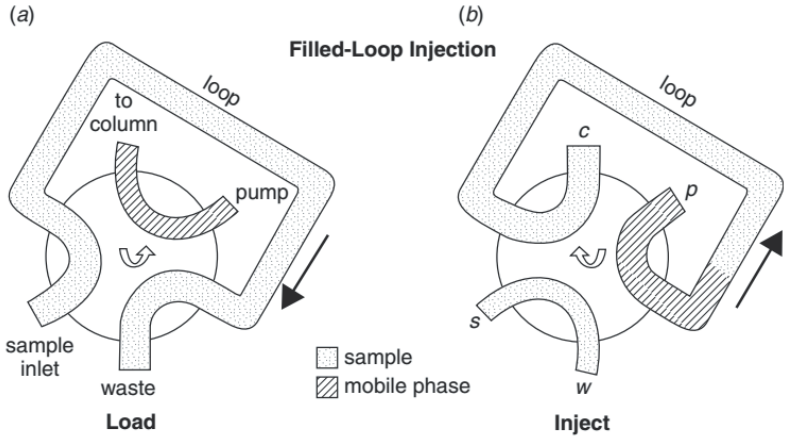

(a) while loading position; (b) while injection position. The direction of the arrow indicates that flow; s, sample inlet; w, to waste; p, mobile phase c, to column (Braumann, Weber & Grimme, 1983)

Figure 6 *Manuel Injection and Auto-Injection with Oto-Sampler*

3.3. HPLC Columns

In the 1960s column was the heart of HPLC system. Column was glass materials but As separations became more difficult, pressure became necessary and pressure-resistant metals were used. Generally the support material is porous-silica particles of column. The performance of an HPLC system is determined by the separation performed on the column that is the selection of the right column packing and the efficiency of the packing.

- **Particle Size:**

The size of the column filler (dp) is generally expressed in micrometers (µm). In validated columns, all particles are equal in size and the dimensions are specified by the manufacturer on the column certificate. There is a contrast station between particle size column efficiency that sep-

aration efficiency increases as the size of the particle filler used decreases.

Precolumns are short that been ≤5-cm and known guard column, used to protect the analytical columns from compenent residues. Analytical HPLC columns are 5 cm, 10 cm, 15 cm, 25 cm long with an internal diameter of 3,2 mm, 4.6 mm or 5 mm. The distance the solute has to travel between the mobile phases and the stationary phase and is also reduced as it passes through small particles. This facilitates stabilization and results in good column efficiencies. Small particles also provide greater flow resistance and higher pressures at the same flow rates. The particles with a diameter of 3 μm, 5 μm and 10 μm are used in analytical columns. For low molecular weight analytes (<500-Da), fillers with a pore diameter of 50-100 angstroms and a surface area of 200-400 m^2/g are used.. For larger molecules, such as polysaccharides and proteins, materials with larger pore diameters (≥300 Å) need to be used (Lough & Wainer, 2008).

- **Detectors**

The most commonly used detector in the HPLC system is based on ultra-viyole absorption that can be photometric and spectrophotometric. An ideal dedector characteristic listed;

• have sensitivity and predictable response.

• respond to all soluble matter.

• don't be affected by changes in temperature and mobile phase.

• respond independently of the mobile phase

• be reliable and convenient to use

• have a response that increases linearly with the amount of solute

• be nondestructive of the solute

• provide qualitative information on the detected peak

The signal, noise and signal-to-noise ratio of the signal generated by the analyte is important for the sensitivity and accuracy of the detector. Short-term noise is used for noise of less than 1 minute (Figure 4-a) The term short-term noise is used for noise with a duration of less than 1 minute and can be calculated manually by peak-to-peak measurements bracketing the endpoints of the baseline, or alternatively it can be determined by the data system by root-mean-square calculation. As seen Figure 8 the signal observed to the top of the peak from the middle of the baseline noise.

Figure 7 *Short Term Noise and Long Term Noise of Dedector*

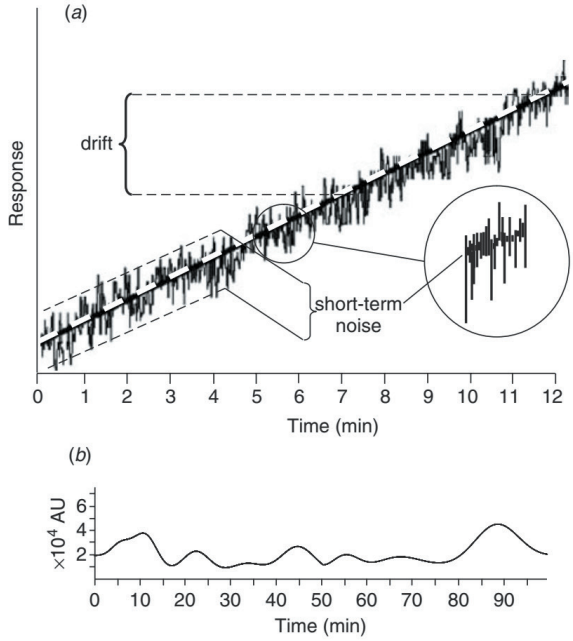

Figure 8 *Schematic representation of signal and noise*

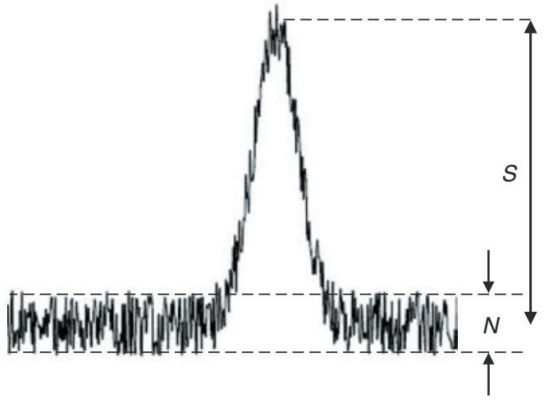

3.4. UV Detectors

UV detectors are very important detectors, also used in liquid and ion exchange chromatography; they are suitable for substances that can absorb light in the range 180-350 nm, their sensitivity is approximately 10^{-8}-10^{-9} g/ml. Based on Lambert Beer's law;

$$\log\left(\frac{I_0}{I}\right) = \varepsilon bc$$

Io is the incident light intensity, I is the intensity of the transmitted light, ε is the molar absorptivity of sample, b is the cell path-length as cm and c is the sample concentration in moles/L.

The HPLC detector is designed to provide a signal in absorbance that is directly proportional to the sample concentration present in the flow and expected to be analyzed. A is the absorbance;

$$\log\left(\frac{I_0}{I}\right) = \varepsilon bc$$

Many compounds such as all olefins, aromatics, >CO, >CS, molecules containing -N=O and -N ≡ N- groups absorb in the UV region (200-350 A); they have single or double bonds (electrons) and unbound electrons (Lough & Wainer, 2008). Fixed Wavelength UV Detectors, Variable (or Multiple) Wavelengths, Variable (or Multiple) Wavelength, Dispersive UV Detector, Diode Array Detector.

Figure 9 *UV Dedector Detailed Schema (Lough & Wainer, 2008)*

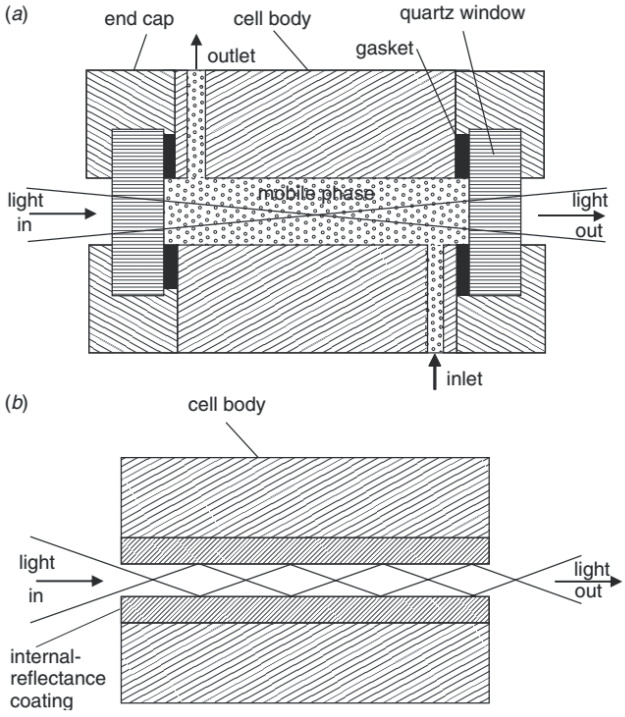

UV light enters the quartz window at one end of the cell and the differential absorbance of the light is monitored by a photosensitive diode at the other end of the cell and converted into an electrical signal, which can be obtained by the data system as a chromatogram.

Figure 10 *Diode-Array UV Dedector (Photodiode- Array PDA dedector)*

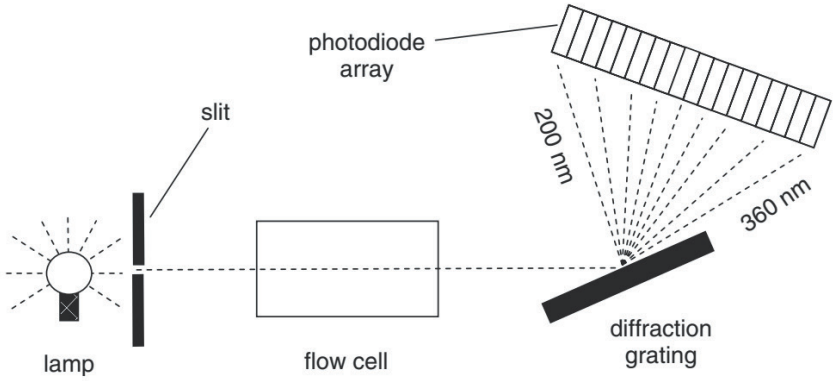

The light source is a source with a wide wavelength range, such as a deuterium or xenon discharge lamp. Distributed light is focused on a flat mirror through a curved mirror and the specific wavelength is selected by adjusting the flat mirror to the appropriate value.

- **Refractive Index Detectors**

Refractive index detectors are very suitable detectors for nonionics, non-absorbing substances in the UV region and non-fluorescent compounds. The detection of the detector changes when the environmental temperature, pressure, flow rate changes.

Figure 11 *Refractive Index Dedector (RI)*

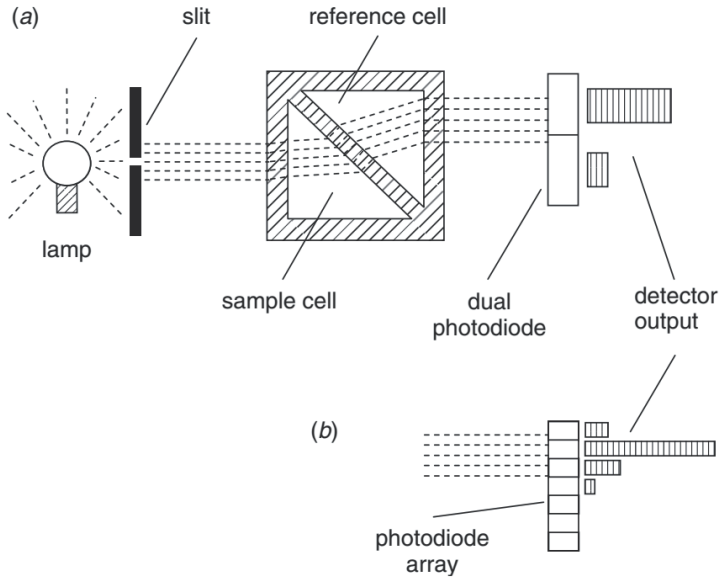

- **Fluorescence Detector**

The most sensitive liquid chromatography detector. It is highly sensitive for substances that can be detected according to the wavelengths at which they absorption and emission. It is ideal dedection for aflatoxin analysis in grains and aromatic hydrocarbons in wasteeater.

- **Electric conductivity detector**

It measures the conductivity of the mobile phase like ion exchange chromatography. Conductivities that may be caused by the ambient conductivity of the itself must be eliminated by appropriate electronic arrangements. If there is a buffer in the mobile phase, the detector will produce a base signal, in which case the measurement will fail. The electrical conductivity detector is a bulk detector and therefore detects all ions in solution and solvent.

4. A Phenolic Application with HPLC

The HPLC chromatogram obtained by phenolic component analysis of a plant extract sample at Figure 8. This chromatogram was obtained by creating and stabilizing several parameters. At first extraction of plant is very important and then chose the analytical coulomn, prefer mobile phase, select the dedector parameters, all of these are steps for HPLC.

Figure 12 *HPLC Chromatogram*

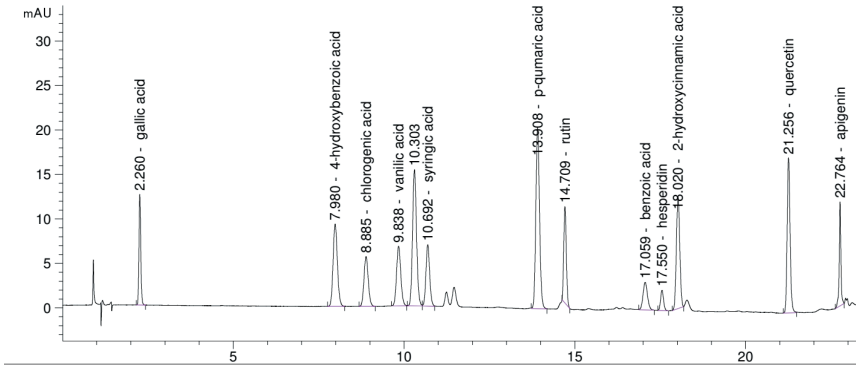

Some phenolic compounds by reversed-phase with multi UV-dedection. Sample preparation and analytical procedures are described in reference Apaydın and Arabacı and Yaşar et al (Apaydın & Arabacı, 2017; Yıldırım, Kadıoğlu, Sağlam &Yaşar, 2017).

As seen in the chromatogram, 13 phenolic acids were separated from each other succesfully. This is an important separation due to the high number of analytes. The mobile was (A) 20 mM phosphate buffer (pH:2.5) and the mobile was (B) acetonitrile (grade). Gradient elution was A and B as follows: 0 min, 5% B; 0–7 min, 5–7% B; 7–12 min, 7–25% B; and 12–25 min, 25–85% B, flow rate of 1.5 mL/min, the sample injection volume was 20 µL. The pH of solutions was adjusted with 3 M HCl. And A mobile phase passed through cellulose acetate membrane filters (47 mm i.d., 0.45 µm pore size,) before use. and flow rate was 1.5 mL/min, multi-UV detection was used at 280 nm, the column temperature was set to 40°C.

Figure 13 *HPLC Chromatograms Compatible with Developing Technology (Yin, Yin & He, 1995)*

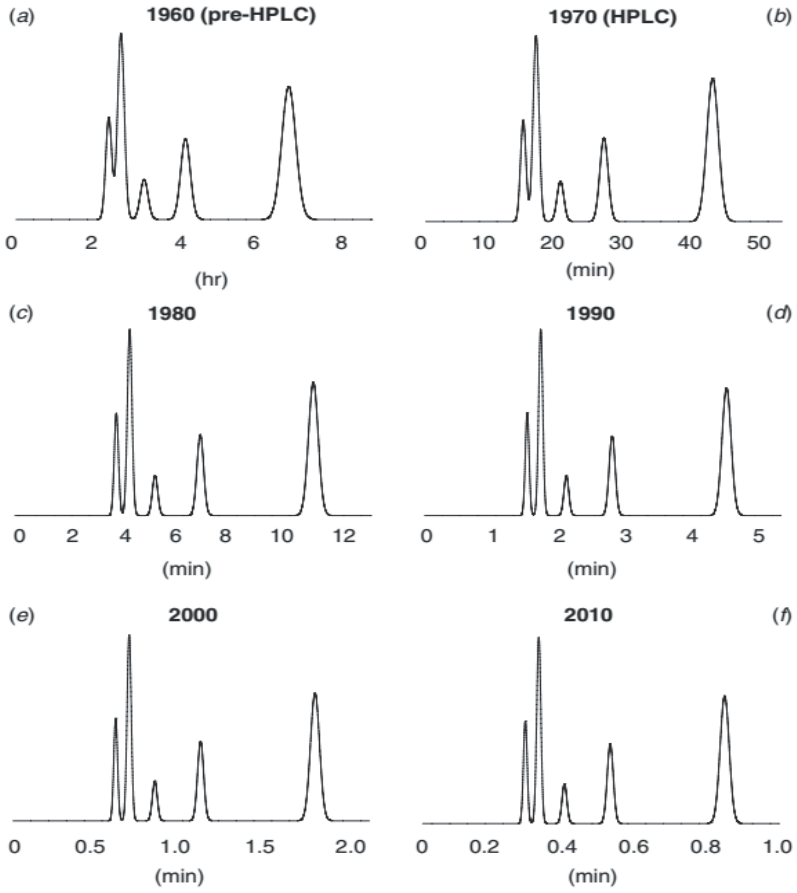

The improvement in the separation of the peaks and the advance of the retantion time are clearly visible.

Eventually HPLC is a selective, rapid chromatographic system for structre been high molecule weight. It is used to separate primary and secondary metabolites of compounds of plant, nutrient or organic nature With the developing technology, a radical change in the HPLC principle is not targeted. It was intended to improve the analysis parameters with studies on the analysis of more groups. As can be seen in Figure 13, the analysis time decreased for each chromatogram. This provided advantages in many aspects such as time, instrument and column life, especially in the amount of solvent used. This provides enormous financial benefits in the production and industrial sector.

REFERENCES

Apaydın E., Arabacı G., (2017). Antioxidant capacity and phenolic compounds with hplc of asphodelus ramosus and comparison of the results with Allium cepa L. and Allium porrum L. Extracts, *Turkish Journal Of Agricultural and Natural Sciences,* 244, 499-505.

Aruoma, G.I., Spencer, J.P.E., Warren, Q.D., Jenner, P., Butler, P. & Halliwell, B., (1997). Characterization of food using commercial garlic antioxidants, *Illustrated and Food Chemistry*, 60, 149-156

Bae, Y.S., Kang, SW. & Seo, MS., (1997). Epidermal growth factor (EGF)-induced generation of hydrogen peroxide. *Journal of Biological Chemistry*, 272: 217-21.

Bidlingmeyer B.A. (1993). Practical HPLC methodology and applications. Wiley, New York.

Braumann T., Weber G. & Grimme L.H., (1983). Determination of hydrophobic parameters by reversed-phase liquid chromatography: theory, experimental techniques, and application in studies on quantitative structure-activity relationships. *Journal of Chromatography A*, 261 329, 1983.

Chopra, S. & Wallace, H.M., (1998) Induction of spermidine/spermine N1-acetyltransferase in human cancer cells in response to increased production of reactive oxygen species, *Biochem Pharmacol*, 55: 1119-23.

Dorsey J.G., Cooper W.T., Siles B.A., Foley J.P. & Barth H..G., (1996). Liquid chromatography: theory and methodology (fundamental review) *Analitical Chemistry,* 68:515R–568R.

Ghosh, J. & Myers, C.E., (1998)Inhibition of arachidonate 5-lipoxygenase triggers massive apoptosis in human prostate cancer cells, *Proceedings of the National Academy of Sciences*, 95: 13182-7.

Halliwell, B., (1994) Free Radicals and Antioxidants: A Personal View, *Nutrition Reviews*, Vol. 52, No. 8: 253-265.

Harborne J. B. & Simmonds N. W., (1964) Biochemistry of Phenolic Compounds, *J. B. Harborne. Academic Press*, London, 77.

Hertog M.G., Feskens E.J., Hollman P.C., Katan M.B. & Kromhout D., (1993). Dietary antioxidant flavonoids and risk of coronary heart disease: the Zutphen Elderly Study, *Lancet*; 342: 1007-1011.

Huang, D., Ou, B. & Prior, R. L., (2005). The Chemistry Behind Capacity Assays, *Journal of Agriculture and Food Chemistry*, 53, 1841-1856.

Kalaycıoğlu, A., Öner, C., (1994). Investigation of antimuogenic effects of some plant extracts by Amest Salmonello test system, *Tr. Botany*, 18, 117-122.

Knekt P., Jarvinen R., Reunanen A. & Maatela J., (1996). Flavonoid in take and coronary mortality in Finland: a cohort study. *British Medical Journal*,

312: 478-481.

Lee, Y.J., Galoforo, S.S. & Berns, C.M., (1998). Glucose deprivation-induced cytotoxicity and alterations in mitogen-activated protein kinase activation are mediated by oxidative stress in multidrug-resistant human breast carcinoma cells, *Journal of Biological Chemistry*, 273: 5294-9.

Lough W.J. & Wainer I,W, (2008). High performance liquid chromatography: fundamental principles and practice. *Springer*, New York.

Rice Evans, C.A., Miller, N.J., Bolwell, P.G., Bramley, P.M,. Pridham, J.B., (1995). The relative activities of plant-derived poliphenolic flavonoids, *Free Radical Research*, 22, 375-383.

Wojtaszek P., (1997). Oxidative burst: an early plant response to pathogen infection, *Biochem Journal*, 322: 681-92.

Yıldırım S., Kadıoğlu A., Sağlam A. & Yaşar A., (2017). Determination of phenolic acids and rutin in Heliotropium thermo philum by high-performance liquid chromatography with photo diode array detection, *Instrumentatıon Science & Technology,* vol. 45,1, .35-48.

Yin, G.Y., Yin, Y.F., He, X.F., (1995). Effect of zhuchun pill on immunity and endocrine function of elderly with kidney-yang deficiency*, Chung Kuo Chung Hsi I Chieh Ho Tsa Chih*, 15: 601-3.

CHAPTER 6

ALDOSE REDUCTASE AND CANCER

Namık KILINÇ[1]

1 Assoc. Prof. Dr. Iğdır University, Vocational School of Health Servi-ces, Department of Medical Services and Techniques, Iğdır, Turkey ORCID: 0000-0002-9102-1370

Polyol pathway

Glycolysis is a fundamental metabolic process that happens in the cytoplasm of cells, which aims to transform glucose into two pyruvate compounds. It operates in both anaerobic and aerobic organisms and can function without oxygen. Hexokinase, an essential enzyme in glycolysis, enables cells to phosphorylate glucose and use it as an energy source. When there is an excessive amount of glucose in the cells, hexokinase becomes saturated, allowing glucose to enter the cells through the polyol pathway (Berrone, Beltramo, Solimine, Ape, & Porta, 2006). Once glucose has been consumed, important enzymes in the polyol pathway go to work, such as aldose reductase (AR), which uses a nucleotide adenine dinucleotide phosphate (NADPH) to convert glucose into sorbitol (Niimi, Yako, Takaku, Chung, & Sango, 2021). Sorbitol dehydrogenase is a different significant enzyme that facilitates the conversion of sorbitol into fructose (SD). As a result of this conversion, nicotinamide adenine dinucleotide (NAD) is transformed into nicotinamide adenine dinucleotide hydrogen (NADH) (Lorenzi, 2007). NADPH is primarily used to facilitate the reduction of glutathione and the subsequent generation of nitric oxide (NO). However, variations in NADPH concentration lead to either a drop in glutathione content or a deficit of it. Glutathione deficiency sets off a chain reaction of oxidative stress (OXS), which promotes hemolysis in those who are affected (Mytilineou, Kramer, & Yabut, 2002). An elevated NADH/NAD^+ ratio, caused by the use of NAD^+ by sorbitol dehydrogenase, is associated with several metabolic and signaling alterations that affect cell functioning and enhance ROS generation (Baynes, 1991; Giacco & Brownlee, 2010; Kinoshita, 1990). This could be a mechanism for the formation of intracellular oxidant species, as the excess NADH could serve as a substrate for NADH oxidase. A reduction in antioxidant defenses and the production of oxidant species would put cells at risk of oxidative stress (oxidant-derived tissue injury), which can set off a cascade of damaging events in the cell.

In diabetic complications, a decrease in NADPH/NADP and an increase in NADH/NAD^+ levels could be responsible for other biochemical abnormalities (Baynes, 1991; Gabbay, 1973, 1975; Giacco & Brownlee, 2010; Kinoshita, 1990). In cells where there is high sorbitol dehydrogenase activity, this can lead to an increase in the NADH/NAD^+ ratio (Figure 1). This ratio change can increase oxidative stress by reducing the regeneration of cellular antioxidants (such as reduced glutathione) and decreasing the availability of NADPH, which decreases the activity of catalase, an enzyme that converts ROS and hydrogen peroxide (H_2O_2) into water. The polyol pathway can reduce the level of reduced glutathione, which makes cells more vulnerable to oxidative stress from within the cell. Hyperglycemia increases the NADH/NAD^+ ratio in cell populations prone to

complications. An elevated NADH/NAD$^+$ ratio can significantly impact the health of the retina (Brownlee, 2001).

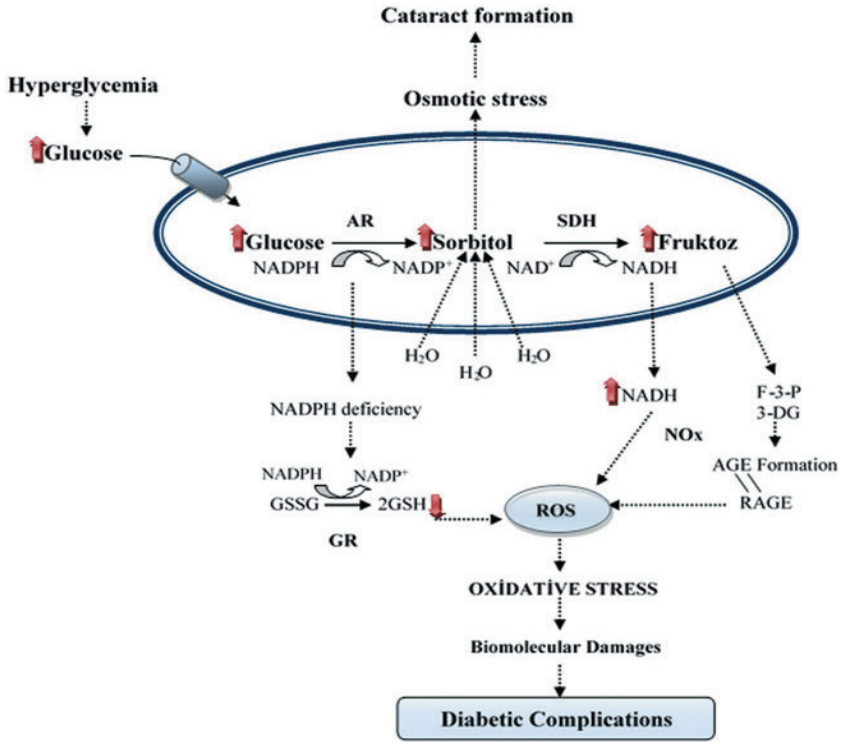

Fig. 1. *Polyol pathway and the link between oxidative stress and diabetic complications: The increased flow of the polyol pathway is crucial in the development of problems related to diabetes. (Alim, Kilinç, Şengül, & Beydemir, 2017).*

Fructose produced in the body can be converted into fructose-3-phosphate, which can then break down into 3-deoxyglucose and 3-deoxyglucosone. These compounds are strong glycating agents that may cause the formation of AGEs. AGEs are a group of compounds that are formed when reducing carbohydrates react non-enzymatically with free amino groups of proteins, nucleic acids, and lipids. They are a major cause of almost all diabetic complications and can be observed in the retinal vessels of diabetic individuals. AGEs can cause an increase in leukocyte adhesion to retinal microvascular endothelial cells by generating intracellular ROS. Hyperglycemia inside the cell leads to an increase in the synthesis of diacylglycerol, which is a crucial stimulating cofactor for protein kinase-C (PKC). Intracellular hyperglycemia can activate PKC, which can

alter gene expression and protein function. This can cause a decrease in factors that promote normal cell function and an increase in those that are harmful to normal function, ultimately leading to cell damage (Brownlee, 2001; González, Barnett, Aguayo, Cheng, & Chylack Jr, 1984; Szwergold, Kappler, & Brown, 1990).

Aldose Reductase

Aldose reductase (AR, EC 1.1.1.21) is an enzyme which can be found throughout a mammal's body (Carper et al., 1989). NADPH is used to convert glucose into sorbitol. Another enzyme called sorbitol dehydrogenase then slowly converts sorbitol to fructose, reducing NAD^+ in the process. The polyol pathway is triggered when there is too much glucose in the blood (hyperglycemia), which leads to numerous metabolic abnormalities in tissues that don't need insulin to take up glucose (Brownlee, 2001).

Many aliphatic and aromatic aldehydes are reduced by the enzyme aldose reductase to the corresponding alcohols (Oates, 2002; Yabe-Nishimura, 1998). The enzyme is essential for turning glucose into the physiologically relevant sorbitol in the polyol pathway. Patients with diabetes mellitus who are exposed to high glucose levels have this route activated. Sorbitol is only slowly converted to fructose by sorbitol dehydrogenase because it cannot readily penetrate cell membranes. As a result, sorbitol builds up in cells that absorb glucose without the help of insulin, increasing osmotic pressure and eventually causing cell damage. Increased glucose processing through the polyol pathway also results in oxidative stress due to the depletion of the NADPH reserve. Several metabolic abnormalities originating from glucose metabolism via the polyol pathway have been connected to many diabetic issues (Miyamoto, 2002).

Under normal blood sugar conditions (euglycemic), AR has a very little part in lowering glucose, accounting for only about 3% of the metabolized quantity. This is due to AR's limited affinity towards glucose as a substrate. In contrast, hexokinase converts glucose to glucose 6-phosphate, the primary substrate for entry into the glycolytic pathway. AR is more effective in reducing various aldehydes, particularly hydrophobic saturated and unsaturated aldehydes, which are produced due to lipid peroxidation, than aldoses like glucose. (Satish K Srivastava, Ramana, & Bhatnagar, 2005; Yabe-Nishimura, 1998). The primary function of AR is to reduce toxic agents or longchain aldehydes that result from lipid peroxidation, including HNE and their glutathione adducts. (bander Jagt et al., 1995; S. Srivastava et al., 2000). AR has also been suggested to regulate cell osmolarity by producing osmotically active compounds such as sorbitol in the kidneys. Additionally, recent research has uncovered AR's involvement in signaling and cell growth, highlighting other physiological functions of the

enzyme (Ramana, Friedrich, Srivastava, Bhatnagar, & Srivastava, 2004; Ramana & Srivastava, 2006).

When there is an excess of glucose in the body (hyperglycemia), aldose reductase (AR) transforms the surplus glucose (which can account for up to one-third of the total glucose quantity, depending on the tissue or organ) to sorbitol in tissues that take up glucose without insulin, such as the retina, lens, kidney, erythrocytes, and peripheral nerves (Brownlee, 2001). After hexokinase saturation, this happens. Reduced blood supply to the nerves, slowed nerve conduction velocity, and tissue and vascular damage may all result from the increasing flow rate of glucose via the polyol pathway. These elements have a role in the emergence of ongoing diabetes-related problems (DM). (Brownlee, 2001; Satish K Srivastava et al., 2005; Satish K. Srivastava et al., 2011; Yabe-Nishimura, 1998).

For example, osmotic stress, swelling, and changes in membrane permeability are brought on by the buildup of osmotically active sorbitol inside lens cell membranes, which may result in cataractogenesis. The concentration of intracellular sorbitol, however, is often too low in other areas, such as retina, neurons, and blood vessels, the to result in any appreciable osmotic imbalance (Brownlee, 2001; Lorenzi, 2007).

AGEs are formed as a consequence of the accelerated breakdown of glucose via the polyol pathway, which results in glycative stress (Hamada et al., 2000). Fructose, which is the final product of the polyol pathway, is more reactive compared to glucose and can potentially react with proteins to form Schiff bases. These bases undergo oxidation and rearrangement to produce advanced glycation end products. (Alexiou, Pegklidou, Chatzopoulou, Nicolaou, & Demopoulos, 2009; Roščić & Horvat, 2006). AGEs can impair the functions of proteins and cellular signaling, and contribute to the formation of reactive oxygen species (ROS) (Costantino, Rastelli, Vianello, Cignarella, & Barlocco, 1999). AGE development is aided by the conversion of fructose to reactive carbonyl molecules (Tang, Martin, & Hwa, 2012). To further increase intracellular ROS generation, dihydroxyacetone phosphate (DHAP) may be converted to glycerol 3-phosphate, a precursor of DAG (diacylglycerol) by activation of PKC (protein kinase C) (Ramana et al., 2005; Ramana & Srivastava, 2006).

Aldose Reductase and Cancer

New research indicates that aldose reductase, a type of protein in the aldo-keto reductase family, is responsible for transmitting inflammatory signals triggered by cytokines, growth factors, carcinogens, and chemokines. In addition to converting excess glucose to sorbitol, aldose reductase can also convert lipid-derived aldehydes and associated metabolites, inc-

luding glutathionyl 1,4-dihydroxynonanol (GS-DHN). These compounds can activate transcription factors such as AP-1 and NF-κB, that regulate the expression of inflammatory cytokine genes. The presence of growth factors and inflammatory cytokines can promote cell proliferation, which is a significant contributor to tumorigenesis. Studies conducted both in vivo and in vitro have demonstrated that inhibiting aldose reductase can curb the growth of cancer cells (Tammali, Ramana, Singhal, Awasthi, & Srivastava, 2006; Tammali, Ramana, & Srivastava, 2007).

In embryonic development, Zeindl-Eberhart et al. discovered that the AR gene is present in the liver, but it disappears in adult rat liver. However, during liver cancer development, AR reappears and functions actively (Zeindl-Eberhart, Jungblut, Otto, & Rabes, 1994). Sa-raswat et al. found that AR is overexpressed in several types of malignant tissues, including breast, lung, prostate, ovarian, cervix, and colon cancers. Moreover, they observed that AR activity was higher in tumor sites compared to non-tumor areas of tissues (Saraswat et al., 2006). Yoshitake et al. discovered that the recurrence of tumors after surgery and keratinization of cervical cancer's squamous cell carcinoma are both linked to the expression of AKR1B10, an enzyme from the aldo-keto reductase family (Yoshitake et al., 2007). Tanimoto et al. isolated AR from tumor cells of the Engelbreth-Holm-Swarm type and described its characteristics, but its exact role in malignancies is still unclear (Tanimoto, Sato, & Kador, 1990).

Reactive oxygen species (ROS) generated by growth factors, cytokines, and chemokines can promote growth or death in different cell types. ROS activates several signaling pathways, such as PKC, PLC, DAG, and PI3-K, which in turn activate transcription factors NF-kB and AP1. These factors can transcribe inflammatory markers and stimulate cell proliferation, which is observed in cancer. The mechanism by which ROS contributes to signaling remains an open question. Lipid peroxidation and the generation of lipid aldehydes due to ROS have been known for some time, but the process by which ROS activate the signaling intermediates that ultimately lead to NF-kappa B and AP1 activation is still not clear. In vitro research has been shown that the human lung cancer cells (A549) respond favorably to beta- and alpha-unsaturated aldehydes. The study further suggests that GS-aldehydes play a role in the signaling pathways triggered by growth factors, chemokines, and cytokines that ultimately lead to AP-1 and NF-kB activation before PI3-K, DAG, PKC, and PLC. When signals induced by LPS, cytokines, growth factors, and chemokines to transcription factors are blocked or removed, inflammatory markers including prostaglandins and COX-2 do not increase significantly. These findings imply that inhibiting AR could be an effective strategy for treating colon, lung, breast,

and prostate cancers that develop due to inflammation (Horton, Mamiya, & Kehrer, 1997; Hung et al., 2007).

Colon cancer is a prevalent type of cancer, ranking third worldwide and second in the USA in terms of cancer-related deaths, with an estimated 1.2 million new cases and 608,700 deaths in 2008 (Globalcancerstatistics, 2011). The development of colon cancer is influenced by both familial and hereditary factors. The transformation of healthy colon tissue to cancerous tissue involves several molecular and biochemical changes, including genetic mutations, increased cell growth and differentiation of intestinal epithelial cells, and inflammation (Kim, 2005). According to recent studies, the aldose reductase (AR) controls the signals produced by reactive oxygen species (ROS), which are brought on by cytokines and growth factors (GF), and which stimulate vascular cell proliferation and differentiation. Inhibiting AR stopped cytokine (TNF-a) or growth factor (bFGF- or PDGF)-induced cell proliferation, Cox-2 expression, PKC activation, NF-kB activation, and PGE2 synthesis in human colon cancer cells (Caco-2). In the nude mice xenograft model, in vivo treatment of AR-small interfering RNA (siRNA) prevented the growth of SW480 human colon cancer cells. The pharmacological AR inhibitor sorbinil stopped BALB/c mice from developing ACF when AOM was present. ACF development, inflammatory marker expression (iNOS and Cox-2), preneoplastic marker protein expression (cyclin D1 and beta-catenin), and NF-kB activation in mice colons were all dramatically inhibited by AOM when the AR gene was knocked out. Cell cycle analysis results showed that AR inhibition also blocked the entrance of cells into the G1/S phase of the cell cycle by aggregating them at the G2/M phase.

Growth factors cause AKT/PI3K to be activated, increasing the production of tumor-promoting proteins including cyclin E, cyclin D1, PCNA, cdks, E2F-1, and c-myc at the G1/S cell cycle transition. Yet, current research suggests that by blocking the E2F-1-mediated G1/S phase cell cycle transition, reducing AR can stop the proliferation of colon cancer cells. Although there is limited research exploring how genetic regulation of aldose reductase (AR) may control carcinogenic signals in mice models, one study has demonstrated that suppressing AR using siRNA in tumor tissues can inhibit colon cancer development in nude mouse xenografts. Moreover, it has been discovered that AOM-induced ACF development and inflammatory protein production do not affect AR-deficient animals. Further research using animal models is required to ascertain how altered AR levels could influence the development of cancer. All things considered, our results imply that AR is a viable new therapeutic target for reducing colon cancer risk.

Hepatocarcinogenesis is a type of liver cancer that usually occurs as a result of viral infections, cirrhosis, or the spread of cancer from other parts of the body, such as the colon (Gustot, Durand, Lebrec, Vincent, & Moreau, 2009). The overexpression of AR (Aldose Reductase) was initially studied in liver cancer development. During fetal development, AR is important in the liver to break down carbohydrates. Its expression increases in the fetal liver up to the 16th week of gestation and disappears in later stages, indicating that it is not required in the normal adult liver (Samanta, Chandra, Ghosh, & Mukherjee, 1984). However, AR is reactivated and functions during hepatocarcinogenesis due to the decreased activity of glycolytic enzymes and increased proliferative activity.

Several studies have suggested that AR is overexpressed during the development of liver cancer (Takahashi et al., 1996). Takahashi and colleagues discovered that the AR gene expression is stimulated in the livers of rats as they develop hepatoma and hereditary hepatitis with age. Additionally, the expression of AR is greater in the cancerous areas of the liver compared to the non-cancerous surrounding tissues (Takahashi, Funjii, Miyoshi, Hoshi, & Taniguchi, 1995).

REFERENCES

Alexiou, P., Pegklidou, K., Chatzopoulou, M., Nicolaou, I., & Demopoulos, V. J. (2009). Aldose reductase enzyme and its implication to major health problems of the 21st century. *Current medicinal chemistry, 16*(6), 734-752.

Alim, Z., Kilinç, N., Şengül, B., & Beydemir, Ş. (2017). Inhibition behaviours of some phenolic acids on rat kidney aldose reductase enzyme: an in vitro study. *Journal of enzyme inhibition and medicinal chemistry, 32*(1), 277-284.

bander Jagt, D. L., Kolb, N. S., bander Jagt, T. J., Chino, J., Martinez, F. J., Hunsaker, L. A., & Royer, R. E. (1995). Substrate specificity of human aldose reductase: identification of 4-hydroxynonenal as an endogenous substrate. *Biochimica et Biophysica Acta (BBA)-Protein Structure and Molecular Enzymology, 1249*(2), 117-126.

Baynes, J. W. (1991). Role of oxidative stress in development of complications in diabetes. *Diabetes, 40*(4), 405-412.

Berrone, E., Beltramo, E., Solimine, C., Ape, A. U., & Porta, M. (2006). Regulation of intracellular glucose and polyol pathway by thiamine and benfotiamine in vascular cells cultured in high glucose. *Journal of Biological Chemistry, 281*(14), 9307-9313.

Brownlee, M. (2001). Biochemistry and molecular cell biology of diabetic complications. *Nature, 414*(6865), 813-820. doi:10.1038/414813a

Carper, D. A., Wistow, G., Nishimura, C., Graham, C., Watanabe, K., Fujii, Y., Hayaishi, O. (1989). A superfamily of NADPH-dependent reductases in eukaryotes and prokaryotes. *Experimental eye research, 49*(3), 377-388.

Costantino, L., Rastelli, G., Vianello, P., Cignarella, G., & Barlocco, D. (1999). Diabetes complications and their potential prevention: aldose reductase inhibition and other approaches. *Medicinal research reviews, 19*(1), 3-23.

Gabbay, K. H. (1973). The sorbitol pathway and the complications of diabetes. *New England journal of medicine, 288*(16), 831-836.

Gabbay, K. H. (1975). Hyperglycemia, polyol metabolism, and complications of diabetes mellitus. *Annual review of medicine, 26*(1), 521-536.

Giacco, F., & Brownlee, M. (2010). Oxidative stress and diabetic complications. *Circulation research, 107*(9), 1058-1070.

Globalcancerstatistics, J. A. (2011). Jemal A, Bray F, Center MM, Ferlay J, Ward E, Forman D. *CA Cancer J Clin, 61*(2), 69-90.

González, R. G., Barnett, P., Aguayo, J., Cheng, H.-M., & Chylack Jr, L. (1984). Direct measurement of polyol pathway activity in the ocular lens. *Diabetes, 33*(2), 196-199.

Gustot, T., Durand, F., Lebrec, D., Vincent, J. L., & Moreau, R. (2009). Severe sepsis in cirrhosis. *Hepatology, 50*(6), 2022-2033.

Hamada, Y., Nakamura, J., Naruse, K., Komori, T., Kato, K., Kasuya, Y., Hotta, N. (2000). Epalrestat, an aldose reductase ihibitor, reduces the levels of Nepsilon-(carboxymethyl) lysine protein adducts and their precursors in erythrocytes from diabetic patients. *Diabetes Care, 23*(10), 1539-1544.

Horton, N. D., Mamiya, B. M., & Kehrer, J. P. (1997). Relationships between cell density, glutathione and proliferation of A549 human lung adenocarcinoma cells treated with acrolein. *Toxicology, 122*(1-2), 111-122.

Hung, H.-S., Wu, W.-J., Cheng, Y.-W., Wu, T.-C., Chang, K.-L., & Lee, H. (2007). Association of cooking oil fumes exposure with lung cancer: involvement of inhibitor of apoptosis proteins in cell survival and proliferation in vitro. *Mutation Research/Genetic Toxicology and Environmental Mutagenesis, 628*(2), 107-116.

Kim, Y.-I. (2005). Nutritional epigenetics: impact of folate deficiency on DNA methylation and colon cancer susceptibility. *The Journal of nutrition, 135*(11), 2703-2709.

Kinoshita, J. H. (1990). A thirty year journey in the polyol pathway. *Experimental eye research, 50*(6), 567-573.

Lorenzi, M. (2007). The polyol pathway as a mechanism for diabetic retinopathy: attractive, elusive, and resilient. *Experimental diabetes research, 2007*.

Miyamoto, S. (2002). Molecular modeling and structure-based drug discovery studies of aldose reductase inhibitors. *Chem-Bio Informatics Journal, 2*(3), 74-85. doi:10.1273/cbij.2.74

Mytilineou, C., Kramer, B. C., & Yabut, J. A. (2002). Glutathione depletion and oxidative stress. *Parkinsonism & related disorders, 8*(6), 385-387.

Niimi, N., Yako, H., Takaku, S., Chung, S. K., & Sango, K. (2021). Aldose reductase and the polyol pathway in schwann cells: old and new problems. *International Journal of Molecular Sciences, 22*(3), 1031.

Oates, P. J. (2002). Polyol pathway and diabetic peripheral neuropathy. *International review of neurobiology, 50*, 325-392.

Ramana, K. V., Friedrich, B., Srivastava, S., Bhatnagar, A., & Srivastava, S. K. (2004). Activation of nulcear factor-κB by hyperglycemia in vascular smooth muscle cells is regulated by aldose reductase. *Diabetes, 53*(11), 2910-2920.

Ramana, K. V., Friedrich, B., Tammali, R., West, M. B., Bhatnagar, A., & Srivastava, S. K. (2005). Requirement of aldose reductase for the hyperglycemic activation of protein kinase C and formation of diacylglycerol in vascular smooth muscle cells. *Diabetes, 54*(3), 818-829.

Ramana, K. V., & Srivastava, S. K. (2006). Mediation of aldose reductase in lipopolysaccharide-induced inflammatory signals in mouse peritoneal macrophages. *Cytokine, 36*(3-4), 115-122.

Roščić, M., & Horvat, Š. (2006). Transformations of bioactive peptides in the

presence of sugars—characterization and stability studies of the adducts generated via the Maillard reaction. *Bioorganic & medicinal chemistry, 14*(14), 4933-4943.

Samanta, B., Chandra, N., Ghosh, S., & Mukherjee, K. (1984). Aldose metabolism in developing human fetal brain and liver. *Experientia, 40*, 1420-1422.

Saraswat, M., Mrudula, T., Kumar, P. U., Suneetha, A., TS, R. R., Srinivasulu, M., & Reddy, B. (2006). Overexpression of aldose reductase in human cancer tissues. *Medical science monitor: international medical journal of experimental and clinical research, 12*(12), CR525-529.

Srivastava, S., Dixit, B. L., Cai, J., Sharma, S., Hurst, H. E., Bhatnagar, A., & Srivastava, S. K. (2000). Metabolism of lipid peroxidation product, 4-hydroxynonenal (HNE) in rat erythrocytes: role of aldose reductase. *Free Radical Biology and Medicine, 29*(7), 642-651.

Srivastava, S. K., Ramana, K. V., & Bhatnagar, A. (2005). Role of aldose reductase and oxidative damage in diabetes and the consequent potential for therapeutic options. *Endocrine reviews, 26*(3), 380-392.

Srivastava, S. K., Yadav, U. C. S., Reddy, A. B. M., Saxena, A., Tammali, R., Shoeb, M., Ramana, K. V. (2011). Aldose reductase inhibition suppresses oxidative stress-induced inflammatory disorders. *Chemico-Biological Interactions, 191*(1), 330-338. doi:https://doi.org/10.1016/j.cbi.2011.02.023

Szwergold, B. S., Kappler, F., & Brown, T. R. (1990). Identification of fructose 3-phosphate in the lens of diabetic rats. *Science, 247*(4941), 451-454.

Takahashi, M., Funjii, J., Miyoshi, E., Hoshi, A., & Taniguchi, N. (1995). Elevation of aldose reductase gene expression in rat primary hepatoma and hepatoma cell lines: implication in detoxification of cytotoxic aldehydes. *International journal of cancer, 62*(6), 749-754.

Takahashi, M., Hoshi, A., Fujii, J., Miyoshi, E., Kasahara, T., Suzuki, K., Taniguchi, N. (1996). Induction of aldose reductase gene expression in LEC rats during the development of the hereditary hepatitis and hepatoma. *Japanese journal of cancer research, 87*(4), 337-341.

Tammali, R., Ramana, K. V., Singhal, S. S., Awasthi, S., & Srivastava, S. K. (2006). Aldose reductase regulates growth factor-induced cyclooxygenase-2 expression and prostaglandin E2 production in human colon cancer cells. *Cancer Research, 66*(19), 9705-9713.

Tammali, R., Ramana, K. V., & Srivastava, S. K. (2007). Aldose reductase regulates TNF-α-induced PGE2 production in human colon cancer cells. *Cancer letters, 252*(2), 299-306.

Tang, W. H., Martin, K. A., & Hwa, J. (2012). Aldose reductase, oxidative stress, and diabetic mellitus. *Frontiers in pharmacology, 3*, 87.

Tanimoto, T., Sato, S., & Kador, P. F. (1990). Purification and properties of aldose reductase and aldehyde reductase from EHS tumor cells. *Biochemical*

pharmacology, 39(3), 445-453.

Yabe-Nishimura, C. (1998). Aldose reductase in glucose toxicity: a potential target for the prevention of diabetic complications. *Pharmacological reviews, 50*(1), 21-34.

Yoshitake, H., Takahashi, M., Ishikawa, H., Nojima, M., Iwanari, H., Watanabe, A., Takamori, K. (2007). Aldo-keto reductase family 1, member B10 in uterine carcinomas: a potential risk factor of recurrence after surgical therapy in cervical cancer. *International Journal of Gynecologic Cancer, 17*(6).

Zeindl-Eberhart, E., Jungblut, P. R., Otto, A., & Rabes, H. M. (1994). Identification of tumor-associated protein variants during rat hepatocarcinogenesis. Aldose reductase. *Journal of Biological Chemistry, 269*(20), 14589-14594.

CHAPTER 7

A CRITICAL REVIEW OF ADDITIVES USED IN PLASTICS

Abdulaziz KAYA[1]

1 Asst.Prof.Dr. Department of Metallurgical and Materials Engineering, Gaziantep University email: akaya@gantep.edu.tr Orcid ID: 0000-0001-8767-1998

1. Introduction

Since they have comparatively long chains and large molecular weights, polymers stand out from all other compounds. Plastics are polymers that have been altered with additives for commercial use (Grossman & Lutz Jr, 2000). Because of its low cost, versatility, durability, and light weight, plastics have considerably enhanced human lives (Pérez-Albaladejo, Solé, & Porte, 2020). In the plastic materials used to make the majority of products, the basic polymer is combined with various additives to enhance the polymer's performance (e.g., during shaping via injection molding, extrusion, blow molding, vacuum molding, etc.), functionality, and ageing characteristics (Hahladakis, Velis, Weber, Iacovidou, & Purnell, 2018). Some of these improvements to properties include better resistance to oxidation, high temperatures, UV radiation and impact loads as well as alteration of a wide variety of other properties. Compounding is the process of incorporating necessary chemicals into polymers to produce these effects (Bolgar, Hubball, Groeger, & Meronek, 2015).

The most often used additives in a variety of polymeric materials include plasticizers, flame retardants, antioxidants, acid scavengers, light and heat stabilizers, lubricants, pigments, antistatic agents, and slip compounds. Each one of them contributes in a particular way to the ultimate functional attributes of a plastic product (Hahladakis et al., 2018). Without additives, polymer industry is unattainable. The capability to overcome processing issues, performance constraints on properties, and environmental stability constraints is made possible by additives in plastics. The need to meet new environmental health requirements, simpler processing, improved physical qualities, better long-term performance, and other factors drive the ongoing evolution and diversification of additive packages (Bart, 2005). A large variety of different additives are employed as auxiliary materials in the manufacturing of polymer goods. The proportion of each additive in the auxiliary market (quantitative breakdown) is depicted in Figure 1. (Kosiński, Rykowska, Gonsior, & Krzyżanowski, 2022).

Many additives affect a plastics compound in multiple ways. Plasticizers frequently assist with lubrication and processing. Weathering is influenced by light stabilizers as well. Often employed as a pigment, carbon black also serves as a reinforcement, an electrically conductive component, and a light shield (Murphy, 2001). The polymer and the additives may be entirely miscible or completely immiscible, as is the case with fillers and fiber reinforcers. Due to their low solubility, the majority of surface property modifiers migrate to the polymer surface where their features are shown. Certain additives, like antioxidants or UV stabilizers, are employed in very small amounts, but others, like fillers, reinforcing fibers, and plasticizers, typically make up a sizeable portion of the final formulation of

the polymer (Stevens, 1993c). This review aims to educate even the most casual reader about additives and how they apply to everyday life.

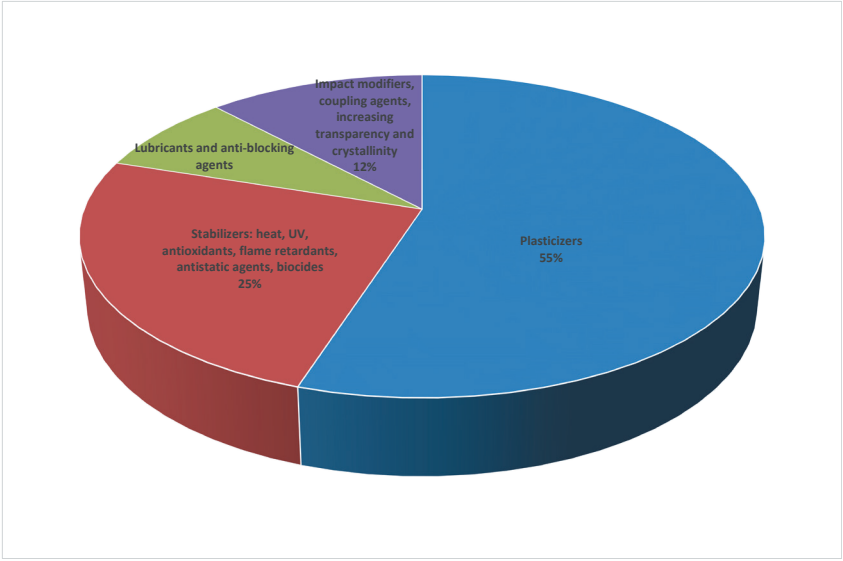

Fig. 1. *The percentage of each additive on the auxiliary market (quantitative breakdown) (Kosiński et al., 2022).*

2. Additives

There are many different types of additives with different functions, but the following are the most significant: Antioxidants, plasticizers, fillers, impact modifiers, lubricants, heat stabilizers, flame retardants, nucleating agents, coupling agents and antistatic additives. These are thoroughly covered in this review.

2.1 Antioxidants

The oxidation-induced polymer degradation phenomena has been the focus of scientific study since the 1940s, concurrent with the expansion of polymeric materials into a wide range of specialty and commodity applications. During the degradation process, oxygen-induced formation of reactive oxygen species takes place, which ultimately results in the change of the macromolecular structure by chain scission or crosslinking. Because it uses an autoaccelerated radical chain mechanism, this process is commonly referred to as autoxidation (Marturano, Cerruti, & Ambrogi, 2017).

Free radicals produced in the polymer by heat or mechanical shear during production, or by exposure to UV or ionizing radiation in the application environment, are the main causes of oxidative degradation of

polymers. Further free radical reactions are facilitated by the radicals' subsequent interactions with oxygen to produce hydroperoxides and peroxy radicals. Eqns. (1) through (7) can serve as a summary of these numerous processes (RH = polymer) (Stevens, 1993a). Therefore, hydroperoxides and the byproducts of their decomposition are responsible for the modifications to the polymer's molecular structure and molecular weight, which are demonstrated in practice by the loss of certain mechanical properties (such as impact strength, flexural strength, tensile strength, and elongation) and the alteration of the surface's physical characteristics (e. g. loss of gloss, reduction in transparency, cracking, yellowing, etc.) (Ambrogi, Carfagna, Cerruti, & Marturano, 2017).

$$RH \xrightarrow{Energy} R\bullet + H\bullet \quad (1)$$

$$R\bullet + O_2 \rightarrow ROO\bullet \quad (2)$$

$$ROO\bullet + RH \;\; ROOH + R\bullet \quad (3)$$

$$ROOH \rightarrow RO\bullet + \bullet OH \quad (4)$$

$$2ROOH \rightarrow RO\bullet + ROO\bullet + H_2O \quad (5)$$

$$2RO\bullet \rightarrow ROOR \quad (6)$$

$$ROOR \rightarrow 2RO\bullet \quad (7)$$

To prevent oxidative deterioration of plastics, antioxidants are utilized. They are also added to prevent heat deterioration during processing and under atmospheric aging. The free radical reactions that happen during autooxidation processes can be slowed down by antioxidants (Subramanian, 2013). Depending on the composition, antioxidants can stop the degradation process by either chain-terminating primary antioxidants or by hydroperoxide-decomposing secondary antioxidants (Eyerer, Weller, & Hübner, 2010). Minor amounts of antioxidants are usually added to the organic polymer matrix to reduce the harmful effects of oxidation. Nevertheless, the exact amount to be utilized will depend on how easily the substrate may oxidize: the more oxidizable the polymer, such as elastomers, the greater the amount required (Al-Malaika, Axtell, Rothon, & Gilbert, 2017).

Primary antioxidants

Hindered phenols and secondary amines are examples of primary antioxidants that serve as radical scavengers, hydrogen donors, or chain reaction inhibitors (Subramanian, 2013). By causing chain terminating reactions, primary antioxidants prevent oxidation. They contain reactive OH or NH groups (hindered phenols and secondary aromatic amines). A proton

is transferred to the free radical species to cause inhibition. The resultant radical cannot abstract a proton from the polymer chain and is stable (Ambrogi et al., 2017). Figures 2 and 3 illustrate, respectively, the mechanisms by which hindered phenols and secondary aromatic amines decompose peroxide radicals (Fink, 2010).

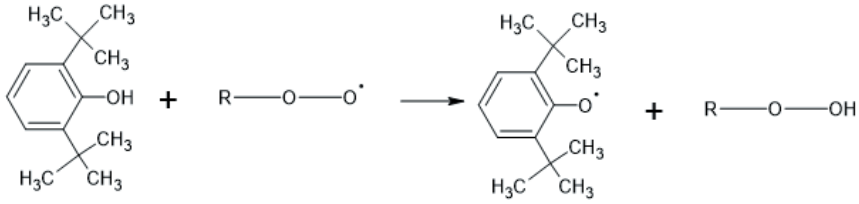

Fig. 2. *The reaction of peroxide radicals with sterically hindered phenols.*

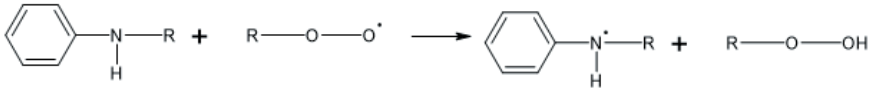

Fig. 3. *The reaction of peroxide radicals with secondary aromatic amines.*

Secondary Antioxidants

Secondary antioxidants are sometimes assigned as "hydroperoxide decomposers" because they react with hydroperoxides to form non-radical compounds (Eyerer et al., 2010). In another regard, hydroperoxides are still reactive since they may produce peroxide radicals. The redox reaction between hydroperoxide decomposers and hydroperoxides convert the latter into stable compounds. For instance, as shown in Eqns. (8-10), phosphites or phosphonites are oxidized into phosphates. The same mechanism of action governs thio compounds as the method of peroxide decomposition employing thio compounds is demonstrated in Eqn. (11) (Fink, 2010). Secondary antioxidants are different from primary phenols and amines in that they react with hydroperoxide to break it down instead of actually containing it. They are especially effective when combined with primary antioxidants in synergistic fashion (Eyerer et al., 2010).

$$H_2P(\text{-O}\Phi)_3 + \text{R-OOH} \rightarrow \text{O=P(-O}\Phi)_3 + \text{R-OH} \quad (8)$$

$$H_2P(\text{-O}\Phi)_3 + \text{R-OO}\bullet \rightarrow \text{O=P(-O}\Phi)_3 + \text{R-O}\bullet \quad (9)$$

$$H_2P(\text{-O}\Phi)_3 + \text{R-O}\bullet \rightarrow \text{O=P(-O}\Phi)_3 + \text{R}\bullet \quad (10)$$

$$\text{H-S(-R)}_2 + \text{R-OOH} \rightarrow \text{O=S(-H)(-R)}_2 + \text{R-OH} \quad (11)$$

2.2 Plasticizers

Polymeric materials are softened by plasticizers. Hence, the main purpose of plasticizers is to increase the plasticity and processability of polymers (Fink, 2010). This is achieved by lowering the viscosity of polymer melts, the glass transition temperature, the melting temperature, and the elastic modulus of final products (Ambrogi et al., 2017). Plasticizers might be polymer impact modifiers or non-polymeric compounds. A certain amount of internal plasticizing can also result from some types of copolymerization (Murphy, 2001).

Plasticizers have a long history of being used successfully to create flexible plastics for a variety of items, from the automotive sector to consumer goods and medical devices. In the beginning, celluloid was plasticized using camphor. Camphor was quickly replaced by tricresyl phosphate. Immediately after that, tricresyl phosphate took the place of camphor. For poly(vinylchloride) (PVC), this compound is still in use. Since its introduction in 1920, phthalic acid esters have remained the most significant category of plasticizers (Fink, 2010).

Many theories have been introduced to explain the plasticization phenomena. One hypothesis is that the plasticizer functions as a lubricant, decreasing intermolecular friction and increasing the freedom of motion of the polymer chains (Stevens, 1993c). Another hypothesis proposed is that the plasticizers are establishing secondary bonds with the polymer chains, therefore extending the distance between them. Alternatively, they separated the polymer chains. Because of this, plasticizers increase the mobility of the macromolecules by reducing the side valence bonding forces of the chains. As a result, a softer, more malleable bulk material is produced. Plasticizers only penetrate the amorphous sections of polymers in crystalline polymers, leaving the crystalline area unaltered (Fink, 2010).

The main two types of plasticizers are primary and secondary. The plasticizer is referred to be a primary plasticizer if a polymer is soluble in it at a high concentration of the polymer (Stipek & Daoust, 2012). The glass transition temperature is lowered by primary plasticizers, which also increase the polymer's elongation and softness (Eyerer et al., 2010). The plasticizer is known as a secondary plasticizer when the polymer solubility is restricted in the technologically significant high concentration range (Stipek & Daoust, 2012). When added to the polymer alone, secondary plasticizers do not reduce the glass transition temperature and do not increase the polymer's elongation and softness. Yet, secondary plasticizers improve the primary plasticizer's ability to plasticize when they are introduced to the polymer in the presence of the main plasticizer (Eyerer et al., 2010).

Around 80% of PVC compounds utilize plasticizers (Murphy, 2001).

PVC is hard and challenging to process on its own. Temperatures as high as 160°C have no effect on it. The polymer, however, softens at ≈160°C and may be press-rolled into semi-rigid sheets for uses like floor tiling if modest quantities of plasticizer are added. PVC is flexible enough to be used in vinyl upholstery and shower curtains at plasticizer concentrations of around 50 wt.% (Stevens, 1993c).

Based on their chemical structure, plasticizers may also be divided into two groups: phthalates and non-phthalates (Ambrogi et al., 2017). At the beginning, 85% of the market for plasticizers was made up of phthalate-based products. Due to safety concerns, their use was curtailed in the last ten years, and terephthalate and bio-based plasticizers were commercialized (Paoli & Waldman, 2019).

Phthalates

Esters of orthophthalic acid are the most widely used commercial plasticizers; isophthalates perform relatively poorly. Typically, monohydric alcohols and phthalic anhydride react to form the phthalate esters (Grossman & Lutz Jr, 2000). The benzene nucleus significantly improves the compatibility of phthalate esters with PVC. Nevertheless, when the alkyl chains get longer, the compatibility goes down. As they diffuse more quickly, phthalates with short alkyl chains are simpler to manufacture. Nonetheless, they have the disadvantage of being more flammable than phthalates with long alkyl chains (Fink, 2010).

The most used phthalate plasticizer, dioctyl phthalate (DOP or DHEP, di-2-ethylhexyl phthalate), accounts for more than 50% of global plasticizer usage. The structure of DOP is shown in Figure 4. Diisononyl phthalate and diisodecyl phthalate are two additional commonly used phthalate plasticizers, whereas butylbenzyl phthalate and diisotridecyl phthalate are classified as specialized phthalates. Dibutylphthalate is primarily utilized in coating applications as a plasticizer to make nitrocellulose resins more flexible. Dimethyl isophthalate is employed as a reactive intermediate for optical plastics as well as a plasticizer and modifier for poly(ethylene terephthalate) (PET) (Eyerer et al., 2010).

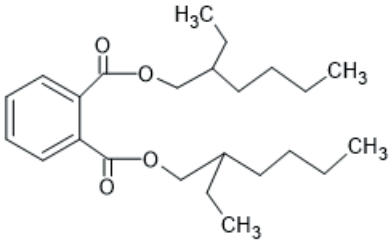

Fig. 4. *Chemical structure of DOP.*

Non-phthalate Plasticizers

Nonphthalate plasticizers are typically defined as other chemical compounds that might replace phthalates in certain applications. Phosphoric esters, citric esters, adipates or sebacates, trimellitic esters, and benzoates are all included in this group. Some of the compounds on the list (such as adipates) are already commonly employed in PVC artifacts, while others are only utilized in specialized goods since their high cost prevents their usage in ordinary applications (Marturano et al., 2017).

2.3 Fillers

Since the beginning of the plastics business, fillers have been utilized. In the start of the 20th century, the industry was essentially founded by the discovery that wood flour made it feasible to mold the liquid resin phenol formaldehyde, and PVC has since proven to be a significant consumer of fillers. Yet, the use of fillers for plastics has drastically evolved throughout the ensuing years (Murphy, 2001).

In the past, fillers were thought of as additives that, because of poor geometrical characteristics, surface areas, or chemical compositions on their surfaces, could only slightly raise the polymer's modulus while the strength (tensile, flexural) stayed the same or even declined. Its main contribution was to replace the more costly polymer, which reduced the cost of materials. Other potential economic benefits included quicker molding cycles due to enhanced heat conductivity and fewer rejected parts because of warpage (Xanthos, 2010). But, lately, their primary application has been to enhance performance. Many benefits exist for the plastic with filler, including high modulus, great chemical resistance, and simplicity of production. This is the rationale behind the substantial increase in plastic usage in the automotive industry (Subramanian, 2013).

Fillers have been categorized in a variety of ways, from their physical features (such as spheres, rods, ribbons, and flakes) to their forms (e.g., conductivity, fire retardancy). For ease of understanding, fillers may be divided into two groups: extenders and functional fillers. Although almost all fillers have certain functional characteristics, the above classification is related to the main function of the filler. By definition, an extender filler is largely employed to take up space and reduce the cost of the formulation. Yet, a functional filler serves a specific and necessary purpose in the formulation in addition to being inexpensive. Examples include antimony oxide for fire resistance and pyrogenic silicas for rheology modification (Grossman & Lutz Jr, 2000). Fillers were first utilized as extenders for polymers, but they are now more concentrated on improving functionality. Nowadays, functional fillers are almost solely used in the polymer sector

to increase stiffness, toughness, dimensional stability, electric insulation, or reduce dielectric loss (Subramanian, 2013).

Calcium Carbonate

Calcite deposits, which range in purity, color, and crystallite size, constitute the basis for entire commercial grades of natural calcium carbonate ($CaCO_3$). These variables are reliant on the origin and ensuing temperature and pressure history. Chalk often has an off-white color and is made up of tiny crystals that are readily broken apart (Pritchard, 2012). Up to 99% of calcite, silica, and other minerals can be found in chalk. Its particles range in size from 1 to 3 μm on average (Hsissou et al., 2021). Large crystals and highly white deposits can be discovered in marble owing to metamorphosis. One of several intermediate types, limestone can range in color from white to grey or buff, primarily due to iron impurities (Pritchard, 2012). Marble and limestone both include silica and magnesium oxide, while calcite makes about 80–90% of the material. The range of the particle size is 0.5 to 30 μm. Calcium carbonate may be the filler that is utilized the most (Hsissou et al., 2021). Several thermosets and thermoplastics employ calcium carbonate as an expensive filler and calcium carbonate is used as an acid acceptor in PVC and as a filler in polypropylene (PP) (Coleman, 2017).

Kaolin

Clay is the mineral with the trade name kaolin. Its chemical formula is $A1_2O_3 \cdot 2SiO_2 \cdot 2H_2O$, which indicates that it is essentially a hydrous aluminosilicate mineral. Hence, theoretically, kaolin is composed of 14.0% water, 46.5% silica, and 39.5% alumina. (Grossman & Lutz Jr, 2000). There are two types: (a) a hydrous form that occurs naturally, and (b) a form that is produced when the clay is heated to a temperature above 600 °C in order to evaporate the water. This is the anhydrous, calcined form. It is more harder than the hydrous form, having a hardness value of 6 to 8 on the Mohs scale as opposed to 2. The natural form's average equivalent spherical diameter ranges from 1.5 to 1.8 μm, however following calcination, it has a broader range (0.9 to 3 μm) (Pritchard, 2012).

Kaolinite is structurally made up of two sheets of silica tetrahedral and alumina octahedral sheets that are layered alternately and joined together on one side. The oxygen atoms serve as the connection between the two sheets of kaolinite, which fit together tightly (Xanthos, 2010). The particles are hexagonal platelets, and when they stack together, they get larger. To make dispersion in a resin easier, the surface must be treated. The surface treatment may have undesirable consequences, preventing epoxy and vinyl polymer reactions. By applying the proper treatment, the particles

are made hydrophobic, resulting in reduced dielectric loss. Additon of very tiny kaolin particles can increase rather than decrease the strength of some thermoplastics (Pritchard, 2012).

Talc

Talc is a hydrated magnesium silicate in terms of chemistry. Pure talc's chemical formula is $3MgO{\cdot}4SiO_2{\cdot}H_2O$. In reality, the MgO to SiO_2 ratio can range from 1:2 to 1:1 (Grossman & Lutz Jr, 2000). By connecting two tetrahedral silica planes to oxygen atoms, the center brucite plane is chemically joined. If talc is not heated above 800 °C, it exhibits a plate-like structure. Talc can delaminate at modest shearing forces because Weak van der Waals forces hold the flat surfaces of the individual platelets together. This explains why the mineral feels slippery and makes it easily dispersible (Xanthos, 2010).

It provides a good mix of stiffness and impact strength in plastics, particularly in PP. The finest talcs can be produced using cutting-edge milling technology without sacrificing the lamellar structure's strength as reinforcement. Compounds of high purity have excellent long-term thermal stability, making them suitable for use in packaging (Murphy, 2001). Talc is a useful filler because it is white and soft. Talc particles' flat structure gives reinforcement value in addition to serving as a filler (Coleman, 2017). Talc-filled compounds are easier to color because of their whiteness and low yellow index, which also means that less pigment is needed. Moreover, some grades will lessen warpage and shrinkage in bigger mouldings (Murphy, 2001).

Silica

There are several crystal shapes and impurity levels of silica (SiO_2). Its inexpensive price and extensive availability are outweighed by its density (2.65 g/cm^3), hardness (7 on the mho scale), and potential toxicity of some but not all grades (Coleman, 2017). In addition to being available as fumed silica and finely divided amorphous diatomaceous earth, silica can also be found as massive crystalline particles like sand and powdered quartz. Burning rice hulls has resulted in the production of reactive silica ash. Furthermore, fluid energy milling and acidification of sodium silicate solutions both yield finely divided silicas (Subramanian, 2013).

The more expensive pyrogenic silica, also known as fumed silica, is produced by the hydrolysis of silicon tetrachloride in an oxygen/hydrogen flame. The product flocculates to create "flocks" with a variety of surface areas that can be up to 200 μm in diameter. The surfaces have silanol groups that cause the particles to engage with one another through their

hydrogen bonds (Pritchard, 2012). To improve the viscosity and thixotropy of liquid resins, fumed silica is utilized (Subramanian, 2013).

At least five different kinds of artificial silicas can be used in polymers. Generally speaking, these are referred to as fumed, arc, fused, gel, and precipitated. The types of silicas that are most frequently employed in thermoplastics are the gel and precipitated varieties, which are used as gloss-reducing agents in polymer sheets and as antiblocking agents in polymer films (Jancar et al., 1999).

Carbon Black

Natural gas, gasoline, coconut shells, and other organic resources, both natural and synthetic, are used as raw materials to make carbon blacks (Coleman, 2017). Carbon black is the most versatile additive. It is utilized to offer reinforcement, color, opacity, UV protection, electrical qualities, and even thermal conductivity. Improved manufacturing techniques have allowed carbon black providers to create a variety of carbon black grades, which in turn give plastics processors a selection of additives tailored to specific end-use characteristics (Pritchard, 2012).

Agglomerates of tiny groups of carbon particles, also known as aggregates, are what make up carbon black. These aggregates are created during the processes that cause solid carbon to condense from vapor. The term "high structure" or "low structure" for carbon blacks refers to how dense they are, with the former having greater dimensions than the latter (Xanthos, 2010). Carbon black's dispersion and viscosity properties are influenced by structure. High structure blacks spread more readily since the attractive forces are weaker because of the greater distances between aggregation centers. Aggregates of high-structure carbon blacks have wider gaps that allow for the incorporation of more resin, increasing compound viscosity (Pritchard, 2012).

Glass Spheres

Thermoplastics and thermosets both make significant use of glass spheres. With densities ranging from 2.5 $g \cdot cm^{-3}$ to 0.1 $g \cdot cm^{-3}$, they can be solid or hollow (Xanthos, 2010). Although spheres obviously lack an aspect ratio (the ratio of length to diameter) that would provide reinforcement characteristics, their geometry offers significant processing benefits. They have the lowest surface area of any shapes, are isotropic in their affects, and have the least impact on melt movement. Due to this and a specific type of ballbearing action, very high loading is possible with only a slight increase in viscosity. Glass sphere composites have minimal distortion and decreased, consistent shrinkage (Stipek & Daoust, 2012). An additional

and crucial feature of hollow spheres is their overall decreased composite density (Xanthos, 2010).

The process of making glass spheres can be done in several distinct ways. They often entail melting fine glass powder or atomisation of molten glass. The majority of the surface treatments employed are silane-based. Although a wide range of particle sizes are available, thermoplastics primarily use the smaller ones (30 μm and lower) (Jancar et al., 1999). Several mechanical qualities, such as tensile strength, flexural strength, compressive strength, and elasticity modulus are improved by solid glass spheres, but ductility, elongation at break, and cold flow are decreased. They are mostly used to fill PVC, poly(acrylonitrile-co-butadiene-co-styrene) and polyamides (Stipek & Daoust, 2012). All the benefits of solid glass spheres are present in hollow glass spheres, but they are also less dense. The decreased density might totally balance the additional cost (when volume or area pricing is used). Hollow spheres with reduced density may frequently replace expensive resin, which is a very good trade-off (Coleman, 2017).

2.4 Impact Modifiers

The majority of plastic materials are extremely brittle; in other words, when under stress, they break without undergoing much deformation. Whereas polyamides (PA) and polyolefins are ductile at ambient temperature and brittle at low temperatures, unmodified PVC or polystyrene (PS) are brittle at ambient temperature (Marturano et al., 2017). A key factor for many applications is the improvement of polymer toughness. Impact toughness expresses how much energy is absorbed from the start of a mechanical stress to the point of final breakage. A plastic's toughness can be increased by adding clearly specified modest doses of impact modifiers with various physical properties (Subramanian, 2013). The polymeric impact modifier must have a glass transition temperature that is significantly lower than the ambient temperature (Stevens, 1993c).

Compared to the polymer matrix, impact modifiers typically have low modulus and glass transition temperature. They are also elastomeric or rubbery in nature. Moreover, the rubbery phase needs to be well-compatible with the host polymer and have a fine particle size distribution (Marturano et al., 2017). Various elastomers have varying proportions of hard (like styrene) and soft (like butadiene or isoprene) building blocks, as well as different molecular weights and molecular structures. The processing and performance characteristics of the finished goods vary as a result of these variances in elastomer structures. For instance, increasing the proportion of rigid blocks produces stiffer (higher modulus) materials, but also makes it harder to melt-process blends. Impact strength of a thermoplastic elastomer typically increases with its molecular mass (Ghosh, 2021).

2.5 Lubricants

A lubricant is a chemical that, when applied in small amounts, significantly reduces the resistance to the movement of chains or segments of a polymer having at least partially amorphous structure without significantly altering the material's observable properties. (Grossman & Lutz Jr, 2000). Lubricants are useful because they either lower the polymer's melt viscosity or lower the heterogeneous friction between the polymer and the stationary and moving walls of the processing machinery. The surface of a finished resin product is smoothed with a lubricant to increase its processability. (Fink, 2010).

External lubrication is the technique of using lubricants to keep polymers that have a tendency to stick from adhering to the metallic components of processing machines. In order to optimize the free flow of the melt bulk polymer by minimizing friction between chain segments, another crucial role is to contribute internal lubrication to the polymer that is being processed. For improved homogeneity of the combination of the polymer and additives, this enables, for instance, higher temperature operation of the mixing process. When these two tasks are integrated, the processing machinery produces a superior product, and mold release is also made easier (Stipek & Daoust, 2012).

Currently, solid materials that are most frequently employed as lubricants include (Xanthos, 2010):

1. Particular fillers (layer-lattice solids) include graphite, and molybdenite or molysulfide (MoS_2).

2. Polymers include silicones, poly(chlorofluoroethylene), and poly(-tetrafluoroethylene).

3. Less often utilized materials include ceramics, such as, boron nitride, aramid or carbon fibers, as well as other materials like calcium fluoride, cerium fluoride, tungsten disulfide, mica, borax, silver sulfate, cadmium iodide, lead iodide, and talc.

Among the materials mentioned above, the two most common solid lubricants are MoS_2 and graphite. These lubricants are efficient in dry powder form because of their lamellar structures. The lamellae face to the surface which is parallel to the direction of motion (Xanthos, 2010).

2.6 Heat Stabilizers

Chemical bonds in certain synthetic polymers are less thermally stable than the chemically pure backbone of the ideal structure. These "weak links" frequently breaks during melt processing, which lowers the perfor-

mance of the plastic item that results. Some commercial polymers have chemical contaminants including catalyst residues and products of thermal breakdown that further weaken the thermal stability of the polymer's backbone chain (Coleman, 2017).

Different types of stabilizers are utilized as plastic additives in order to increase the virgin resin's resistance to degradation and preserve the physical and chemical properties of the compounded materials at optimal values during the processing and lifespan of the material and/or the components made from it as well. In order to prevent thermal deterioration of plastics even in the absence of oxygen during production as well as during the useful life of the completed goods, heat stabilizers are added to plastics (Eyerer et al., 2010).

By preventing the negative impacts of polymer defects and impurities, thermal stabilizers reduce molecular weight change during melt processing. PVC, PP, and polyoxymethylene are the polymers that are most susceptible to heat, although even molar mass of high-density polyethylene can change during melt processing (Coleman, 2017).

PVC is highly heat-sensitive due to its structure. In fact, the PVC industry is the one that uses heat stabilizers the most and has the most demand for them (Ambrogi et al., 2017). When PVC is heated, it tends to release hydrogen chloride and produce highly colored conjugated units in the polymer backbone. This also happens to cause corrosion of processing equipment. On heating, the polymer's scattered allylic chloride sites are thought to be what initiates the dehydrohalogenation reaction (Stevens, 1993b):

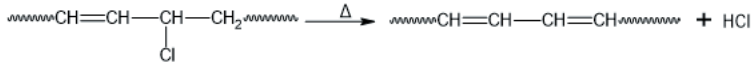

(12)

There are several different stabilizers for plastics, based on the kind and products of oxidation. Formerly, metallic salts based on barium, cadmium, lead, or zinc were used to stabilize PVC. These salts were frequently combined to have a synergistic effect. Also employed are organometallic compounds, mostly based on tin. The third category consists of non-metallic organic stabilizers, where phosphites are significant contributors that enhance transparency, initial color, and light fastness. Epoxies, especially those made from soy bean oil, are also utilized in non-toxic goods as plasticizers (Murphy, 2001).

2.7 Flame Retardants

The basis of all organic polymeric compounds is carbon, which is a fundamental component. In addition to hydrogen, many of them also include significant amounts of nitrogen, oxygen, sulphur, fluorine, and chlorine.

Due to the existence of heteroatoms in the main chains, some of the polymer backbones also include carbon-nitrogen and carbon-oxygen bonds on a regular basis. If exposed to enough heat, all of these organic polymers experience thermal degradation (Pritchard, 2012). The initial step in the burning process for polymers is melting, followed by the melt's thermal or thermo-oxidative destruction. When deterioration occurs, volatiles are created. When they come into contact with heat and oxygen, they ignite a combustion process that produces heat and flames for the process' self-sustenance. This cycle continues until one of the "heat- fuel- oxygen" trio components is absent (Paoli & Waldman, 2019).

Burning of plastics is a highly important issue that restricts the use of plastics in construction industry, in the automotive and aviation sectors, in mining, and other applications. The majority of common commercial polymers are very flammable. Burning of plastics is a complex process that is mostly influenced by the chemical nature of polymers and a few physical variables. Plastics are very combustible when the fundamental polymers are depolymerized to create flammable monomers or active substances. The same is true for natural rubber, poly(oxymethylene), poly(methylmethacrylate), PS, and other materials (Stipek & Daoust, 2012).

Flame retardant (FR) additives function by severing one of the three components that cause and maintain combustion—heat, fuel, and air. They can put out a flame by stripping it of oxygen, or they can take in heat and turn it into water, which lowers the temperature. There is a growing trend toward the combined usage of flame retardant chemicals, which frequently has a synergistic effect (Murphy, 2001).

A primary flame retardant is recognized as one that is capable of creating a level of flame retardancy that is economically useful on its own. A secondary additive, often known as a synergist, can greatly increase the efficiency of a main flame retardant while having little of its own flame retardant impact (Al-Malaika et al., 2017). Depending on the technology used, there are three different types of flame retardants (Ambrogi et al., 2017): Halogen-based flame retardants, phosphorus based flame retardants and metal hydrate flame retardants.

Halogen-based Flame Retardants.

The halogenated additives that are employed are organic compounds of chlorine or bromine and have high halogen content relative to their weight. Their efficacy rises as the halogen content rises, and certain brominated chemicals can have halogen contents as high as 80% by weight. There are many different halogenated compounds available; they must be robust enough to withstand the host polymer's processing conditions while also breaking down and releasing halogen at a temperature comparable to

the polymer's own disintegration (Al-Malaika et al., 2017). They operate by interfering with the chemical radical mechanism of combustion when in the vapor or gas phase. Unfortunately, several of the flame retardants in this class, particularly the brominated ones, are thought to be detrimental to the environment (Ambrogi et al., 2017).

Phosphorus-based Flame Retardants.

Based on the oxidation state of the element, phosphorus-based flame retardants can be classified as phosphates ($(RO)_3PO$), phosphites ($(RO)_3P$), phosphonites ($(RO)_2PR'$), phosphinates ($(RO)R_2'PO$), phosphine oxides (R_3PO), phosphines (R_3P), and phosphonium salts (R_xPX). The most efficient molecules appear to contain phosphorus in the oxidation states -3, -1, and 1. These flame retardants work in both the gaseous and solid phases (Stipek & Daoust, 2012). In reality, phosphorus-based flame retardants are more frequently referred to as "char formers" because, while burning, they generate phosphoric acids. These acids react with the substrate to create a char that serves as a protective covering for the substrate. Phosphorus-based flame retardants are primarily used in the formulation of PA, polyesters, polyolefins, and PS, particularly in electrical and electronic insulation components (Marturano et al., 2017).

Metal hydrate flame retardants

Typical members of this family of FRs are magnesium hydroxide ($Mg_2(OH)_4$) and aluminum trihydroxide ($Al(OH)_3$). They break down endothermically and release a lot of water of hydration (30%) for cooling of the system. As a result, the material's flaming ignition is postponed and, in certain situations, even prevented. There is a need for high additive concentrations, and considerable mechanical property deterioration is predicted (Grossman & Lutz Jr, 2000). They are not employed in many of the high temperature thermoplastics, like PA, polybutylene terephthalate, polycarbonate (PC), etc., since they work by breaking down to release water at temperatures above the melt processing temperatures of many polymers. Aluminum trihydrooxide can not be utilized as an additive for PP. The breakdown of aluminum trihydrooxide produces steam. The polymer foams if this happens during melt processing. A more thermally stable inorganic hydrate than aluminum trihydrooxide is magnesium hydroxide. It may be utilized in high melting thermoplastics like PP and others (Coleman, 2017).

2.8 Nucleating Agents

A polymer begins to crystallize when it is cooled below its melting point, and this process includes nucleation and growth phases. When a new crystalline phase begins at locations known as nuclei, the process is

known as nucleation. Nucleation processes control the kinetics of polymer crystallization. Following the establishment of the initial nuclei, further nucleation stages in macromolecular crystallization control the growth rate (Libster, Aserin, & Garti, 2007).

While a crystal is growing, polymer chains are oriented in a 3D pattern around the original nucleation site, or nucleus, most frequently creating a spherical crystal cluster known as a spherulite. Spherulites form individual crystals during the early stages of crystal formation and define separate crystalline domains when they come into contact with other spherulites or the material interface. When the crystalline and noncrystalline domains fills the available space, complete crystallization takes place. The size and form of these domains, which are frequently determined by the initial nucleation density and growth rate, describe the final material (Seven, Cogen, & Gilchrist, 2016).

Homogeneous and heterogeneous nucleation are the two main forms of nucleation, with the latter being significantly more prevalent. The volume of a typical polymer chain varies from 10^2 to 10^4 nm^3, whereas the dimensions of a homogeneous nucleus are typically on the order of 10^2 nm^3. As a result, the formation of a nucleus only involves a small piece of the chain. Heterogeneous nucleation, which mostly develops on impurities left over from catalytic systems, on filler particles, or as a result of the action of nucleating chemicals purposefully introduced to encourage nucleation, has a far higher practical significance. When the critical nucleus size is reduced due to the presence of solid surfaces, heterogeneous nucleation and subsequent crystallization can happen at lower undercooling since the free enthalpy for critical nucleation is considerably reduced (Jancar et al., 1999).

Higher polymer crystallization temperatures are provided by nucleating agents, which result in smaller spherulites and better optical and mechanical characteristics. Rigidity and flexural modulus may be enhanced by small spherulites. The optical characteristics of the plastics are improved by the size reduction of spherulites, which lowers haze and increases clarity. Higher polymer crystallization temperatures allow for much shorter cycle times and increased product output (Libster et al., 2007).

The duration, temperature, and type of nucleant can all affect which crystalline form of a polymer predominates when there are several possible crystalline forms. The monoclinic (α) and hexagonal (β) forms of PP serve as the most typical examples. Depending on the nucleating agent employed, PP can crystallize to produce one of its crystalline forms (Pritchard, 2012). As a result, whereas sodium benzoate can create the α-(monoclinic) form present in nonnucleated PP, a number of nucleating chemicals, such

as disodium phthalate, can create the β-(hexagonal) form, which can create enhanced mechanical characteristics (Al-Malaika et al., 2017).

Crystallization can be initiated by a wide variety of chemicals. The effect is distinctive to the chemical and the polymer. Some polymers can start crystallizing because of the presence of glass fibers, colors, talc, etc (Coleman, 2017). For the purpose of processing polymers, nucleating agents can be classified into three categories: organic nucleating agents, inorganic nucleating agents, and nanoparticles. Examples of organic nucleating agents are metal aromatic carboxylates, sorbitol derivatives, and organic phosphates and whereas examples of inorganic nucleating agents are talc and silica. Nanoparticles include nanoclay and carbon nanotubes (Subramanian, 2013).

2.9 Coupling Agents

Many of the characteristics that fillers offer are associated with the surface attributes of the particles, particularly their surface area, structure, and nature of the reactive group. Modifying the filler surface is frequently helpful to maximize the balance of qualities in a particular composition (Grossman & Lutz Jr, 2000). The surface properties of the fillers and their reinforcements are modified using coupling agents. Coupling agents aid plastic composites' mechanical and chemical resistance by enhancing the adhesion between the plastic and the filler (Subramanian, 2013).

Coupling agents can either be fixed to fillers before being added to polymers or added directly to polymers. Compared to the scenario when the coupling agent is bonded to the filler first, this final procedure has the drawbacks of requiring higher amounts of coupling agents and longer intervals to get excellent adhesion between the filler and the polymer (Stipek & Daoust, 2012). The silanes and titanates are the two most common types of coupling agents.

Silanes

Chemical substances with a silicon-hydrogen bond are known as silanes. These substances are also known as silicon hydrides (e.g. SiH_4 or $SiCl_3H$). Despite having organic groups in place of the hydrogen atoms that silanes have, organosilanes are still frequently referred to as silanes in the context of reinforced plastics even though they may not necessarily have the silicon hydrogen bond (Pritchard, 2012). The silane molecule should have bifunctional groups that may individually react with the two phases, so generating a bridge between them, in order to efficiently connect the fillers and polymer matrices. The chemical formula for silane coupling agents is $R_{(4-n)}–S–(R'X)_n$ (n = 1,2), where R is an alkoxy group, X is an

organofunctionality, and R′ is an alkyl bridge (or alkyl spacer) that attachs the silicon atom to the organofunctionality. Inorganic reinforcements like glass fiber and organic polymer matrices have been coupled using a variety of silane structures that have been tested over the past few decades (Xie, Hill, Xiao, Militz, & Mai, 2010).

Silane coupling agents are frequently used in the manufacturing of composite materials composed of organic polymers and inorganic fillers such as glass, minerals, metals, and their oxides. (Stipek & Daoust, 2012). For instance, vinyltrimethoxysilane (CH_2=$CHSi(OCH_3)_3$) is typically employed with polymers that incorporate glass fiber reinforcement. As shown in Figure 5, the coupling agent's alkoxy groups that are bound to silicon atoms undergo hydrolysis to become hydroxyl groups, which then establish siloxane linkages with silicon atoms on the glass surface. The vinyl group is copolymerized into the crosslinked network which is formed by copolymerization of unsaturated polyesters with styrene (Stevens, 1993b).

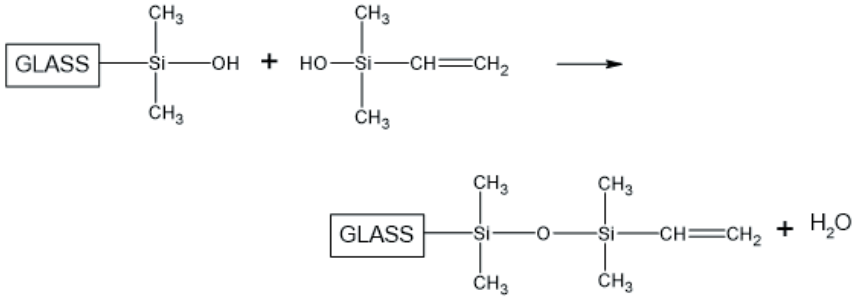

Fig. 5. *The reaction of vinyltrimethoxysilane with glass fiber.*

Titanates

Plastic fillers using titanate coupling agents have greater functionality. By proton coordination, titanium esters join or chemically link two different species, such as an organic polymer and an inorganic filler or particle or fiber. This enables coupling to organic substrates like carbon black and nitramines as well as inorganic substrates like $CaCO_3$ and boron nitride without the requirement for water or condensation, unlike with silanes, which are non-hydroxyl bearing and consequently non-silane reactive. Neoalkoxy organometallics' thermally stable quaternary carbon structure allows for in-mold reactions to occur with thermoplastic melt (Xanthos, 2010).

The benefit of titanate coupling agents is that they only produce a monomolecular layer. Because multimolecular layer does not exist at the interface and titanates have a different chemical nature than other coupling

agents, their surface energy is altered, resulting in lower melt viscosities for polymers (Stipek & Daoust, 2012). Titanates have a variety of uses, including coating the surfaces of minerals, pigments, carbon black, metals, metal oxides, and fibers (Pritchard, 2012).

2.10 Antistatic Additives

Several organic macromolecules exhibit properties of dielectrics. In most cases, the electrons involved in chemical interactions are confined, and at room temperature, the specific conductance of polymers ranges from 10^{-9} to 10^{-2} $S \cdot cm^{-1}$ (Stipek & Daoust, 2012). Materials with high resistivity, or low electrical conductivity, are subject to static electrification. The excessive buildup of electric charges on their surface is the cause of this phenomena. Electrification may be applied to items manufactured of, among other things, PC, PET, polyurethane, PVC, PP, or polyethylene (Kosiński et al., 2022). Surface charge makes plastic film adhere to one another, attracts dirt like a magnet, and makes cloth cling. Static charge can produce interference when electrical equipment is present, and in some settings (like grain elevators, for example), it poses an explosion risk (Stevens, 1993b).

Antistatic additives need to be added to polymers for the reasons mentioned above. Antistatic additives are substances that are applied to material surfaces to reduce or completely remove static electricity buildup caused by the triboelectric effect or other non-contact processes. An antistatic additive has the ability to slightly conduct the material's surface on its own (Kosiński et al., 2022). Antistatic additives are available in two different types: internal antistatic additives and external antistatic additives.

Internal antistatic additives are typically compounded at 0.1-3.0% by weight and they are barely compatible with the polymer; nevertheless, because of the hydrophilic head on the molecule, it is forced to migrate to the surface and draw moisture from the air, increasing the surface conductivity. They are simple to use, have low addition rates, and frequently offer additional advantages including enhanced processability and mould release (Murphy, 2001). Internal antistatic additives are frequently favored because, even if some of them are removed from the surface by different processes, including erosion, additional additive is available within the polymer to migrate and replace what was lost (Pritchard, 2012).

Because they are sprayed to the plastic surface as a coating, external antistatic additives are occasionally referred to as topical antistatic additives. The coating process just needs a tiny amount of additive that takes effect right away. The antistatic qualities are less durable, though. When the surface is cleaned, for instance, the specific properties could be readily lost (Fink, 2010).

Antistatic additives can also be divided into groups based on their chemical nature. Ionic and non-ionic additives are both available. Ionic antistatic substances can be either cationic or anionic. The first of these include quaternary ammonium salts. They can be produced by treating a long-chain aliphatic tertiary amine, for instance, with dialkyl sulfates and dialkyl halides. N-cetyl-N, N, N-trimethylammonium bromide (Figure 6) is an illustration of such an antistatic (Kosiński et al., 2022). Alkali salts of alkyl sulphonic, and phosphonic, or carboxylic acids are frequently used as anionic antistatic additives. For styrenics, sodium alkyl sulphonates are suggested (Murphy, 2001).

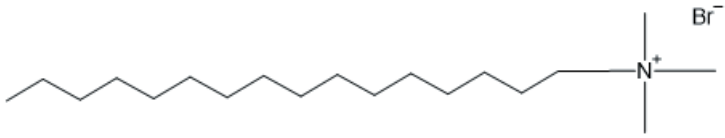

Fig. 6. *Structure of N-cetyl-N, N, N-trimethylammonium bromide.*

The ethoxylated fatty alkylamines, fatty diethanolamines, and mono- and di-glycerides are examples of the non-ionic antistatic additives. In some styrenated polymers and hydrocarbon-rich plastics like polyolefins, ethoxylated fatty alkylamines are utilized. They remain effective even at low relative humidity levels and can be utilized in low concentrations (Pritchard, 2012).

3. Conclusions

Herein, we reviewed the most signficant additives developed and sold by the plastics industry. It has been known since the beginning of the plastics and rubber industries that certain additives should be incorporated into polymers in order to produce useful products. These additives have made it feasible to promote the mechanical characteristics and processability of plastics while also preventing oxidative and thermal degradation. The massive increase in the amount of plastics that modern society consumes and the emergence of new applications for plastics have led to a desire for more effective additives and a superior knowledge of their fuctions in plastics. The significance of additives in plastics will not only endure, but also grow as a result of the tendency in plastics toward higher quantities and fewer grades, offering new uses and new effects. In a summary, plastic additives are and will continue to be crucial elements in polymer formulas, and they will offer creative solutions to resin producers, plastic converters, and an increasing number of consumers of plastic goods.

REFERENCES

Al-Malaika, S., Axtell, F., Rothon, R., & Gilbert, M. (2017). Additives for plastics. In *Brydson's plastics materials* (pp. 127-168): Elsevier.

Ambrogi, V., Carfagna, C., Cerruti, P., & Marturano, V. (2017). Additives in polymers. In *Modification of polymer properties* (pp. 87-108): Elsevier.

Bart, J. C. (2005). *Additives in polymers: industrial analysis and applications*: John Wiley & Sons.

Bolgar, M., Hubball, J., Groeger, J., & Meronek, S. (2015). *Handbook for the chemical analysis of plastic and polymer additives*: CRC Press.

Coleman, E. A. (2017). Plastics additives. In *Applied Plastics Engineering Handbook* (pp. 489-500): Elsevier.

Eyerer, P., Weller, M., & Hübner, C. (2010). *Polymers-Opportunities and Risks II: sustainability, product design and processing* (Vol. 12): Springer.

Fink, J. K. (2010). *A concise introduction to additives for thermoplastic polymers*: John Wiley & Sons.

Ghosh, A. (2021). Performance modifying techniques for recycled thermoplastics. *Resources, Conservation and Recycling, 175*, 105887.

Grossman, R. F., & Lutz Jr, J. T. (2000). *Polymer modifiers and additives*: CRC Press.

Hahladakis, J. N., Velis, C. A., Weber, R., Iacovidou, E., & Purnell, P. (2018). An overview of chemical additives present in plastics: Migration, release, fate and environmental impact during their use, disposal and recycling. *Journal of hazardous materials, 344*, 179-199.

Hsissou, R., Seghiri, R., Benzekri, Z., Hilali, M., Rafik, M., & Elharfi, A. (2021). Polymer composite materials: A comprehensive review. *Composite structures, 262*, 113640.

Jancar, J., Fekete, E., Hornsby, P., Jancar, J., Pukánszky, B., & Rothon, R. (1999). *Mineral fillers in thermoplastics I: raw materials and processing*: Springer.

Kosiński, S., Rykowska, I., Gonsior, M., & Krzyżanowski, P. (2022). Ionic liquids as antistatic additives for polymer composites–a review. *Polymer Testing*, 107649.

Libster, D., Aserin, A., & Garti, N. (2007). Advanced nucleating agents for polypropylene. *Polymers for advanced technologies, 18*(9), 685-695.

Marturano, V., Cerruti, P., & Ambrogi, V. (2017). Polymer additives. *Physical Sciences Reviews, 2*(6).

Murphy, J. (2001). *Additives for plastics handbook*: Elsevier.

Paoli, M. A. D., & Waldman, W. R. (2019). Bio-based additives for thermoplastics. *Polímeros, 29*.

Pérez-Albaladejo, E., Solé, M., & Porte, C. (2020). Plastics and plastic additives as inducers of oxidative stress. *Current Opinion in Toxicology, 20*, 69-76.

Pritchard, G. (2012). *Plastics additives: an AZ reference* (Vol. 1): Springer Science & Business Media.

Seven, K. M., Cogen, J. M., & Gilchrist, J. F. (2016). Nucleating agents for high-density polyethylene—A review. *Polymer Engineering & Science, 56*(5), 541-554.

Stevens, M. P. (1993a). Polymer additives: II. Chemical and aesthetic property modifiers. *Journal of chemical education, 70*(7), 535.

Stevens, M. P. (1993b). Polymer additives: III. Surface property and processing modifiers. *Journal of chemical education, 70*(9), 713.

Stevens, M. P. (1993c). Polymer additives: Part I. Mechanical property modifiers. *Journal of chemical education, 70*(6), 444.

Stipek, J., & Daoust, H. (2012). *Additives for plastics* (Vol. 5): Springer Science & Business Media.

Subramanian, M. N. (2013). *Plastics additives and testing*: John Wiley & Sons.

Xanthos, M. (2010). *Functional fillers for plastics*: John Wiley & Sons.

Xie, Y., Hill, C. A., Xiao, Z., Militz, H., & Mai, C. (2010). Silane coupling agents used for natural fiber/polymer composites: A review. *Composites Part A: Applied Science and Manufacturing, 41*(7), 806-819.

CHAPTER 8

SEMI-MARKOV VS CONDITIONAL COPULAS: A COMPARATIVE STUDY IN SEISMIC HAZARD ANALYSIS

Serpil ÜNAL[1]

1 Dr. Öğr. Üyesi, Usak University, Faculty of Arts and Sciences, Department of Mathematics, Uşak, Turkey, E-mail:serpil.unal@usak.edu.tr
ORCHID: 0000-0002-4043-6832

Introduction

Turkey is located in the Alpine-Himalaya or Mediterranean Environment earthquake belt, which is one of the 3 important earthquake belts on the world, and where approximately 20-25% of the earthquakes occurred in the world every year. It is also a country having an extremely high earthquake risk with regard to geological, historical and instrumental current period earthquake activities of this belt. Tsapanos and Burton (1991) supported this with a study using the Gumbel extreme value theory and showed that Turkey ranks tenth among the 50 active countries in the world in terms of seismicity. West Anatolia, which is considered as the application region in this study, is also among the important mechanisms of active tectonics in Turkey. Due to its highly complex tectonic appearance, the region is constantly exposed to earthquakes and creates a region with high earthquake potential in the future. For this reason, studies on the prediction of earthquakes in the West Anatolia region including big cities, especially such as the third largest city of Turkey, İzmir, have become very important.

Today, it is thought that it is not possible to know exactly where, when and how large earthquakes will occur and to prevent this destructive natural event. However, many researchers have tried to estimate the parameters of possible earthquakes and the intensity of the ground motion they create with the statistical studies available in fields such as geophysics, geology. The Poisson model, one of the most frequently used statistical models, is on the assumption that the time and place occurrences of earthquakes are independent of each other. Since it can not be a realistic approach to assume that earthquakes that occurred in a local area are independent from each other, although risk determinations with the Poisson model give good results in large areas, they are insufficient in local studies. Considering this problem, the need to use a more valid model has emerged in studies to be conducted in a local area (Altınok, 1988). Therefore, in later studies, the Markov model, which is on the assumption that earthquakes are dependent on space and time, in conjunction with the Elastic Rebound Theory, the Semi-Markov model based on this model (Altınok, 1988; Altınok, 1991; Altınok and Kolçak, 1999; Sadeghian et al, 2008; Sadeghian, 2012; Causapin, 2018) and Hidden Markov model, which is a special case of the

Markov model, where the states of the system cannot be observed directly, and the observations are defined as the output of another process under the influence of the process followed by the system have been used. It is useful to apply the Markov model in certain areas and regions with the same structural discontinuity, due to the dependency characteristic of the sequences of events, in other words, the dependence of events on their predecessors. The drawback of the model is that it is also time dependent. This dependency is the requirement that an event occur in each unit of time selected in the time dimension. However, it is not obligatory for an earthquake to occur in every selected unit of time in earthquakes. This led researchers to use the Semi-Markov model. According to the Semi-Markov model, the energy accumulation in the earth's crust depends on the time elapsed between two consecutive earthquakes. The absence of an earthquake for a long time after a major earthquake indicates that a major earthquake may occur in the future. The magnitude of an earthquake in the future depends on the magnitude of the previous earthquake and the elapsed time (Altınok, 1988). The other statistical method used to estimate earthquake occurrences is also the Conditional Copulas. Copulas are the connections between one-dimensional marginal distribution functions and multivariate distribution functions. A copula that is parametric and has a parameter change depending on the covariate is known as a conditional copula. Both copulas and conditional copulas (Li et al., 2008; Nikoloulopoulos, et al., 2008; Goda and Ren, 2010; Liu and Zhang, 2016; Ünal Karaçam, 2019; Shen and Chen, 2020; Bai et al., 2022; Qian and Dong, 2022; Rivera-Vargas and Heredia-Zavoni, 2022) have been used in seismology for long years.

In this study, using the earthquake data in the years 1901-2013 with the magnitude $M_l \geq 4,$ on the areas limited by 36°-39.5° N latitudes and 26°-31° E longitudes of West Anatolia, it is aimed to compare earthquake occurences of next years for mentioned above two models: Semi-Markov model, based on the assumption that consecutive earthquakes within the same structural discontinuity are not independent events and that the occurrence of earthquakes should be affected by the time elapsed between them and Conditional Copulas, based on modeling the dependency structure of Semi-Markov models.

1. Methods

1.1. Semi-Markov model

Let $\{X(t)\}_{t\in[0,\infty)}$ be a continuous time chain having discrete state space. If the development of the chain after each transition is independent of its behavior before that time, the chain is called Semi-Markov. More clearly, with T_n being the nth transition time, the distribution of its holding time $T_n - T_{n-1}$ is independent of its behaviour before T_{n-1} but may be a function of $X_{n-1} \equiv X(T_{n-1}), X_n \equiv X(T_n)$.

The transition probability G_{ij}, being the ijth element of the transition matrix P,

$$G_{ij} = P\{X(T_n) = j \mid X(T_{n-1}) = i\}$$
$$G_{ij} \geq 0 \;\; ; \quad i,j = 1,2,\dots,N \quad \text{and} \quad \sum_{j=1}^{N} G_{ij} = 1.$$

Before the transition from state i to state j, the process remains in state i for some time t_{ij} which is called the holding times. All holding times t_{ij} are positive random variables with integer values and each one is at least equal to one time unit.

The probability of the joint event in which a system entered state i at time 0 and makes its next transition to state j after a holding time m_1, the ijth element $C_{ij}(m_1)$ of the core matrix $C(m_1)$, is obtained by:

$$C_{ij}(m_1) = P\{X_n = j \mid X_{n-1} = i, t_{ij} = m_1\}$$
$$= P\{X_n = j \mid X_{n-1} = i\} \;\; P\{t_{ij} = m_1\}$$
$$= G_{ij} \;\; T_{ij}(m_1) \quad ; \;\; i,j = 1,2,\dots,N \;\; ; m_1 = 1,2,\dots,n$$

To be $T_{ij}(m_1)$ is the ijth element of the holding time mass function $T(m_1)$ and $\otimes$ is the multiplication of corresponding elements of the congruent matrices, the obtained equation is denoted in congruent matrix multiplication form by

$$C(m_1) = P \otimes T(m_1).$$

Therefore, the interval transition probability matrix $F(n)$ is as follows:

$$F(n) = GW(m_1) + \sum_{m=0}^{n} P \otimes T(m_1)F(n-m_1) = PW(m_1) + \sum_{m=0}^{n} C(m_1)F(n-m_1)$$

such that $n = 0,1,2,\ldots\ ; 0 \le m_1 \le n$, where $PW(m_1)$ is a diagonal matrix with ith element equal to $1 - \sum_j^N C_{ij}(m_1)$. However, because of $T(0) = 0$, $F(n)$ is obtained for $1 \le m_1 \le n$. If $n = 0$, $F(n)$ is equal to the Kronecker Delta or identity matrix (Sadeghian, 2012).

1.2. Copulas and Conditional Copulas

A copula is a function that combines a multivariate distribution function with one-dimensional marginal distribution functions.

Definition 1. A two-dimensional copula $C: [0,1]^2 \to [0,1]$ provide the conditions follows:

1. $C(u,0) = C(0,v) = 0$ and $C(u,1) = u, C(1,v) = v$; $\forall u,v \in [0,1]$.

2. $C(u_2,v_2) - C(u_1,v_2) - C(u_2,v_1) + C(u_1,v_1) \ge 0$; $\forall u_1,u_2,v_1,v_2 \in [0,1]$ such that $u_1 \le u_2$ ve $v_1 \le v_2$.

Theorem 1. (Sklar's theorem) Let H be a joint distribution function with margins F and G. Then there exists a copula C such that for all x, y in $\overline{\mathrm{R}}$,

$$H(x,y) = C\big(F(x), G(y)\big) \qquad (1)$$

If F and G are continuous, then C is unique; otherwise, C is uniquely determined on $RanF \times RanG$. Conversely, if C is a copula and F and G are distribution functions, then the function H defined by (1) is a joint distribution function with margins F and G (Nelsen, 2006).

Table 1. Some of the one-parameter copula families

Family	$C_\theta(u,v)$	Range of θ
Clayton	$\left(u^{-\theta}+v^{-\theta}-1\right)^{-1/\theta}$	$(0,\infty)$
Frank	$-\theta^{-1}\ln\left(\left[\left(e^{-\theta}-1\right)+\left(e^{-\theta u}-1\right)\left(e^{-\theta v}-1\right)\right]/\left(e^{-\theta}-1\right)\right)$	$(-\infty,\infty)-\{0\}$
Gumbel	$exp\left(-\left((-\ln u)^\theta+(-\ln v)^\theta\right)^{1/\theta}\right)$	$[1,\infty)$
Çelebioğlu-Cuadras	$uv\,exp\left(\theta(1-u)(1-v)\right)$	$[-1,1]$
FGM	$uv+\theta uv(1-u)(1-v)$	$[-1,1]$
Galambos	$uv\,exp\left\{\left[(-\ln u)^{-\theta}+(-\ln v)^{-\theta}\right]^{-1/\theta}\right\}$	$[0,\infty)$
Tawn	$uv\,exp\left(-\theta\frac{\ln u\ln v}{ln(uv)}\right)$	$(0,1)$
Joe	$1-\left[(1-u)^\theta+(1-v)^\theta-(1-u)^\theta(1-v)^\theta\right]^{1/\theta}$	$[1,\infty)$

In modeling the dependency between two or more random variables, you must model not with copulas when a covariate is added to the model, but with conditional copulas, where the copula parameter changes according to the values of the covariate.

Definition 2. The conditional copula of $(X,Y)|Z=z$, where $X|Z=z\approx F_{X|Z}(.|z)$ and $Y|Z=z\approx F_{Y|Z}(.|z)$, is the joint distribution function of $U\equiv F_{X|Z}(.|z)$ and $V\equiv F_{Y|Z}(.|z)$ given $Z=z$.

Proposition 1. A two-dimensional conditional copula is a function $C\colon[0,1]\times[0,1]\times\chi\to[0,1]$ with the following properties:

1. $C(u,0|z)=C(0,v|z)=0$; $C(u,1|z)=u, C(1,v|z)=v$; $\forall u,v\in[0,1]$ and $\forall z\in\chi$.
2. $C(u_2,v_2|z)-C(u_1,v_2|z)-C(u_2,v_1|z)+C(u_1,v_1|z)\geq 0$; $\forall u_1,u_2,v_1,v_2\in[0,1]$ such that $u_1\leq u_2$ and $v_1\leq v_2$ and $\forall z\in\chi$.

Theorem 2. Let $F_{X|Z}(.|z)$ be the conditional distribution of $X|Z=z$, $F_{Y|Z}(.|z)$ be the conditional distribution of $Y|Z=z$, $H_Z(.,.|z)$ be the joint distribution of $(X,Y)|Z=z$ and χ be the support of Z. Then,

there exists a unique conditional copula $C(.,.|z)$, whenever $F_{X|Z}(.|z)$ and $F_{Y|Z}(.|z)$ are continuous in x and y, for all $z \in \chi$, such that

$$H_Z(x,y|z) = C\big(F_{X|Z}(x|z), F_{Y|Z}(y|z)|z\big) \quad (2)$$

Conversely, if $\{C(.,.|z)\}$ is a family of conditional copulas measurable in z, then the function $H_Z(.,.|z)$ defined in (2) is a conditional bivariate distribution function with conditional marginal distributions $F_{X|Z}(.|z)$ and $F_{Y|Z}(.|\boldsymbol{z})$ (Patton, 2003; Patton, 2006; Unal Karacam, 2019).

1.3. Entropy and Markov Chains

According to Shannon, who defines entropy as a measure of the level of uncertainty of a system, obtaining information about an event can only happen if that event contains uncertainty. According to this, the formation of events with a high probability does not bring much information; on the contrary, the formation of unlikely events carries more information. Based on Shannon (1948), Jaynes also stated that if a distribution with a smaller entropy than the maximum entropy is chosen, this decrease in entropy may be due to some additional information used consciously or unconsciously, but using a distribution with less entropy would not be correct if this information is not given stated that only the maximum entropy distribution should be used (Giriftinoğlu, 2005).

Definition 3 Let $\{X_n\}$ be a Markov Chain with stationary distribution π and transition matrix P. Then the entropy rate of the Markov Chain $H(P)$,

$$H(P) = \sum_{i,j} \pi_i P_{ij} \log P_{ij}.$$

2. Application to Earthquake Data

Western Anatolia is one of the important mechanisms of active tectonics in Turkey. Due to its highly complex tectonic appearance, the region is constantly exposed to earthquakes and creates a region with high earthquake potential in the future. Due to the randomness of the

earthquakes according to the parameters and the presence of various uncertainties, probabilistic methods are used in the estimation of earthquake occurrences. The fact that the Semi-Markov model, which is the most frequently used among these methods, gives good results in places with tectonic relations such as structural discontinuities, suggests that this model can be applied to similar tectonic areas (Altınok, 1988; Altınok, 1991). For this reason, area limited by 36°-39.5° N latitudes and 26°-31° E longitudes of West Anatolia was chosen as the application area (Ünal, 2010; Ünal and Çelebioğlu, 2011; Ünal Karaçam, 2016; Ünal Karaçam; 2019):

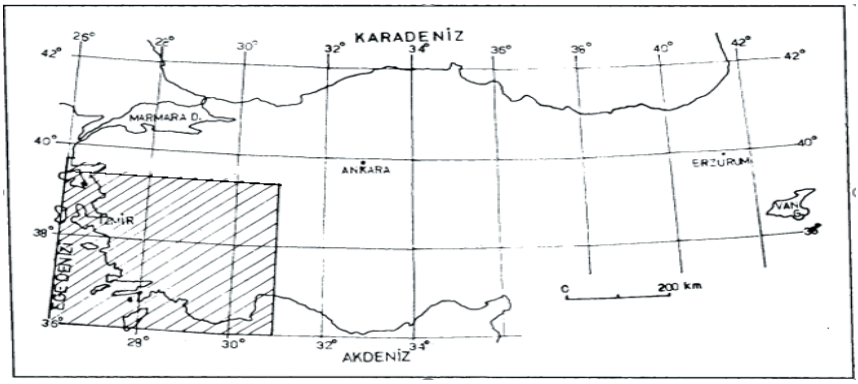

Figure 1. Investigated area

At the first stage of modeling with Semi-Markov, entropy principle was applied for the clustering of magnitudes chosen as states. Table 2 shows the transition matrix P, the stationary distribution π and the entropy values $H(P)$ for all considered threshold magnitudes. From the table 2, we can see that how the results vary for different threshold magnitudes and which results will be useful in hazard estimates.

Table 2. The transition matrix P, the stationary distribution π and the entropy values H(P) for all threshold magnitudes considered

States	***P***	***π***	***H(P)***
M_1: $M < 4.5$ M_2: $4.5 \leq M < 5$ M_3: $5 \leq M$	$\begin{bmatrix} 0{,}726876 & 0{,}212914 & 0{,}060209 \\ 0{,}440433 & 0{,}395307 & 0{,}16426 \\ 0{,}304348 & 0{,}391304 & 0{,}304348 \end{bmatrix}$	[0,592255 0,287712 0,120033]	**0,3728**

M_1: $M < 4.4$ M_2: $4.4 \leq M < 5$ M_3: $5 \leq M$	$\begin{bmatrix} 0{,}663664 & 0{,}276276 & 0{,}060060 \\ 0{,}398003 & 0{,}459344 & 0{,}142653 \\ 0{,}247826 & 0{,}447826 & 0{,}304348 \end{bmatrix}$	[0,517620 0,363210 0,119170]	**0,3923**
M_1: $M < 4.5$ M_2: $4.5 \leq M < 5.1$ M_3: $5.1 \leq M$	$\begin{bmatrix} 0{,}726876 & 0{,}226876 & 0{,}046248 \\ 0{,}447412 & 0{,}419032 & 0{,}133556 \\ 0{,}248649 & 0{,}47027 & 0{,}281081 \end{bmatrix}$	[0,594522 0,309699 0,095779]	**0,3610**
M_1: $M < 4.5$ M_2: $4.5 \leq M < 4.9$ M_3: $4.9 \leq M$	$\begin{bmatrix} 0{,}726876 & 0{,}190227 & 0{,}082897 \\ 0{,}461373 & 0{,}345494 & 0{,}193133 \\ 0{,}311321 & 0{,}27044 & 0{,}418239 \end{bmatrix}$	[0,594508 0,240828 0,164664]	**0,3810**
M_1: $M < 4.5$ M_2: $4.5 \leq M < 4.8$ M_3: $4.8 \leq M$	$\begin{bmatrix} 0{,}726876 & 0{,}167539 & 0{,}105585 \\ 0{,}505291 & 0{,}261905 & 0{,}232804 \\ 0{,}302956 & 0{,}211823 & 0{,}485222 \end{bmatrix}$	[0,594479 0,195276 0,210244]	**0,3813**
M_1: $M < 4.4$ M_2: $4.4 \leq M < 4.9$ M_3: $4.9 \leq M$	$\begin{bmatrix} 0{,}663664 & 0{,}254254 & 0{,}082082 \\ 0{,}417618 & 0{,}414356 & 0{,}168026 \\ 0{,}251572 & 0{,}330189 & 0{,}418239 \end{bmatrix}$	[0,517672 0,317567 0,164760]	**0,4047**
M_1: $M < 4.3$ M_2: $4.3 \leq M < 4.9$ M_3: $4.9 \leq M$	$\begin{bmatrix} 0{,}584541 & 0{,}332126 & 0{,}083333 \\ 0{,}353316 & 0{,}498724 & 0{,}147959 \\ 0{,}210692 & 0{,}371069 & 0{,}418239 \end{bmatrix}$	[0,429018 0,406215 0,164766]	**0,4171**
M_1: $M < 4.2$ M_2: $4.2 \leq M < 4.9$ M_3: $4.9 \leq M$	$\begin{bmatrix} 0{,}474960 & 0{,}450727 & 0{,}074313 \\ 0{,}276939 & 0{,}583082 & 0{,}139980 \\ 0{,}157233 & 0{,}424528 & 0{,}418239 \end{bmatrix}$	[0,320718 0,514512 0,164767]	**0,4104**

According to maximum entropy, in the investigated area, three groups according to the magnitudes so that each is called a state were formed as follows:

$$M_1\colon\ M < 4.3$$
$$M_2\colon\ 4.3 \leq M < 4.9$$
$$M_3\colon\quad M \geq 4.9$$

With respect to the investigated area in Figure 1, the transition matrix P is as follows:

$$P = \begin{bmatrix} 0.584541 & 0.332126 & 0.083333 \\ 0.353316 & 0.498724 & 0.147959 \\ 0.210692 & 0.371069 & 0.418239 \end{bmatrix}$$

According to the matrix P, the most probable transition of earthquake is of transition M_1 to M_1 with a probability of 0.584541 followed by the transition M_2 to M_2 and M_3 to M_3 with probabilities 0.498724 and 0.418239 respectively and the least probable transition with a probability of 0.083333 in the transition M_1 to M_3.

The holding time mass functions of the magnitude state with unit interval of one month, each obtained by determining the probability of holding times in which the process remains in state i before entering state j, are presented as follows:

$$T_m(1) = \begin{bmatrix} 0{,}880165 & 0{,}847273 & 0{,}811594 \\ 0{,}906137 & 0{,}879795 & 0{,}698276 \\ 0{,}865672 & 0{,}762712 & 0{,}548872 \end{bmatrix}$$

$$T_m(2) = \begin{bmatrix} 0{,}095041 & 0{,}134545 & 0{,}101449 \\ 0{,}061372 & 0{,}058824 & 0{,}077586 \\ 0{,}134328 & 0{,}067797 & 0{,}082707 \end{bmatrix}$$

$$T_m(3) = \begin{bmatrix} 0{,}020661 & 0{,}010909 & 0{,}072464 \\ 0{,}032491 & 0{,}033248 & 0{,}086207 \\ 0 & 0{,}050847 & 0{,}112782 \end{bmatrix}$$

$$T_m(4) = \begin{bmatrix} 0{,}002066 & 0{,}007273 & 0{,}014493 \\ 0 & 0{,}007673 & 0{,}025862 \\ 0 & 0{,}059322 & 0{,}075188 \end{bmatrix}$$

$$T_m(5) = \begin{bmatrix} 0{,}002066 & 0 & 0 \\ 0 & 0{,}002558 & 0{,}017241 \\ 0 & 0{,}033898 & 0{,}037594 \end{bmatrix}$$

$$T_m(6) = \begin{bmatrix} 0 & 0 & 0 \\ 0 & 0{,}002558 & 0{,}017241 \\ 0 & 0 & 0{,}022556 \end{bmatrix}$$

$$T_m(7) = \begin{bmatrix} 0 & 0 & 0 \\ 0 & 0{,}002558 & 0{,}017241 \\ 0 & 0 & 0{,}007519 \end{bmatrix}$$

$$T_m(8) = \begin{bmatrix} 0 & 0 & 0 \\ 0 & 0{,}005115 & 0{,}017241 \\ 0 & 0{,}008475 & 0 \end{bmatrix}$$

$$T_m(9) = \begin{bmatrix} 0 & 0 & 0 \\ 0 & 0{,}002558 & 0 \\ 0 & 0{,}008475 & 0{,}022556 \end{bmatrix}$$

$$T_m(10) = \begin{bmatrix} 0 & 0 & 0 \\ 0 & 0{,}002558 & 0 \\ 0 & 0 & 0{,}037594 \end{bmatrix}$$

$$T_m(11) = \begin{bmatrix} 0 & 0 & 0 \\ 0 & 0 & 0{,}008621 \\ 0 & 0 & 0{,}015038 \end{bmatrix}$$

The matrices show that earthquakes with transitions from M_2 $(4.3 \leq M < 4.9)$ to M_1 $(M < 4.3)$ with time interval of one (1) month have the highest probability with 0,906137. In addition, earthquakes are likely to occur every time in one (1) to ten (10) months at M_2 given that an earthquake would occur first in M_2.

Considering the widest time interval in the transitions of earthquakes from years 1901-2013, that is three (3) years, holding time mass functions of the magnitude state with unit interval of one year were presented as follows:

$$T_y(1) = \begin{bmatrix} 1 & 1 & 1 \\ 1 & 0{,}997442 & 0{,}965517 \\ 1 & 0{,}991525 & 0{,}962406 \end{bmatrix}$$

$$T_y(2) = \begin{bmatrix} 0 & 0 & 0 \\ 0 & 0{,}002558 & 0{,}017241 \\ 0 & 0{,}008475 & 0{,}030075 \end{bmatrix}$$

$$T_y(3) = \begin{bmatrix} 0 & 0 & 0 \\ 0 & 0 & 0{,}008621 \\ 0 & 0 & 0 \end{bmatrix}$$

Accordingly, the interval transition probability matrices of magnitude state with unit interval of one month were presented as follows:

$$F_m(1) = \begin{bmatrix} 0{,}650967 & 0{,}281401 & 0{,}067633 \\ 0{,}320153 & 0{,}576537 & 0{,}103316 \\ 0{,}18239 & 0{,}283019 & 0{,}534593 \end{bmatrix}$$

$$F_m(2) = \begin{bmatrix} 0{,}520679 & 0{,}370844 & 0{,}10848 \\ 0{,}389412 & 0{,}476899 & 0{,}133697 \\ 0{,}279511 & 0{,}304622 & 0{,}415871 \end{bmatrix}$$

$F_m(3) = \begin{bmatrix} 0{,}4665 & 0{,}393011 & 0{,}140494 \\ 0{,}403521 & 0{,}436741 & 0{,}159749 \\ 0{,}302129 & 0{,}323665 & 0{,}374212 \end{bmatrix}$
$F_m(4) = \begin{bmatrix} 0{,}435226 & 0{,}401091 & 0{,}16369 \\ 0{,}398653 & 0{,}423441 & 0{,}17792 \\ 0{,}317491 & 0{,}348859 & 0{,}333658 \end{bmatrix}$
$F_m(5) = \begin{bmatrix} 0{,}416453 & 0{,}403316 & 0{,}180241 \\ 0{,}390405 & 0{,}418878 & 0{,}190733 \\ 0{,}332211 & 0{,}363924 & 0{,}303875 \end{bmatrix}$
$F_m(6) = \begin{bmatrix} 0{,}402882 & 0{,}404674 & 0{,}192396 \\ 0{,}383063 & 0{,}416382 & 0{,}200573 \\ 0{,}342162 & 0{,}365012 & 0{,}292838 \end{bmatrix}$
$F_m(7) = \begin{bmatrix} 0{,}392756 & 0{,}405096 & 0{,}202114 \\ 0{,}377152 & 0{,}413593 & 0{,}209257 \\ 0{,}345437 & 0{,}367681 & 0{,}286885 \end{bmatrix}$
$F_m(8) = \begin{bmatrix} 0{,}384843 & 0{,}404779 & 0{,}210305 \\ 0{,}372420 & 0{,}410492 & 0{,}217084 \\ 0{,}345382 & 0{,}372752 & 0{,}281864 \end{bmatrix}$
$F_m(9) = \begin{bmatrix} 0{,}378444 & 0{,}404007 & 0{,}217418 \\ 0{,}369051 & 0{,}409154 & 0{,}221776 \\ 0{,}344583 & 0{,}375682 & 0{,}279723 \end{bmatrix}$
$F_m(10) = \begin{bmatrix} 0{,}373329 & 0{,}40331 & 0{,}223173 \\ 0{,}365936 & 0{,}407908 & 0{,}226108 \\ 0{,}345418 & 0{,}377478 & 0{,}277073 \end{bmatrix}$
$F_m(11) = \begin{bmatrix} 0{,}369213 & 0{,}402639 & 0{,}227898 \\ 0{,}363258 & 0{,}405393 & 0{,}231266 \\ 0{,}34768 & 0{,}382081 & 0{,}270182 \end{bmatrix}$

According to the above matrices, the highest probability is in one (1) month with a probability of 0,650967 where the transition is from M_1 $(M < 4.3)$ to M_1 .

Similarly, interval transition probability matrices of magnitude state with unit interval of a year were presented as follows:

$F_y(1) = \begin{bmatrix} 0{,}584541 & 0{,}332126 & 0{,}083333 \\ 0{,}353316 & 0{,}503828 & 0{,}142857 \\ 0{,}210692 & 0{,}367925 & 0{,}421385 \end{bmatrix}$
$F_y(2) = \begin{bmatrix} 0{,}476591 & 0{,}392136 & 0{,}131273 \\ 0{,}412383 & 0{,}424363 & 0{,}163256 \\ 0{,}337959 & 0{,}406588 & 0{,}255456 \end{bmatrix}$
$F_y(3) = \begin{bmatrix} 0{,}443713 & 0{,}404044 & 0{,}152244 \\ 0{,}422795 & 0{,}410588 & 0{,}166619 \\ 0{,}391935 & 0{,}408625 & 0{,}199444 \end{bmatrix}$

According to the matrices, like with the matrices with unit interval of one month, the most probable transition given one (1) year as unit interval is M_1 $(M < 4.3)$ to M_1. Based on the interval transition probabilities, for the whole region, the probability of the second earthquake with M_3 $(M \geq 4.9)$ magnitude in one year is 42%.

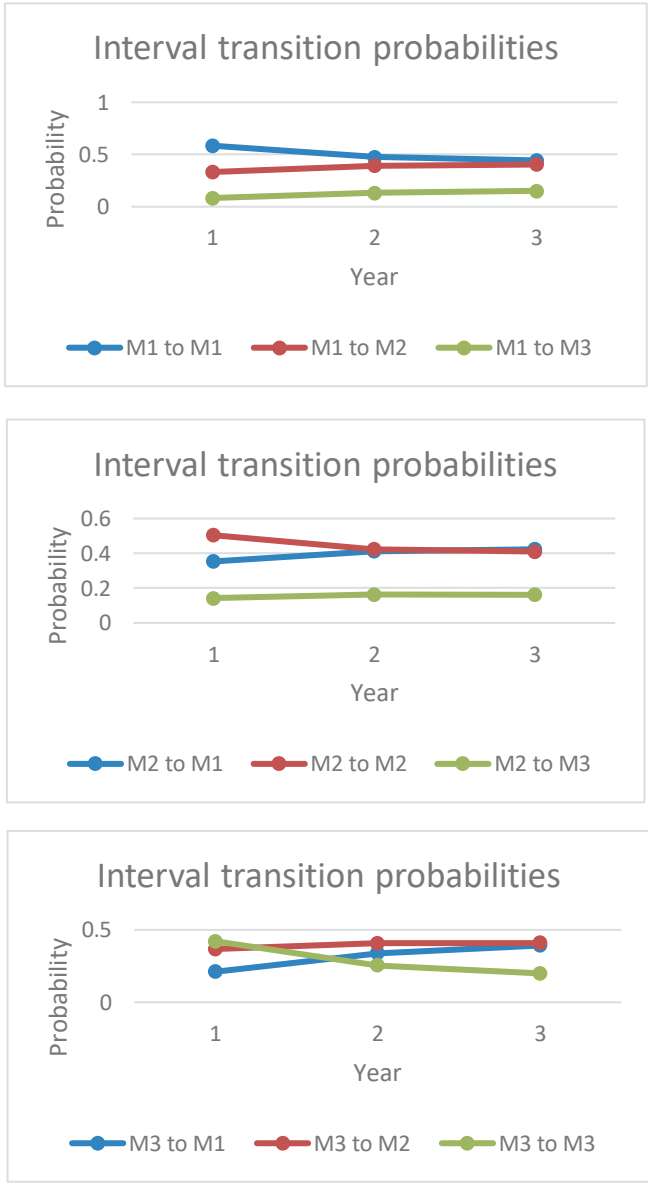

Figure 2. Interval transition probability functions from magnitude to magnitude

From the graphics above, it is inferred that the probability of a second earthquake with M_1 $(M < 4.3)$ magnitude is the highest for the investigated area. The probability of an earthquake of equal magnitude following one of M_1 $(M < 4.3)$ decrease while the probability of M_1 $(M < 4.3)$ magnitude earthquake coming after M_2 $(4.3 \leq M < 4.9)$ and M_3 $(M \geq 4.9)$ increases with time. The probability of an earthquake of equal magnitude following one of M_2 $(4.3 \leq M < 4.9)$ and M_3 $(M \geq 4.9)$ decrease while the probabilities of M_2 $(4.3 \leq M < 4.9)$ and M_3 $(M \geq 4.9)$ magnitude earthquake coming after M_2 $(4.3 \leq M < 4.9)$ stabilize with time.

On the other hand, from the results obtained regarding the investigated area in Unal Karaçam (2016; 2019), to be X_{t_i} and Y_{i-1}, the magnitude at time t_i and elapsed time between consecutive earthquakes (holding time), respectively, since the influence of $X_{t_{i-1}}$ on the strength of the dependency between X_{t_i} and Y_{i-1} was statistically significant, the dependency structure of Semi-Markov model would be modeled with a Conditional Copula:

To be Frank (unconditional) copula with $\hat{\theta} = 2.5237$ within many copula families the best representation of the dependency structure between $X_{t_{i-1}}$ and X_{t_i} and $X_{t_i} \approx$ Gen-Pareto $(k = -0.14549; \sigma = 0.57414; \mu = 3.9454)$ the conditional marginal distribution could be given as:

$$P\left(X_{t_i} \leq x_2 | X_{t_{i-1}} = x_1\right) = \frac{A(B-1)}{(exp(-2.5237)-1)+(A-1)(B-1)} \quad (3)$$

where $A = exp\left(-2.5237F(x_1)\right)$ and $B = exp\left(-2.5237F(x_2)\right)$.

In addition to these, to be Gumbel (unconditional) copula with $\hat{\theta} = 1.0362$ within many copula families the best representation of the dependency structure between $X_{t_{i-1}}$ and Y_{i-1}, $X_{t_i} \approx$Gen-Pareto $(k = -0.14549; \sigma = 0.57414; \mu = 3.9454)$ and $Y_{i-1} \approx$ Weibull $(\alpha = 0.42366; \sigma = 0.02322; \gamma = 0)$, the conditional marginal distribution could be given as:

$$P\left(Y_{i-1} \le y_1 | X_{t_{i-1}} = x_1\right) = exp\left(-E^{\frac{1}{1,0362}}\right)\left(\frac{\left(-ln\left(F(x_1)\right)\right)^{0.0362}}{F(x_1)}\right)\left(E^{\left(\left(1/1.0362\right)-1\right)}\right) \qquad (4)$$

where $E = \left(\left(-ln\left(F(x_1)\right)\right)^{1.0362} + \left(-ln\left(G(y_1)\right)\right)^{1.0362}\right)$.

To be $P\left(Y_{i-1} \le y_1 | X_{t_{i-1}} = x_1\right) = U_1$ and $P\left(X_{t_i} \le x_2 | X_{t_{i-1}} = x_1\right) = U_2$ from the equations (3) and (4), and Conditional Galambos Copula with $\hat{\theta}_1(x_1) = exp(-2.67621255 + 0.32528955x_1)$ within many copula families the best representation of the dependency structure between $X_{t_{i-1}}$ and Y_{i-1}, the conditional joint distribution could be given as:

$$P\left\{X_{t_i} \le x_2, Y_{i-1} \le y_1 | X_{t_{i-1}} = x_1\right\} = u_1 u_2 S \qquad (5)$$

where $S = exp\left(\left\{\left[(-ln(u_1))^{-\hat{\theta}_1(x_1)} + (-ln(u_2))^{-\hat{\theta}_1(x_1)}\right]^{-1/\hat{\theta}_1(x_1)}\right)$.

The following table, prepared by taking into account the above results, shows (a) the interval transition probabilities within unit interval of one year obtained from Semi-Markov and Conditional Copula models, (b)-(c) expected frequencies from the possibilities and observed frequencies from data for the years 2014-2022, respectively, (d) success percentages for the years 2014-2022.

Table 3. (a) Interval transition probabilities **(b)-(c)** The Expected and Observed Frequencies **(d)** The Success percentages of the two models: Semi-Markov (SM) and Conditional Copulas (CC) (for $Y_{i-1} \le 1$ (year))

States	(a)Interval transition probabilities		(b) The Expected Frequencies		(c) The Observed Frequencies (for the years 2014-2022)	(d) The Success percentages (for the years 2014-2022)	
	SM	CC	SM	CC		SM	CC
$M_1 \to M_1$	0,584500	0,633100	138	149	142	97,18%	95,07%
$M_1 \to M_2$	0,332126	0,290822	78	69	69	86,96%	100,00%
$M_1 \to M_3$	0,083333	0,076078	20	18	25	75,00%	72,00%

$M_2 \to M_1$	0,353316	0,373791	59	63	71	83,10%	88,73%
$M_2 \to M_2$	0,503828	0,437500	85	74	76	88,16%	97,37%
$M_2 \to M_3$	0,142857	0,188754	24	31	21	85,71%	52,38%
$M_3 \to M_1$	0,210692	0,212449	12	13	23	52,17%	56,52%
$M_3 \to M_2$	0,367925	0,445252	22	26	23	95,65%	86,96%
$M_3 \to M_3$	0,421385	0,342299	25	20	13	7,69%	46,15%

The goodness-of-fit of the Semi-Markov and Conditional Copula models are tested by Chi-square analysis. From the results in Table 3 ($\chi^2_{SM} = 22{,}06,\ \chi^2_{CC} = 17{,}83$), both models were found to be fitted for the data. Moreover, we concluded that with the Conditional Galambos Copula $\hat{\theta}_1(x_1) = exp(-2.67621255 + 0.32528955x_1)$, we have an aftcast success percentage of about 77,24% on average, better than Semi-Markov (about 74,62%). Furthermore, it is seen that the success percentages of the conditional copula are much better than those of the Semi-Markov model, especially for large magnitudes. In addition, since the maximum time between two consecutive earthquakes in the investigated area is 3 years, it is possible to estimate only up to 3 years with Semi-Markov, while there is no such limit for Conditional Copula.

3. Results

Seismic activity or earthquakes are destructive catastrophes that cannot be prevented; thus, preparation is significant in order to survive such hazardous catastrophe (Causapin, 2018). By using the Semi-Markov model and the conditional copulas based on it, it will be possible to provide an approach to seismic hazard by determining the probability of earthquakes, and it will also contribute to the studies of predicting earthquakes. Regardless of the impossibility in determining the exact occurences of earthquakes in the future, probabilistically estimating earthquake parameters likewise, time, location and magnitude have already been established through stochastic processes. It is understandable that such probabilities cannot prevent seismic activities but can help in

providing various measures against this disaster that would likely reduce the casualities and damages to some extent (Ünal and Çelebioğlu, 2011).

In this study, which we have prepared considering all these, using the earthquake data of the area limited by $36° - 39.5°$ N latitudes and $26° - 31°$ E longitudes of West Anatolia in the years 1901-2013 with magnitude $M_l \geq 4$, it is aimed to compare earthquake occurences of the next years for two models: Semi-Markov and Conditional Copulas based on the modeling the dependency structure of Semi-Markov. Considering the earthquake occurrence probabilities within one year, it is concluded that both models were fitted for the data and the conditional Galambos copula ($\hat{\theta}_1(x_1) = exp(-2.67621255 + 0.32528955x_1)$ with a success percentage of about 77,24% is better than the only using Semi-Markov model in terms of earthquake prediction of West Anatolia, Turkey. Moreover, since the maximum time between two consecutive earthquakes is 3 years for the earthquakes occured in the area, the forecastings can only be made up to 3 years with the Semi-Markov model, while there is no such a limitation for the Conditional Copulas.

REFERENCES

Altınok, Y. (1988). Seismic risk estimation of the North Anatolian Faulth Zone Using Semi-Markov model. Jeofizik, 2: 44-58.

Altınok, Y. (1991). Evaluation of earthquake risk in West Anatolia by Semi-Markov model. Jeofizik, 5: 135-140.

Altınok, Y., Kolçak, D. (1999). An application of the Semi-Markov model for earthquake occurrences in North Anatolia, Turkey. Journal of Balkan Geophysical Society, 2: 90–99.

Bai, X., Jiang H., Song, G. (2022). Conditional probability modeling of intensity measures for offshore mainshock-aftershock sequences. Soil Dynamics and Earthquake Engineering, 161.

Causapin, H. P. A. (2018). Semi-Markov chain modeling on earthquake occurrences in selected areas in Luzon. TILAMSIK: The Southern Luzon Journal of Arts and Sciences, 10 (1): 67-90.

Giriftinoğlu, Ç. (2005). Kesikli Rassal Değişkenler için Entropi Optimizasyon Prensipleri ve Uygulamaları. Yüksek Lisans Tezi, Ankara Üniversitesi Fen Bilimleri Enstitüsü, Ankara.

Goda, K., Ren, J. (2010). Assessment of Seismic Loss Dependence Using Copula. Risk Analysis, 30(7): 1076-1091.

Li, Y., Shi, B., Zhang, J. (2008). Copula joint function and its application in probability seismic hazard analysis. Acta Seismologica Sinica, 21(3): 296-305.

Liu, X. and Zhang, Q. (2016). Analysis of the return period and correlation between the reservoir-induced seismic frequency and the water level based on a copula: A case study of the Three Gorges reservoir in China. Physics of the Earth and Planetary Interiors, 260: 32-43.

Nelsen, R.B. (2006). An introduction to copulas. Springer, New York.

Nikoloulopoulos, A.K. and Karlis, D. (2008). Fitting copulas to bivariate eartquake data: The Seismic Gap Hypothesis revisited. Environmetrics, 19: 251-269.

Patton, A. J. (2003). Modelling Asymmetric Exchange Rate Dependence. Working paper, University of California, San Diego.

Patton, A.J. (2006). Modelling Asymmetric Exchange Rate Dependence. International Economic Review, 47: 527-556.

Qian, J., Dong, Y. (2022) Surrogate-assisted seismic performance assessment incorporating vine copula captured dependence. Engineering Structures, 257.

Rivera-Vargas, D., Heredia-Zavoni, E. (2022). Seismic demand analysis using environmental contours of vector-valued ground motion intensity measures. Engineering Structures, 265.

Sadeghian, R., Jalali-Naini, G.R., Sad-jadi, J., Fard, N.H. (2008). Applying Semi-Markov Models for Forecasting the Triple Dimensions of Next Earthquake Occurences: with Case Study in Iran Area. International Journal of Industrial Engineering & Production Research, 19 (4): 57-67.

Sadeghian, R. (2012). Forecasting time and place of earthquakes using a Semi-Markov model (with case study in Tehran province)", Journal of Industrial Engineering International, 8(20): 1-7.

Shannon, C.E. (1948). A Mathematical Theory of Communication. The Bell System Technical Journal, 27:379–423, 623–656.

Shen, J., Chen, J. (2020). A Copula-based random function model of sequential ground motions. The 17th World Conference on Earthquake Engineering, Japan.

Tsapanos, T.M., Burton, P.W. (1991). Seismic Hazard Evaluation for Specific Seismic Regions of the World. Tectonophysics, 194(1), 153-169.

Ünal, S. (2010). Modelling the earthquakes occuring on Turkey by Markov Chains. Dissertation, Gazi University, Ankara.

Ünal, S., Çelebioğlu, S. (2011). A Markov Chain modelling of the earthquakes occurring in Turkey. Gazi University Journal of Science, 24: 263–274.

Ünal Karaçam, S. (2016). Investigation of the Dependence Structure in Seismic Hazard Analysis: An application for Turkey. Dissertation, Gazi University, Ankara.

Ünal Karaçam, S. (2019). Investigation of the dependence structure in seismic hazard analysis: an application for Turkey. Communications Faculty of Sciences University of Ankara Series A1 mathematics and statistics, 68(2), 1528-1542.

CHAPTER 9

A NEW RESEARCH ON SOME SPECIAL TYPES OF SURFACES

Ayşe YAVUZ[1]

1 Assoc. Prof. Dr. Ayşe Yavuz, Necmettin Erbakan University, Ahmet Keleşoğlu Education Faculty, Konya, Turkey. Orcid ID: 0000-0002-0469-3786.

1. Introduction

One of the topics of differential geometry was indeed curves and surfaces with special properties. Ruled surfaces are well-known surface classes with many interesting properties. They are defined as families of smooth single-parameter lines. A ruled surface is a surface that is "swept away" by a straight line moving through space. Many ruled surface structures exist, including the hyperboloid, hyperbolic paraboloid, and cylinder.

Another important type of surface is the constant slope surface, which is a type of ruled surface. A surface is called a constant slope surface if its position vector makes a constant slope with the normal at each point on the surface. Munteanu examined these type surfaces and classified them in (Munteanu, 2010). In recent years, constant slope surfaces have been investigated in many studies (Fu and Yang, 2012; Fu and Wang, 2013; Munteanu, 2010, Maleček at all, 2009). In a surface with a constant slope, if the base curve α is a circle and the director vector is given by constant slope, then the surface is a rotational surface.

Frenet-Serret frames along a space curve are the most well-known frame fields. The Serret-Frenet frame describes the kinematic properties of a particle moving in Euclidean space along a continuous and differentiable curve.

Clifford algebra provides a unified algebraic framework for the direct expression of geometric ideas that underlies algebraic mathematical theories of differential geometry, projective geometry, and affine geometry.

Quaternions are examples of geometric algebras (Ablamowicz, 2004; Ablamowicz and Sobczyk, 2004). Quaternions are used in both theoretical and applied mathematics, particularly in three-dimensional rotation calculations. Geometric algebra, which includes the concept of direction, is a natural extension of the actual number system. Various physical applications of the quaternion calculus are discussed, including crystallography, the kinematics of rigid body motion, the special theory of relativity, classical electromagnetism, the equation of motion of the general theory of relativity, and Dirac's relativistic wave equation (Girard, 1984; Erdoğdu, 2019; Erdoğdu and Özdemir, 2015; Erdoğdu and Özdemir, 2020). Quaternion numbers are the natural physics analysis tools. Their properties as rotation generators make them extremely useful in Newtonian mechanics, scattering experiments like crystallography, and quantum mechanics (Girard, 1984).

2. Preliminaries

Let M be a surface in $\mathbb{R}^3$ and $\alpha(s)$ be an arbitrary speed curve on this surface. If the curve $\alpha(s)$ is parameterized by time s with belonging to the interval $[a, b]$, then it can be said that the tangent to the curve is given by $\alpha'(s)$ and points in the direction of motion along the curve. It was shown that the unit tangent is given by

$$t(s) = \alpha'(s)$$

We also showed that the curve since t has unit norm that $\langle t(s), t'(s)\rangle = 0$, so that the derivative of the unit tangent is orthogonal to the vector $t(s)$. Using this relation, we define the vector field

$$n(s) = \frac{\alpha''(s)}{\|\alpha''(s)\|}$$

and the binormal vector is defined as

$$b(s) = t(s) \wedge n(s).$$

The triple $\{t, n, b\}$ defines a frame in $\mathbb{R}^3$ and called the Frenet frame. The Frenet equations of the curve $\alpha(s)$ is given by

$$t'(s) = \kappa(s)n(s)$$

$$n'(s) = -\kappa(s)t(s) - \tau(s)b(s)$$

$$b'(s) = -\tau(s)n(s)$$

(Hacısalihoğlu, 2000). A space curve is planar if and only if it has zero torsion everywhere. Circles are the only planar curves with nonzero constant curvature. A line is a space curve if and only if its curvature is zero everywhere. A curve is general helix if and only if $\frac{\kappa}{\tau}$ is constant. The planes spanned by $\{t, n\}$,$\{t, b\}$,$\{n, b\}$ are called as the osculating plane, the rectifying plane and the normal plane, respectively (Erdoğdu, 2019).

On a surface M, the standard unit normal vector field N can be described as

$$N = \frac{M_s \wedge M_v}{\|M_s \wedge M_v\|}.$$

The internal geometry of the surface in the neighborhood of a specific point is characterized by the first fundamental form. This implies that measurements can be made using it on the surface. The first fundamental form is provided by

$$I = Eds^2 + 2Fdsdv + Gdv^2$$

such that

$$E = \langle M_s, M_s \rangle, \qquad F = \langle M_s, M_v \rangle \; G = \langle M_v, M_v \rangle.$$

The second fundamental form is given by

$$II = eds^2 + 2fdsdv + gdv^2$$

where

$$e = \langle M_{ss}, N \rangle, \qquad f = \langle M_{sv}, N \rangle, \qquad g = \langle M_{vv}, N \rangle.$$

Weingarten map is used to define Gauss curvature

$$K = \det S$$

and mean curvature is associated to the trace in the following way

$$H = \frac{1}{2} trS.$$

The Gauss and mean curvatures of a parametrized surface can be determined by calculating as

$$K = \frac{\det II}{\det I} = \frac{eg - f^2}{EG - F^2},$$

$$H = \frac{Eg + Ge - 2Ff}{2(EG - F^2)}.$$

A surface is said to be minimal if its mean curvature vanishes (Do Carmo, 1976).

A ruled surface is defined by parameterizing it using a curve $\alpha(s)$ and then evaluating the surface obtained by adding a line through each points on the curve. If directions of such lines are provided by $X(s)$, then the surface can be parametrized by

$$M(s,v) = \alpha(s) + v(X(s)).$$

Without loss of generality, we can suppose that X is a unit field. To obtain a parametrized surface, $\frac{\partial M}{\partial s} = X$ and $\frac{\partial M}{\partial v} = \frac{d\alpha}{dv} + v\frac{dX}{dv}$ should be linearly independent. It is always possible to obtain a surface for all parameter values. The extended lines in the rulings for all values of s must be taken into account.

One example of a ruled surface where X is constant is a generalized cylinder. A ruled surface where α can be designed to be constant is known as a generalized cone.

Ruled surfaces have non-positive Gauss curvature. The vanishing Gauss curvature of generalized cylinders, generalized cones, and tangent developables is particularly notable. A developable surface has vanishing Gauss curvature and no umbilics. If there are certain tangent planes along the generating lines of the ruled surface, the surface may be a developable ruled surface (Hacısalihoğlu, 2000).

The dral of the ruled surface is given by

$$P_X = \frac{\det\left(\frac{d\alpha}{ds}, X, X'\right)}{\|X'\|^2}$$

The dral of the ruled surface vanishes if and only if the surface is developable. The striction curve on the surface is determined as below

$$\overline{\beta}(\mathrm{s}) = \alpha(s) - \frac{\left\langle \vec{t}(s), \vec{X}(s) \right\rangle}{\left\langle \overrightarrow{X'}(s), \overrightarrow{X'}(s) \right\rangle} \vec{X}(s)$$

(Hacısalihoğlu, 2000).

Hamilton defines the real quaternion algebra H as the following multiplication

$$i^2 = j^2 = k^2 = ijk = -1.$$

The identity element of H is 1 and the basis of quaternions is $\{1, i, j, k\}$. i, j and k are standard orthonormal bases in $\mathbb{R}^3$. A quaternion can be given as $q = a_0 + a_1 i + a_2 j + a_3 k$ where vector and the scalar component of q are $V(q) = w \in \mathbb{R}^3$ and $S(q) = a_0 \in \mathbb{R}$, respectively. The quaternion can be obtained as $q = S(q) + V(q)$. If $S(q) = 0$, q is

referred to as pure quaternion. The conjugate of a quaternion, sum of two quaternions, and multiplication of a quaternion with a scalar λ can be provided by

$$\bar{q} = S(q) - V(q)$$

$$q + p = (S(q) + S(p)) + (V(q) + V(p))$$

$$\lambda q = \lambda S(q) + \lambda V(q).$$

We can compute the quaternion product of two quaternions p and q using dot and cross-product as follows

$$q \times p = S(q)S(p) - < V(q), V(p) > \\ + S(q)V(p) + S(p)V(q) + V(q) \wedge V(p)$$

where $\times$ is quaternion product. The norm of the quaternion q is $\|q\| = a_0^2 + a_1^2 + a_2^2 + a_3^2$. A quaternion is called a unit quaternion if its norm is 1. The unit quaternion is written as $q = cos\theta + vsin\theta$, where $v \in \mathbb{R}^3$ and $\|v\| = 1$ (Hamilton, 1844).

3 CSR Surface with Respect to Osculating Planes

The CSR surface (surface of constant slope rulling) with regard to osculating planes is introduced in this section. Then, some of the characteristics of this surface are discussed, along with some particular result based on these characteristics. Eventually, quaternions are used to describe this surface.

The generating lines of CSR surface $M_1(s, v)$ are given by points on the curve $X_1(s)$ and have the constant slope σ with respect to the osculating planes to the curve at every point on the curve $X(s)$. The direction vector of generating lines of the surface is

$$X_1(s) = \sin w(s)t(s) + \cos w(s)n(s) + \sigma b(s).$$

CSR surface is parametrized by

$$M_1(s, v) = \alpha(s) + v(X(s))$$

for $s \epsilon I, v \epsilon \mathbb{R}$ such that $\sigma = tg\gamma$, $\gamma \epsilon \left[0, \frac{\pi}{2}\right]$ and $\sigma \epsilon [0, \infty]$.

Theorem 3.1. If κ and τ satisfy the following equation

$$\kappa\sigma\sin w(s) - \tau(\cos^2 w(s) + \sigma^2) = \sigma\sin w(s)w'(s),$$

then CSR surface $M_1(s,v)$ is developable.

Corollary 3.1. It is considered that $w'(s) = 0, \cos w(s) = x_1 = const$ and $\sin w(s) = x_2 = const$. CSR surface is developable if and only if the base curve is general helix with

$$\frac{\kappa}{\tau} = \frac{(x_1)^2 + \sigma^2}{\sigma . x_2}.$$

Theorem 3.2. The striction line on CSR surface $M_1(s,v)$ is given by

$$\overline{\beta} = \alpha(s) - \frac{\cos w(s)(w'(s) - \kappa)}{(w'(s) - \kappa)[(w'(s) - \kappa) - 2\tau\sigma\sin w] + \tau^2(\sigma^2 + \cos^2 w)} X(s).$$

Corollary 3.2. If $w(s) = \int \kappa ds$ or $X_1(s)$ is spanned by rectifying planes, then the striction line of the surface $M_1(s,v)$ is equal to base curve.

Theorem 3.3. The Gauss curvature K and the mean curvature H of the $M_1(s,v)$ are given as

$$K = -\frac{\tau^2[-\sigma^2 + \cos^2 w(s)]^2}{\| M_s \wedge M_v \|^2 \left[\left[1 + v^2\tau^2\left(\sigma^2 + \cos^2 w(s)\right)\right][1 + \sigma^2] - \sin^2 w(s)\right]}$$

$$H = \frac{(1 + \sigma^2)vA - 2\tau\sin w(s)\left(-\sigma^2 + \cos^2 w(s)\right)}{2\| M_s \wedge M_v \| \left\{\left[1 + v^2\tau^2\left(\sigma^2 + \cos^2 w(s)\right)\right](1 + \sigma^2) - \sin^2 w(s)\right\}}$$

such that

$$A = -2\cos w(s)(\sigma\tau^2 + \sin w(s)\kappa) + v\tau\begin{bmatrix} \tau^2\sin w(s)\left(\sigma^2 + \cos^2 w(s)\right) \\ +\kappa\sigma(-\tau\cos^2 w(s) + \sin^2 w(s) - \sigma^3\kappa) \end{bmatrix}$$

and $w(s) = \int \kappa ds$.

Proof The normal of CSR surface $M_1(s,v)$ is given by

$$N = \frac{1}{\| M_s \wedge M_V \|}\begin{pmatrix} v\tau\left(-\sigma^2 - \cos^2 w(s)\right), \\ \sigma - v\tau\sin w(s)\cos w(s), \\ \cos w(s) - \sigma v\tau\sin w(s) \end{pmatrix}$$

$$\| M_S \wedge M_V \| = \sqrt{\begin{matrix} v^2\tau^2\left(\cos^2 w(s) + \sigma^2\left(1+\cos^2 w(s)\right)\right) \\ +\cos^2 w(s) - 4\sigma v\tau \cos w(s)\sin w(s) \end{matrix}}.$$

The coefficients E, F and G of the first fundamental form of CSR surface $M_1(s,v)$ are obtained as follows

$$E = 1 + v^2\tau^2\left(\sigma^2 + \cos^2 w(s)\right),$$

$$F = \sin w(s),$$

$$G = 1 + \sigma^2.$$

We can obtain the coefficients e, f, and g of the second fundamental form of CSR surface $M_1(s,v)$ as

$$e = \frac{v\left[\begin{matrix} -2\cos w(s)(\sigma\tau^2 + \sin w(s)\kappa) + v\tau \\ \left[\tau^2 \sin w(s)\left(\sigma^2 + \cos^2 w(s)\right) + \kappa\sigma(-\tau\cos^2 w(s) + \sin^2 w(s) - \sigma^3\kappa)\right] \end{matrix}\right]}{\| M_s \wedge M_v \|}$$

$$f = \frac{1}{\| M_s \wedge M_v \|}\tau[-\sigma^2 + \cos^2 w(s)]$$

$$g = 0$$

such that $w(s) = \int \kappa ds$.

Corollary 3.3. It is known that the necessary condition for CSR surface $M_1(s,v)$ to be a developable surface is to satisfy the condition $K = 0$. If $\tau = 0$ or $\sigma = \pm\cos w(s)$ where $w(s) = \int \kappa ds$, then CSR surface $M_1(s,v)$ is developable.

Corollary 3.4. It is known that minimal surface is surface satisfying $H = 0$. Hence, we can obtained the $M_1(s,v)$ is a minimal surface if

$$(1+\sigma^2)vA = 2\tau \sin w(s)\left(-\sigma^2 + \cos^2 w(s)\right)$$

where $w(s) = \int \kappa ds$.

As the CSR surface $M_1(s,v)$, now we will examine some geometric properties of the surface that the base curve is planar to see the above results. These type surfaces are investigated in (Maleček , at all 2009). The generating lines of the surface are given by points on the curve $X_2(s)$ and have constant slope σ with respect to the given surface to the curve at every point on the curve $X_2(s)$. The direction vector of generating lines of

the surface is given by

$$X_2(s) = \sin w(s)t(s) + \cos w(s)n(s) + \sigma e_3.$$

The surface with constant slope $M_2(s,v)$ is parametrized by

$$M_2(s,v) = \alpha(s) + v\big(X(s)\big).$$

Example 3.1. Let a curve is logarithmic spiral with following parametric expression

$$\alpha(s) = \big(e^s\cos(s), e^s\sin(s)\big).$$

Then Frenet frames are obtained

$$t(s) = \left(\frac{\cos(s) - \sin(s)}{\sqrt{2}}, \frac{\cos(s) + \sin(s)}{\sqrt{2}}\right)$$

$$n(s) = \left(-\frac{\cos(s) + \sin(s)}{\sqrt{2}}, \frac{\cos(s) - \sin(s)}{\sqrt{2}}\right).$$

The parametric expression of surface with constant slope with respect to rectifying plane $M_2(s,v)$ calculated as

$$x = e^s\cos(s) + v\left[\sin w(s)\frac{\cos(s) - \sin(s)}{\sqrt{2}} + \cos w(s) - \frac{\cos(s) + \sin(s)}{\sqrt{2}}\right]$$

$$y = e^s\sin(s) + v\left[\sin w(s)\frac{\cos(s) + \sin(s)}{\sqrt{2}} + \cos w(s)\frac{\cos(s) - \sin(s)}{\sqrt{2}}\right]$$

$$z = \sigma v.$$

The surface is visualized for $w(s) = \frac{\pi}{2}$, $\sigma = \sqrt{3}$, $t\epsilon[-\pi,\pi]$ and $v\epsilon[-15{,}15]$ in Figure 1.

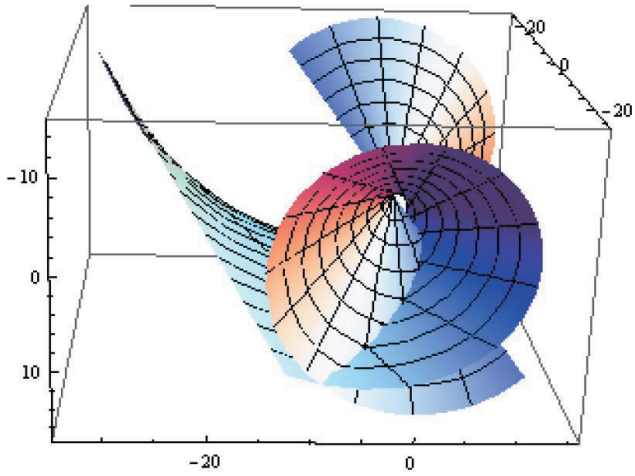

Figure 1

Theorem 3.4. The ruled surface $M_2(s,v)$ is developable if and only if $w(s) = \int \kappa ds$ or $w(s) = 2k\pi, k\epsilon Z$.

Theorem 3.5. The striction line on the surface $M_2(s,v)$ is given by

$$\overline{\beta} = \alpha(s) - \cos^2 w(s) X(s).$$

Corollary 3.5. If $X_2(s)\epsilon Span\ \{t(s), e_3\}$, then the striction line of the surface $M_2(s,v)$ is equal to base curve.

Theorem 3.6. From the Theorem 3.4., it is known that if $w(s) = \int \kappa ds$, the surface is developable. Under this condition, the mean curvature H of developable surface $M_2(s,v)$ are given as

$$H = \frac{(1+\sigma^2)v[-2\cos w(s)(\sin w(s)\kappa)]}{2\sqrt{\cos^2 w(s)}\{1+\sigma^2-\sin^2 w(s)\}}$$

such that $\sin w(s) \neq 2k\pi$.

Corollary 3.6. If $w(s) = k\frac{\pi}{2}, k\epsilon Z$, then the surface $M_2(s,v)$ is a minimal surface.

Corollary 3.7. If $X_2(s)$ is spanned by $\{n(s), e_3\}$ or by $\{t(s), e_3\}$ plane, then the surface $M_2(s,v)$ is a minimal surface.

Now, we express CSR surface with respect to osculating planes by

means of quaternions and rotational motions.

Remark 3.1. Surface $M_1(s,v)$ can be obtained by using quaternion product three types as follows

$$\textbf{a)}\ M_1(s,v) = \alpha(s) + v\big(Q_1 \times b(s)\big)$$

such that

$$Q_1 = \sigma + \sin w(s)n(s) - \cos w(s)t(s)$$

$$\textbf{b)}\ M_1(s,v) = \alpha(s) + v\big(Q_2 \times t(s)\big)$$

such that

$$Q_2 = \sin w(s) + \cos w(s)b(s) - \sigma n(s)$$

$$\textbf{c)}\ M_1(s,v) = \alpha(s) + v\big(Q_3 \times n(s)\big)$$

such that

$$Q_3 = \cos w(s) + \sin w(s)b(s) + \sigma t(s)$$

where $\times$ is the quaternion product.

Theorem 3.8. The Q_1 is obtained that rotation of $b(s)$ around $\vec{v}$.

Proof

$$Q_1 = \cos\theta + \vec{v}\sin\theta$$

is a rotation of $b(s)$ about the $\vec{v}$ through an angle θ

$$Q_1 \times b(s) = \cos\theta b(s) + \sin\theta \vec{v} \times b(s)$$

$$v \times b(s) = -\langle \vec{v}, b(s) \rangle + \vec{v} \wedge b(s)$$

And for $\sin\theta(-\langle \vec{v}, b(s) \rangle) = 0$, $\theta = 0$ or $\vec{v} \perp b(s)$. Because of θ is rotation angle, $\theta \neq 0$. So $\vec{v} \perp b(s)$. Then

$$\vec{v} = xt(s) + yn(s).$$

Vector product of $\vec{v}$ and $b(s)$ given by

$$\vec{v} \wedge b(s) = -xn(s) + yt(s).$$

and so

$$Q_1 \times b(s) = \cos\theta b(s) + \sin\theta(-xn(s) + yt(s))$$

$$Q_1 \times b(s) = X(s).$$

To ensure equality, the following equalities are given

$$\sigma = \cos\theta,$$

$$y\sin\theta = \sin w(s),$$

$$-x\sin\theta = \cos w(s).$$

So we give the equality of Q_1 as follow

$$Q_1 = \sigma + \sin w(s)n(s) - \cos w(s)t(s).$$

Remark 3.2. The Q_2 is obtained that rotation of $n(s)$ around $\vec{v}$ and similarly Q_3 is rotation of $t(s)$ around $\vec{v}$.

4. CSR surface with Respect to Rectifying Planes

The CSR surface with regard to rectifying planes is defined. Some of the characteristics of this surface are discussed, along with some particular result based on these characteristics. Finally, quaternions are used to describe this surface.

The rulings of CSR surface $\tilde{M}_1(s,v)$ are given by points on the curve $\tilde{X}(s)$ and have the constant slope σ with respect to the rectifying planes to the curve at every point on the curve $\tilde{X}(s)$. The direction vector of the generating lines of the surface is given by

$$\tilde{X}(s) = \sin w(s)t(s) + \cos w(s)b(s) + \sigma n(s).$$

CSR surface $\tilde{M}_1(s,v)$ is parametrized by

$$\tilde{M}_1(s,v) = \alpha(s) + v\big(\tilde{X}(s)\big)$$

Example 4.1. Let a unit speed curve as

$$\alpha(s) = \left(\frac{1}{\sqrt{2}}\cos(s), \frac{1}{\sqrt{2}}\cos(s), \sin(s)\right),$$

then the Frenet frames are obtained as

$$t(s) = \left(-\frac{1}{\sqrt{2}}\sin(s), -\frac{1}{\sqrt{2}}\sin(s), \cos(s)\right)$$

$$b(s) = \left(\frac{1}{\sqrt{2}}, -\frac{1}{\sqrt{2}}, 0\right)$$

$$n(s) = \left(-\frac{1}{\sqrt{2}}\cos(s), -\frac{1}{\sqrt{2}}\cos(s), -\sin(s)\right).$$

The parametric expression of CSR surface with respect to the rectifying plane $\widetilde{M}_1(s,v)$ calculated as follows

$$x = \frac{1}{\sqrt{2}}\cos(s) + v\left[-\frac{1}{\sqrt{2}}\sin w(s)\sin(s) + \frac{1}{\sqrt{2}}\cos w(s) - \frac{1}{\sqrt{2}}\sigma\cos(s)\right]$$

$$y = \frac{1}{\sqrt{2}}\cos(s) + v\left[-\frac{1}{\sqrt{2}}\sin w(s)\sin(s) - \frac{1}{\sqrt{2}}\cos w(s) - \frac{1}{\sqrt{2}}\sigma\cos(s)\right]$$

$$z = \sin(s) + v[\sin w(s)\cos(s) - \sigma\sin(s)]$$

and surface is visualized in the following Figure 2, for $w(s) = \frac{s}{\pi}$, $\sigma = \sqrt{3}$, $v\epsilon[0,1]$ and $s\epsilon[-\pi,\pi]$.

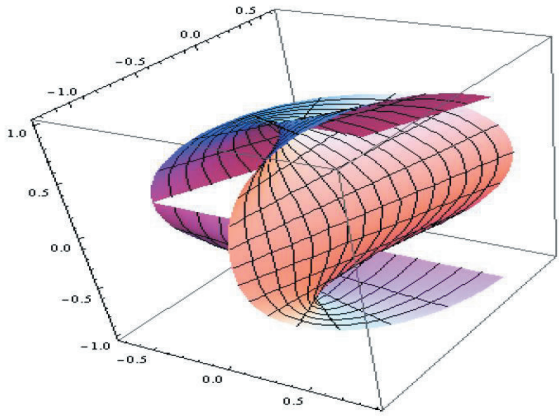

Figure 2

Remark 4.1. CSR surface $\widetilde{M}_1(s,v)$ can be obtained by using quaternion product three types as follows

a)

$$\widetilde{M}_1(s,v) = \alpha(s) + v\left(\tilde{Q}_1 \times b(s)\right)$$

where

$$\tilde{Q}_1 = \cos w(s) + \sin w(s)n(s) - \sigma t(s)$$

b) $$\widetilde{M}_1(s,v) = \alpha(s) + v\left(\tilde{Q}_2 \times t(s)\right)$$

where

$$\tilde{Q}_2 = \sin w(s) + \cos w(s).n(s) + \sigma b(s)$$

c) $$\widetilde{M}_1(s,v) = \alpha(s) + v\left(\tilde{Q}_3 \times n(s)\right)$$

where

$$\tilde{Q}_3 = \sigma - \sin w(s)b(s) + \cos w(s)t(s).$$

Remark 4.2. $\tilde{Q}_1$ is a rotation of $b(s)$ about the $\vec{v}$ through an angle θ and $\tilde{Q}_2$ is a rotation of $t(s)$ about the vector $\vec{v}$. And similarly, $\tilde{Q}_3$ is a rotation of $n(s)$ about the vector $\vec{v}$.

Theorem 4.1. If κ and τ satisfy the following equation

$$\kappa \cos w(s)\sin w(s) - \tau(\cos^2 w(s) + \sigma^2) = -w'(s)\sin w(s)\sigma,$$

then CSR surface $\widetilde{M}_1(s,v)$ is a developable surface.

Corollary 4.1. It is considered that $w'(s) = 0, \cos w(s) = x_1 = const$ and $\sin w(s) = x_2 = const$. Therefore CSR surface is developable if and only if the base curve is a general helix with

$$\frac{\kappa}{\tau} = \frac{x_1^2 + \sigma^2}{x_1 x_2}.$$

Theorem 4.2 The striction line on CSR surface $\widetilde{M}_1(s,v)$ is given by

$$\overline{\beta} = \alpha(s) - \frac{w'(s)\cos w(s) - \sigma\kappa}{w'(s)^2 + \sigma^2(\kappa^2 + \tau^2) - 2w'(s)\sigma(\cos w(s)\kappa + \sin w(s)\tau) + (\sin w(s)\kappa - \cos w(s)\tau)^2} X(s).$$

Corollary 4.2. If

$$w(s) = \arcsin\sigma \int \kappa ds,$$

then the striction line of surface $\widetilde{M}_1(s,v)$ is equal to the base curve.

In this chapter, in the subsequent investigations, the base curve of the surface is cylindrical helix with

$$\kappa = mx_1, \qquad \tau = mx_2, \qquad m\epsilon Z$$

and $w(s) = const.$, $\cos w(s) = x_1 = const$, $\sin w(s) = x_2 = const$ will be considered.

Theorem 4.3. The Gauss curvature K and the mean curvature H in regular points of $\widetilde{M}_1(s,v)$ are given as

$$K = -\frac{(-\sigma^2\tau)^2}{\| M_s \wedge M_v \| (1 + v^2\sigma^2m^2 - 2v\sigma mx_1)(1+\sigma^2) - x_2^2}$$

$$H = \frac{(1+\sigma^2)m[x_1 - v\sigma m]^2 - 2x_2(-\sigma^2 mx_2)}{\| M_s \wedge M_v \| (2[1 + v^2\sigma^2m^2 - 2v\sigma mx_2](1+\sigma^2) - x_2^2)}.$$

Proof. The normal of the ruled surface $\widetilde{M}_1(s,v)$ is given by

$$N = \frac{1}{\| M_s \wedge M_V \|}(vmx_2\sigma^2, \sigma - vmx_1\sigma^2, x_1 - \sigma vm).$$

The coefficients E, F and G of the first fundamental form of $\widetilde{M}_1(s,v)$ are obtained as follows

$$E = 1 + v^2\sigma^2m^2 - 2v\sigma mx_1,$$

$$F = x_2,$$

$$G = 1 + \sigma^2$$

and we can obtain coefficients e, f and g of the second fundamental form of $\widetilde{M}_1(s,v)$ as

$$e = \frac{1}{\| M_s \wedge M_v \|} m[x_1 - v\sigma m]^2,$$

$$f = \frac{1}{\| M_s \wedge M_v \|}(-\sigma^2 mx_2),$$

$$g = 0.$$

Corollary 4.3. If $\sigma = 0$, then CSR surface $\widetilde{M}_1(s,v)$ is developable. This result is supported by Theorem 4.1.

Corollary 4.4. If the following equality is satisfy

$$(1+\sigma^2)(x_1 - v\sigma m)^2 = -2x_2^2\sigma^2,$$

then the surface is a minimal.

Remark 4.3. The striction line on the surface $\widetilde{M}_1(s,v)$ is given by

$$\overline{\beta} = \alpha(s) - \frac{x_1}{\sigma m}X(s).$$

5. CSR surface with Respect to Normal Plane

The CSR surface with regard to normal planes is introduced in this section. Then, some of the characteristics of this surface are discussed, along with some particular result based on these characteristics. Finally, quaternionic representations of the surface are given in three types.

The generating lines of the surface $\overline{M}_1(s,v)$ are given by points on the curve $\overline{X}(s)$ and have the constant slope σ with respect to the normal planes to the curve at every point on the curve $\overline{X}(s)$. The direction vector of generating lines of the surface is given by

$$\overline{X}(s) = \sin w(s)n(s) + \cos w(s)b(s) + \sigma t(s).$$

CSR surface $\overline{M}_1(s,v)$ is parametrized as follows

$$\overline{M}_1(s,v) = \alpha(s) + v\big(\overline{X}(s)\big).$$

Example 5.1. The parametric expression of CSR surface $\overline{M}_1(s,v)$ is as follows

$$x = \frac{1}{\sqrt{2}}\cos\big(s\sqrt{2}\big) + v\left(-\sin w(s)\cos\big(s\sqrt{2}\big) - \sigma\sin\big(s\sqrt{2}\big)\right)$$

$$y = \frac{1}{\sqrt{2}}\sin\big(s\sqrt{2}\big) + v\left(-\sin w(s)\sin\big(s\sqrt{2}\big) + \sigma\cos\big(s\sqrt{2}\big)\right)$$

$$z = -\frac{1}{2} + v\sigma.$$

In Figure 3, the surface choosing $\sigma = \sqrt{5}$, $w(s) = \frac{\pi}{2}$, $s\epsilon[0,\pi]$, $v\epsilon[-1,1]$ can be seen.

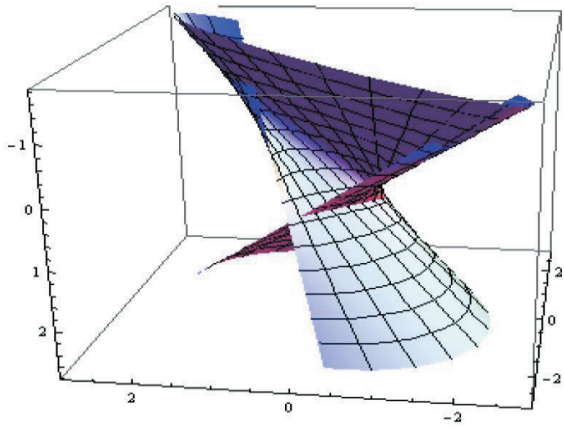

Figure 3

Remark 5.1. CSR surface with respect to the normal planes can be given with quaternion product in three types as follows

$$\textbf{i)}\ \overline{M}_1(s,v) = \alpha(s) + v\left(\overline{Q}_1 \times b(s)\right)$$

where

$$\overline{Q}_1 = \cos w(s) - \sin w(s)t(s) + \sigma n(s)$$

$$\textbf{ii)}\ \overline{M}_1(s,v) = \alpha(s) + v\left(\overline{Q}_2 \times t(s)\right)$$

where

$$\overline{Q}_2 = \sigma - \cos w(s)n(s) + \sin w(s)b(s)$$

$$\textbf{iii)}\ \overline{M}_1(s,v) = \alpha(s) + v\left(\overline{Q}_3 \times n(s)\right)$$

where

$$\overline{Q}_3 = \sin w(s) + \cos w(s)t(s) - \sigma b(s).$$

Remark 5.2. For quaternion $\overline{Q}_1$ and for vector $\vec{v}$, we can say that $\overline{Q}_1$ is a rotation of $b(s)$ about the $\vec{v}$ through an angle θ and $\overline{Q}_2$ is a rotation of $t(s)$ about the vector $\vec{v}$. And similarly, $\overline{Q}_3$ is a rotation of

$n(s)$ about the vector $\vec{v}$.

Theorem 5.1. If κ and τ satisfy the following equation

$$(w'(s) - \tau) + \cos w(s)\kappa\sigma = 0,$$

then CSR surface $\overline{M_1}(s, v)$ is a developable.

Corollary 5.1. The CSR surface is developable if and only if $\int \tau ds = \frac{(2k-1)\pi}{2}, k\epsilon Z^+$.

Corollary 5.2. If it is considered that $\cos w(s) = x_1 = const$, the surface is developable where

$$\frac{\kappa}{\tau} = \frac{1}{x_1\sigma}.$$

Namely, the base curve is the helix.

Theorem 5.2. The striction line on CSR surface $\overline{M_1}(s, v)$ is given as follows

$$\overline{\beta} = \alpha(s) + \frac{\kappa \sin w(s)}{(w'(s) - \tau)^2 + \kappa^2(\sin^2 w(s) + \sigma^2) - 2\sigma\kappa\cos w(s)(w'(s) - \tau)} X(s).$$

Corollary 5.3. If base curve is a line or $\overline{X}(s)$ is spanned by rectifying plane, striction line of CSR surface is equal to base curve.

In the subsequent investigations it is considered that $w(s) = \int \tau ds$.

Theorem 5.3. The mean curvature H and the Gauss curvature K of CSR surface $\overline{M_1}(s, v)$ is given by

$$K = -\frac{\kappa^2\sigma^2\cos^2 w(s)\big(1 - v\kappa\sin w(s)\big)^2}{\| M_s \wedge M_v \|^2 \left[(1 + \kappa^2\sigma^2)(1 + \sigma^2) - \big(\sigma + \sigma\kappa\sin w(s)\big)^2\right]},$$

$$H = \frac{\begin{matrix}\big(1 - v\kappa\sin w(s)\big)\big[\kappa(1 + \sigma^2)(-\cos w(s) + v\sigma\sin w(s)\tau) + 2\sigma^2\cos w(s)\big(1 + \kappa\sin w(s)\big)\big] \\ +(1 + \sigma^2)\big(\kappa^2\sigma^2v^2(\tau - \kappa)\big)\end{matrix}}{2 \| M_s \wedge M_v \| \left[(1 + \kappa^2\sigma^2)(1 + \sigma^2) - \big(\sigma + \sigma\kappa\sin w(s)\big)^2\right]}.$$

Corollary 5.4. The CSR surface is a developable**,** if the following

equality is satisfy

$$1 = v\kappa \sin w(s)$$

or $\overline{X}(s)$ is spanned by osculating plane.

REFERENCES

Ablamowicz, R. (2004), *Clifford Algebras: Applications to Mathematics, Physics, and Engineering*, Boston: Birkhauser.

Ablamowicz, R., Sobczyk, G. (2004), *Lectures on Clifford (Geometric) Algebras and Applications*, Boston: Birkhauser.

Do Carmo, M. P., (1976) *Differential Geometry of Curves and Surfaces*, Portland, U.S.A.: Prentice-Hall

Fu, Y., Yang, D. (2012), On constant slope space-like surfaces in 3-dimensional Minkowski space. *Journal of Mathematical Analysis and Applications*, Vol. 385.(1); pp. 208-220.

Fu, Y., Wang X. (2013), Classification of Timelike Constant Slope Surfaces in 3-Dimensional Minkowski Space. *Results. Math.* 63, 1095–1108.

Girard, P. R. (1984), The quaternion group and modern physics. *European Journal of Physics*, 5(1), 25.

Hamilton, W.R. (1844), On quaternions; or on a new system of imagniaries in algebra. *Lond. Edinb. Dublin Philos. Mag. J. Sci*. 25(3), 489–495.

Hacısalihoğlu H.H. (2000), *Differential Geometry*. Ankara, Faculty of Science Publ,.

Maleček K, Szarka J, Szarková D. (2009), Surfaces with Constant Slope and Their Generalization. *J. Polish Society Geometry Eng. Graphics*, 19:67-77.

Munteanu, M.I. (2010), From golden spirals to constant slope surfaces, *Journal of Mathematical Physics*, Vol. 51 (7), 073507, 1-9.

Shifrin, T. (2015), Differential Geometry: A first Course in Curves and Surfaces, University of Georgia. AMS Open Math. Notes.

Erdoğdu, M. (2019), Reflections with Respect to Line and Hyperplane from Quaternionic Point of View . *Journal of the Institute of Science and Technology* , 9 (3) , 1612-1621.

Erdoğdu, M., Özdemir, M. (2015), Split Quaternion Matrix Representation of Dual Split Quaternions and Their Matrices. *Adv. Appl. Clifford Algebras.* 25, 787–798.

Erdoğdu, M., Özdemir, M. (2020), Real Matrix Representations of Complex Split Quaternions with Applications. *Mathematical Methods in the Applied Sciences*, 43(12), 7227-7238.

CHAPTER 10

FIRST TESS LIGHT CURVE SOLUTION OF CP AUR

Oğuz ÖZTÜRK[1]

1 Research Asst. Oğuz ÖZTÜRK, PhD, Çanakkale Onsekiz Mart University, Faculty of Science, Department of Physics, Çanakkale Onsekiz Mart University, Astrophysics Research Centre and Observatory
ORCID: 0000-0002-9135-9865

Introduction

In binary star systems with orbital inclinations close to 90 degrees, the stars periodically eclipse each other during their orbital motion. Such binary star systems are called as eclipsing binary star systems.

Eclipsing binary star systems are of great importance to astrophysicists because of the information they contain. The geometric parameters can be obtained reliably from their precise ground and space based observations. From spectral and photometric observations of such systems, the masses, temperatures, and radii of the components can be found. In this way, it is possible to obtain information about the evolutionary processes of stars.

Table 1. Some parameters of CP Aur taken from literature.

Parameter	Description	Unit	Value	Reference
$\alpha_{\mathrm{J2000.0}}$	Right ascension	h, m, s	06 00 51.57	[1]
$\delta_{\mathrm{J2000.0}}$	Declination	°, ′, ″	+39 44 38.7	[1]
B	B-band magnitude	Mag.	14.025 ± 0.414	[2]
V	V-band magnitude	Mag.	13.377 ± 0.378	[2]
$d_{\mathrm{Gaia\ DR3}}$ $(= 1/\pi_{\mathrm{Gaia\ DR3}})$	Distance	pc	~1073	[3]

[1] (https://www.aavso.org/vsx). [2] AAVSO Photometric All Sky Survey DR9 (Henden et al. 2015). [3] Gaia DR3 data base (van Leeuwen et al., 2022).

CP Aur considered in this study is a neglected eclipsing binary star system. However the system has been included in some binary star catalogs (see Qian et al. 2018, Malkov et al. 2006, Hoogeveen 2005, Guthnick and Schneller 1939, Morgenroth 1933). Some parameters of CP Aur is presented in Table 1 with their references.

In this study, the Transiting Exoplanet Survey Satellite (TESS) (Ricker et al., 2015) light curve of CP Aur was solved for the first time. The absolute physical parameters were also estimated and results are discussed.

TESS Observations

Detailed information on the TESS observations can be found in the study of Ricker et al. (2015). The TESS observations of CP Aur were made between 28 November 2019 and 23 December 2019 (sector 19). The observations were made with a broad band filter (600-1000nm) and an exposure time of 1800s

was given (Mikulski Archive for Space Telescopes database). The light curve was constructed using the SAP_FLUX measurements given in the database. In total, 1155 observation points were taken, but 777 of them were determined as the most sensitive data (i.e., observations with quality flag value of 0). In the analysis, the 777 observation points were used (see Figure 1).

To phase the light curve presented in Figure 1, the updated light element of CP Aur is needed. For this, first of all, minimum time were determined from the TESS observations (Kwee & van Woerden, 1956).

Then, the O-C diagram of CP Aur was made using the light element below.

$$C_{1,\mathrm{CP\ Aur}}(\mathrm{Min\ I/Min\ II}) = \mathrm{BJD}\ 2458827.66586(122) + 2^{\mathrm{d}}.7649341 \times E \quad (1)$$

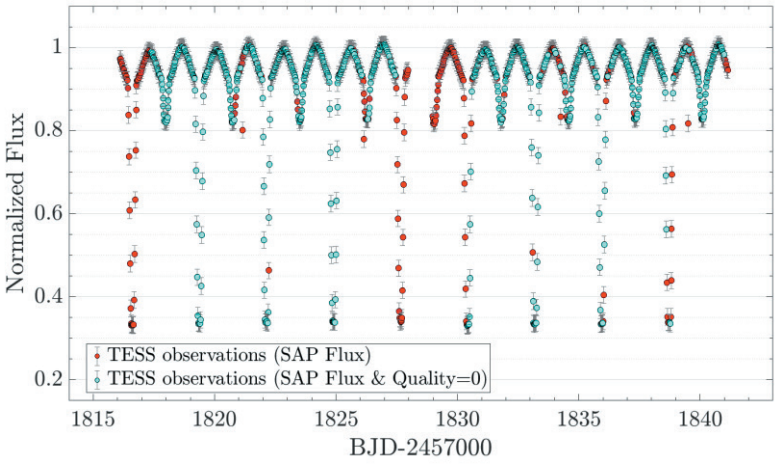

Figure 1. TESS light curve of CP Aur.

Table 2. TESS minimum times of CP Aur.

Minimum time (BJD)	Error	Minimum type
2458816.60764	0.00130	Min I
2458817.98637	0.00077	Min II
2458819.37193	0.00053	Min I
2458820.75170	0.00163	Min II
2458822.13653	0.00101	Min I
2458823.51617	0.00145	Min II

2458824.90119	0.00114	Min I
2458826.28035	0.00163	Min II
2458827.66586	0.00122	Min I
2458830.43035	0.00018	Min I
2458831.81212	0.00146	Min II
2458833.19530	0.00086	Min I
2458834.57601	0.00056	Min II
2458835.95941	0.00108	Min I
2458837.34121	0.00094	Min II
2458838.72446	0.00014	Min I
2458840.10627	0.00120	Min II

The time 2458827.66586(122) BJD seen in equation (1) is the TESS minimum time obtained in this study (see Table 1) and the orbital period of 2.7649341 days was taken from the ASAS-SN database (Shappee et al. 2014). The O-C diagram of CP Aur is presented in Figure 2.

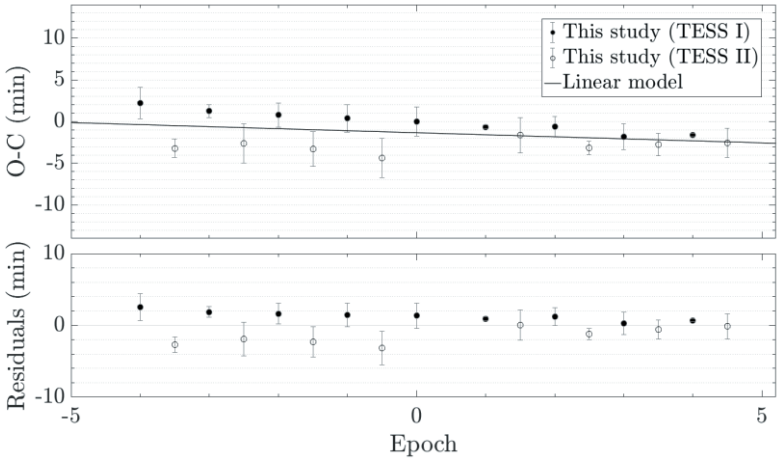

Figure 2. O-C diagram of CP Aur obtained using TESS minimum times and linear fit to O-C dataset. Lower panel: O-C residues from linear fit.

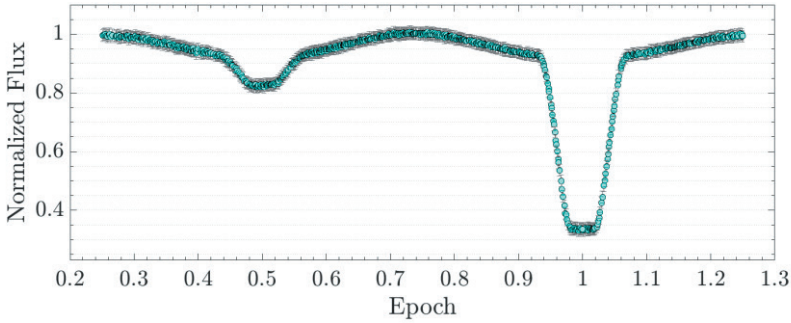

Figure 3. Phased TESS light curve of CP Aur.

Linear fit was made to the O-C dataset of CP Aur (see Figure 2) and the new light element obtained as a result of linear correction is given below.

$$C_{2,\text{CP Aur}}(\text{Min I/Min II}) = \text{BJD } 2458827.66493(30) + 2^{\text{d}}.76477(11) \times E \quad (2)$$

The light curve phased with the light element given by Equation (2) is shown in Figure 3.

Light Curve Solution

The analysis of CP Aur was performed using Wilson-Devinney software (Wilson & Devinney, 1971; Wilson, 2012) in semi-detached configuration (mod5). The effective wavelength is taken as 786.5nm in the solution. According to the convective (T<7200) stellar atmospheres, the bolometric gravitational darkening coefficients (g_1 and g_2) were taken as 0.32 (von Zeipel, 1924; Lucy, 1967). The bolometric albedo of the components (A_1 and A_2) is fixed at 0.5 for stellar atmospheres with convective atmospheres (Ruciński, 1969). The second order limb darkening coefficients were taken from Claret (2017). The rotation parameters were taken as $F_1 = F_2 = 0$ and the eccentricity as $e = 0$.

There is a slight difference in the maximum levels (see Figure 4). Therefore, the solution was made separately by assuming that there is a hot/cold spot on the primary or a hot/cold spot on the secondary. The spot parameters (see Table 3) were also adjusted as free parameters.

Undoubtedly, one of the most important parameters in the analysis is the assumed effective temperature value of the primary, T_1. There are two different temperature values given in the literature for CP Aur. One of them is given as 5741.33 K in the Gaia DR2 database (Gaia Collaboration, 2018; Andrae et al., 2018), and the other as 7934.7 in the Gaia DR3 database (Gaia Collaboration, 2022).

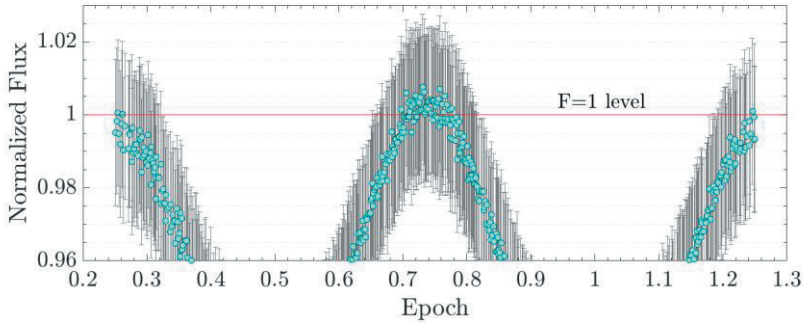

Figure 4. Diagram showing the maximum levels of light curve of CP Aur.

On the other hand, it is also possible to estimate the effective temperature from the intrinsic color index, $(B-V)_0$, using the method presented by Tunçel Güçtekin et al. (2016). Firstly, V band total absorption of CP Aur, $A_{(\infty,V)}$, is determined from Schlafly and Finkbeiner (2011) (NASA Extragalactic Database). Later the interstellar absorption for the distance $d_{\text{Gaia DR3}}$ (see Table 1), $A_{d_{\text{Gaia DR3,V}}}$ was calculated using the equation given by Bahcall and Soneira (1980) to be 0.771 mag. The color excess of CP Aur ($E_{d_{\text{Gaia DR3}}}(B-V)$)was then estimated from equation below to be 0.249 mag.

$$E_{d_{\text{Gaia DR3}}}(B-V) = A_{d_{\text{Gaia DR3}},V}/3.1 \tag{3}$$

$(B-V)_0$ of CP Aur was calculated to be 0. 0.40 ± 0.09 mag using equation below, where B and V magnitudes are taken from Table 1.

$$(B-V)_0, = (B-V) - E_{d_{\text{Gaia DR3}}}(B-V) \tag{4}$$

Finally, T_1 was estimated as 6809 ± 200 K, according to Drilling and Landolt (2000)'s $(B-V)_0$ – effective temperature calibration for main sequence stars.

As a result, we have 3 different temperature values. Since the system does not have any spectrally determined temperature value, an effective temperature search was performed for the primary component to decide which of these temperatures will be used in the analysis. In the temperature search process, the solution is made for different values of T_1. The variation of $T_1$with the sum of squares residuals obtained from the model fit ($\sum(O-C)^2$) is given in Figure 5. The minimum value of $\sum(O-C)^2$ is obtained under the cold spot assumption on the primary component. Therefore the final solution was made under the cold spot assumption.

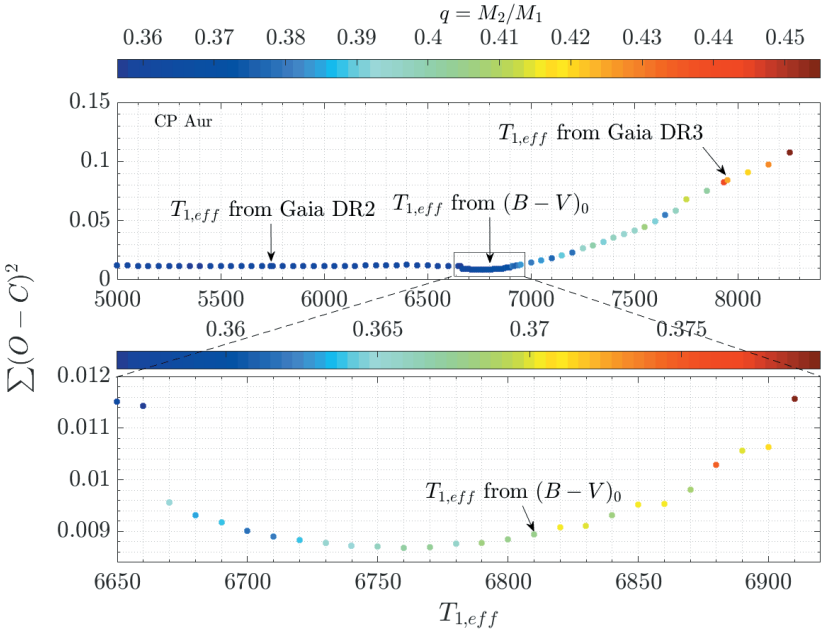

Figure 5. $T_{1,eff}$-$\sum(O-C)^2$ diagram obtained for CP Aur under assumption of a cold spot on primary component.

Table 3. Parameters obtained from light curve analysis of CP Aur.

Parameter	Description	Value
T_0 (BJD)	Conjunction time	2458827.66493±0.00030
P (days)	Orbital period	2.76477± 0.00011
ϕ	Phase shift	0.0002±0.0001
i (deg)	Inclination	86.69±0.17
T_1 (K)	Eff. temp. of pri.	6809 (fixed)
T_2 (K)	Eff. temp. of sec.	4090±120
$q(=M_2/M_1)$	Mass ratio	0.361±0.006
Ω_1	Surface potential of pri.	7.848±0.009
Ω_2	Surface potential of sec.	2.642
$r_1(=R_1/A)$ (vol.)	Fractional radius of primary	0.134±0.004
$r_2(=R_r/A)$ (vol.)	Fractional radius of sec.	0.313±0.006
L_1/L_{tot}	Fractional luminosity of pri.	0.590±0.007
L_2/L_{tot}	Fractional luminosity of sec.	0.410
	Spot parameters	
Co-lat. (deg.)	Co-latitude of spot	98±18
Lon. (deg.)	Longitude	277±12
Spot radius (deg.)		8.3±0.6
T_{spot}/T_2	Fractional temperature of spot	0.74±0.06
$\sum(O-C)^2$	Sum of squared residuals	0.0085

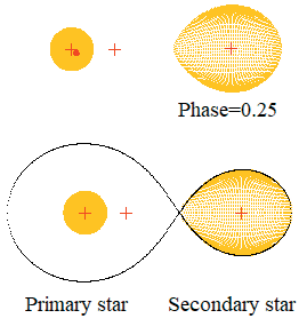

Figure 6. Roche geometry of CP Aur. Red area represents cold spot on primary component.

The minimum value of $\sum(O-C)^2$ was reached at the temperature value estimated from $(B-V)_0$ of CP Aur (see Figure 5). For this reason, T_1 was taken as 6809 ± 200 K and kept constant in the solution. At the same time, the minimum $\sum(O-C)^2$ value was reached at $q = 0.36$ in the temperature search process. For this reason, the initial value of the mass ratio parameter ($q = M_2/M_1$) in the light curve solution is taken to be 0.36. Final solution parameters are given in Table 3. The Roche geometry of CP Aur obtained using Binary Maker 3.0 software (Bradstreet and Steelman 2002) and the parameters in Table 3 is also shown in Figure 6.

Results and Discussion

Table 4. Estimated absolute parameters of CP Aur.

Parameter	Description	Primary star	Secondary star
A ($R_\odot$)	Semi-major axis	10.40±0.21	
M ($M_\odot$)	Mass	1.45±0.15	0.53±0.11
R ($R_\odot$)	Radius	1.39±0.12	3.25±0.48
$\log g$ (cgs)	Surface gravity	4.31±0.11	3.13±0.09
M_{bol} (mag)	Absolute bolometric magnitude	3.32±0.41	3.69±0.48
M_V (mag)	Absolute visual magnitude	3.34±0.43	4.65±0.62
M_V (system)	Absolute visual magnitude of system	3.05±0.40	
d (pc)	Distance	813±215	

The estimated physical parameters of CP Aur are given in Table 4. Assuming $T_1 = 6809$ K (see Light Curve Solution Section), the mass of the component is estimated as 1.45 $M_\odot$ using the mass-temperature calibration given for main-sequence stars by Drilling and Landolt (2000). 10% of the primary mass was accepted as the error value, and the errors of the other parameters given in Table 4 were calculated accordingly. The semi-major axis of the system was calculated using Kepler's third law. Mass of the secondary is calculated from the photometric mass ratio given in Table 3. Radii of components were estimated using the fractional radii given in Table 3. M_{bol} and $\log g$ were estimated using the solar values ($T_{eff} = 5771.8 \pm 0.7\,K$ mag, $M_{bol} = 4.7554 \pm 0.0004$ and $g = 27423.2 \pm 7.9$ cm/s^2) given by Pecaut and Mamajek (2013). Absolute visual magnitudes were estimated using equation below, where the bolometric corrections were calculated using the effective temperature-bolometric correction calibration presented by Pecaut & Mamajek (2013).

$$M_{V,1,2} = M_{bol,1,2} - BC_{V,1,2} \tag{5}$$

M_V (system) of CP Aur was estimated using equation below.

$$M_V(\text{system}) = -2.5\log_{10}(10^{-0.4M_{V,1}} + 10^{-0.4M_{V,2}}) \tag{6}$$

The distance of the system is calculated from equation below.

$$d = 10^{\frac{V - M_V(system) + 5 - A_{d_{\text{Gaia DR3}},V(b)}}{5}} \quad (7)$$

As a result, the absolute parameters of CP Aur calculated in this study were estimated using only the geometric parameters obtained as a result of TESS light curve analysis together with the calibrations given in the literature. Therefore, precise radial velocity measurements and spectroscopic observations of the system are needed to obtain the absolute parameters reliably. It was concluded that the secondary component filled its Roche lobe (see Light Curve Analysis Section). Therefore, a mass transfer from the secondary component to the primary can occur. To examine the predicted mass transfer mechanism, precise minimum time observations of the system to be made in the future are needed.

REFERENCES

Andrae, R., Fouesneau, M., Creevey, O., et al., 2018, Astronomy & Astrophysics, Volume 616, id.A8, 29 pp.

Bahcall, J.N., Soneira, R.M., 1980. The universe at faint magnitudes, I. Models for the Galaxy and the predicted star counts. Astrophys. J. Suppl. 44, 73–110

Bradstreet, D. H., Steelman, D. P., 2002, Binary Maker 3.0 - An Interactive Graphics-Based Light Curve Synthesis Program Written in Java. American Astronomical Society, 201st AAS Meeting, id.75.02; Bulletin of the American Astronomical Society, Vol. 34, p.1224

Claret, A., 2017, Limb and gravity-darkening coefficients for the TESS satellite at several metallicities, surface gravities, and microturbulent velocities. A&A 600, id.A30.

Drilling, J.S., Landolt, A.U., 2000. In: Cox, Arthur N. (Ed.), Allen's Astrophysical Quantities, fourth ed. AIP Press; Springer, New York, ISBN: 0-387-98746-0, p. 381

Gaia Collaboration, 2018, Gaia Data Release 2. Summary of the contents and survey properties. A&A 616, id.A1.

Gaia Collaboration, 2022, VizieR Online Data Catalog: Gaia DR3 Part 1. Main source (Gaia Collaboration, 2022), p. I/355

Guthnick P., Schneller H., 1939, Astron. Nachr. 268, p.165-190.

Henden, A.A., Levine, S., Terrell, D., Welch, D.L., 2015. APASS- The latest data release. In: AAS Meeting #225. 336,16.

Hoogeveen G. J., 2005, IAU Inform. Bull. Var. Stars 5652, p.1-6.

Kwee, K. K., van Woerden, H., 1956, A method for computing accurately the epoch of minimum of an eclipsing variable. BAN 12,327-330.

Lucy, L. B., 1967, Gravity-Darkening for Stars with Convective Envelopes. ZA 65, 89-92.

Malkov O. Yu., Oblak E., Snegireva E. A., Torra J., 2006, Astron. Astrophys. 446 (2), p.785-789.

Morgenroth O., 1933, Astron. Nachr. 250, p.75-80.

Pecaut, M.J., Mamajek, E.E., 2013. Intrinsic colors, temperatures, and bolometric corrections of pre-main-sequence stars. Astrophys. J. Suppl. 208 (1), 9.

Qian S. -B., Zhang J., He J. -J. et al., 2018, Astrophys. J., Suppl. Ser. 235 (1), article id. 5, 12 pp.

Ricker G. R., Winn J. N., Vanderspek R., et al., 2015, J. Astron. Telesc. Instrum. Syst. 1 (1), 014003.

Ruciński S. M., 1969, The Proximity Effects in Close Binary Systems. II. The Bolometric Reflection Effect for Stars with Deep Convective Envelopes. AcA 19, 245-255

Schlafly, E.F., Finkbeiner, D.P., 2011. Measuring reddening with sloan digital sky survey stellar spectra and recalibrating SFD. Astrophys. J. 737 (2).

Shappee, B. J., Prieto, J. L., Grupe, D. ve ark. 2014, The Man behind the Curtain: X-Rays Drive the UV through NIR Variability in the 2013 Active Galactic Nucleus Outburst in NGC 2617. ApJ 788 (1), id.48.

Tunçel Güçtekin, S., Bilir, S., Karaali, S., et al., 2016, Metallicity calibration and photometric parallax estimation: I. UBV photometry, Astrophysics and Space Science, Volume 361, Issue 6, article id.186, 18 pp.

van Leeuwen F., de Bruijne J., Babusiaux C., et al., 2022, Gaia DR3 documentation, European Space Agency; Gaia Data Processing and Analysis Consortium Online at https://gea.esac.esa.int/archive/documentation/GDR3/index.html, id. 1

von Zeipel, H., 1924. The radiative equilibrium of a rotating system of gaseous masses. MNRAS 84, 665–683.

Wilson, R. E., 2012, Spotted Star Light Curves with Enhanced Precision. AJ 144 (3), id.73.

Wilson, R.E., Devinney, E.J., 1971. Realization of accurate close-binary light curves: Application to MR cygni. Astrophys. J. 166, 605–619.

CHAPTER 11

LEFT-COVARIANT DIFFERENTIAL CALCULUS ON THE Z_2-GRADED HOPF SUPERALGEBRA

Fatma BULUT[1]

1 Doç. Dr. Fatma BULUT, Department of Mathematics, University of Bitlis Eren, Bitlis, Turkey, ORCID: 0000-0002-7684-6796

In the mathematical modeling, Lie group differential geometry is important and it can be tempting to also generalize the equivalent notions of differential geometry when a quantum group (or a Hopf algebra) is viewed as a generalization of the notion of a group. In this paper, we prepared a left-covariant noncommutative differential calculus on the Hopf superalgebra $F(\mathbb{C}_q^{2|1})$. This calculus contain functions on the superspace $\mathbb{C}_q^{2|1}$ and differentials. In the cause of establish a differential diagram, we use the left-covariance. Finally, we explicitly construct a vector field quantum Lie superalgebra.

1. Introduction

In recent years, the notion of differential calculus on algebras has been playing important role in mathematics and physics dated from Connes' work [1] on noncommutative geometry. Noncommutative geometry is the idea that the geometric structure is constructed by considering the generators of an algebra that need not be commutative as coordinate functions. If an algebra is associative, it can be aimed to extend it to a differential algebra as in commutative geometry. Woronowicz is responsible for the groundbreaking work on covariant differential calculi on the quantum groups [2, 3]. Several authors, including [4-10], have studied specific examples of covariant noncommutative calculus on quantum spaces and groups.

Wess and Zumino [11] introduced another approach and defined differential forms as differential of coordinates for the quantum space defined by Manin [12]. Also in [13], Manin investigated a multiparametric deformation of the general linear supergroup.

The extension to the superspace has been discussed in many papers like as [14-18]. In particular, the coordinates of a plane have been deformed to become noncommutative objects in order to obtain the quantum groups $\mathbb{R}_q(1|2)$ [9] and $\mathbb{R}_h(1|2)$ [19].

In this paper, we construct a left covariant noncommutative calculus on the Hopf superalgebra $O(\mathbb{C}_q^{2|1})$ using the left covariance perspective. This calculus involves functions on the $\mathbb{Z}_2$-graded space (or quantum superspace) $\mathbb{C}_q^{2|1}$, differentials of generators, differential forms and partial derivatives.

2. The Hopf Superalgebra $F(\mathbb{C}_q^{2|1})$

In this section, we briefly mention some definitions and theorems from [16] as much as we need.

2.1 The superalgebra of polynomials on $\mathbb{C}_q^{2|1}$

The elements of the $\mathbb{Z}_2$-graded (2+1)-space $\mathbb{C}_q^{2|1}$ are $\mathbb{Z}_2$-graded vectors (or supervectors) formed by three components, two even and one odd. Let us denote components of a supervector in $\mathbb{C}_q^{2|1}$ by x, y and θ and the polynomial superalgebra $\mathbb{C}[x,y,\theta]$ by $O(\mathbb{C}^{2|1})$Let us also assume that the degrees of x and y are 0, the degree of θ is 1.

Definition 2.1 Let I_q be the two-sided ideal of the superalgebra $\mathbb{C}\langle x,y,\theta\rangle$, which is created by the components $xy-yx$, $x\theta-q\theta x$, $y\theta-q\theta y$ and θ^2.

Let $\mathbb{C}\langle x, y, \theta\rangle$ be a free superalgebra with a unit generated by x, y and θ, where $q \in \mathbb{C} - \{0\}$. The quantum superalgebra $O(\mathbb{C}_q^{2|1})$ is then defined by

$$O(\mathbb{C}_q^{2|1}) = \mathbb{C}\langle x, y, \theta\rangle / I_q .$$

This associative, unital superalgeba is called superalgebra of polynomials on $\mathbb{C}_q^{2|1}$. According to Definition 2.1, if $(x, y, \theta)^t$ belongs to $\mathbb{C}_q^{2|1}$ then we have

$$xy = yx, \quad x\theta = q\theta x, \quad y\theta = q\theta y, \quad \theta^2 = 0, \tag{1}$$

where $q \in \mathbb{C} - \{0\}$.

Definition 2.2 Assume that the algebra $\Lambda(\mathbb{C}_q^{2|1})$ contains the ξ generators, η and z which provide the relations

$$\xi^2 = 0 = \eta^2, \quad \xi\eta = -q^{-2}\eta\xi, \quad \xi z = q^{-1} z\xi, \quad \eta z = q^{-1} z\eta \tag{2}$$

where the degrees of the coordinates ξ and η are 1 and the degree of the coordinate z is 0.

2.2 The Hopf superalgebra $F(\mathbb{C}_q^{2|1})$

We suppose that the inverse u^{-1} of u exists such that $uu^{-1} = 1 = u^{-1}u$ for $u \in \{x, y\}$. So, we have the extended $\mathbb{Z}_2$-graded quantum algebra, denoted by $F(\mathbb{C}_q^{2|1})$, to be the $\mathbb{Z}_2$-graded algebra containing $O(\mathbb{C}_q^{2|1})$ with the formal inverses x^{-1}, y^{-1} and $\mathbf{1}$.

We denote by $p(a)$ the degree of an element a in a superalgebra. The rule for the tensor product of two superalgebras is defined as follows:

Definition 2.3 If U and V are two superalgebras, then the tensor product $U \otimes V$ is given by

$$(u_1 \otimes u_2)(v_1 \otimes v_2) = (-1)^{p(u_2)p(v_1)}(u_1 v_1 \otimes u_2 v_2),$$

where u_i and v_i are homogeneous elements in U and V, respectively [16] .

Theorem 2.4 The superalgebra $F(\mathbb{C}_q^{2|1})$ is a Hopf superalgebra with the co-maps Δ, ϵ and S the actions of these co-maps on the generators of $F(\mathbb{C}_q^{2|1})$ is given by

$$\Delta(x) = x \otimes x, \quad \Delta(y) = y \otimes y, \quad \Delta(\theta) = \theta \otimes x^{-1}y + 1 \otimes \theta.$$

$$\epsilon(x) = 1, \quad \epsilon(y) = 1, \quad \epsilon(\theta) = 0.$$

$$S(x) = x^{-1}, \quad S(y) = y^{-1}, \quad S(\theta) = -q^{-1}x\theta x^{-1}. \tag{3}$$

3. THE RESEARCH FINDINGS AND DISCUSSION

Functions typically commute with 1-forms or differentials, as is widely known geometry using algebra. To put it another way, differentials can multiply functions in the same way whether they come from the left or the right. Because the algebra of functions is noncommutative, this condition is not possible. If the outcomes of multiplying functions by 1-forms on the left and right sides do not match, the differential calculus is said to be noncommutative.

We shall establish a left-covariant differential calculus on the associative unital $\mathbb{Z}_2$-graded algebra $F(\mathbb{C}_q^{2|1})$ in this section. Differentials,

differential forms, and functions on the $\mathbb{Z}_2$-graded space $\mathbb{C}_q^{2|1}$ are all components of this calculus.

Now, we identify the relationship(s) between the superalgebra's generators and their differentials.

3.1 $\mathbb{Z}_2$-graded Differential algebra and left-covariance

Definition 3.1 First order $\mathbb{Z}_2$-graded differential calculus over A is referred to as a pair (Γ, d) if Γ is an A-bimodule, $d: A \longrightarrow \Gamma$ is a linear map that complies with the $\mathbb{Z}_2$-graded Leibniz rule

$$d(a \cdot b) = (da) \cdot b + (-1)^{p(a)}\, a \cdot db, \quad \forall a, b \in A,$$

such that

$$\Gamma = \mathrm{Lin}\{a \cdot db : a, b \in A\}$$

and A is a $\mathbb{Z}_2$-graded associative algebra. A one-form is a type of Γ. Any $w \in \Gamma$ can be expressed as $w = \sum_k a_k \cdot db_k$, where $a_k, b_k \in A$.

We use left covariance to construct a differential scheme. First, note that the differential algebra is a $\mathbb{Z}_2$-graded associative algebra produced by the elements of $\{x, y, \theta, dx, dy, d\theta\}$ due to the consistency of a differential calculus with relations (2). If H is a Hopf superalgebra and Γ is a free left module over H generated by the elements of this set, then $\Gamma = \Gamma^0 \cup \Gamma^1$, where $\Gamma^0 \simeq H$. In this case, we say that (Γ, d) is a differential calculus of first order over H with a $\mathbb{Z}_2$-graded.

Definition 3.2 Assume that (Γ, d) be a $\mathbb{Z}_2$-graded differential calculus and $\tau: H \longrightarrow H$ be the linear map of degree zero which gives

$\tau(\rho) = (-1)^{p(\rho)}\rho$ for all $\rho \in H$. If there is a left coaction, or linear map $\Delta_L: \Gamma^1 \longrightarrow H \otimes \Gamma^1$, such that

$$\Delta_L(a \cdot db) = \Delta(a)(\tau \otimes d)\Delta(b), \quad \forall a,b \in H, \tag{4}$$

then the pair (Γ, d) is called left-covariant.

3.2 First order differential calculations with a left covariant

Suppose that the $F(\mathbb{C}_q^{2|1})$-bimodule Γ^1 is a free right $F(\mathbb{C}_q^{2|1})$-module generated by the differentials dx, dy and $d\theta$. The algebra's generators and their differentials do not commute, as far as we are aware. Therefore, we can think of possible commutation relations between differentials and generators as follows

$$u_i \cdot dv_j = \sum_{k,l=1}^{3} B_{ij}^{kl}\, dv_k \cdot u_l, \tag{5}$$

where some constants B_{ij}^{kl} being zero and some depending on the parameter q. We obtain these constants in the following two lemmas. Then, we combine all the results in the next theorem.

Lemma 3.3 If Δ_L is applied to both sides of the equality (5), we have 10 constants left.

Proof. The identity in (4) allows us to write

$$\begin{aligned} &\Delta_L(dx) = x \otimes dx, \qquad \Delta_L(dy) = y \otimes dy, \\ &\Delta_L(d\theta) = \theta \otimes x^{-1}\left(dx.x^{-1}y - dy\right) + 1 \otimes d\theta. \end{aligned} \tag{6}$$

If we use the operator Δ_L on both sides of the equation (5), the following six constants are obtained.

$$B_{11}^{11} = r, \quad B_{12}^{21} = A, \quad B_{12}^{12} = B, \quad B_{21}^{12} = C, \quad B_{21}^{21} = D, \quad B_{22}^{22} = s.$$

And this operation imposes the following restriction on another contants as follow

$$B_{ii}^{kl} = 0, \quad kl \neq ii; B_{ij}^{kl} = 0, \quad kl \neq \{ij, ji\};$$

$$B_{13}^{13} = r^{-1}B_1 - 1, B_{31}^{31} = qA, \quad B_{23}^{32} = q[C + (s - B_2)B(B_1)^{-1}],$$

$$B_{23}^{23} = (s - B_2)(B_1)^{-1}, B_{31}^{13} = -q^{-1}r^{-1}B_2, \quad B_{31}^{31} = -D,$$

$$B_{32}^{23} = -q^{-1}s(B_1)^{-1}, B_{32}^{32} = -sA(B_1)^{-1}, \quad B_{33}^{33} = B_2(B_1)^{-1}$$

where $B_1 = A + B$ and $B_2 = C + D$.

Lemma 3.4 Consistency with the relations (1) leaves only two constants in (5).

Proof. (i) The differential d is first applied to commutation relations (1) from the left and here, we replace relations associated with the new commutation relations (5) obtained with Lemma 4.1, thus, we find as

$$C = 1 + A, \quad D = B - 1$$

Thus 2 more of those constants are eliminated.

(ii) We multiply the commutation relations (1) from left by differentials and we get how the commutation relations between their own of the remaining four constant. When this relations are examined by considering the consistency, it is seen that there are two situations which

two constants fixed as free parameters and another two constants depend on them. These are as follows

$$\text{CaseI:}\quad A=0,\quad B=r,\quad \text{CaseII:}\quad A=s-1,\quad B=1.$$

Then, by combining the two aforementioned lemmas, we arrive at the following theorem, where (5) still contains two arbitrary constants.

Theorem 3.5 There are two $\mathbb{Z}_2$-graded first-order differential calculi $\Gamma^1(\mathbb{C}_q^{2|1})$ on the $\mathbb{Z}_2$-graded Hopf algebra $F(\mathbb{C}_q^{2|1})$ that are covariant with regard to one another, and $\{dx, dy, d\theta\}$ is a free right $F(\mathbb{C}_q^{2|1})$-module basis of $\Gamma^1(\mathbb{C}_q^{2|1})$. The relations

$$\begin{aligned}
&xdx = r\,dxx, ydx = dxy + (r-1)dyx,\\
&xdy = r\,dyx, yd\theta = q\,d\theta y + (sr^{-1}-1)\,dy\theta,\\
&xd\theta = qr\,d\theta x, \theta dx = -q^{-1}\,dx\theta + (1-r)\,d\theta x,\\
&ydy = s\,dyy, \theta dy = -q^{-1}r^{-1}s\,dy\theta,\\
&\theta d\theta = d\theta\theta,
\end{aligned} \tag{7}$$

for Type I, and

$$\begin{aligned}
&xdx = r\,dxx, xdy = r\,dyx + (s-1)\,dxy,\\
&ydx = s\,dxy, xd\theta = q\,d\theta x + (r^{-1}s-1)\,dx\theta,\\
&ydy = s\,dyy, \theta dx = -q^{-1}r^{-1}s\,dx\theta,\\
&yd\theta = qs\,d\theta y, \theta\cdot dy = -q^{-1}\,dy\theta + (1-s)\,d\theta y,\\
&\theta d\theta = d\theta\theta,
\end{aligned} \tag{8}$$

for Type II, we determine the bimodule structures for these calculi.

Remark 3.6 In Section 3.3 we will see that the relations (8) are not consistent with higher order differential calculus (look Remark 3.14).

Theorem 3.7 There is a map $\sigma: F(\mathbb{C}_q^{2|1}) \to M_3(F(\mathbb{C}_q^{2|1}))$ preserving the relations (7).

Proof. Since $\Gamma(\mathbb{C}_q^{2|1})$ has the homogeneous basis $\{dx, dy, d\theta\}$, there is a map $\sigma: F(\mathbb{C}_q^{2|1}) \to M_3(F(\mathbb{C}_q^{2|1}))$ given

$$f \cdot dx_j = \sum_{i=1}^{3} (-1)^{p(f)p(dx_i)} dx_i \cdot \sigma_{ij}(f), \quad (9)$$

for all $f \in F(\mathbb{C}_q^{2|1})$ and $x_1 = x$, $x_2 = y$, $x_3 = \theta$. Indeed, we can easily see that the relations (9) for

$$\sigma(x) = \begin{pmatrix} r\,x & 0 & 0 \\ 0 & r\,x & 0 \\ 0 & 0 & qr\,x \end{pmatrix}, \quad \sigma(\theta) = \begin{pmatrix} q^{-1}\theta & 0 & 0 \\ 0 & q^{-1}r^{-1}s\theta & 0 \\ (r-1)\,x & 0 & \theta \end{pmatrix}, \quad (10)$$

$$\sigma(y) = \begin{pmatrix} y & 0 & 0 \\ (r-1)\,x & s\,y & (sr^{-1}-1)\theta \\ 0 & 0 & q\,y \end{pmatrix},$$

are equivalent to the relations (7). Here the constants r and s are arbitrary complex numbers different from zero.

Theorem 3.8 The map σ is a $\mathbb{Z}_2$-graded $\mathbb{C}$-linear homomorphism such that

$$\sigma_{ij}(fg) = \sum_{k=1}^{3} (-1)^{p(f)[p(x_k)-p(x_j)]} \sigma_{ik}(f)\sigma_{kj}(g), \quad \forall f, g \in F(\mathbb{C}_q^{2|1}) \quad (11)$$

where $x_1 = x$, $x_2 = y$ and $x_3 = \theta$.

Remark 3.9 It can be easily seen that operator σ preserves the commutation relations (1)

Corollary 3.10 We define operator $\tau: F(\mathbb{C}_q^{2|1}) \to M_3(F(\mathbb{C}_q^{2|1}))$ by the formulas

$$dx_i \cdot u = \sum_{j=1}^{3} (-1)^{p(u)p(dx_j)} \tau_{ij}(u) \cdot dx_j \qquad (12)$$

for all $u \in F(\mathbb{C}_q^{2|1})$ and $x_1 = x$, $x_2 = y$ and $x_3 = \theta$. We have

$$\tau(x) = \begin{pmatrix} r^{-1}x & 0 & 0 \\ 0 & r^{-1}x & 0 \\ 0 & 0 & q^{-1}r^{-1}\,x \end{pmatrix}, \quad \tau(y) = \begin{pmatrix} y & (r^{-1}-1)\,x & 0 \\ 0 & s^{-1}y & 0 \\ 0 & (1-rs^{-1})\theta & q^{-1}\,y \end{pmatrix},$$

$$\tau(\theta) = \begin{pmatrix} q\theta & 0 & (r^{-1}-1)\,x \\ 0 & qrs^{-1}\theta & 0 \\ 0 & 0 & \theta \end{pmatrix} \qquad (13)$$

for the relations (7).

Corollary 3.11 Operator τ is a $\mathbb{Z}_2$-graded $\mathbb{C}$-linear homomorphism in the sense (11).

Remark 3.12 Using Result 3 it can be easily shown that the relations in (1) are preserved under the action of operator τ.

3.3 Differential calculus of higher order on $F(\mathbb{C}_q^{2|1})$

We initially provide the definition of the $\mathbb{Z}_2$-graded differential calculus before moving on to higher order differential calculus.

Definition 3.13 A $\mathbb{Z}_2$-graded differential calculus over A is a $\mathbb{Z}_2$-graded algebra $\Omega^{\wedge} = \bigoplus_{n=0}^{\infty} \Omega^{\wedge n}$ if A is an arbitrarily associative

superalgebra. Here $\Omega^{\wedge 0} = A$ and the spaces $\Omega^{\wedge n}$ are generated as A-bimodules via the action of a linear mapping $d: \Omega^{\wedge} \longrightarrow \Omega^{\wedge}$ of degree 1 such that [16]

1. $d^2 = 0$,
2. $d(u \wedge w) = (du) \wedge w + (-1)^{p(u)}\, u \wedge (dw)$ for $u, w \in \Omega^{\wedge}$.
3. $\Omega^{\wedge n} = \mathrm{Lin}\{f_0 \cdot df_1 \wedge \cdots \wedge df_n : f_0, f_1, \ldots, f_n \in A, n \in \mathbb{N}\}$.

Now let us assume that the first order differentials of the generators of the superalgebra $F(\mathbb{C}_q^{2|1})$ are ξ, η and z respectively, i.e. $dx = \xi$, $dy = \eta$ and $d\theta = z$. The criteria in Definition 3.13 specifically define differential d in this situation, and the commutation relations between the differentials take the following form:

$$dx \wedge dy = -q^{-2} dy \wedge dx, \quad dx \wedge d\theta = q^{-1} d\theta \wedge dx, \quad dy \wedge d\theta = q^{-1} d\theta \wedge dy,$$

$$dx \wedge dx = 0 = dy \wedge dy. \tag{14}$$

Remark 3.14 We can use conditions 1 and 2 in Definition 3.13, to forming an opinion for the two constants, which are r and s, in the relation (7) and (8) which first order differential calculus. Indeed, if we apply the operator d to the relations (8) from the left and right, we will see that the relations we obtain are not consistent with the relations (14). However for consistent of the relations (7), we get the arbitrary constants in these relations must be like as $r = q^{-2}$ and $s = 1$. So, we continue with relations (7) in Theorem 3.5.

3.4 The $\mathbb{Z}_2$-graded partial derivatives

In this chapter, we introduce the partial derivatives of the generators of the superalgebra $F(\mathbb{C}_q^{2|1})$ and proceed to the construction of differential calculus.

Definition 3.15 The vector fields $\partial_x, \partial_y, \partial_\theta : F(\mathbb{C}_q^{2|1}) \longrightarrow F(\mathbb{C}_q^{2|1})$ dual to $\{dx, dy, d\theta\}$ is defined by

$$df = dx\ \partial_x(f) + dy\ \partial_y(f) + d\theta\ \partial_\theta(f), \quad f \in F(\mathbb{C}_q^{2|1}) \tag{15}$$

where $p(\partial_x) = 0 = p(\partial_y)$ and $p(\partial_\theta) = 1$. The partial derivatives of the calculus $(\Omega^\wedge, d)$ are the name given to these operators [16].

Theorem 3.16 Commutation relationships between partial derivatives and $F(\mathbb{C}_q^{2|1})$'s generators have the following form:

$$\partial_x x = 1 + q^{-2} x \partial_x, \partial_y x = q^{-2} x \partial_y, \partial_\theta x = q^{-1} x \partial_\theta,$$

$$\partial_y y = 1 + y\partial_y + (q^{-2} - 1)(x\partial_x - q^2\theta\partial_\theta), \partial_x y = y\partial_x, \partial_\theta y = qy\partial_\theta, \tag{16}$$

$$\partial_\theta \theta = 1 - \theta\partial_\theta + (q^{-2} - 1)\ x\partial_x, \partial_x \theta = q^{-1}\theta\partial_x, \partial_y \theta = q\theta\partial_y.$$

Proof. If f is a differentiable function, then we can write

$$df = (dx\ \partial_x + dy\ \partial_y + d\theta\ \partial_\theta) f, \tag{17}$$

We now replace f with xf in the left hand side of the equation in (17). Then, we have

$$d(xf) = dx\ f + x\ (dx\ \partial_x + dy\ \partial_y + d\theta\ \partial_\theta x) f$$

$$= \{dx(1 + q^{-2}x\partial_x) + dy(q^{-2}x\partial_y) + d\theta(q^{-1}x\partial_\theta)\}f.$$

On the other hand, since the right-hand side of the equality in (17) is of the form

$$d(xf) = [dx\ (\partial_x x) + dy\ (\partial_y x) + d\theta\ (\partial_\theta x)]f \quad .$$

We obtain some relations in (16) by comparing the right hand sides of these two equalities. We follow similar ways to find other relations.

Theorem 3.17 The following commutation relations

$$\partial_x\partial_y = q^{-2}\partial_y\partial_x, \quad \partial_x\partial_\theta = q^{-1}\partial_\theta\partial_x, \quad \partial_y\partial_\theta = q^{-1}\partial_\theta\partial_y, \quad \partial_\theta^2 = 0. \tag{18}$$

are satisfied by the partial derivatives.

Proof. We use the fact that $d^2f = 0$ for a differentiable function f with the relations given in (14).

3.5 $\mathbb{Z}_2$-graded left-invariant Maurer-Cartan 1-forms

In this section we will define three 1-forms from the generators of the Hopf superalgebra $F(\mathbb{C}_q^{2|1})$ and find their relations with the generators and with themselves. Let us give the following definition [16] .

Using the generators of the Hopf superalgebra $F(\mathbb{C}_q^{2|1})$, three 1-forms can be defined as

$$w_i := w(x_i) = m(S' \otimes d)\Delta(x_i), \quad x_i \in F(\mathbb{C}_q^{2|1}). \tag{19}$$

where $S'(x_i) := (-1)^{p(x_i)}S(x_i)$.

Lemma 3.18 The 1-forms w_1, w_2 and w_3 are left-invariant, that is,

$$\Delta_L(w_i) = 1 \otimes w_i, \quad (i = 1,2,3).$$

Theorem 3.19 If $(\Omega^\wedge, \Delta_L)$ is a left-covariant bimodule over the Hopf superalgbera $F(\mathbb{C}_q^{2|1})$ and $\{w_k\}$ is a basis in the vector space of all left-invariant elements of $\Omega^\wedge$, then there is a linear map $\mu: F(\mathbb{C}_q^{2|1}) \longrightarrow M_3(F(\mathbb{C}_q^{2|1}))$ such that

$$w_i \cdot u = \sum_{j=1}^{3} (-1)^{p(u)p(w_i)} \mu_{ij}(u) \cdot w_j \tag{20}$$

for all $u \in F(\mathbb{C}_q^{2|1})$.

Proof. If we use (19) and (7), we have the matrices $\mu(f)$ for $f \in F(\mathbb{C}_q^{2|1})$ as

$$\mu(x) = \begin{pmatrix} q^2x & 0 & 0 \\ 0 & q^2x & 0 \\ 0 & 0 & qx \end{pmatrix}, \quad \mu(y) = \begin{pmatrix} y & (q^2-1)y & 0 \\ 0 & y & 0 \\ 0 & 0 & q^{-1}y \end{pmatrix},$$

$$\mu(\theta) = \begin{pmatrix} q^{-2}\theta & (1-q^{-2})\theta & 1-q^2 \\ 0 & q^{-2}\theta & 0 \\ 0 & 0 & \theta \end{pmatrix}. \tag{21}$$

Now if we substitute these matrices in (20), we obtain the relations of Maurer-Cartan 1-forms with the generators of the Hopf superalgebra $F(\mathbb{C}_q^{2|1})$.

Corollary 3.20 The map μ is a $\mathbb{Z}_2$-graded algebra homomorphism such that

$$\mu_{ij}(u \cdot v) = \sum_{k=1}^{4} (-1)^{p(v)[p(x_k)-p(x_i)]}\, \mu_{ik}(u)\mu_{kj}(v), \qquad (i,j = 1,2,3)$$

where $x_i, x_k, u, v \in F(\mathbb{C}_q^{2|1})$ [16] .

We find the forms' commutation rules by using (7) and (20).

Theorem 3.21 The commutation relations between the forms are of the form

$$w_1 \wedge w_1 = 0, w_1 \wedge w_2 = -w_2 \wedge w_1, \quad w_3 \wedge w_2 = q^2 w_2 \wedge w_3,$$

$$w_2 \wedge w_2 = 0, w_1 \wedge w_3 = q^2\, w_3 \wedge w_1 - (q^{-2} - 1)\, w_3 \wedge w_2. \qquad (22)$$

Theorem 3.22 The Maurer-Cartan equations for $\Omega^{\wedge}$ have the form

$$dw_1 = 0, \quad dw_2 = 0, \quad dw_3 = q^{-2}(w_2 - q^{-2}w_1) \wedge w_3. \qquad (23)$$

3.6 Quantum Lie superalgebra

In order to construct the Lie superalgebra of vector fields, Maurer-Cartan commutation rules are used.

In general, it is possible to connect a specific superalgebra to a Lie superalgebra.

A quantum Lie superalgebra of vector fields is created by first writing the exterior differential operator, denoted by d , in the following manner:

$$df = (\omega_1 X_1 + \omega_2 X_2 + \omega_3 \nabla) f, \quad f \in F(\mathbb{C}_q^{2|1}).$$

Here X_1, X_2 and ∇ are the quantum Lie superalgebra generators.

Theorem 3.23 The relations of the quantum vector fields are of the form

$$[X_1, X_2] = 0, \quad [X_1, \nabla]_{q^2} = q^{-2}\Theta, \tag{24}$$

$$[X_2, \nabla]_{q^{-2}} = -q^{-6}\nabla + (1 - q^{-2})\nabla X_1, \quad \nabla^2 = 0 \tag{25}$$

where $[u, v]_t = uv - (-1)^{p(u)p(v)}tvu$.

Proof. Suppose that f is an arbitrary function f of the generators of the superalgebra $F(\mathbb{C}_q^{2|1})$. In this case, the use of relations (22) and (23) with $d^2 = 0$, will give the desired commutation relations of the vector fields.

Let us denote by L the algebra formed by the generators X_1, X_2 and ∇ and the relations (24). In this case, we have the following theorem.

Theorem 3.24 The algebra L is a Lie superalgebra.

Proof. For this, it is sufficient to provide the Jacobi identity. If we arrange the second and third relations in the theorem 3.23 as follows:

$$[X_1, \nabla] = q^{-2}\nabla + \left(q^2 - 1\right)\nabla X_1,$$
$$[X_2, \nabla] = -q^{-6}\nabla + \left(1 - q^{-2}\right)\nabla\left(X_1 - X_2\right).$$

So, we get

$$\begin{aligned}\left[X_1,\left[X_2,\nabla\right]\right]&=\left[X_1,\ -q^{-6}\nabla+\left(1-q^{-2}\right)\left(\nabla X_1-\nabla X_2\right)\right]\\&=-q^{-6}\left[X_1,\nabla\right]+\left(1-q^{-2}\right)\left(\left[X_1,\nabla\right]X_1-\left[X_1,\nabla\right]X_2\right)\\&=-q^{-8}\nabla+q^{-2}\left(q^{-2}-1\right)^2\nabla X_1+q^{-2}\left(q^{-2}-1\right)\nabla X_2\\&\quad+q^{-2}\left(q^2-1\right)^2\left(\nabla X_2-\nabla X_1\right)X_1,\end{aligned}$$

$$\begin{aligned}\left[X_2,\left[\nabla,X_1\right]\right]&=q^{-8}\nabla-q^{-2}\left(q^{-2}-1\right)^2\nabla X_1-q^{-2}\left(q^{-2}-1\right)\nabla X_2\\&\quad+q^{-2}\left(q^2-1\right)^2\left(\nabla X_1-\nabla X_2\right)X_1,\end{aligned}$$

and following this

$$\left[\nabla,\left[X_1,X_2\right]\right]=0.$$

Therefore, we obtain

$$\left[X_1,\left[X_2,\nabla\right]\right]+\left[X_2,\left[\nabla,X_1\right]\right]+\left[\nabla,\left[X_1,X_2\right]\right]=0,$$

which completes the proof.

4. RESULTS

A noncommutative associative superalgebra's coordinates are part of a quantum superspace, which is a space in which a quantum supergroup transforms the space with linear operations. Standard and nonstandard (or Jordanian) generic Lie (super)group deformations are two separate deformations. One of them is the well- known (q-deformed) quantum group and the other is so-called h-deformed group. Quantum supergroups and quantum superalgebras are significantly more complex than Lie supergroups and Lie superalgebras. The differential calculus on the $\mathbb{Z}_2$-graded quantum (2+1)-space involves functions, differentials, differential

forms and derivatives on the superspace. The extended $\mathbb{Z}_2$-graded algebra of polynomials denoted by $F(\mathbb{C}_q^{2|1})$, is a $\mathbb{Z}_2$-graded Hopf algebra. In conclusion, we construct a left-covariant differential calculus on the $\mathbb{Z}_2$-graded Hopf algebra $F(\mathbb{C}_q^{2|1})$ by applying related methods to the problems in quantum theory.

REFERENCES

[1] Connes A. Non-commutative differential geometry. Publications Mathematiques de l'Institut des Hautes Etudes Scientifiques. 1985;62:41-144.

[2] Woronowicz SL. Twisted $SU_q(2)$ group an example of a non-commutative differential calculus. Publications of the Research Institute for Mathematical Sciences. 1987;23:117-184.

[3] Woronowicz SL. Differential calculus on compact matric pseudogroups (quantum groups). Communications in Mathematical Physics. 1989;122:125-170.

[4] Brzezinski T, Majid S. A class of bicovariant differential calculi on Hopf algebras. Letters in Mathematical Physics. 1992;26:67-78.

[5] Celik S. Differential geometry of the q-superplane. Journal of Physics A: Mathematical and General. 1998;31:9695-9701.

[6] Celik SA, Celik S. Differential geometry of the q-plane, International Journal of Modern Physics A. 2000;15:3237-3243.

[7] Celik S. Differential geometry of $\mathbb{Z}_3$-graded quantum superplane. Journal of Physics A: Mathematical and General. 2002;35:4257-4268.

[8] Celik S. Cartan calculi on the quantum superplane. Journal of Mathematical Physics. 2006;47(8):083501.

[9] Celik S. Bicovariant differential calculus on the quantum superspace $\mathbb{R}_q(1|2)$. Journal of Algebras and its Applications. 2016;15(9):1650172.

[10] Celik SA. Differential calculi on super-Hopf algebra $F(\mathbb{R}_q(1|2))$. Advanced in Applied Clifford Algebras. 2018;28(85):1-16.

[11] Wess J, Zumino B. Covariant differential calculus on the quantum hyperplane. Nucleer Physics B. 1990;18:302-312.

[12] Manin YI. Quantum Groups and Noncommutative Geometry. Springer Nature Switzerland AG:Second Edition; 2018.

[13] Manin YI. Multiparametric quantum deformation of the general linear supergroup. Communications in Mathematical Physics. 1989;123:163-175.

[14] Soni S. Differential calculus on the quantum superplane. Journal of Physics A: Mathematical and General. 1990;24:619-624.

[15] Celik S. Covariant differential calculi on quantum symplectic superspace $SP_q^{1|2}$. Journal of Mathematical Physics. 2017;58:023508.

[16] Celik S. Right-covariant differential calculus on $F(\mathbb{C}_q^{2|1})$. 2021; https://arxiv.org/pdf/2103.16307.

[17] Fakhri H, Laheghi S. $GL_{r,s}(n)$-covariant differential calculi on the quantum n-space. Advanced in Applied Clifford Algebras. 2019; 29(52):1-10.

[18] Kobayashi T, Uematsu T. Differential calculus on the quantum superspace and deformation of phase space. Zeitschrift für Physik C: Particles and Fields. 1992;56: 193-199.

[19] Bulut F, Celik S. A Differential Calculus on Superspace $\mathbb{R}_h(1|2)$ and Related Topics. Advances in Applied Clifford Algebras. 2017;27:1019-1030.

CHAPTER 12

A RESEARCH ON GEOMETRIC APPROACH FOR EM WAVES IN MINKOWSKI SPACE

Melek ERDOĞDU[1]

1 Assoc. Prof. Dr. Melek Erdoğdu, Department of Mathematics and Computer Sciences, Faculty of Science, Necmettin Erbakan University. ORCID ID: 0000-0001-9610-6229

1. Introduction

Electric and magnetic fields vibrate together to produce EM waves (electromagnetic waves). Electric and magnetic fields oscillate, which causes electromagnetic waves to form. This is exactly where physics and geometry work together. More precisely, $(\vec{t}, \vec{\mathcal{E}}, \vec{\mathcal{B}})$ are investigated by means of Serret Frenet frame of the curve $\mathfrak{I}$. There is a new study which use these relationships by rotation transformation (Yavuz, 2022). In this context, this paper investigates these relationships in Minkowski space.

Studying EM wave equations just in Euclidean space is an incomplete strategy given the significance of Minkowski space in other areas of physics. Details on EM wave theory can be found in many studies (Van Bladel, 2007; Wangsness, 1979; Feibelman, 1982; Chen and Chan 2007; Ishimaru, 2017; Polo and Lakhtakia, 2011). This allows for the investigation of the differential geometric and physical properties of EM waves in Minkowski space. EM wave vector fields are Lorentzian orthogonal to one another along a nonnull electromagnetic wave. An adjusted nonnull frame $\{\vec{t}, \vec{\mathcal{E}}, \vec{\mathcal{B}}\}$ is established on EM wave as a consequence. $\{\vec{t}, \vec{n}, \vec{b}\}$ of nonnull curve $\mathfrak{I}$ provides EM wave vectors (Körpınar et al., 2020). Anholonomic coordinates with eight parameters and three partial differential equations are described by a vector field (Marris and Passman, 1969; Rogers and Schief, 2003). According to geometric approach, circular (hyperbolic) rotation occurs in normal plane of $\mathfrak{I}$ with geometric phase (angle) θ. There are many studies examining circular or hyperbolic rotations (Özdemir and Erdoğdu, 2014; Erdoğdu and Özdemir 2020; Erdoğdu and Özdemir, 2015). There is a linear transformation between $\{\vec{t}, \vec{n}, \vec{b}\}$ and $\{\vec{t}, \vec{\mathcal{E}}, \vec{\mathcal{B}}\}$. Rytov's law also explains the parallel propagation of $\vec{\mathcal{E}}$ and $\vec{\mathcal{B}}$ across the tangent direction of an electromagnetic wave. See (Erdoğdu, 2015) for more details on parallel frames. Moreover, it is recommended to examine studies (Hacısalihoğlu, 2000; Do Carmo, 1976; Shifrin, 2015) for the basic rules of differential geometry used in the study.

This study's main objective is to investigate electromagnetic waves in Minkowski space. Depending on the characteristics of the tangent direction, and it is also the direction of the electromagnetic wave, three different cases are examined independently. Generalized Serret Frenet formulas are used for further calculations. The relations between the frames Serret Frenet and EM wave vectors are obtained. It is proved that the hyperbolic or circular rotation takes places of normal plane of $\mathfrak{I}$ with the geometric phase θ. An application is investigated by physical and geometric approach.

2. Rytov's Law for EM Wave Vectors

In the first two subsection, the direction of electromagnetic wave is spacelike and electric and magnetic vector fields are timelike, respectively. In the last subsection, the direction of the electromagnetic wave is timelike and both the electric and magnetic field are spacelike. For all these cases, generalized Serret Frenet formulas are expressed since they are necessary for further calculations.

2.1. Rytov's Law for Timelike Electric Wave Vector

In this subsection, let $\Im = \Im(s,n,b)$ be a curve where Serret Frenet frame of curve $\Im$ has signature $(1,-1,1)$.

Theorem 1. Let $\Im = \Im(\mathrm{s},\mathrm{n},\mathrm{b})$ be a unit speed spacelike curve with timelike normal. Then, derivative formulas of $\{\vec{t},\vec{n},\vec{b}\}$ are presented as

$$\text{i) } \frac{\partial}{\partial s}\vec{t} = \kappa\vec{n}, \qquad \frac{\partial}{\partial s}\vec{n} = \kappa\vec{t} + \tau\vec{b}, \qquad \frac{\partial}{\partial s}\vec{b} = \tau\vec{n} \tag{1}$$

$$\text{ii) } \frac{\partial}{\partial n}\begin{bmatrix}\vec{t}\\ \vec{n}\\ \vec{b}\end{bmatrix} = \begin{bmatrix}0 & -\ell_{ns} & \varrho_b - \tau\\ -\ell_{ns} & 0 & -div\vec{b}\\ \tau - \varrho_b & -div\vec{b} & 0\end{bmatrix}\begin{bmatrix}\vec{t}\\ \vec{n}\\ \vec{b}\end{bmatrix} \tag{2}$$

$$\text{iii) } \frac{\partial}{\partial b}\begin{bmatrix}\vec{t}\\ \vec{n}\\ \vec{b}\end{bmatrix} = \begin{bmatrix}0 & \tau - \varrho_n & \ell_{bs}\\ \tau - \varrho_n & 0 & div\vec{n} - \kappa\\ -\ell_{bs} & div\vec{n} - \kappa & 0\end{bmatrix}\begin{bmatrix}\vec{t}\\ \vec{n}\\ \vec{b}\end{bmatrix} \tag{3}$$

where

$$\ell_{ns} = \left\langle \vec{n}, \frac{\partial\vec{t}}{\partial n}\right\rangle_L, \qquad \ell_{bs} = \left\langle \vec{b}, \frac{\partial\vec{t}}{\partial b}\right\rangle_L$$

and

$$\varrho_n = \langle curl\vec{n},\vec{n}\rangle_L, \quad \varrho_b = \left\langle curl\vec{b},\vec{b}\right\rangle_L$$

(Körpınar et al., 2020).

Proposition 2. Let $\Im = \Im(\mathrm{s},\mathrm{n},\mathrm{b})$ be a unit speed spacelike curve with timelike normal. The following relations are satisfied:

$$\begin{bmatrix}\vec{t}\\ \vec{\mathcal{E}}\\ \vec{\mathcal{B}}\end{bmatrix}=\begin{bmatrix}1 & 0 & 0\\ 0 & \cosh\theta & -\sinh\theta\\ 0 & -\sinh\theta & \cosh\theta\end{bmatrix}\begin{bmatrix}\vec{t}\\ \vec{n}\\ \vec{b}\end{bmatrix} \tag{4}$$

and

$$\begin{bmatrix}\vec{t}\\ \vec{n}\\ \vec{b}\end{bmatrix}=\begin{bmatrix}1 & 0 & 0\\ 0 & \cosh\theta & \sinh\theta\\ 0 & \sinh\theta & \cosh\theta\end{bmatrix}\begin{bmatrix}\vec{t}\\ \vec{\mathcal{E}}\\ \vec{\mathcal{B}}\end{bmatrix} \tag{5}$$

where θ is the geometric phase.

Proof. Since tangent vector field of curve $\mathfrak{I}$ is spacelike vector field, rotation axis should be a spacelike vector field. This implies that a hyperbolic rotation takes place of the normal plane with geometric phase θ. There is a linear transformation between Serret Frenet frame and EM wave vector fields. This linear transformation corresponds to hyperbolic rotation on normal plane with geometric phase (rotation angle) θ.

Theorem 3. Let $\mathfrak{I}=\mathfrak{I}(\mathrm{s},\mathrm{n},\mathrm{b})$ be a unit speed spacelike curve with timelike normal. Then, the following derivative formulas are satisfied:

$$\text{i)}\ \frac{\partial}{\partial s}\begin{bmatrix}\vec{t}\\ \vec{\mathcal{E}}\\ \vec{\mathcal{B}}\end{bmatrix}=\begin{bmatrix}0 & \kappa\cosh\theta & \kappa\sinh\theta\\ \kappa\cosh\theta & 0 & -\frac{\partial\theta}{\partial s}+\tau\\ -\kappa\sinh\theta & -\frac{\partial\theta}{\partial s}+\tau & 0\end{bmatrix}\begin{bmatrix}\vec{t}\\ \vec{\mathcal{E}}\\ \vec{\mathcal{B}}\end{bmatrix} \tag{6}$$

$$\text{ii)}\ \frac{\partial}{\partial n}\begin{bmatrix}\vec{t}\\ \vec{\mathcal{E}}\\ \vec{\mathcal{B}}\end{bmatrix}=$$

$$\begin{bmatrix}0 & \sinh\theta(\varrho_b-\tau)-\ell_{ns}\cosh\theta & \cosh\theta(\varrho_b-\tau)-\ell_{ns}\sinh\theta\\ \sinh\theta(\varrho_b-\tau)-\ell_{ns}\cosh\theta & 0 & -\frac{\partial\theta}{\partial n}-div\vec{b}\\ \ell_{ns}\sinh\theta-\cosh\theta(\varrho_b-\tau) & -\frac{\partial\theta}{\partial n}-div\vec{b} & 0\end{bmatrix}\begin{bmatrix}\vec{t}\\ \vec{\mathcal{E}}\\ \vec{\mathcal{B}}\end{bmatrix} \tag{7}$$

$$\text{iii)}\ \frac{\partial}{\partial b}\begin{bmatrix}\vec{t}\\ \vec{\mathcal{E}}\\ \vec{\mathcal{B}}\end{bmatrix}=$$

$$\begin{bmatrix}0 & (\tau-\varrho_n)\cosh\theta+\ell_{bs}\sinh\theta & (\tau-\varrho_n)\sinh\theta+\ell_{bs}\cosh\theta\\ (\tau-\varrho_n)\cosh\theta+\ell_{bs}\sinh\theta & 0 & -\frac{\partial\theta}{\partial b}+div\vec{n}-\kappa\\ (\varrho_n-\tau)\sinh\theta-\ell_{bs}\cosh\theta & -\frac{\partial\theta}{\partial b}+div\vec{n}-\kappa & 0\end{bmatrix}\begin{bmatrix}\vec{t}\\ \vec{\mathcal{E}}\\ \vec{\mathcal{B}}\end{bmatrix}. \tag{8}$$

Proof. Directional derivatives of $\{\vec{t},\vec{\mathcal{E}},\vec{\mathcal{B}}\}$ along s parameter curve on $\mathfrak{I}$ are obtained as follows:

$$\frac{\partial}{\partial s}\vec{t} = \kappa\vec{n} = \kappa(\cosh\theta\vec{\mathfrak{E}} + \sinh\theta\vec{\mathfrak{B}}),$$

$$\frac{\partial}{\partial s}\vec{\mathfrak{E}} = \frac{\partial}{\partial s}(\cosh\theta\vec{n} - \sinh\theta\vec{b})$$

$$= \sinh\theta(\tfrac{\partial\theta}{\partial s})\vec{n} + \cosh\theta(\kappa\vec{t} + \tau\vec{b}) - \cosh\theta(\tfrac{\partial\theta}{\partial s})\vec{b} - \sinh\theta(\tau\vec{n})$$

$$= \kappa\cosh\theta\vec{t} + (-\frac{\partial\theta}{\partial s} + \tau)(-\sinh\theta\vec{n} + \cosh\theta\vec{b})$$

$$= \kappa\cosh\theta\vec{t} + (-\frac{\partial\theta}{\partial s} + \tau)\vec{\mathfrak{B}}$$

and

$$\frac{\partial}{\partial s}\vec{\mathfrak{B}} = \frac{\partial}{\partial s}(-\sinh\theta\vec{n} + \cosh\theta\vec{b})$$

$$= -\cosh\theta(\tfrac{\partial\theta}{\partial s})\vec{n} - \sinh\theta(\kappa\vec{t} + \tau\vec{b}) + \sinh\theta(\tfrac{\partial\theta}{\partial s})\vec{b} + \cosh\theta(\tau\vec{n})$$

$$= -\kappa\sinh\theta\vec{t} + (-\frac{\partial\theta}{\partial s} + \tau)(\cosh\theta\vec{n} - \sinh\theta\vec{b})$$

$$= -\kappa\sinh\theta\vec{t} + (-\frac{\partial\theta}{\partial s} + \tau)\vec{\mathfrak{E}}$$

by using the Equations 1 and 5. Directional derivatives of $\{\vec{t}, \vec{\mathfrak{E}}, \vec{\mathfrak{B}}\}$ along n parameter curve on $\Im$ are obtained as follows:

$$\frac{\partial}{\partial n}\vec{t} = -\ell_{ns}(\cosh\theta\vec{\mathfrak{E}} + \sinh\theta\vec{\mathfrak{B}}) + (\varrho_b - \tau)(\sinh\theta\vec{\mathfrak{E}} + \cosh\theta\vec{\mathfrak{B}})$$

$$= (-\ell_{ns}\cosh\theta + (\varrho_b - \tau)\sinh\theta)\vec{\mathfrak{E}}$$

$$+(-\ell_{ns}\sinh\theta + (\varrho_b - \tau)\cosh\theta)\vec{\mathfrak{B}},$$

$$\frac{\partial}{\partial n}\vec{\mathfrak{E}} = \frac{\partial}{\partial n}(\cosh\theta\vec{n} - \sinh\theta\vec{b})$$

$$= \sinh\theta\left(\frac{\partial\theta}{\partial n}\right)\vec{n} + \cosh\theta\left(-\ell_{ns}\vec{t} - div\vec{b}\vec{n}\right)$$

$$-\cosh\theta(\frac{\partial\theta}{\partial n})\vec{b} - \sinh\theta((\tau - \varrho_b)\vec{t} - div\vec{b}\vec{n})$$

$$= (-\ell_{ns}\cosh\theta - (\tau - \varrho_b)\sinh\theta)\vec{t}$$
$$+(-\frac{\partial\theta}{\partial n} - div\vec{b})(-\sinh\theta\vec{n} + \cosh\theta\vec{b})$$

$$= (-\ell_{ns}\cosh\theta - (\tau - \varrho_b)\sin\theta)\vec{t} + (-\frac{\partial\theta}{\partial n} - div\vec{b})\vec{\text{ß}}$$

and

$$\frac{\partial}{\partial n}\vec{\text{ß}} = \frac{\partial}{\partial n}(-\sinh\theta\vec{n} + \cosh\theta\vec{b})$$

$$= -\cosh\theta\left(\frac{\partial\theta}{\partial n}\right)\vec{n} - \sinh\theta\left(-\ell_{ns}\vec{t} - div\vec{b}\vec{b}\right) + \sinh\theta\left(\frac{\partial\theta}{\partial n}\right)\vec{b}$$
$$+\cosh\theta((\tau - \varrho_b)\vec{t} - div\vec{b}\vec{n})$$

$$= (\ell_{ns}\sinh\theta + (\tau - \varrho_b)\cosh\theta)\vec{t}$$
$$+(-\frac{\partial\theta}{\partial n} - div\vec{b})(\cosh\theta\vec{n} - \sinh\theta\vec{b})$$

$$= (\ell_{ns}\sinh\theta + (\tau - \varrho_b)\cosh\theta)\vec{t} + (-\frac{\partial\theta}{\partial n} - div\vec{b})\vec{\text{Ɛ}}$$

by using Equations 2 and 5. Finally, we have

$$\frac{\partial}{\partial b}\vec{t} = (\tau - \varrho_n)(\cosh\theta\vec{\text{Ɛ}} + \sinh\theta\vec{\text{ß}}) + \ell_{bs}(\sinh\theta\vec{\text{Ɛ}} + \cosh\theta\vec{\text{ß}})$$

$$= \left((\tau - \varrho_n)\cosh\theta - \ell_{bs}\sinh\theta\right)\vec{\text{Ɛ}}$$
$$+((\tau - \varrho_n)\sinh\theta + \ell_{bs}\cosh\theta)\vec{\text{ß}},$$

$$\frac{\partial}{\partial b}\vec{\text{Ɛ}} = \frac{\partial}{\partial b}\left(\cosh\theta\vec{n}\,\sinh\theta\vec{b}\right)$$
$$= \sinh\theta\left(\frac{\partial\theta}{\partial b}\right)\vec{n} + \cosh\theta\left((\tau - \varrho_n)\vec{t} + (div\vec{n} - \kappa)\vec{b}\right)$$
$$-\cosh\theta\left(\frac{\partial\theta}{\partial b}\right)\vec{b} - \sinh\theta(-\ell_{bs}\vec{t} + (div\vec{n} - \kappa)\vec{n})$$

$$= \left((\tau - \varrho_n)\cosh\theta + \ell_{bs}\sinh\theta\right)\vec{t}$$
$$+(-\frac{\partial\theta}{\partial b} + div\vec{n} - \kappa)(-\sinh\theta\vec{n} + \cosh\theta\vec{b})$$

$$= ((\tau - \varrho_n)\cosh\theta + \ell_{bs}\sinh\theta)\vec{t} + (-\frac{\partial\theta}{\partial b} + div\vec{n} - \kappa)\vec{\text{ß}}$$

and

$$\frac{\partial}{\partial b}\vec{\mathfrak{B}} = \frac{\partial}{\partial b}(-\sinh\theta\vec{n} + \cosh\theta\vec{b})$$

$$= -\cosh\theta(\frac{\partial\theta}{\partial b})\vec{n} - \sinh\theta((\tau - \varrho_n)\vec{t} + (div\vec{n} - \kappa)\vec{b})$$
$$+\sinh\theta(\frac{\partial\theta}{\partial b})\vec{b} + \cosh\theta(-\ell_{bs}\vec{t} + (div\vec{n} - \kappa)\vec{n})$$

$$= (-(\tau - \varrho_n)\sinh\theta - \ell_{bs}\cosh\theta)\vec{t} + (-\frac{\partial\theta}{\partial b} + div\vec{n} - \kappa)\vec{\mathfrak{E}}$$

by Equation 3 and Equation 5.

Theorem 4. Let $\mathfrak{I} = \mathfrak{I}(\mathrm{s},\mathrm{n},\mathrm{b})$ be a unit speed spacelike curve with timelike normal. $\{\vec{t},\vec{\mathfrak{E}},\vec{\mathfrak{B}}\}$ is parallel transportation of $\{\vec{t},\vec{n},\vec{b}\}$ if and only if followings are satisfied

$$\frac{\partial\theta}{\partial s} = \tau,$$

$$\frac{\partial\theta}{\partial n} = -div\vec{b}, \tag{9}$$

$$\frac{\partial\theta}{\partial b} = div\vec{n} - \kappa.$$

Proof. Based on the parallel transportation criterion, partial derivatives of $\{\vec{t},\vec{\mathfrak{E}},\vec{\mathfrak{B}}\}$ only need to have a tangent direction. By Equations 6, 7 and 8, we obtain the proof.

2.2. Rytov's Law for Timelike Magnetic Wave Vector

In this subsection, let $\mathfrak{I} = \mathfrak{I}(s,n,b)$ be a curve where Serret Frenet frame of curve $\mathfrak{I}$ has signature $(1,1,-1)$.

Theorem 5. Let $\mathfrak{I} = \mathfrak{I}(s,n,b)$ be a unit speed spacelike curve with timelike binormal. Then, following derivative formulas are satisfied:

i) $\frac{\partial}{\partial s}\vec{t} = \kappa\vec{n}, \quad \frac{\partial}{\partial s}\vec{n} = -\kappa\vec{t} + \tau\vec{b}, \quad \frac{\partial}{\partial s}\vec{b} = \tau\vec{n}$ (10)

ii) $$\frac{\partial}{\partial n}\begin{bmatrix}\vec{t}\\ \vec{n}\\ \vec{b}\end{bmatrix} = \begin{bmatrix}0 & \ell_{ns} & \tau+\varrho_b\\ -\ell_{ns} & 0 & div\vec{b}\\ \tau+\varrho_b & div\vec{b} & 0\end{bmatrix}\begin{bmatrix}\vec{t}\\ \vec{n}\\ \vec{b}\end{bmatrix} \tag{11}$$

iii) $$\frac{\partial}{\partial b}\begin{bmatrix}\vec{t}\\ \vec{n}\\ \vec{b}\end{bmatrix} = \begin{bmatrix}0 & \varrho_n-\tau & -\ell_{bs}\\ \tau-\varrho_n & 0 & -(div\vec{n}+\kappa)\\ -\ell_{bs} & -(div\vec{n}+\kappa) & 0\end{bmatrix}\begin{bmatrix}\vec{t}\\ \vec{n}\\ \vec{b}\end{bmatrix} \tag{12}$$

(Körpınar et al., 2020).

Proposition 6. Assume that $\mathfrak{I} = \mathfrak{I}(\mathrm{s}, \mathrm{n}, \mathrm{b})$ is a unit speed spacelike curve with timelike binormal. The following relations are satisfied:

$$\begin{bmatrix} \vec{t} \\ \vec{\mathcal{E}} \\ \vec{\mathcal{B}} \end{bmatrix} = \begin{bmatrix} 1 & 0 & 0 \\ 0 & \cosh\theta & -\sinh\theta \\ 0 & -\sinh\theta & \cosh\theta \end{bmatrix} \begin{bmatrix} \vec{t} \\ \vec{n} \\ \vec{b} \end{bmatrix} \tag{13}$$

and

$$\begin{bmatrix} \vec{t} \\ \vec{n} \\ \vec{b} \end{bmatrix} = \begin{bmatrix} 1 & 0 & 0 \\ 0 & \cosh\theta & \sinh\theta \\ 0 & \sinh\theta & \cosh\theta \end{bmatrix} \begin{bmatrix} \vec{t} \\ \vec{\mathcal{E}} \\ \vec{\mathcal{B}} \end{bmatrix} \tag{14}$$

where θ is the geometric phase.

Proof. Since tangent vector field of curve $\mathfrak{I}$ is spacelike vector field, rotation axis should be a spacelike vector field. This implies that a hyperbolic rotation takes place of normal plane with geometric phase θ.

Theorem 7. Let $\mathfrak{I} = \mathfrak{I}(\mathrm{s}, \mathrm{n}, \mathrm{b})$ be a spacelike curve with timelike binormal. Then, following derivative formulas are stated:

i) $$\frac{\partial}{\partial s} \begin{bmatrix} \vec{t} \\ \vec{\mathcal{E}} \\ \vec{\mathcal{B}} \end{bmatrix} = \begin{bmatrix} 0 & \kappa\cosh\theta & \kappa\sinh\theta \\ -\kappa\cosh\theta & 0 & -\frac{\partial\theta}{\partial s} + \tau \\ \kappa\sinh\theta & -\frac{\partial\theta}{\partial s} + \tau & 0 \end{bmatrix} \begin{bmatrix} \vec{t} \\ \vec{\mathcal{E}} \\ \vec{\mathcal{B}} \end{bmatrix} \tag{15}$$

ii) $$\frac{\partial}{\partial n} \begin{bmatrix} \vec{t} \\ \vec{\mathcal{E}} \\ \vec{\mathcal{B}} \end{bmatrix} =$$

$$\begin{bmatrix} 0 & \ell_{ns}\cosh\theta + \sinh\theta(\varrho_b + \tau) & \ell_{ns}\sinh\theta + \cosh\theta(\varrho_b + \tau) \\ -\ell_{ns}\cosh\theta - \sinh\theta(\varrho_b + \tau) & 0 & -\frac{\partial\theta}{\partial n} + div\vec{b} \\ \ell_{ns}\sinh\theta + \cosh\theta(\varrho_b + \tau) & -\frac{\partial\theta}{\partial n} + div\vec{b} & 0 \end{bmatrix} \begin{bmatrix} \vec{t} \\ \vec{\mathcal{E}} \\ \vec{\mathcal{B}} \end{bmatrix} \tag{16}$$

iii) $$\frac{\partial}{\partial b} \begin{bmatrix} \vec{t} \\ \vec{\mathcal{E}} \\ \vec{\mathcal{B}} \end{bmatrix} =$$

$$\begin{bmatrix} 0 & (\varrho_n - \tau)\cosh\theta - \ell_{bs}\sinh\theta & (\varrho_n - \tau)\sinh\theta - \ell_{bs}\cosh\theta \\ (\tau - \varrho_n)\cosh\theta + \ell_{bs}\sinh\theta & 0 & -\frac{\partial\theta}{\partial b} - div\vec{n} - \kappa \\ (\varrho_n - \tau)\sinh\theta - \ell_{bs}\cosh\theta & -\frac{\partial\theta}{\partial b} - div\vec{n} - \kappa & 0 \end{bmatrix} \begin{bmatrix} \vec{t} \\ \vec{\mathcal{E}} \\ \vec{\mathcal{B}} \end{bmatrix}. \tag{17}$$

Proof. The followings are the directional derivatives of $\{\vec{t}, \vec{\mathfrak{E}}, \vec{\mathfrak{B}}\}$ along s parameter curve on $\mathfrak{I}$:

$$\frac{\partial}{\partial s}\vec{t} = \kappa\vec{n} = \kappa(\cosh\theta\vec{\mathfrak{E}} + \sinh\theta\vec{\mathfrak{B}}),$$

$$\frac{\partial}{\partial s}\vec{\mathfrak{E}} = \frac{\partial}{\partial s}(\cosh\theta\vec{n} - \sinh\theta\vec{b})$$

$$= \sinh\theta(\frac{\partial\theta}{\partial s})\vec{n} + \cosh\theta(-\kappa\vec{t} + \tau\vec{b}) - \cosh\theta(\frac{\partial\theta}{\partial s})\vec{b} - \sinh\theta(\tau\vec{n})$$

$$= -\kappa\cosh\theta\vec{t} + (-\frac{\partial\theta}{\partial s} + \tau)(-\sinh\theta\vec{n} + \cosh\theta\vec{b})$$

$$= -\kappa\cosh\theta\vec{t} + (-\frac{\partial\theta}{\partial s} + \tau)\vec{\mathfrak{B}}$$

and

$$\frac{\partial}{\partial s}\vec{\mathfrak{B}} = \frac{\partial}{\partial s}(-\sinh\theta\vec{n} + \cosh\theta\vec{b})$$

$$= -\cosh\theta\left(\frac{\partial\theta}{\partial s}\right)\vec{n} - \sinh\theta\left(-\kappa\vec{t} + \tau\vec{b}\right) + \sinh\theta(\frac{\partial\theta}{\partial s})\vec{b} + \cosh\theta(\tau\vec{n})$$

$$= \kappa\sinh\theta\vec{t} + (-\frac{\partial\theta}{\partial s} + \tau)(\cosh\theta\vec{n} - \sinh\theta\vec{b})$$

$$= \kappa\sinh\theta\vec{t} + (-\frac{\partial\theta}{\partial s} + \tau)\vec{\mathfrak{E}}$$

by using the Equations 10 and 14. Then, we also have

$$\frac{\partial}{\partial n}\vec{t} = \ell_{ns}(\cosh\theta\vec{\mathfrak{E}} + \sinh\theta\vec{\mathfrak{B}}) + (\varrho_b + \tau)(\sinh\theta\vec{\mathfrak{E}} + \cosh\theta\vec{\mathfrak{B}})$$

$$= (\ell_{ns}\cosh\theta + (\varrho_b + \tau)\sinh\theta)\vec{\mathfrak{E}} + (\ell_{ns}\sinh\theta + (\varrho_b + \tau)\cosh\theta)\vec{\mathfrak{B}},$$

$$\frac{\partial}{\partial n}\vec{\mathfrak{E}} = \frac{\partial}{\partial n}(\cosh\theta\vec{n} - \sinh\theta\vec{b})$$

$$= (-\ell_{ns}\cosh\theta - (\tau + \varrho_b)\sinh\theta)\vec{t} + (-\frac{\partial\theta}{\partial n} + div\vec{b})(-\sinh\theta\vec{n} + \cosh\theta\vec{b})$$

$$= (-\ell_{ns}\cosh\theta - (\tau - \varrho_b)\sin\theta)\vec{t} + (-\frac{\partial\theta}{\partial n} + div\vec{b})\vec{\mathfrak{B}}$$

and

$$\frac{\partial}{\partial n}\vec{\mathfrak{B}} = \frac{\partial}{\partial n}(-\sinh\theta\vec{n} + \cosh\theta\vec{b})$$

$$= (\ell_{ns}\sinh\theta + (\tau + \varrho_b)\cosh\theta)\vec{t} + (-\frac{\partial\theta}{\partial n} + div\vec{b})(\cosh\theta\vec{n} - \sinh\theta\vec{b})$$

$$= (\ell_{ns}\sin\theta + (\tau + \varrho_b)\cos\theta)\vec{t} + (-\frac{\partial\theta}{\partial n} + div\vec{b})\vec{\mathcal{E}}$$

by using Equations 11 and 14. Finally, we get

$$\frac{\partial}{\partial b}\vec{t} = (\varrho_n - \tau)(\cosh\theta\vec{\mathfrak{E}} + \sinh\theta\vec{\mathfrak{B}}) - \ell_{bs}(\sinh\theta\vec{\mathfrak{E}} + \cosh\theta\vec{\mathfrak{B}})$$

$$= \big((\varrho_n - \tau)\cosh\theta - \ell_{bs}\sinh\theta\big)\vec{\mathfrak{E}} + ((\varrho_n - \tau)\sinh\theta - \ell_{bs}\cosh\theta)\vec{\mathfrak{B}},$$

$$\frac{\partial}{\partial b}\vec{\mathfrak{E}} = \frac{\partial}{\partial b}(\cosh\theta\vec{n} - \sinh\theta\vec{b})$$

$$= \big((\tau - \varrho_n)\cosh\theta + \ell_{bs}\sinh\theta\big)\vec{t} + (-\frac{\partial\theta}{\partial b} - div\vec{n} - \kappa)(-\sinh\theta\vec{n} + \cosh\theta\vec{b})$$

$$= ((\tau - \varrho_n)\cosh\theta + \ell_{bs}\sinh\theta)\vec{t} + (-\frac{\partial\theta}{\partial b} - div\vec{n} - \kappa)\vec{\mathfrak{B}}$$

and

$$\frac{\partial}{\partial b}\vec{\mathfrak{B}} = \frac{\partial}{\partial b}(-\sinh\theta\vec{n} + \cosh\theta\vec{b})$$

$$= (-(\tau - \varrho_n)\sinh\theta - \ell_{bs}\cosh\theta)\vec{t} + (-\frac{\partial\theta}{\partial b} - div\vec{n} - \kappa)\vec{\mathfrak{E}}$$

by using Equations 12 and 14.

Theorem 8. Assume that $\mathfrak{I} = \mathfrak{I}(s, n, b)$ is a unit speed spacelike curve with timelike binormal. EM wave vector fields are parallel transportation of Serret Frenet frame if and only if followings are satisfied

$$\frac{\partial\theta}{\partial s} = \tau,$$

$$\frac{\partial\theta}{\partial n} = div\vec{b}, \tag{18}$$

$$\frac{\partial\theta}{\partial b} = -div\vec{n} - \kappa.$$

Proof. Based on the parallel transportation criterion, partial derivatives of $\{\vec{t}, \vec{\mathcal{E}}, \vec{\mathcal{B}}\}$ only need to have a tangent direction if and only if

$$-\frac{\partial\theta}{\partial s} + \tau = 0,$$

$$-\frac{\partial\theta}{\partial n} + div\vec{b} = 0,$$

$$-\frac{\partial\theta}{\partial b} - div\vec{n} - \kappa = 0$$

by Equations 15, 16 and 17.

2.3. Rytov's Law for Spacelike EM Wave Vectors

In this subsection, let $\mathfrak{I} = \mathfrak{I}(s, n, b)$ be a given unit speed timelike curve. In this case, Serret- Frenet frame of curve $\mathfrak{I}$ has signature $(-1,1,1)$.

Theorem 9. Let $\mathfrak{I} = \mathfrak{I}(\mathrm{s}, \mathrm{n}, \mathrm{b})$ be a unit speed timelike curve. Then, the derivative formulas are satisfied:

$$\text{i)}\ \frac{\partial}{\partial s}\vec{t} = \kappa\vec{n}, \qquad \frac{\partial}{\partial s}\vec{n} = \kappa\vec{t} + \tau\vec{b}, \qquad \frac{\partial}{\partial s}\vec{b} = -\tau\vec{n} \tag{19}$$

$$\text{ii)}\ \frac{\partial}{\partial n}\begin{bmatrix}\vec{t}\\ \vec{n}\\ \vec{b}\end{bmatrix} = \begin{bmatrix}0 & \ell_{ns} & -\tau-\varrho_b\\ \ell_{ns} & 0 & -div\vec{b}\\ -\tau-\varrho_b & div\vec{b} & 0\end{bmatrix}\begin{bmatrix}\vec{t}\\ \vec{n}\\ \vec{b}\end{bmatrix} \tag{20}$$

$$\text{iii)}\ \frac{\partial}{\partial b}\begin{bmatrix}\vec{t}\\ \vec{n}\\ \vec{b}\end{bmatrix} = \begin{bmatrix}0 & \tau-\varrho_n & \ell_{bs}\\ \tau-\varrho_n & 0 & div\vec{n}+\kappa\\ \ell_{bs} & -(div\vec{n}+\kappa) & 0\end{bmatrix}\begin{bmatrix}\vec{t}\\ \vec{n}\\ \vec{b}\end{bmatrix} \tag{21}$$

(Körpınar et al, 2020).

Proposition 10 Let $\mathfrak{I} = \mathfrak{I}(\mathrm{s}, \mathrm{n}, \mathrm{b})$ be a unit speed timelike curve. The following relations are stated:

$$\begin{bmatrix}\vec{t}\\ \vec{\mathcal{E}}\\ \vec{\mathcal{B}}\end{bmatrix} = \begin{bmatrix}1 & 0 & 0\\ 0 & \cos\theta & -\sin\theta\\ 0 & \sin\theta & \cos\theta\end{bmatrix}\begin{bmatrix}\vec{t}\\ \vec{n}\\ \vec{b}\end{bmatrix} \tag{22}$$

and

$$\begin{bmatrix}\vec{t}\\ \vec{n}\\ \vec{b}\end{bmatrix}=\begin{bmatrix}1 & 0 & 0\\ 0 & \cos\theta & \sin\theta\\ 0 & -\sin\theta & \cos\theta\end{bmatrix}\begin{bmatrix}\vec{t}\\ \vec{\mathcal{E}}\\ \vec{\mathcal{B}}\end{bmatrix} \tag{23}$$

where θ is the geometric phase.

Proof. Since tangent vector field of curve $\mathfrak{I}=\mathfrak{I}(s,n,b)$ is timelike vector field, rotation axis will be a timelike vector field. This implies that a circular rotation takes place of normal plane of curve $\mathfrak{I}$ with θ.

Theorem 11. Let $\mathfrak{I}=\mathfrak{I}(\mathrm{s},\mathrm{n},\mathrm{b})$ be a unit speed timelike curve. Then, the following derivative formulas are stated:

$$\text{i)}\ \frac{\partial}{\partial s}\begin{bmatrix}\vec{t}\\ \vec{\mathcal{E}}\\ \vec{\mathcal{B}}\end{bmatrix}=\begin{bmatrix}0 & \kappa\cos\theta & \kappa\sin\theta\\ \kappa\cos\theta & 0 & -\frac{\partial\theta}{\partial s}+\tau\\ \kappa\sin\theta & \frac{\partial\theta}{\partial s}-\tau & 0\end{bmatrix}\begin{bmatrix}\vec{t}\\ \vec{\mathcal{E}}\\ \vec{\mathcal{B}}\end{bmatrix} \tag{24}$$

$$\text{ii)}\ \frac{\partial}{\partial n}\begin{bmatrix}\vec{t}\\ \vec{\mathcal{E}}\\ \vec{\mathcal{B}}\end{bmatrix}=\begin{bmatrix}0 & \ell_{ns}\cos\theta+\sin\theta(\tau+\varrho_b) & \ell_{ns}\sin\theta-\cos\theta(\tau+\varrho_b)\\ \ell_{ns}\cos\theta+\sin\theta(\tau+\varrho_b) & 0 & -\frac{\partial\theta}{\partial n}-div\vec{b}\\ \ell_{ns}\sin\theta-\cos\theta(\tau+\varrho_b) & \frac{\partial\theta}{\partial n}+div\vec{b} & 0\end{bmatrix}\begin{bmatrix}\vec{t}\\ \vec{\mathcal{E}}\\ \vec{\mathcal{B}}\end{bmatrix} \tag{25}$$

$$\text{iii)}\ \frac{\partial}{\partial b}\begin{bmatrix}\vec{t}\\ \vec{\mathcal{E}}\\ \vec{\mathcal{B}}\end{bmatrix}=\begin{bmatrix}0 & (\tau-\varrho_n)\cos\theta-\ell_{bs}\sin\theta & (\tau-\varrho_n)\sin\theta+\ell_{bs}\cos\theta\\ (\tau-\varrho_n)\cos\theta-\ell_{bs}\sin\theta & 0 & -\frac{\partial\theta}{\partial b}+div\vec{n}+\kappa\\ (\tau-\varrho_n)\sin\theta+\ell_{bs}\cos\theta & \frac{\partial\theta}{\partial b}-div\vec{n}-\kappa & 0\end{bmatrix}\begin{bmatrix}\vec{t}\\ \vec{\mathcal{E}}\\ \vec{\mathcal{B}}\end{bmatrix}. \tag{26}$$

Proof. Directional derivatives of $\{\vec{t},\vec{\mathcal{E}},\vec{\mathcal{B}}\}$ along s parameter curve on $\mathfrak{I}$ are obtained as follows:

$$\frac{\partial}{\partial s}\vec{t}=\kappa(\cos\theta\vec{\mathcal{E}}+\sin\theta\vec{\mathcal{B}}),$$

$$\frac{\partial}{\partial s}\vec{\mathcal{E}}=-\sin\theta(\frac{\partial\theta}{\partial s})\vec{n}+\cos\theta(-\kappa\vec{t}+\tau\vec{b})-\cos\theta(\frac{\partial\theta}{\partial s})\vec{b}-\sin\theta(-\tau\vec{n})$$

$$=-\kappa\cos\theta\vec{t}+(-\frac{\partial\theta}{\partial s}+\tau)\vec{\mathcal{B}}$$

and

$$\frac{\partial}{\partial s}\vec{\mathfrak{B}} = \cos\theta(\frac{\partial\theta}{\partial s})\vec{n} + \sin\theta(-\kappa\vec{t} + \tau\vec{b}) - \sin\theta(\frac{\partial\theta}{\partial s})\vec{b} + \cos\theta(-\tau\vec{n})$$

$$= -\kappa\sin\theta\vec{t} + (\frac{\partial\theta}{\partial s} - \tau)(\cos\theta\vec{n} - \sin\theta\vec{b})$$

$$= -\kappa\sin\theta\vec{t} + (\frac{\partial\theta}{\partial s} - \tau)\vec{\mathfrak{E}}$$

by using the Equations 19 and 23. Then, we also have

$$\frac{\partial}{\partial n}\vec{t} = \ell_{ns}(\cos\theta\vec{\mathfrak{E}} + \sin\theta\vec{\mathfrak{B}}) - (\tau + \varrho_b)(-\sin\theta\vec{\mathfrak{E}} + \cos\theta\vec{\mathfrak{B}})$$

$$= (\ell_{ns}\cos\theta + (\tau + \varrho_b)\sin\theta)\vec{\mathfrak{E}} + (\ell_{ns}\sin\theta - (\tau + \varrho_b)\cos\theta)\vec{\mathfrak{B}},$$

$$\frac{\partial}{\partial n}\vec{\mathfrak{E}} = -\sin\theta\left(\frac{\partial\theta}{\partial n}\right)\vec{n} + \cos\theta\left(\ell_{ns}\vec{t} - div\vec{b}\vec{b}\right)$$
$$-\cos\theta(\frac{\partial\theta}{\partial n})\vec{b} - \sin\theta((-\tau - \varrho_b)\vec{t} + div\vec{b}\vec{n})$$

$$= (\ell_{ns}\cos\theta + (\tau + \varrho_b)\sin\theta)\vec{t} + (-\frac{\partial\theta}{\partial n} - div\vec{b})\vec{\mathfrak{B}}$$

and

$$\frac{\partial}{\partial n}\vec{\mathfrak{B}} = \cos\theta\left(\frac{\partial\theta}{\partial n}\right)\vec{n} + \sin\theta\left(\ell_{ns}\vec{t} - div\vec{b}\vec{b}\right)$$
$$-\sin\theta(\frac{\partial\theta}{\partial n})\vec{b} + \cos\theta((-\tau - \varrho_b)\vec{t} + div\vec{b}\vec{n})$$

$$= (-\ell_{ns}\sin\theta - (\tau + \varrho_b)\cos\theta)\vec{t} + (\frac{\partial\theta}{\partial n} + div\vec{b})\vec{\mathfrak{E}}$$

by using Equations 20 and 23. Finally, it is obtained that

$$\frac{\partial}{\partial b}\vec{t} = (\tau - \varrho_n)(\cos\theta\vec{\mathfrak{E}} + \sin\theta\vec{\mathfrak{B}}) + \ell_{bs}(-\sin\theta\vec{\mathfrak{E}} + \cos\theta\vec{\mathfrak{B}})$$

$$= ((\tau - \varrho_n)\cos\theta - \ell_{bs}\sin\theta)\vec{\mathfrak{E}} + ((\tau - \varrho_n)\sin\theta + \ell_{bs}\cos\theta)\vec{\mathfrak{B}},$$

$$\frac{\partial}{\partial b}\vec{\mathfrak{E}} = -\sin\theta\left(\frac{\partial\theta}{\partial b}\right)\vec{n} + \cos\theta\left((\tau - \varrho_n)\vec{t} + (\kappa + div\vec{n})\vec{b}\right)$$
$$-\cos\theta(\frac{\partial\theta}{\partial b})\vec{b} - \sin\theta(\ell_{bs}\vec{t} - (\kappa + div\vec{n})\vec{n})$$

$$= \left((\tau - \varrho_n)\cos\theta - \ell_{bs}\sin\theta\right)\vec{t}$$
$$+(-\frac{\partial\theta}{\partial b} + div\vec{n} + \kappa)(\sin\theta\vec{n} + \cos\theta\vec{b})$$

$$= ((\tau - \varrho_n)\cos\theta - \ell_{bs}\sin\theta)\vec{t} + (-\frac{\partial\theta}{\partial b} + div\vec{n} + \kappa)\vec{\mathcal{B}}$$

and

$$\frac{\partial}{\partial b}\vec{\mathcal{B}} = \cos\theta\left(\frac{\partial\theta}{\partial b}\right)\vec{n} + \sin\theta\left((\tau - \varrho_n)\vec{t} + (\kappa + div\vec{n})\vec{b}\right)$$
$$-\sin\theta(\frac{\partial\theta}{\partial b})\vec{b} + \cos\theta(\ell_{bs}\vec{t} - (\kappa + div\vec{n})\vec{n})$$

$$= ((\tau - \varrho_n)\sin\theta + \ell_{bs}\cos\theta)\vec{t} + (\frac{\partial\theta}{\partial b} - div\vec{n} - \kappa)\vec{\mathcal{E}}$$

by using Equations 21 and 23.

Theorem 12. Assume that $\mathfrak{I} = \mathfrak{I}(s, n, b)$ is a unit speed timelike curve. EM wave vector fields are parallel transportation of Serret-Frenet frame if and only if θ satisfies the followings

$$\frac{\partial\theta}{\partial s} = \tau,$$

$$\frac{\partial\theta}{\partial n} = -div\vec{b}, \tag{27}$$

$$\frac{\partial\theta}{\partial b} = \kappa + div\vec{n}.$$

Proof. Based on the parallel transportation criterion, partial derivatives of $(\vec{t}, \vec{\mathcal{E}}, \vec{\mathcal{B}})$ only need to have a tangent direction if and only if

$$-\frac{\partial\theta}{\partial s} + \tau = 0,$$
$$-\frac{\partial\theta}{\partial n} - div\vec{b} = 0,$$
$$-\frac{\partial\theta}{\partial b} + div\vec{n} + \kappa = 0$$

by Equations 24, 25 and 26.

3. A Physical and Geometric Application

It is known that

$$curl\vec{t} = -\varrho_s\vec{t} + \kappa\vec{b} \tag{28}$$

for a given timelike curve. Since $curl\vec{t}$ has no component with $\vec{n}$ direction, there is a surface which contains both s and b parameter curves if and only if

$$\varrho_n = 0. \tag{29}$$

Let Υ be a given surface which contains both s and b parameter curves as follows

$$\Upsilon(s,b) = (\sqrt{2}\sinh(s+\tfrac{b}{\sqrt{2}}), \sqrt{2}\cosh(s+\tfrac{b}{\sqrt{2}}), s+\sqrt{2}b).$$

The tangent vector is obtained as follows:

$$\vec{t}(s,b) = (\sqrt{2}\cosh(s+\tfrac{b}{\sqrt{2}}), \sqrt{2}\sinh(s+\tfrac{b}{\sqrt{2}}),1)$$

which is also direction of the electromagnetic wave. We have found

$$\kappa(s,b) = \sqrt{2}, \qquad \tau(s,b) = -1$$

respectively. The spacelike vector fields are found as follows:

$$\vec{n}(s,b) = (\sinh(s+\tfrac{b}{\sqrt{2}}), \cosh(s+\tfrac{b}{\sqrt{2}}),0),$$

$$\vec{b}(s,b) = (\cosh(s+\tfrac{b}{\sqrt{2}}), \sinh(s+\tfrac{b}{\sqrt{2}}), \sqrt{2}).$$

Moreover, we get

$$\frac{\partial}{\partial s}\theta(s,b) = \tau(s,b) = -1,$$
$$\frac{\partial}{\partial b}\theta(s,b) = div\vec{n} + \kappa(s,b) = -\frac{1}{2}$$

by Theorem 9. Therefore, we have found $\theta = \theta(s,b)$ as follows:

$$\theta(s,b) = -s - \tfrac{b}{2}.$$

The geometric phase θ is defined by the rotation of vectors $\vec{\mathcal{E}}$ and $\vec{\mathcal{B}}$ with respect to $(\vec{n},\vec{b})$ basis with an angular velocity. Then, $\vec{\mathfrak{E}}$ and $\vec{\mathfrak{B}}$ are stated as follows:

$$\vec{\mathfrak{E}}(s,b) = (\sinh(s+\tfrac{1}{2}\sqrt{2}b)\cos\theta - \cosh(s+\tfrac{1}{2}\sqrt{2}b)\sin\theta,$$
$$\cosh(s+\frac{1}{2}\sqrt{2}b)\cos\theta - \sinh(s+\frac{1}{2}\sqrt{2}b)\sin\theta, -\sqrt{2}\sin\theta)$$

$$\vec{\mathfrak{B}}(s,b) = (\sin\theta\sinh(s+\tfrac{b}{\sqrt{2}}) + \cos\theta\cosh(s+\tfrac{b}{\sqrt{2}}),$$
$$\sin\theta\cosh(s+\frac{b}{\sqrt{2}}) + \cos\theta\sinh(s+\frac{b}{\sqrt{2}}), \sqrt{2}\cos\theta).$$

Then, figures of $\vec{\mathfrak{E}}(s,b)$, $\vec{\mathfrak{B}}(s,b)$ and the one-parameter family of surface $\Upsilon = \Upsilon(s,b)$ are all illustrated as follows:

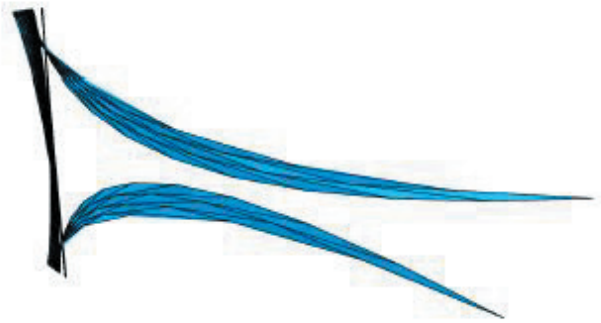

Figure 1: Image of electromagnetic wave vector fields

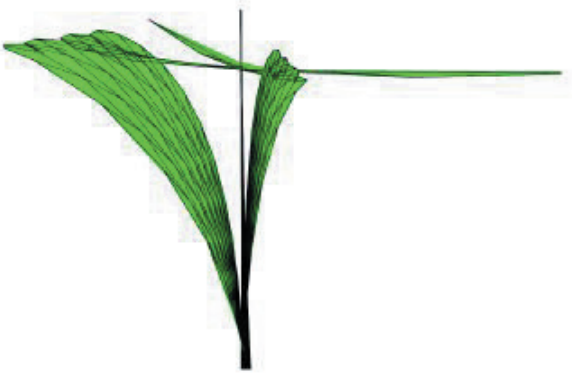

Figure 2: Image of magnetic wave vector fields

Figure 3: Image of the surface and EM wave vector fields

REFERENCES

Körpınar, T., Demirkol, R. C., Körpınar, Z., & Asil, V. (2020). Maxwellian Evolution Equations Along the Uniform Optical Fiber in Minkowski Space. *Revista Mexicana de Fisica*, 66(4), 431-439.

Yavuz, A. (2022). On Normal Congruence of Surfaces and Position Vector of Optical Fiber by Electromagnetic Wave Vectors. *Optik*, 260, 168994.

Rogers, C., & Schief, W.K. (2003). Novel İntegrable Reductions in Nonlinear Continuum Mechanics via Geometric Constraints. *Journal of Mathematical Physics*, 44(8), 3341-3369.

Marris, A. W., Passman, S. L. (1969). Vector Fields and Flows on Developable Surfaces. *Archive for Rational Mechanics and Analysis*, 32(1), 29-86.

Özdemir, M., Erdoğdu, M. (2014). On The Rotation Matrix in Minkowski Space-Time. *Reports on Mathematical Physics*, 74(1), 27-38.

Erdoğdu, M., Özdemir, M. (2020). Simple, Double and Isoclinic Rotations with a Viable Algorithm. *Mathematical Sciences and Applications E-Notes*, 8(1), 11-24.

Erdoğdu, M., Özdemir, M. (2015). On Reflections and Rotations in Minkowski 3-Space of Physical Phenomena. *Journal of Geometry and Symmetry in Physics*, 39, 1-16.

Erdoğdu, M. (2015). Parallel Frame of Non-Lightlike Curves in Minkowski Space-Time. *International Journal of Geometric Methods in Modern Physics*, 12(10), 1550109.

Do Carmo, M. P., (1976). *Differential Geometry of Curves and Surfaces*, Portland, U.S.A. Prentice-Hall.

Hacısalihoğlu H.H. (2000), *Differential Geometry*. Ankara, Faculty of Science Publ,.

Shifrin, T. (2015), *Differential Geometry: A first Course in Curves and Surfaces*, University of Georgia. AMS Open Math. Notes.

Van Bladel, J. G. (2007). *Electromagnetic Fields* (Vol. 19). John Wiley & Sons.

Wangsness, R. K. (1979). *Electromagnetic Fields* (Vol. 2). New York: Wiley.

Feibelman, P. J. (1982). Surface Electromagnetic Fields. *Progress in Surface Science*, *12*(4), 287-407.

Chen, H., & Chan, C. T. (2007). Transformation Media That Rotate Electromagnetic Fields. *Applied Physics Letters*, *90*(24), 241105.

Ishimaru, A. (2017). Electromagnetic Wave Propagation, Radiation, and Scattering: From Fundamentals to Applications. John Wiley & Sons.

Polo Jr, J. A., & Lakhtakia, A. (2011). Surface Electromagnetic Waves: A Review. *Laser & Photonics Reviews*, *5*(2), 234-246.